DSE - Steps to Mars - Boots on Phobos

Design a Solar Electric Propulsion tug and lander necessary to pre-position a human habitat on Phobos by 2033.

I. Akkerhuis	4271750	F.C. Schornagel	4307348
A.O. Bianchi	4276973	F. Schoutetens	4358341
E. Ghys	4368568	M. Touw	4135474
T. Govaert	4345436	R.C. van der Grift	4341279
F. Sasse	4174992	N.W.H. van Tent	4383206

Final Report

Design Synthesis Excercise

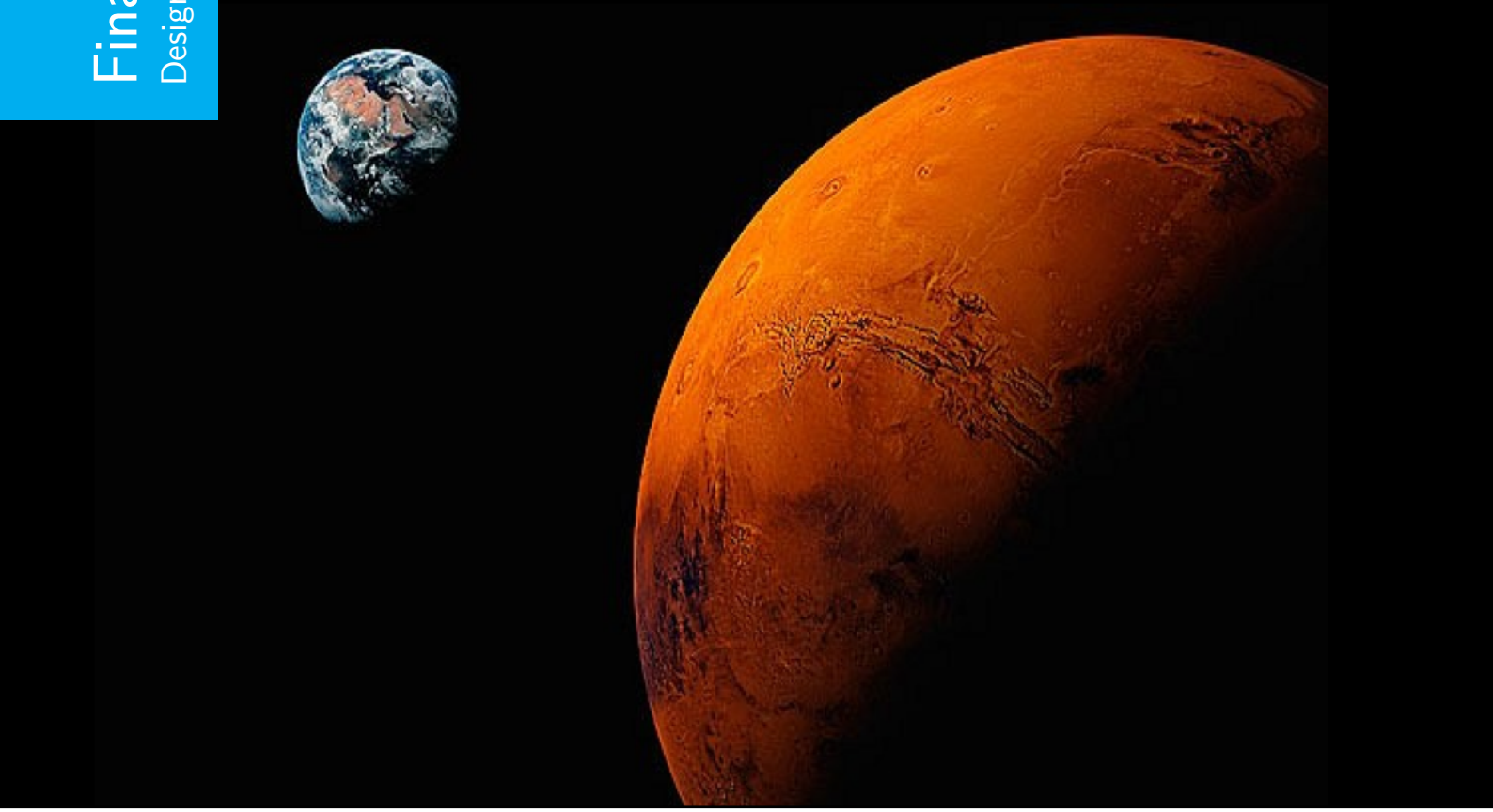

TU Delft Delft University of Technology

Aerospace Engineering

July 5, 2017

[THIS PAGE WAS INTENTIONALLY LEFT BLANK]

Preface

This report is the final and solely published progress report on a mission to Phobos, one of Mars' moons. It was conducted by ten students from the Aerospace Engineering faculty at the Delft University of Technology. The Planetary Society proposed a plan for a mission to Phobos. These reports provide the means to perform this mission. This report should provide an insight in the possibilities for this type of mission and can thus be used as reference for future designs. The preceding reports are described in Figure 1 to give an idea on how this final report came to be.

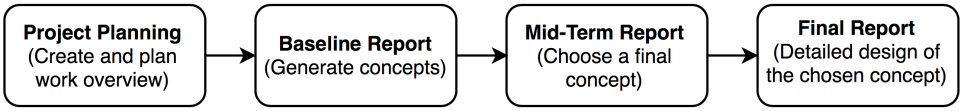

Figure 1: Outline of the reports delivered for this DSE-project.

Important to note about this report is that it has been structured according to the Pyramid Principle. This method highlights the most significant results first. The questions of 'why' and 'how' are answered at lower levels of the pyramid. This method is used to fortify the mentioned results. In other words, each layer of the pyramid provides the reader with a new level of detail.

The authors would like to thank K. Cowan, G. Mahapatra and M. Roelofs for their inexhaustible effort and support, together with the responsible persons organising this Design Synthesis Exercise.

Title page figure taken from https://oncirculation.com/2011/12/

[THIS PAGE WAS INTENTIONALLY LEFT BLANK]

Summary

The Planetary Society forged a plan to conduct a mission that transports a habitat from Earth to the surface of Phobos. The mission would start in Low Earth Orbit (LEO). There, a transportation tug would pick up the 50 tonne habitat and bring it to the surface of Phobos. This could be accomplished with the configuration of choice, while the main requirement was that it should be propelled by a solar electric propulsion system. Completing this interplanetary transport challenge was the main focus of this report.

During the previous report, the Mid-Term Report, the goal was to choose the final concept by trading off five configurations. Structures, power, propulsion and navigation contributed to the system-level trade-off, where the other subsystems performed an independent trade-off. The trade-off criteria were the following: size, cost, risk, sustainability and sensitivity.

The concept that was chosen to conduct the mission is the PICARD (Phobos Interplanetary Cargo and Reconnaissance Design). The PICARD's body consists of a tug and lander module, interconnected by structural fairing. The total wet masses of the tug and lander are 83,693 kg and 8,297 kg, respectively. To reach Mars within acceptable time limits, a total velocity increment of 10,321 m/s is required. The PICARD is propelled by two electromagnetic VASIMR-engines which require a total 400 kW of power that is provided by two solar array wings with a total area of 2,752 m^2. This is significantly less than the 4,438 m^2 found in the Mid-Term Report [1] due to the preliminary orbit times and power required by the various subsystems, and also due to the lower performance assumed for the solar arrays. During eclipse times, 80 Li-Ion secondary batteries are used to keep delivering the average power. The lander has no external power source. It is purely powered by 50 batteries which are charged just in time before decoupling of tug and lander. Whenever communication with Earth is necessary during transfer, the Attitude Determination & Control System (ADCS) is able to point within an accuracy of 0.1 degree. Both tug and lander have an independent ADCS, capable of achieving this accuracy. The tug uses 16 thrusters, four control moment gyroscopes, 12 sun sensors and two star trackers, each with three optical heads. The lander uses 40 thrusters, eight sun sensors and two star trackers, each with three optical heads. When needed, the antennas can send data on both Ka- and X-band. A total of four antennas on the tug and one on the lander were found to provide communication with proper redundancy. Of course, all incoming data has to be processed, and that is done with three RAD750 processors for both tug and lander. This is once again for redundancy. Memory modules of 2,048 MB in the lander for the main system and several instruments can provide sufficient storage in case of communication eclipses. For the tug, this value turned out to be 1,024 MB.

During the design process, sustainability and risk were taken into account as the major parameters when trading-off between subsystem design options. Sustainability was evaluated by looking at environmental and societal aspects, where e.g. off-the-shelf technology was very influential, since it limited the amount of resources required.
Whenever risks with a high probability and/or catastrophic risks would come into play, a mitigation strategy was established to decrease their likelihood of occurrence and severity.

The mission was divided into eight phases. Concerning the launch phase, John F. Kennedy Space Center would be the preferred launch location with a launch date at the 31st of September 2028. Having a travel time of about four years, the expected arrival date is the 4th of July 2032. The PICARD will be launched by two Space Launch Systems (SLS) Block II. Once in orbit, tug, lander and habitat will dock to prepare the transfer to Mars. To escape Earth's Sphere of Influence (SOI), the propulsion system will continuously increase the orbit, resulting into a low thrust trajectory. After leaving Earth's SOI, the PICARD will travel towards Mars. The propulsion system will be shut off before the arrival at Mars to ensure easier and less propellant consuming insertion into capture orbit. When in orbit around Mars, the tug and lander will separate using the same coupling mechanism as for the docking. While the lander module proceeds to approach the surface of Phobos, the tug will travel to a pre-determined relay orbit and function as relay satellite for lander-to-Earth communication. During the awaiting of the astronauts, the lander will monitor the surface of Phobos and maintain the habitat. To keep the mission sustainable, the End-of-Life (EOL) strategy includes the disposal of the tug after the arrival of the astronauts.

In the last phase of this project, all the post-design operations up to the actual launch were considered. A plan was set up explaining how to produce and transport elements in order to meet the actual launch window. A Gantt chart and cost breakdown show the schedule and costs for these post-design activities.

Throughout the entire design process, verification and validation had been applied to ensure the feasibility of the design. Regarding the model, the numerical values were checked to ensure their correctness and references provided their validity. Products were verified and validated by proposing tests to check whether they meet requirements and whether configurations within the subsystem actually produced a working system.

Contents

List of Figures

List of Tables

Nomenclature

List of Abbreviations

ADCS	Attitude Determination & Control Subsystem
ATV	Automated Transfer Vehicle
AU	Astronomical Unit
BER	Bit Error Probability
BIRD	Bispectral and Infrared Remote Detection
BOL	Beginning of Life
BPSK	Binary Phase-Shift Keying
C&DH	Command & Data Handling
CBS	Cost Breakdown Structure
CMG	Control Moment Gyroscopes
CMOS	Complementary Metal Oxide Semiconductor
COSPAR	Committee on Space Research
DSE	Design Synthesis Exercise
DSN	Deep Space Network
EBD	Electrical Block Diagram
EOL	End of Life
EPS	Electrical Power System
ESA	European Space Agency
FBS	Functional Breakdown Structure
FFD	Functional Flow Diagram
GMAT	General Mission Analysis Tool
GN&C	Guidance, Navigation & Control
HEOMD	Human Exploration and Operations Missions Directorate
HOM	Humans Orbiting Mars
IEEE	Institute of Electrical and Electronics Engineers
IGNC	Integrated GN&C
IMU	Inertia Measurement Unit
ISS	International Space Station
ITU	International Telecommunication Union
LEO	Low Earth Orbit
LIDAR	Light Detection and Ranging
MJ	Multi-Junction
MLB	Mobile Launcher Platform
MLI	Multi Layer Insulation
MMH	Monomethylhydrazine
MOLA	Mars Orbiter Laser Altimeter
MRO	Mars Reconnaissance Orbiter
MSS	Mechanical Support System
NASA	National Aeronautics and Space Agency
PCU	Power Control Unit
PD&D	Project Design & Development Logic
PICARD	Phobos Interplanetary Cargo and Reconnaissance Design
PLP	Pre-landing Phase
PMD	Power Management & Distribution
PPP	Planetary Protection Policy
PSP	Phobos Staying Phase
RAMS	Reliability, Availability, Maintainability and Safety
RHU	Radioisotope Heater Unit
ROSA	Roll-Out Solar Arrays
RTG	Radioisotope Thermoelectric Generator
SA	Solar Array
SAM	Sample Analysis at Mars
SEP	Solar Electric Propulsion
SLOC	Source Lines of Code
SLS	Space Launch System
SOI	Sphere of Influence
SPENVIS	Space Environment Information System
SPF	Single Point of Failure
STMD	Space Technology Mission Directorate
TRL	Technology Readiness level
VASIMR	Variable Specific Impulse Rocket

List of Symbols

α	Absorptance factor [-]
$\alpha_{1/2}$	Half-power angle [deg]
β	Solar incidence angle [rad]
ΔV	Change in velocity [m/s]
$\dot{Q}$	Heat flow rate [W]
η_{BAT}	Battery discharge efficiency [-]
$\frac{E_b}{N_0}$	Signal-to-noise ratio [-]
κ	Coefficient of thermal conductivity [W /m /K]
λ	Wavelength [m]
λ_M	Magnetic amplification factor [-]
μ	Gravitational parameter [m^2/s^3]
ω	Angular velocity
ϕ	Roll angle [rad]
ρ	Density [kg/m^3]
σ	Stefan-Boltzmann constant [$W/m^2/K^4$]
σ_y	Yield stress [Pa]
τ	Torque [Nm]
θ	Angle [deg]
υ	Poisson ratio [-]
ε	Emittance factor [-]
A	Area [m^2]
a	Planetary albedo [-]
C	Heat capacity [J/K]
C_D	Drag coefficient [-]
cm	Centre of mass location [m]
cp_a	Aerodynamic centre of pressure [m]
D	Diameter [m]
d	Arm [m]
$d\theta$	Angular step [°]
D_{res}	Residual dipole [Am^2]
DOD	Depth of Discharge [-]
dt	Time step [s]

E	Youngs modulus [Pa]
e_t	Pointing offset [deg]
E_δ	Energy density [Wh/l]
E_e	Eclipse energy [Wh]
E_{sp}	Specific energy [Wh/kg]
f	Frequency [Hz]
F_T	Thrust [N]
F_{cr}	Critical buckling force [N]
f_{cr}	Dynamic crush strength [Pa]
FoS	Factor of Safety [-]
G	Gain [-]
g_0	Average gravitational acceleration at sea level on Earth [m/s^2]
G_C	Gravitational constant [m^3/kg /s^2]
H	Angular momentum [kg m^2/s]
I	Area moment of inertia [m^4]
I_d	Inherent degradation [-]
I_{sp}	Specific impulse [s]
J	Solar radiation intensity [W/m^2]
k	Boltzmann constant [m^{2}kg/s^2/K]
L	Loss [-]
l	Distance length [m]
L_d	Lifetime degradation [-]
M	Magnetic field strength [Tm^3]
m	Mass [kg]
P	Power [W]
p	Pressure [Pa]
P_δ	Power density [W/m^2]
P_{sp}	Specific power [W/kg]
Q	Internal generated heat [W]
q	Reflectivity [-]
R	Required data rate [bits/s]
r	Radius [m]
T	Temperature [K]
t	Time [s]
T_s	System noise temperature [K]
t_t	tank wall thickness [m]
V	Volume [m^3]
v	Velocity [m/s]
V_f	Visibility factor [-]
w	Width of the structure

Chapter 1 Introduction

In 1969 mankind landed on the Moon with the Apollo missions. Ever since these missions ended, there has never been another manned space mission to go beyond LEO . To revive this age of exploration and to set the next step, plans are being made to send humans into outer space again. These plans entail sending humans to Mars and safely land on its surface, while enabling a return home. In these plans, landing on Phobos is considered a precursor to human landing on Mars, since Phobos has very low gravity and no atmosphere. These two factors make the process of landing easier [7], while the habitat can be used as a stop or fallback base for astronauts.
The difference from other Mars missions is the fact that it should be solely powered by solar power. This is the main problem to be solved, hence the report will focus on transporting a habitat and lander module from LEO to the surface of Phobos by means of a Solar Electric Propulsion (SEP) tug. From this problem, the Mission Need Statement and Project Objective Statement were derived.

Mission Need Statement
Create a programme for the sustainable human exploration of Mars, with the ultimate goal of safely landing humans on Mars.

Project Objective Statement
Design a Solar Electric Propulsion tug and lander to pre-position a human habitat on Phobos by 2033 and maintain it until the arrival of astronauts.

This mission is especially important since it tests the feasibility of this sustainable method of transportation. At the same time, the future colonisation of space is studied, which will become increasingly important throughout the coming years.

To identify whether this mission is feasible and what the design would look like one posed the question: 'Is SEP a possible option for a mission to Mars and if so, what would its detailed design look like when considering all the design challenges?'. The design challenges include sustainability, risk and pre-launch operations. This would not only test its feasibility in space, but also in a realistic manner by testing more than just the spacecraft itself.
This question was answered by doing a detailed design of the space probe and evaluating how this entire craft would function through the different mission phases that were thought of. Information on the design of subsystems were gathered from literature, conversations with professors at the Delft University of Technology and external sources from space related companies. To be certain that these designs were actually sensible and achievable, a verification and validation analysis had been executed throughout the design phases on requirements, models and products. The model verification and validation was accomplished by analysing whether the elements of the model were correct and whether adequately integrated, using experience in application of similar models, or by comparing it to valid and independent models or test data. For this comparison with valid models or data, it was opted to implement an allowed margin of error of 10 %, as this was assumed to represent the appropriate complexity of the models created [8]. The products would then be treated by verifying whether they actually perform what they were designed for by means of, for example, a test or inspection. A final validation would be done by testing the design as a whole, both subsystem- and system-wise, to validate that all components are correctly working together.
To know what to design for, or what to verify or validate, a list of requirements were set up as reference. Initially, the customer requirements came from the Planetary Society, which formed the building blocks for this research [9]. Major constraints were that of the electric propulsion and a proper sustainability approach. Of course, this project was limited to certain extent: investigating whether what was designed is actually available on the market proved to be very difficult, since much of it is either confidential or not available to the public. Best efforts were made, but further research is required. All these requirements constrained the extent to which the mission could be designed, but if required, these requirements could be discarded in case of a killer requirement situation.

Ultimately, the report is structured to answer the main question that was posed. The steps towards doing so were laid out in this introduction. The final design for this mission will be presented up first, in chapter 2. The explanation of how all elements of this spacecraft are used and interact during the mission is found in chapter 3. Special attention was paid to the design of the landing and EOL strategy,

which were given shape in chapter 4. To comprehend the philosophy behind these elements of different subsystems, a detailed design is discussed in chapter 5. This chapter also contains the verification and validation per subsystem. After that, the design and the main mission is elaborated on. With chapter 6, the phases between design and launch are set-up, like production and transportation. Continuing with a system level analysis, chapter 7 provides insight in the available budget and market developments. This is followed up by the Reliability, Availability, Maintainability and Safety (RAMS), chapter 8, to check the entire design for each of these four parameters. Subsequently, the design is then checked for risk, sustainability and sensitivity in chapter 9, chapter 10 and chapter 11, respectively, finalising the idea of the design in chapter 12 by showing its system level verification and validation. This report is ended with a conclusion and a discussion with recommendations in chapter 13 and chapter 14, respectively.

Chapter 2 PICARD Specifications

After a trade-off, the final concept was chosen. This was the goal of the Mid-Term Report [1]. The concept was given the name "PICARD" (Phobos Interplanetary Cargo and Reconnaissance Design). The general overview of this design, resulting from design calculations and iterations described in chapter 5, is given in this chapter. It consists of the hardware configuration in section 2.1. Afterwards, the performance of the PICARD is discussed in section 2.2. The resource allocation, which includes the mass, power and propellant budgets, can be found in section 2.3. The scientific instruments used for this mission are presented in section 2.4. Lastly, a hardware diagram that depicts all components of the system and their interfacing is presented in section 2.5.

2.1 Configuration

To give a clear indication on the PICARD's hardware configuration, the spacecraft was divided into external and internal configuration. This section contains the general layout of the design.

2.1.1 External Configuration

Many of the designed components are stored inside the spacecraft, others are attached externally. The external layout of the PICARD, illustrated in Figure 2.1, Figure 2.2 and Figure 2.3, shows that the PICARD's body consists of two main parts: the transportation tug and the lander. They are connected by a fairing structure. The body of the spacecraft has a base of 5x5 m. The tug, fairing and lander have a height of 5, 2.4 and 1.1 m, respectively. During the escape from Earth's SOI and the transfer to Mars, the PICARD is propelled by two electromagnetic Variable Specific Impulse Rocket (VASIMR) engines. After the arrival at Mars, the lander module uses a chemical propulsion system to perform the landing procedure. The tug's subsystems will be powered by two solar wings, each consisting of 14 deployable Roll-Out Solar Arrays (ROSA) in combination with 80 secondary internal batteries for powering during Solar eclipses. The lander is powered by 50 batteries and has no power generation system. Further external components, necessary for the communication with Earth, are antennas. The tug has four antennas, three pointed towards Earth and one towards the lander. The last one is present so that the tug can function as a relay satellite for the lander communication. The external components of the ADCS are actuators and sensors. The tug uses 16 thrusters, 12 sun sensors, 2 star trackers and 4 control moment gyroscopes. The lander uses 40 thrusters, 8 sun sensors and 2 star trackers.

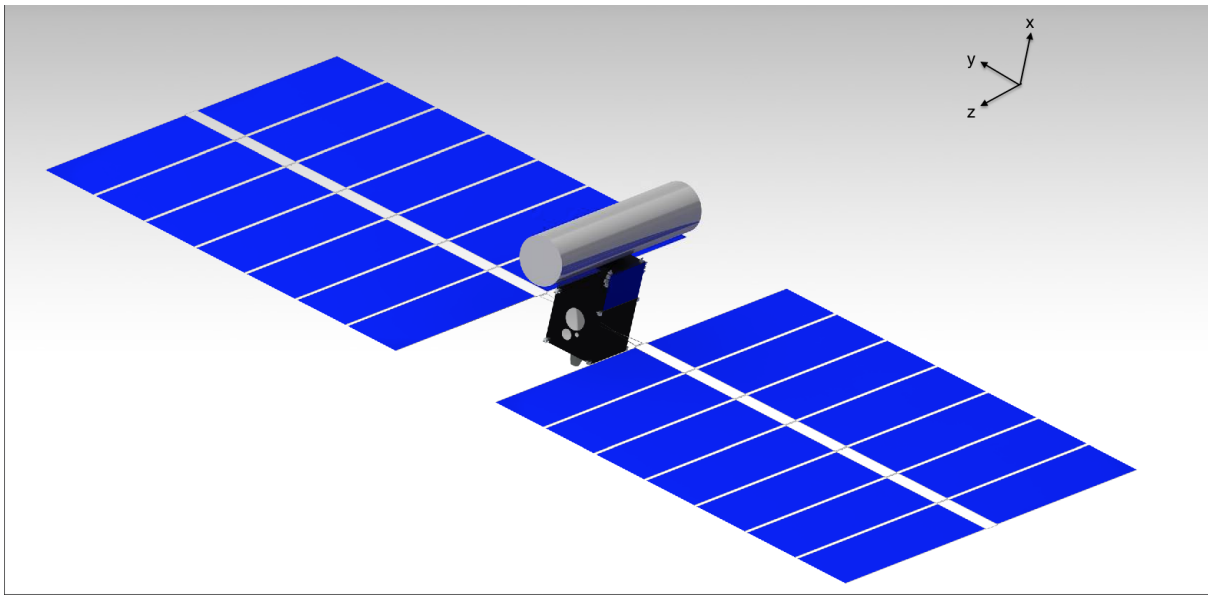

Figure 2.1: Isometric view of the PICARD.

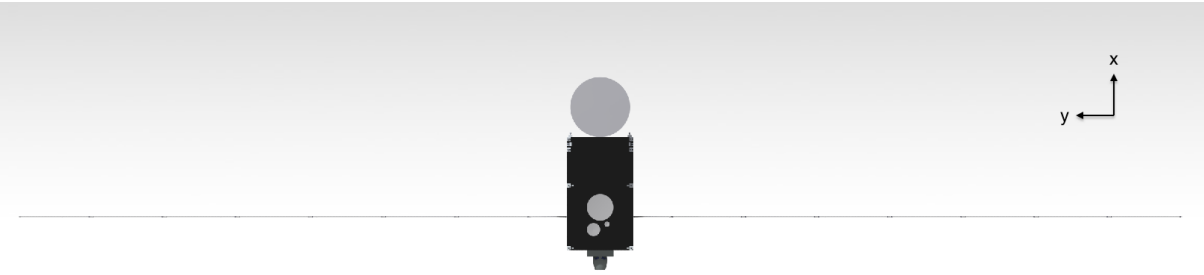

Figure 2.2: Front view of the PICARD.

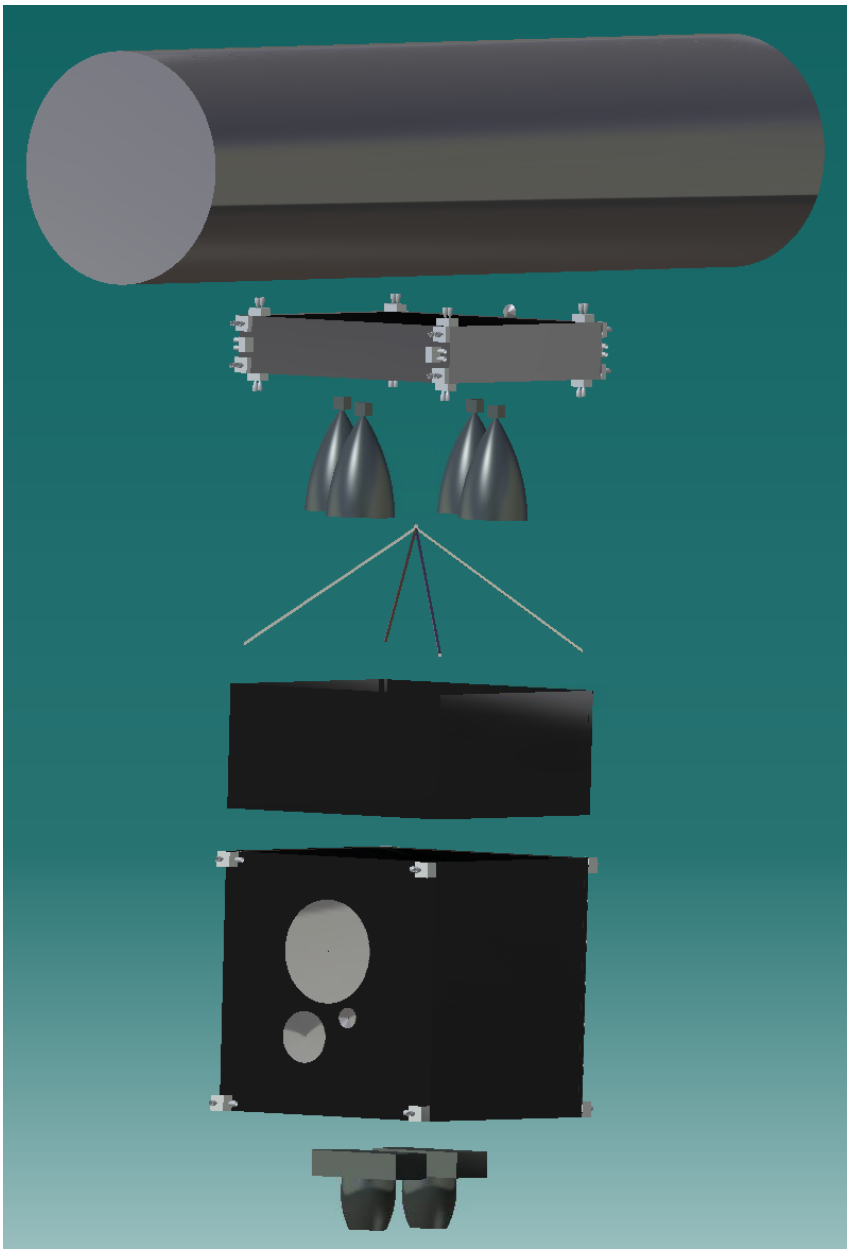

Figure 2.3: Exploded view of the PICARD, excluding the solar arrays.

2.1.2 Internal Configuration

The internal configuration of the tug and lander can be found in Figure 2.4 and Figure 2.5, respectively. These figures do not contain small parts such as the board computers, wiring and small scientific payload (like temperature measurement units and bolometers) to improve the clarity of the figure. As it can be observed in Figure 2.4, the tug embodies two fuel, two oxidiser and two pressure tanks to provide propellant to the thrusters of the ADCS. Each corner of the tug, seen from the top view, reserves some space for the attachment of the thrusters. Furthermore, the tug fits a xenon (propulsion) tank to fuel the two VASIMR-engines. As previously mentioned, the tug uses batteries for power provision during eclipse times. When observing Figure 2.5 and comparing it to the internal layout of the tug, the main difference in components is the absence of the xenon tank due to the use of a chemical propulsion system. The lander module was designed in such a way the ADCS and propulsion system can share the same tanks. Further differences are the inclusion of scientific instruments, which are further elaborated on in section 2.4.

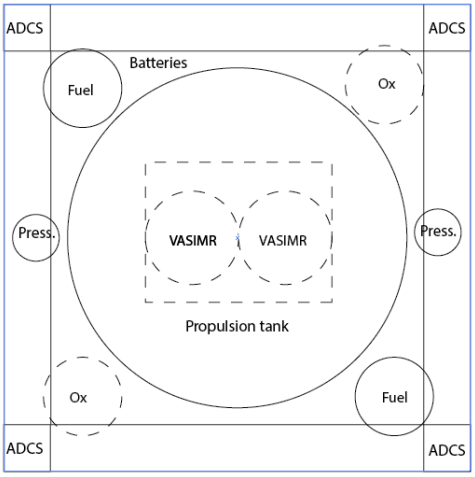

(a) Top view of the internal configuration of the tug.

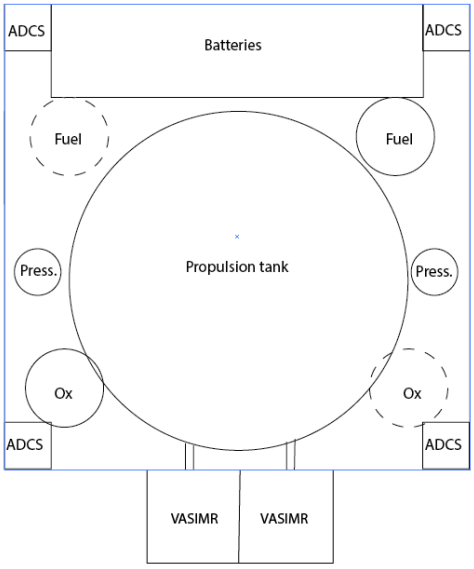

(b) Front view of the internal configuration of the tug.

Figure 2.4: Internal lay-out of the tug.

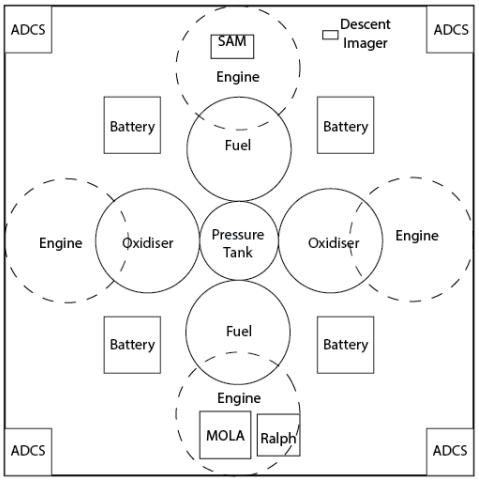

(a) Top view of the internal configuration of the lander.

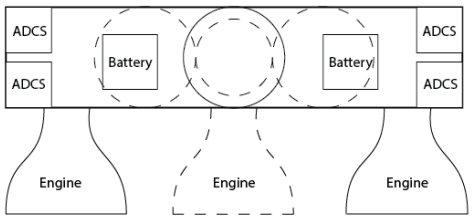

(b) Front view of the internal configuration of the lander.

Figure 2.5: Internal lay-out of the lander.

2.2 System Performance

The spacecraft is planned to launch from Cape Canaveral in August 2028 and arrive on Phobos in October 2032. The loading struts of the PICARD, with aluminium as main material, are designed to carry a load of 4 g during launch. The tug, lander and habitat are coupled together using the same mechanism, which is based of lead screws. The same mechanism is used in a later stage of the mission, where the lander is decoupled from the transportation tug. The PICARD uses low-thrust trajectories. This requires the tug propulsion system to provide a total ΔV of 9,237.1 m/s which is achieved with a maximum thrust level of 11.4 N by means of two VASIMR-engines having a combined mass of 2,052 kg. The propellant used for these engines is xenon and has a total mass of 34,326 kg. One spherical tank is used to store the xenon, which has a mass of 3,854 kg and a diameter of 3.65 m. After separation of the tug, the lander performs a Hohmann transfer from Mars orbit to Phobos. This requires a total ΔV of 67.5 m/s which is achieved by four Aestus-engines with a total thrust level of 118.4 kN and a combined mass of 444 kg. The engines for the propulsion system and the thrusters of the ADCS both run on Monomethylhydrazine (MMH) fuel + N_2O_4 oxidiser with helium pressurant and therefore use the same propellant tanks. A combined fuel mass of 1,140 kg, oxidiser mass of 2,058 kg and pressurant mass of 12 kg is found. This results in two fuel tanks both with a diameter of 1.07 m and a mass of 322 kg, two oxidiser tanks both with a diameter of 1.10 m and a mass of 353 kg and two pressurant tanks with a diameter of 0.26 m and mass of 42 kg per tank. To land on Phobos, a four-legged landing mechanism is designed, which makes use of crushed honeycomb material for touch-down. Besides, two harpoons and screws at each leg of the landing mechanism provide anchoring.

During space travel, the tug communicates with Earth using the Deep Space Network (DSN) and on-board antennas. The communication has to be done during a frequency of eight hours. This communication requires a pointing accuracy of 0.1° which is provided by the ADCS. A downlink data rate of at least 200 kbits/s can be achieved. When Earth and Mars are at minimum distance, data rates up to 5 Mbits/s can be achieved. During the communication eclipse the tug is not able to communicate with Earth, this happens 0.88 hours per orbit and 17 days every 26 months. Communication eclipses between tug and lander last 52.2 hours every 5.78 days. At this time, the data is stored by the Command & Data Handling (C&DH) subsystem, with memory modules to accommodate the data generated during these eclipses. The tug was designed for the longer eclipse of 17 days. This resulted in 1,024 MB of memory for the tug. The eclipse of 52.2 hours was the constraint for the lander, which required 2,048 MB accordingly. To provide redundancy for failing modules, the scientific instruments have their own modules of 2,048 MB. The choice of processor was the RAD750 for both tug and lander, both having an amount of three. This third processor runs on different software to provide override whenever deviation between the first and second would arise.

The electrical power system of the tug includes GaAs/GaInp Multi-Junction (MJ) solar panels with an area of 2,752 m^2 and a mass of 4,403.91 kg, able to produce a continuous power level of 473.62 kW. This output is sufficient to provide the average power consumption of 402.41 kW by the subsystems and charge the on-board Li-Ion secondary batteries with 5,668.10 kWh of energy. Such a high battery capacity is necessary to ensure sufficient power provision during the longest eclipse time of 10.14 hours. This requires a total battery mass and volume of 18.89 tonnes and 14.17 m^3, respectively. As mentioned before, the lander uses no external component for power generation. As a matter of fact, the batteries on-board of the lander are of the same type as the ones on-board of the tug. They are charged by the solar arrays of the tug, just in time before the decoupling of the two modules, and are able to store 240.5 kWh of energy. This is a sufficient output to provide all subsystems during the 8.04 hours landing approach with 128.93 W of continuous power. Furthermore, it can provide 13.67 W of power over the worst case duration of two years until the arrival of astronauts.

All of these different subsystems are protected from the harsh environmental aspects the spacecraft has to endure during its travel. To protect the spacecraft against radiation, particles and small debris, it is equipped with lead and aluminium panels, covered with an insulation layer for thermal protection. Further thermal control components installed are radiators, heaters and heat pipes.

The analysis of the performance was done in verification and validation. In that section, the spacecraft was checked to be in line with the requirements.

2.3 Resource Allocation

In this section, the major budgets are shown. These include the mass, power and propellant budgets. The cost budget is shown in section 6.4.

2.3.1 Mass Budget

The mass budget of the PICARD can be found in Table 2.1. This budget consists of the final masses, resulting from the detailed design in chapter 5. The masses are calculated by taking worst-case scenario and adding safety factors. Only the mass of the thermal subsystem does not come from calculations, but it is an estimation. The mass of the habitat is 50 tonnes and it is not included in the table as it is assumed to be launched before the tug and lander, thus being considered a separate element.

Table 2.1: Mass budget of the PICARD design.

Mass Budget	Tug [kg]	%	Lander [kg]	%
Structures	4,603	5.5	1,175	14.2
Thermal	500	0.52	100	1.2
Navigation	1	neglectable	1	neglectable
Propellant main propulsion	34,326	41.1	3,210	38.7
Propellant ADCS	1,840	2.2	3,210	-
Propulsion	6,189	7.4	1,970	23.7
Power	34,773	41.6	1,642	19.8
ADCS	1,388	1.6	98	1.2
CDH	10	0.01	20	0.24
Communication	62	0.07	0.5	neglectable
Payload	1	neglectable	80	0.96
Total Wet Mass	**83,693**	100	**8,296.5**	100
Total Dry Mass	**47,527**	56.7	**5,086.5**	61.3

2.3.2 Power Budget

The power required P_{req} by the subsystems found in the tug and lander is presented in Table 2.2 and Table 2.3, respectively. From these tables, the average power required by the tug and lander can be derived for each mission phase. Considering the tug, the P_{req} is the same for all subsystems for all mission phases, as they keep performing the same operations. For the Earth-to-Mars Transfer phase, since the power system sizing was performed taking into account the total transfer time instead of a single orbit (see section 5.7), time is displayed as not applicable. In case of the lander, however, the operations during the Pre-Landing Phase (PLP) and Phobos Staying Phase (PSP) are different, hence the different P_{req} values. A more elaborate explanation of the methodology for the power budget can be found in section 5.7.

Table 2.2: Power budget of the tug.

Tug Subsystem	Power Setting	P_{req} [W]	t [h] Earth Escape	t [h] Earth-to-Mars Transfer	t [h] Mars Capture
Thermal control	On	60	2,460.44	N.A.	2,982.20
	Stand-by	0	0		0
Structures	On	5	2,460.44		2,982.20
	Stand-by	0	0		0
Propulsion	On	400,000	2,460.44		0
	Stand-by	5	0		2,982.20
ADCS	On	1,942	2,460.44		2,982.20
	Stand-by	5	0		0
Communication	On	1,100	820.15		994.07
	Stand-by	5	1,640.29		1,988.13
C&DH	On	30	2,460.44		2,982.20
	Stand-by	5	0		0

Table 2.3: Power budget of the lander.

Lander Subsystem	Power Setting	P_{req} [W]		t [h]	
		PLP	PSP	PLP	PSP
Thermal control	On	0	0	0	0
	Stand-by	0	0	0	0
Structures	On	2	2	8.04	0
	Stand-by	1	1	0	17,520
Propulsion	On	2	2	8.04	0
	Stand-by	1	1	0	0
ADCS	On	93	5	8.04	0
	Stand-by	1	1	0	17,520
Communication	On	5	5	2.68	5,840
	Stand-by	1	1	5.36	0
C&DH	On	30	10	8.04	17,520
	Stand-by	2	2	0	0

2.3.3 Propellant Budget

The types of propellant and their mass usage for different mission phases and subsystems varies. The propellant budget is shown for the tug and lander separately in Table 2.4 and Table 2.5, respectively.

Firstly the actual required propellant masses are given, after which the residual propellant, required for contingency, is given and finally the total masses are given. Considering the tug, xenon is used as fuel for the VASIMR propulsion engines. The mass values shown for the individual segments are as found to be required from section 5.2. The actual available propellant is much higher, as the calculations for the final propulsion system sizing are based on the second to last iteration, giving a relatively high residual propellant mass. As for the tug's ADCS, MMH and N_2O_4 propellant is used, with a helium pressurant. Helium is included in the total mass, as this is not an actual propellant bus that is used in the system. In the relay orbit segment, the propulsion propellant to actually get to the relay orbit is used, whereas the ADCS propellant used in the relay orbit itself is shown. In the lander, both the propulsion system and ADCS use MMH and N_2O_4 propellant, as shown in Table 2.5. Both use helium as a pressurant.

Table 2.4: Propellant budget of the tug.

Mission Segment	Subsystem	Fuel Type	Mass [kg]
Earth Escape	Propulsion	Xenon	10,453
	ADCS	MMH	123
		N_2O_4	204
Earth-to-Mars Transfer	Propulsion	Xenon	11,299
	ADCS	MMH	166
		N_2O_4	273
Mars Capture	Propulsion	Xenon	4,000
	ADCS	MMH	91
		N_2O_4	150
Relay orbit	Propulsion	Xenon	82
	ADCS	MMH	139
		N_2O_4	230
Residual	Propulsion	Xenon	8,492
	ADCS	MMH	53
		N_2O_4	87
Total	Propulsion	Xenon	34,326
	ADCS	MMH	572
		N_2O_4	944
		Helium	6

Table 2.5: Propellant budget of the lander.

	Fuel Type	Mass [kg]
Propulsion	MMH	374
	N_2O_4	767
ADCS	MMH	587
	N_2O_4	969
Residual	MMH	178
	N_2O_4	322
Total	MMH	1,139
	N_2O_4	2,058
	Helium	12

2.4 Instruments

To fulfil the key requirements on monitoring the surface of Phobos, which are MTP-KEY-SYS02 and MTP-KEY-SYS03, several instruments were required for proper maintaining. For the lander the following list of instruments was set-up:

- **Laser altitude determination**: To land on Phobos, detailed real-time data of the position with respect to Phobos has to be provided to the navigation system, preventing the lander from approaching too fast. This was previously done with the Mars Orbiter Laser Altimeter (MOLA)[1]. The idea is very comparable to a LIght Detection And Ranging (LIDAR), frequently used on Earth.
- **On-board camera**: To image the surface of Phobos, an on-board camera is present to provide imagery to the ground station. Currently the best images of Phobos are from satellites orbiting Mars, where terrain is visible to a limited extent. Detailed terrain images will then be the first with this camera, but can also be used to confirm the landing.
- **Spectrometer**: With a spectrometer experiments can be performed to analyse whether in-situ production is feasible by analysing the composition of present elements. Also, the composition of Phobos can be further analysed, supplying valuable information on the origin of Phobos. Speculation on the captured asteroid theory could then be cleared up[2]. Curiosity has used the Sample Analysis at Mars (SAM) instrument for these purposes, which is applicable for this mission as well [10].
- **Infrared camera**: Whether the surface proves to be habitable also depends on other parameters like temperature. The infrared imager (named Ralph in Figure 2.5) takes care of gathering these parameters, to ensure future astronauts are not exposed to extreme conditions.
- **Descent imager**: During descent, the process has to be captured in order to evaluate the landing. If a failure occurs during the descent, these images help in understanding the landing procedure on these surfaces. This instrument fulfils requirement MTP-OTH-01 as well.
- **Bolometer**: To ensure that radiation levels are not beyond critical limits for future astronauts, the bolometer will send data on radiation levels.
- **Landing sensors**: This includes multiple sensors like accelerometers, touchdown-pressure and velocity sensors. These are necessary during the final descent[3].
- **Electra transceiver**: To avoid a loss of communications, the Electra package is taken on-board. This sender and transceiver make sure communications with other Mars orbiting satellites, like the Mars Reconnaissance Orbiter, is possible. The Electra package supports any navigation, command or data-return needs that a new incoming spacecraft, in this case the lander, might have[4].

To ensure that the tug is fulfilling its scientific requirements as well, the following payload is included in the tug.

[1] URL `https://tharsis.gsfc.nasa.gov/MOLA/Background/spec.php` [cited: 23 May 2017]
[2] URL `http://sci.esa.int/mars-express/31031-phobos/` [cited: 23 June 2016]
[3] URL `http://www.msss.com/mars/mars9x/penetratorpayload.html` [cited: 22 May 2017]
[4] URL `https://mars.nasa.gov/mro/mission/instruments/electra/` [cited: 22 May 2017]

- **Bolometer**: As for the lander, during travel, the radiation levels should be monitored. To save power, the bolometer will be turned off in the lander during transfer, hence the second sensor.
- **Detachment camera**: Although sensors could confirm decoupling, a visual confirmation is required for redundancy and safety. Installing a camera like the Visual Monitoring Camera by the European Space Agency (ESA) would be ideal in this case[5]. Note that this camera should not be seen as the sole confirmation, but a visual guidance whenever odd readings indicate an incorrect separation.
- **Temperature sensors**: In deep space and with an engine turned on, a lot of variation in temperature can occur. Bringing temperature sensors is vital to make sure that all critical values are monitored[6].

2.5 Hardware Diagram

The hardware diagram illustrates the components the PICARD consists of and its top-level interactions. The diagram is shown in Figure 2.6. The top of the diagram shows the four major components of the PICARD: the transportation tug, fairing, lander and habitat. Note that the ground segment DSN is included as well. Below, the transportation tug and lander components are broken down. It shows the power, propulsion, ADCS, structures, communications, on-board computers and scientific instruments. Furthermore, some relations are added which are not discussed in the separate diagrams discussed below. The first one is the pointing accuracy, coming from the ADCS-subsystem, required to communicate. The second point continues on the first one, as the antennas are pointed to communicate with Earth. The third point concerns the tanks in the lander. The ADCS and propulsion subsystems share the same tanks. The last interface is related to power, as the batteries for the lander are charged by the solar arrays of the tug, before the lander is separated from the tug. Note that more detailed diagrams are included in this report:

- **Fuel block diagrams**: Figure 5.18 and Figure 5.19 (Propulsion), Figure 5.22 (ADCS).
- **Communication flow diagram**: Figure 5.28.
- **Data handling diagram**: Figure 5.31 and Figure 5.32.
- **Electrical block diagram**: Figure 5.33 and Figure 5.37.

[5]URL `http://blogs.esa.int/vmc/faq/` [cited: 22 May 2017]
[6]URL `http://www.msss.com/mars/mars9x/penetratorpayload.html` [cited: 22 May 2017]

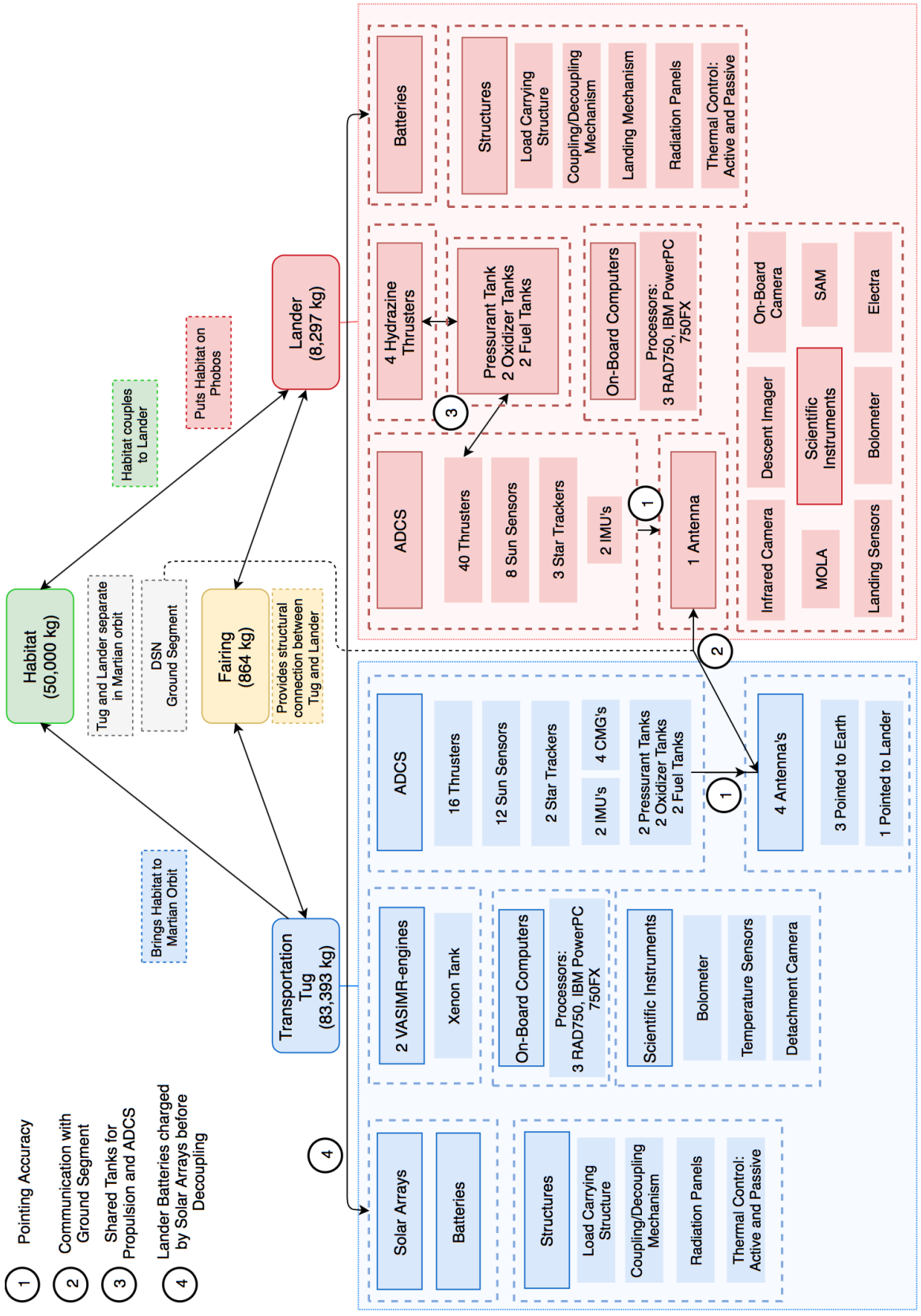

Figure 2.6: Hardware diagram.

[THIS PAGE WAS INTENTIONALLY LEFT BLANK]

Chapter 3 Mission Phases

The spacecraft will have to perform multiple operations to make the mission a success. In this chapter, the mission phases and the associated operations are discussed. These operations show how the subsystems work together to perform the mission. The Functional Flow Diagram (FFD) and the Functional Breakdown Structure (FBS) give a visual representation of these operations. They can be found in Appendix C. There are eight mission phases, from launch until EOL, which are discussed in section 3.1 through section 3.8.

3.1 Launch

The first part of the mission is to get the tug and lander into space. This is done by the SLS Block II which can be loaded with a payload mass of 50 tonnes while being able to reach a trans-lunar trajectory. Unfortunately, the spacecraft is heavier than that. Therefore, the spacecraft is launched by two launchers. Methods for achieving this are further elaborated on in section 5.2.

The payload fairing has a diameter of 8.3 m while having a height of 25 m [11]. The spacecraft was designed to fit into this fairing. The external components such as the solar panels and the antennas are folded and strapped tightly to the spacecraft to minimise vibrations. The solar panels are folded according to the ROSA-method[1]. The spacecraft itself will be structurally supported inside the SLS to also minimise vibrations and lateral loads.

The spacecraft is launched from Cape Canaveral, enabling the use of the SLS launcher. This is further discussed in section 6.2.

3.2 Rendez-vous with Habitat

As explained in section 3.1, the transportation tug and lander are launched separately using two launchers. Due to this choice, assembly in space is required. The exact assembly method is still to be determined.

After the assembly of the lander and tug, the habitat needs to be docked to the lander. It was proven feasible for the habitat to launch to the same delivery orbit as the tug and lander, at which docking has to occur, as explained in section 5.2. Docking of tug, lander and habitat is supported by a mechanical coupling system, the Mechanical Support System (MSS), designed in section 5.1. This operation was chosen to be performed with non-deployed Solar Arrays (SA), thus using power from pre-charged batteries. The reason behind this choice is mainly risk related: if a hazard occurs during the docking operation with deployed SAs, these or the habitat may get heavily damaged. Therefore, arrays are deployed immediately after docking.

3.3 Escaping Earth's Sphere of Influence

After launch and docking of the spacecraft (tug and lander) with the habitat, the tug will activate its propulsion system to start a slow continuous increase of orbit radius, shaping the trajectory into a spiral. This trajectory continues until the spacecraft reaches the limit of Earth's Sphere of Influence (SOI) at a radius of about 924,000 km.

Before this altitude is reached, however, a total of 350 to 400 full orbits will be completed. The spacecraft will take approximately 1.4 years to complete this first journey. About nine months of this journey will be spent in the second Van Allen belt around Earth. This does not significantly affect the trajectory, but did require a structural design for extensive radiation protection.

3.4 Transfer to Mars

After escaping Earth's SOI, the longest part of the mission begins: the interplanetary trajectory. The journey from Earth to Mars will take 1.78 Earth years in which it will make 1.29 spirals around the Sun. The engines are shut off before reaching the target orbit around Mars to make the entry velocity lower for an easier insertion.

After entry into Mars SOI is achieved, arrival at a capture orbit with 10,000 km radius is the next step. For this purpose, another low-thrust trajectory is performed by the spacecraft. This time the

[1] URL `https://www.nasa.gov/mission_pages/station/research/experiments/2139.html` [cited 22 June 2017]

spiral is heading towards a lower Martian orbit. The trajectory takes 0.532 years, and it is also the last fuel intensive phase of the total trajectory, requiring 4 tonnes of fuel, meaning the tug burns most of its remaining fuel.

3.5 Separation of Tug & Lander

The same coupling mechanism as discussed in section 3.3, the MSS, is used to decouple the transportation tug from the lander with the habitat. This decoupling happens when the capture orbit is reached, after which both spacecraft go their own way. However, before separation the tug's solar arrays must charge the lander's batteries. This operation is performed at this stage to prevent battery discharge during the travel to Mars.

Once separated, the tug travels to the pre-determined graveyard orbit with 9,278 km radius using low-thrust trajectory. This graveyard orbit was chosen based on an optimisation between relay eclipse times and periods of continuous communication. Although the tug could carry the lander to an even lower trajectory, due to this early separation of tug and lander, less fuel is required by the tug to perform its final burn to the graveyard orbit while keeping the lander fuel required relatively low. This is the last active phase for the transportation tug, after which it becomes a relay for the lander's communication.

At the same time, the lander transports the habitat to a lower orbit where it intersects Phobos by using a Hohmann transfer. This Hohmann transfer becomes possible due to the selection of chemical high-thrust engines for this phase.

3.6 Land on Phobos

When the lander arrives in the vicinity of Phobos, the landing procedure must be started. This procedure involves shutting down the main chemical engine and switching to full ADCS attitude and translation control. This is done due to the high accuracy of the ADCS thrusters, while the thrust required is relatively low for this phase. After touchdown, the lander is mechanically anchored and landing is confirmed. The exact landing spot is identified in section 4.1.

3.7 Mission on Phobos

During the lifespan of the lander after touchdown, Phobos must be monitored by scientific instruments included in the lander as scientific payload. The lander is equipped with a small antenna which enables communication with the tug, which in turn relays the signals and data from Martian orbit to Earth. At the same time, the habitat is kept attached to the lander to ensure its survival and maintenance while its condition can be relayed back to Earth through the lander and tug.

3.8 End of Life

Since the tug is no longer required as a relay for the lander at the end of the mission, its disposal was considered. This disposal should be a sustainable solution. This means it shall not pose danger for any future missions, the Martian atmosphere or environment or space environment around Mars (explained in detail in chapter 10). After some analysis it was found that no new orbit was necessary. Keeping the tug on its relay orbit would be the best option, even after relaying has stopped.

The lander itself is left on the surface of Phobos when the mission ends, which is when astronauts arrive on the surface of Phobos. This way no extra systems have to be designed and no dangers are introduced to the environment or other missions by keeping its future position and condition predictable.

Chapter 4 Mission Design

The landing on Phobos and EOL-solution are part of the mission design. For the landing on Phobos (section 4.1) suitable landing sites and a landing procedure were investigated. In section 4.2 multiple EOL strategies were investigated.

4.1 Landing Design

This section considers the landing on Phobos. This is split into the selection of the landing site and the actual landing procedure.

4.1.1 Landing Site

No further information besides the dimensions and mass of the habitat were available, thus no investigation was done into the preferred circumstances for humans residing in the habitat. Instead, four possible landing sites are proposed, of which one could be chosen based on the design of the habitat or other limitations. These landing sites, illustrated in Figure 4.1, mainly differ in expected surface composition and differing levels of sunlight exposure, but other advantages and disadvantages are also presented. The level of sunlight exposure may be considered both as an advantage and a disadvantage, since it allows for visibility, and thus easier surface monitoring, but also requires including radiators in the design, which are more power consuming than heaters [12].

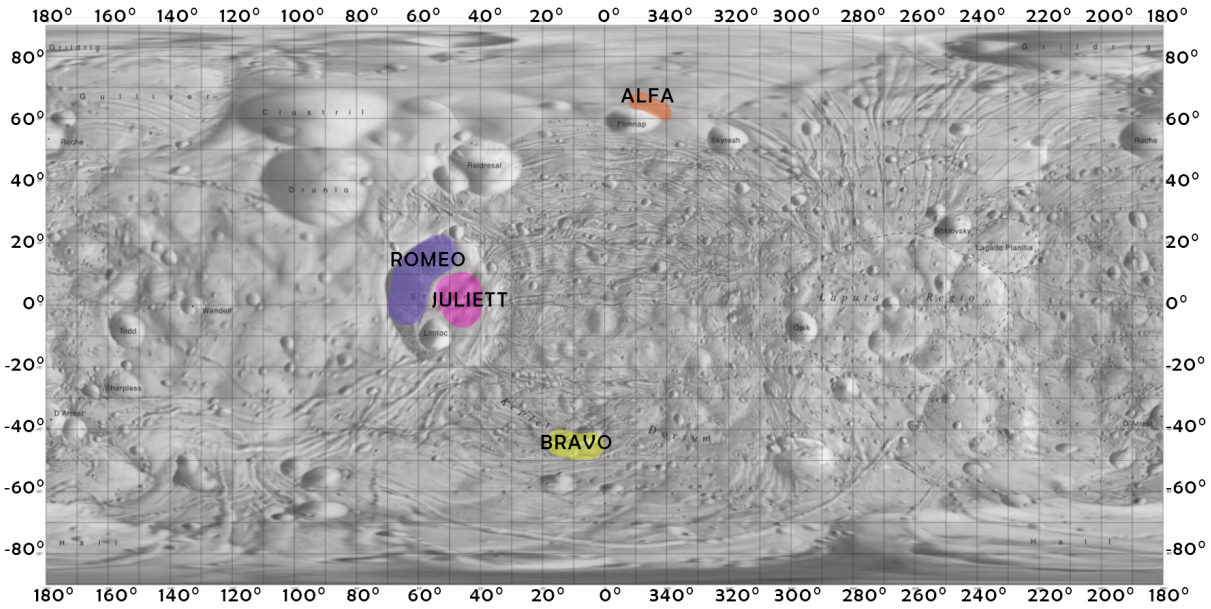

Figure 4.1: Suitable landing sites on Phobos, [2].

Site Alfa
This site is located in the north between 60° and 70° N and between 10° and 20° E, as can be seen in Figure 4.1. It has continuous sunlight during the northern summer, which is from August 10th 2034 until January 1st 2035 [13]. Moreover, it also has a full view of Mars. It can communicate to the relay during the entire orbit of the relay, except when it is eclipsed by Mars. The dust layer at this site is expected to be thicker than the dust layer at sites Romeo and Juliett [14].

Site Bravo
Site Bravo is located closer to the southern pole of Phobos between 40° S and 50° S and between 20° W and 0° E, as can be seen in Figure 4.1. In contrast to site Alfa, site Bravo has continuous sunlight during the southern summer which is from September 22nd 2033 until December 21st 2033 (90 days) [13]. Similar to the Alfa landing site, site Bravo also has full view of Mars. However, the dust layer thickness is expected to be higher than the dust layer of the Romeo and Juliett sites [14].

Site Juliett
Site Juliett is located on the east side of Stickney. Stickney is the largest crater on the Phobian surface

and located between 20° N and 20° S and between 70° W and 30° W, as can be seen in Figure 4.1. The location is Mars centred and there is no continuous sunlight in contrast to site Alfa and Bravo [13]. The advantage of a landing site within Stickney is the size of the dust layer which is expected to be significantly lower than the dust layer surrounding Stickney. A more specific advantage of the Juliett site is that it is located outside the landslide zone of the crater and the site can be advantageous as it consists of so called "red" and "blue" materials which are interesting to investigate for scientific purpose, as can be seen in Figure 4.2[1] [15]. However, the disadvantage is that there is no full view of Mars [13].

Site Romeo
Similar to the previous site, this landing spot is located in the Stickney crater as well, but more to the West side between 5° S and 15° N and between 55° W and 65°, W as can be seen in Figure 4.1. Contrary to site Juliett, it does have a full view of Mars and the orbit of the relay. On the other hand, it has similar sunlight conditions to the Juliett site. Romeo also has the same advantage as Juliett of having a thinner dust layer compared to Alfa and Bravo. The biggest risk of site Romeo concerns landslides that may occur at this location [15]. These could displace or cover the habitat, or even roll it over, although it is not known how frequent their occurrence is. This site does have the same scientific value as Juliett, because it lies near another intersection of three different types of soil [15]. The small dust layer and good communication time makes this site preferred over other sites for the lander. The habitat designers may still choose another site though if they consider other aspects more important.

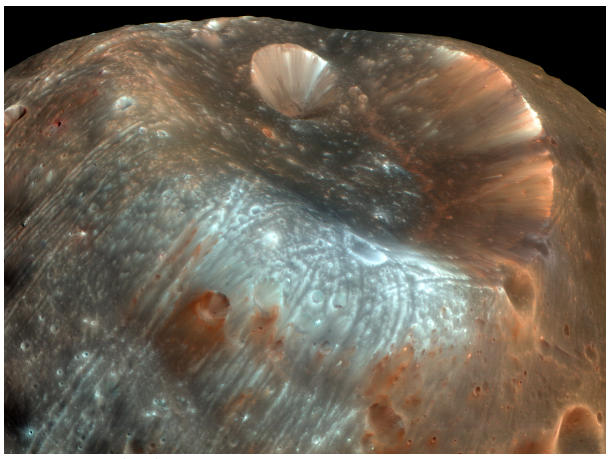

Figure 4.2: Image from NASA showing 'blue' and 'red' material near crater Stickney[1].

4.1.2 Landing Procedure

The final landing site must be selected before the habitat arrives at Phobos. This can be done based on more detailed flybys of satellites already orbiting Mars or a new mission that explores the preferred landing site. The Hohmann transfer to Phobos will bring the lander to a point of approximately two kilometres above the landing site, which is the starting point of the landing procedure.

Upon arrival at the starting point, the spacecraft will rotate to a nadir attitude and check its altitude. It will then start its descent and record the surface conditions during this descent. This recording includes radar sensing and optical imagery during the descent. As it comes closer to the surface, it will be able to more accurately determine the ideal landing location within the indicated landing spots and correct its course towards that point.

During the descent and landing, it will consider three parameters for finding this ideal landing location, which are the slope of the surface, the flatness of the surface and the size of irregularities such as rocks and debris at the landing site. The slope is important for the stability, because it may cause landslides or the spacecraft may not be able to attain a stable position. The flatness and irregularities are considered to ensure that the entire structure is resting on the landing struts while keeping a separation between the habitat edges and the surface. This consideration also includes the requirement for the habitat to remain accessible for astronauts once they arrive.

[1] URL `https://apod.nasa.gov/apod/ap130118.html` [cited: 2 June 2017]

Once the lander closes in at the landing spot, it will perform a soft landing onto the surface of Phobos. This would induce a high load on the landing struts and load bearing structure of the lander. The landing struts consist of a four-legged landing gear, allowing for the required damping during touch-down. Synchronous with touch-down, downward-thrust is generated by the ADCS-thrusters to prevent bouncing back from the surface of Phobos. Firing a harpoon will anchor the lander and habitat to Phobos' surface. Screws in the feet of the landing gear provide additional anchoring.

To enable a soft landing at a safe spot, specific instruments were chosen to detect the altitude and surface during the descent to Phobos.

- **Optical camera**: An optical camera enables surface position recognition, when comparing captured images with known maps of Phobos' surface. This allows to pinpoint positioning and landing trajectory adjustments.
- **Laser altimeter**: By using laser pulses the altitude of the lander can be determined accurately. These pulses are shot with a certain frequency and are reflected back to the lander by the surface. From this reflection the altitude and the approach speed can be determined.
- **Radar**: To ensure a safe landing spot, a radar will be used in combination with the laser altimeter. Radars are useful to detect small objects like rocks and the slope of the surface. Radar was for example used during the descent of the Curiosity rover[2]. Another option considered for object and surface detection was LIDAR. However, radar was determined to be more suitable as it performs better in cloudy conditions which could arise by the upsweep of dust when approaching the surface of Phobos.

4.2 End of Life Design

After the mission is completed, the tug and lander will not suddenly cease to exist. What is planned to do with them at that point is discussed in this section. First, the EOL-strategy for the tug is discussed followed by the EOL-strategy for the lander.

4.2.1 Tug End of Life Strategy

It was decided that the tug would be used as a communication relay, after separation of the tug and lander. This saves weight on the lander, since a smaller transmitter and less power for transmission are required [1]. This also maximises utilisation of the tug, which will be in an orbit around Mars regardless.

At the end of the mission, when the lander goes out of service, the tug is no longer required as a relay. For this reason its disposal was considered. Four options were found for the EOL-solution of the tug. With every option, the tug will be put into standby or passive mode after transfer:

- Move to a lower orbit, let it decay and crash into Mars. This must take more than 50 years to adhere to the Committee on Space Research (COSPAR) regulations.
- Keep it in the relay orbit.
- Move into a higher orbit and crash it into Phobos.
- Move into a higher orbit beyond Phobos and leave it there.

Eventually the second option was chosen as this is by far the the easiest to perform. This strategy will not contradict the COSPAR regulations or cause much space debris, since the spacecraft is kept in one piece while avoiding collision with other celestial objects.

The altitude of this orbit above Martian surface and atmosphere, combined with the almost negligible effect of Phobos on the tug's trajectory ensure an orbital decay rate close to zero. This way the tug will remain in its relay orbit for a relatively long period, potentially remaining available for reuse as transportation tug or as a communication relay for future missions. With both of these options kept open, sustainability of the disposal of the transportation tug is ensured.

[2]URL `https://mars.jpl.nasa.gov/msl/news/index.cfm?FuseAction=ShowNews&NewsID=1005` [cited: 2 June 2017]

4.2.2 Lander End of Life Strategy

The lander will be left on the surface of Phobos. It is not convenient and does not add value to the sustainability of the mission to put the lander into a graveyard orbit or to remove it from its landing spot. Leaving the lander on the Phobian surface does not contradict the COSPAR regulations as no contamination occurs to a target body that could host Earth-life [16]. Phobos will only be inhabited temporarily and leaving the lander in its current position will not endanger any future human missions.

Chapter 5 PICARD Detailed Design

To fully design the spacecraft, the subsystems were designed separately from each other, while still keeping track on the way in which they interact. This chapter discusses these subsystems in the following order: structures in section 5.1, navigation in section 5.2, propulsion in section 5.3, ADCS in section 5.4, communication in section 5.5, C&DH in section 5.6 and power in section 5.7. Results obtained and presented in chapter 2 are obtained through methods explained in this chapter. Designing a complex system is a highly iterative process. For this reason the iterative calculations are repeated several times for all subsystems, while constantly achieving more accurate outputs. The calculations presented here are based on outputs obtained from the second to last iteration, and are thus not equal to the results presented in chapter 2, which includes the final system-level results. The most important of these inputs was a preliminary mass budget, which can be found in Appendix B. Each subsystem has its own verification and validation to verify and validate the design on a subsystem level. The full system verification and validation is performed in chapter 12.

5.1 Structures

The task of the structures subsystem is to house and protect all other subsystems while also enabling performance of mechanical tasks. In the Mid-Term Report [1] the decision was made to have a rectangular structure consisting of struts on each edge to carry the loads. Also the general dimensions were given a first estimate in the Mid-Term Report. In the first section further detailed design of the structure of the complete spacecraft is discussed. Lastly, the subsystem is verified and validated.

5.1.1 Detail Design

This section contains the detail design of the structures subsystem. This includes the supporting structure, but also the coupling and landing system, and the thermal and radiation control.

Launch Loads Sizing

The spacecraft is mechanically loaded during the entire mission. These loads were determined based on the mass budget of a previous estimation as further elaborated in Appendix B. The structure shape, consisting of struts and panels, was designed in a way that it can withstand all loads, and is illustrated in Figure 5.1 as rendered in CATIA [1], [17]. The struts in this structure are all designed with a square cross-section, as to simplify structural analysis.

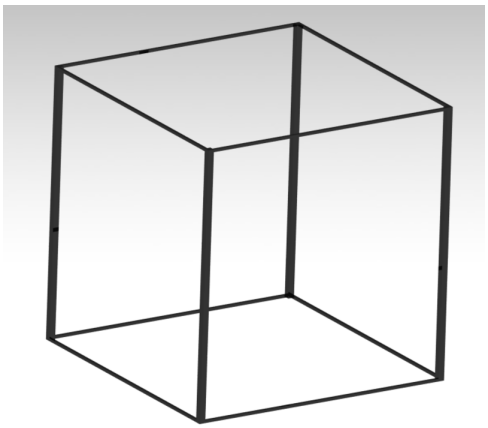

Figure 5.1: Load carrying structure of the tug and lander.

During the entire mission the structure is loaded, but during launch the highest loads are found. Launch loads of 4 g were assumed based on data obtained from the Saturn V. This data was taken since little public information is available as of yet on the performance of the SLS, while the Saturn V is the only launcher that comes close to its size[1] [1]. These loads are driving for the design of the structure, consisting of axial and lateral loads and vibrations. To size the structure, a load and vibrational analysis was performed. For the load analysis the critical buckling force F_{cr} was calculated with Equation 5.1 for the struts and Equation 5.2 for the panels. This was done for the structure of the tug and lander

[1] URL `http://www.braeunig.us/apollo/saturnV.htm` [cited: 21 June 2017]

separately and as a combined structure. The structure was optimised so that it can withstand the compressive launch loads. Because the calculations are still preliminary, a safety factor of two was applied.

$$F_{cr} = \frac{\pi^2 \, E \, I}{L^2} \tag{5.1}$$

$$F_{cr} = A \, \frac{E}{(1-\upsilon)} \left(\frac{t}{w}\right)^2 \tag{5.2}$$

For the calculations the struts and panels were analysed separately. Here I is the area moment of inertia and is calculated for the struts with Equation 5.3. The E-modulus for the aluminium struts and the panels are 68 and 71 GPa, respectively. The different critical buckling loads are then combined to give a thickness of the struts and panels. Note the struts carry most of the stresses, while the panels are mostly used for radiation protection, which will be discussed later.

$$I = I_{xx} = I_{yy} = 4 \left[\frac{t_{struts}^4}{12} + t_{struts}^2 \left(\frac{w}{2}\right)^2 \right] \tag{5.3}$$

For the tug this optimisation gives an axial strut thickness of 11.5 cm, a lateral strut thickness of 5 cm and a panel thickness of 4 mm. For the lander this gives an axial and lateral strut thickness of 3.1 cm and a panel thickness of 4 mm. These panels are not fully made of aluminium but from a different combination of material, including lead. This second material is not used to carry any loads for easier calculations. These panels will be discussed later in the radiation and material section.

The fairing is assumed not to carry the high launch loads, but is loaded in transfer. This is due to the fact that the lander and tug will be launched separately. Therefore it was chosen to only use panels for the fairing since these carry loads and protect the engines from radiation and debris. Struts to carry high loads are not necessary.

After the initial sizing, the natural frequency of the structure was calculated. The natural frequency of the structure should be higher than 25 Hz to withstand the vibrations of the launch [12]. Again, the tug and lander are treated both separately and combined. When treated separately Equation 5.4a and Equation 5.4b were used. In these equations the structure was assumed to be a uniform beam for simplification. Here m_B is the mass of this uniform beam. A full structure with all its components is too complex to analyse vibration-wise without having a full working program with all data.

$$f_{nat} = 0.560 \sqrt{\frac{EI}{m_B L^3}} \tag{5.4a}$$

$$f_{nat} = 0.250 \sqrt{\frac{AE}{m_B L}} \tag{5.4b}$$

When considering the tug, the lander can be seen as payload or additional mass on top of the structure. To take this into consideration, Equation 5.5a and Equation 5.5b are used. Again m_B is the mass of the beam and m is the mass of the lander.

$$f_{nat} = 0.276 \sqrt{\frac{EI}{mL^3 + 0.236 m_B L^3}} \tag{5.5a}$$

$$f_{nat} = 0.160 \sqrt{\frac{AE}{mL + 0.333 m_B L}} \tag{5.5b}$$

The natural frequencies of the tug and lander can be found in Table 5.1. The natural frequency in all directions is higher than 25 Hz and thus passes the vibrational analysis without any extra structural components. The large deviations between the tug and the lander is because of the enormous mass difference. Further vibrations such as acoustic vibrations during launch and shock analysis during decoupling should be further analysed in a later stage.

Table 5.1: Natural frequency of the structure.

Components	f_{nat} Lateral [Hz]	f_{nat} Axial [Hz]
Lander	222	3,517
Tug	-	-
Uniform Beam	31	676
Beam + Mass	51	642

Coupling/Decoupling System

The habitat has to be coupled to the lander to travel to Mars, using the Mechanical Support System (MSS) [3]. Once in Martian orbit, the tug separates from the lander and habitat. The same mechanism is used to decouple. The MSS, consisting of three lead screws of 24 cm each, is used as the coupling and decoupling system, as illustrated in Figure 5.2. This MSS was used and proven to work during the Rosetta mission. The same coupling/decoupling system will be used for this mission. However, it is recommended to test the MSS on the PICARD. The MSS is equipped with a push-off device to separate the tug from the lander. It is able to separate with high accuracy and pre-adjustable velocity between 0.05 m/s and 0.52 m/s. In case of failure, an emergency release ejects the lander from the transportation tug by means of a spring. Note that the fairing is placed in between the tug and lander. This means the fairing will be equipped with the MSS as well. The fairing will not separate from the tug when it travels to its disposal/relay orbit, to limit space debris.

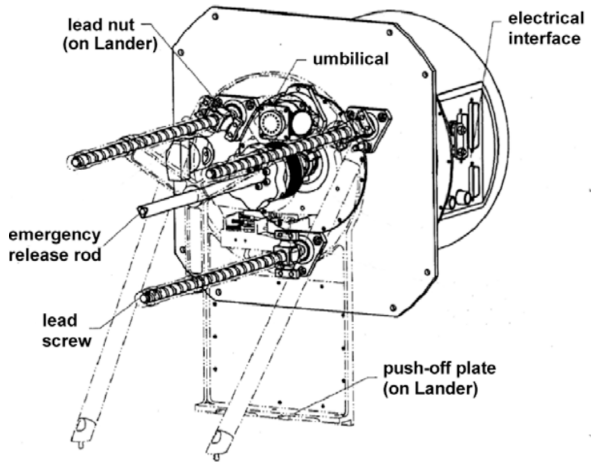

Figure 5.2: The Mechanical Support System as coupling and decoupling system, [3].

Landing Mechanism

An elaborate literature study on landing on microgravity resulted in the Philae landing mechanism as a proper representation for this mission [3]. The Philae lander was required to land on a comet. Therefore, the requirement to land in microgravity is a common one. The Philae landing gear is illustrated in Figure 5.3. The two main aspects of landing on Phobos' surface are to touch down on an appropriate landing spot and to stay on that surface. A tripod landing gear is used to allow touch-down. The tripod is connected to the lander in such a way the lander can rotate to adjust for the surface slope by means of a joint. The landing gear allows for the required damping during touch-down. The damping mechanism is based on a motor that serves as a generator to convert the kinetic impact energy into electrical energy. Moreover, downward thrust is generated by the ADCS-thrusters to prevent bouncing from the surface of Phobos. Firing two harpoons will anchor the lander and habitat to Phobos' surface. The harpoon consists of a projectile, a firing device and a cable re-tensioning mechanism. Once the projectile is fired into the ground, the motor will produce tension in the cable. Therefore, the lander will be tethered to the surface of Phobos. Screws in the feet of the landing gear provide additional anchoring. Note there is one significant difference with the Philae landing mechanism. The landing mechanism of the PICARD landing stage is not a tripod, but consists of four legs. The reasoning behind this decision is

the following. The four propulsion-engines make it challenging to fit a tripod as landing mechanism. Four landing struts are more appropriate as it can be configured better within the fairing, taking into account the positioning of the propulsion-engines.

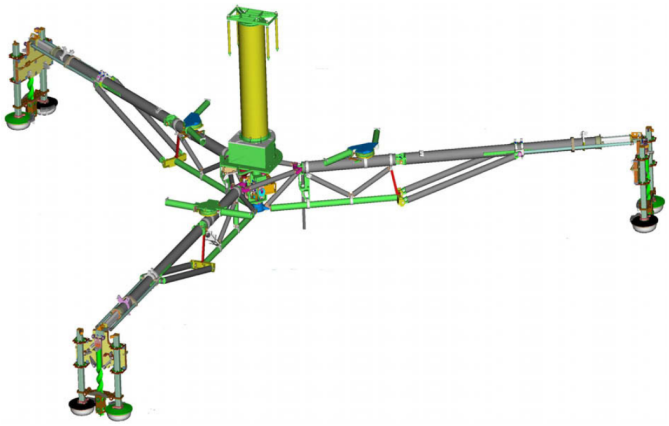

Figure 5.3: The Philae landing gear, [3].

During touch-down, the impact energy is absorbed by using a crushed honeycomb structure, as it was incorporated in Apollo's Lunar Module [18]. This crushed honeycomb develops a uniform level of stress near the optimum response desired to absorb the impact energy [19]. To determine the size of the honeycomb material, the following procedure was used, based on reference material [19]. The touch-down on Phobos was assumed to be a horizontal motion, as landing on microgravity is similar to docking. First, the stopping distance l was determined with Equation 5.6:

$$l = \frac{v^2}{2\,g\,g_{max}} \tag{5.6}$$

Where v is the approach velocity and g_{max} (-) is the ratio of maximum acceleration the object can be subjected to and the gravitational acceleration on Earth (i.e. 4). With confirmation of the ADCS-subsystem, the approach velocity was set to 0.25 m/s considering the soft landing requirement with the possibilities of the ADCS-subsystem and taking into account the increase in stopping distance when the approach velocity increases. This means, the lower the approach velocity the better. However, the performance of the ADCS-thrusters needs to increase when the approach velocity decreases. With the set approach velocity of 0.25 m/s both the stopping distance and ADCS-thrusters performance requirements are taken into account. Furthermore, considering the habitat on top of the landing system, this approach speed should be in the range of 0.05 - 0.3 m/s in order to have a proper settling time of the habitat [20]. This resulted in a stopping distance of 14 cm. Assuming the stopping distance to be 70 % (from [19]) of the total length of the honeycomb core, the total length was found to be 20.3 cm, taking into account a pre-crush of 3.2 mm.

The next step was to choose a suitable material. The reference considered used aluminium honeycomb structures. Therefore, CRIII Aluminium 1/8-5052-8.1 material was decided, trading-off the area necessary to successfully land. This material has a static crush strength of 5.2 MPa [19]. Assuming a five percent crush strength increase for the dynamic crush strength, the dynamic crush strength f_{cr} was found to be 5.46 MPa. This assumption was incorporated based on [19].

The last step in this process was to calculate the required cross-sectional area, based on the chosen material. The area was found with Equation 5.7.

$$\frac{1}{2}\,m\,v^2 = f_{cr}\,A_{cr}\,l \tag{5.7}$$

where m is the mass of 55,100 kg (habitat and lander), v is the approach velocity found before, f_{cr} is the dynamic crush strength of 5.46 MPa, A_{cr} is the crushed impact area and l is the above determined

stopping distance. This resulted in an area of 22.57 cm^2. Assuming a square cross-sectional shape, the width and the thickness were both found to be 4.75 cm.

From what is discussed above, it was found that the landing gear needs to carry 12,324 N, based on the dynamic crush strength and the area found before. Using the aluminium 6061-T6 material (explained in the below material section) and keeping the same cross-sectional area for the landing gear struts, the struts are overdesigned for worst case scenario by considering a safety margin. It was decided to keep the same area for the landing gear struts, to take into account the same safety factor applied to the struts of the tug and lander. Finally, it was checked if these landing gear struts can carry the critical buckling load. Based on Equation 5.1, a critical buckling load of 25.7 kN was found. For this calculation, a length of 3.33 m was found for the landing gear legs. Therefore, it can be concluded that a cross-sectional area of 4.75 cm is sufficient to carry the loads on the landing gear struts. With the dimensions known, the weight of the landing mechanism was found to be 110 kg, including the struts, honeycomb structure and additional elements similar to the Philae landing mechanism.

Thermal Control

The thermal control provides the ability to keep the spacecraft on the right temperature, but what is the right temperature? Each system in the spacecraft has its own operational and survivable temperature. These temperatures can be found in Table 5.2. Some systems are constantly active and need to be operational at all times.

Table 5.2: Operational and survivable temperatures for the different systems.

Temperature [°C]	Operational	Survivable
Coupling Mechanism	0 - +50	
Power		
- Batteries	-20 - +40	0 - +40
- Solar Cells	-150 - +110	-200 - +130
ADCS		
- Reaction Wheels	-10 - +40	-20 - +50
- Star Tracker	-30 - +60	
- Sun Sensor	-25 - +50	
- IMU	-30 - +65	
C&DH & Comm.		
- Board Computer	-10 - +50	
- Antennas	-100 - +100	-120 - +120
Propulsion		
- Hydrazine	+15 - +40	+5 - +50
- Thrusters	+7 - +65	
Maximum Range	+15 - +30	+5 - +40

The first step in designing the spacecraft for thermal control was the analysis of the space environment. The spacecraft is heated by four different aspects: directly by the Sun, the sunlight reflected by the planets (the albedo effect), the heat radiated from the planets themselves and the internal heat of the different instruments of the spacecraft. For this analysis, the temperature of the spacecraft was calculated at different times during the mission. A Python program was written taking into account the distance from the planets and Sun and the orientation of the spacecraft at this point in time [21]. Using Equations 5.8, 5.9 and 5.10 this temperature was calculated.

$$(A_{solar}\ J_s + A_{albedo}\ J_a)\ \alpha + A_{planetary}\ J_p\ \varepsilon + Q = A_{surface}\ \sigma\ T^4\ \varepsilon \tag{5.8}$$

Here A_{solar}, A_{albedo} and $A_{planetary}$ are the areas lit by solar radiation, albedo reflection and planetary radiation, respectively. In this calculation it was assumed that solar radiation intensity of these different radiations J_s, J_a and J_p remain constant.

$$J_a = J_s \, a \, V_f \tag{5.9}$$

$$J_p = 237 \left(\frac{r_{planet}}{r_{orbit}} \right) \tag{5.10}$$

The maximum temperature was calculated, but the spacecraft is not always closest to the Sun or in full sunlight. To calculate temperature differences due to heat flows, Equation 5.11 was used. During this transfer the spacecraft will be in eclipse up to a maximum of 10.14 hours, which makes the core temperature of the spacecraft drop significantly. Therefore heaters are installed on the most temperature sensitive components such as the reaction wheels. The heaters chosen are Radioisotope Heater Units (RHU), they produce 1 W each and have a mass of 40 g [22]. A total of 60 RHUs were chosen from extrapolating reference missions[2].

$$\Delta T = \frac{\dot{Q} \, \Delta t}{m \, C} \tag{5.11}$$

When not in eclipse, one side of the spacecraft is always pointed to the Sun. This side will be heated, requiring a cooling system. This cooling system was chosen to be a radiator which is able to reject heat. The radiators have a heat extraction of 100-350 W/m^2 while having a weight of 12 kg/m^2 [23]. Another system to cool down the spacecraft are louvers, a turning mechanism with panels with a reflective and non reflective side. Placing of louvers on top of the radiator will strengthen the effect up to six times, but are relatively heavy [4]. If louvers are necessary, is still to be determined.

Further difficulties arose when looking at the integration of the different subsystems. Unfortunately, the spacecraft is not isothermal and will therefore not have a constant temperature throughout the spacecraft. Heat conducting from the heated outside panels or internal components travel through the spacecraft heating its surroundings. This is why the placing of the subsystems in the spacecraft is important. In chapter 2 the internal and external layout of the tug and lander are given. The most noticeable parameters for the thermal control are the electronics and the ADCS, which are also temperature sensitive as can be seen in Table 5.2 . This transfer of heat through the spacecraft happens through empty space in the spacecraft but also through conduction and can be calculated with Equation 5.12.

$$\dot{Q} = \frac{\kappa \, A}{l} (T_2 - T_1) \tag{5.12}$$

To have a more isothermal spacecraft, heat pipes are used to distribute the excess heat towards the colder parts of the spacecraft or radiators. The fluid used is ammonia, as it has a low freezing point. This is also used in the International Space Station (ISS) and found to be the most optimum fluid [24].

Lastly, the outer layer of the spacecraft was chosen. Most long term space missions, such as the Mars Reconnaissance Orbiter, use an Multi Layer Insulation (MLI) to cover up most of the spacecraft[3]. The exact material and density of this material is still to be determined.

The differences between the tug and lander are small, in the case of thermal control, since their trajectory is the same. The main difference is the internal heat generated during transfer and after separation. In the tug, the heat generated by the batteries and the constantly active VASIMR engines is significantly higher than the heat generated in the lander. Thus, the tug requires a heavier cooling system. During transfer the lander is inactive and will only activate just before separation. Until that time the heaters and radiator will be powered by the tug.

Radiation Control

To protect the spacecraft against radiation, radiation shielding is applied. During the travel away from Earth, the spacecraft will fly through the outer Van Allen belt for 284 days. In this belt high energy electrons are trapped which harm the spacecraft if not protected for.

Active shielding, such as the creation of an electrostatic field or plasma shields, is under development and needs further investigation [25]. For this reason only passive control is used. Panels with lead

[2]URL `https://solarsystem.nasa.gov/rps/cassini.cfm` [cited: 19 June 2017]
[3]URL: `https://mars.nasa.gov/mro/mission/spacecraft/parts/thermal/` [cited: 23 June 2017]

and aluminium layers were chosen, since this is a recent breakthrough proven to work under harsh environments such as the Van Allen belt[4].

A total panel thickness of 4 mm was determined; alternating 1 mm aluminium and 1 mm lead layers. These panels are also used as a load carrying structure in the previous calculations.

Further radiation investigation is necessary to be able to protect the spacecraft more efficiently. Using the Space Environment Information System (SPENVIS) program from ESA the radiation which the spacecraft has to withstand can be modelled[5]. With this program an effective shielding can also be modelled.

Material

From the Mid-Term Report [1], it was concluded that aluminium is the material to be used for the spacecraft, after a trade-off between aluminium, steel and titanium. After a more elaborate study in this design phase in the sense of doing research into other deep space spacecraft, the alloy of the aluminium material for the struts and plates were decided to be different. For the struts aluminium 6061-T6 was chosen, where aluminium 7075-T73 was chosen for the plates, with their properties explained in Table 5.3. These materials were chosen from a list of most commonly used materials in spacecraft design [26].

Table 5.3: Design properties for aluminium.

Material	Alloy and Form	Mass density, [10^3 kg/m^3]	Tensile Ultimate Strength [10^6 N/m^2]	Tensile Yield Strength [10^6 N/m^2]	Young's Modulus E [10^9 N/m^2]	Elongation [%]	Coefficient of Thermal Expansion [10^{-6}/°C]
Aluminium	6061-T6 Bar	2.71	290	240	68	10	22.9
Aluminium	7075-T73 Sheet	2.80	460	390	71	8	22.1

For the plates, lead and aluminium are used, which is explained in the above radiation control section. Lead has a density of 11,360 kg/m^3 and a Young's modulus of 15 GPa [27]. The yield stress is 14 MPa, where the tensile yield strength is 20 MPa.

5.1.2 Verification & Validation

In this section verification and validation is applied to the model and product for the structures subsystem.

Model Verification

For the calculations an Excel sheet was designed to obtain the stresses and thicknesses. To be able to verify the model a few tests were performed. In the first test the values were calculated by hand in order to check the results. The hand and tool calculations do not differ much. The small differences are due to round-off errors.

The model was further verified by a sanity check where input parameters were changed and checked if the change in output was logical. The driving inputs of the system are the loads and the material characteristics. The results of the sanity check are given in Table 5.4.

Model Validation

To validate this model a CATIA model was build. With this model a load test was performed to check if the structure can withstand the applied loads. As the struts were designed to carry the launch loads, only the struts were analysed. The result of this analysis is shown in Figure 5.4 and Figure 5.5 where the tug and lander struts are illustrated, respectively.

From the analysis in CATIA, it was proven the struts can carry the loads during launch. From Table 5.3, the yield strength is 240 MPa, where the analysis for the landing struts showed a maximum

[4]Based on personal conversation with Dr. A. Menicucci, Assistant Professor at TU Delft
[5]URL: `https://www.spenvis.oma.be/` [cited: 22 June 2017]

Table 5.4: Sanity check of the structure.

Quantity	Change	Expectations	Model
Applied Load	Increase	Thickness increases	True True
Young's modulus	Decrease	P_{cr} decreases f_{nat} Decreases	True True
Approach speed	Increase	l increases	True

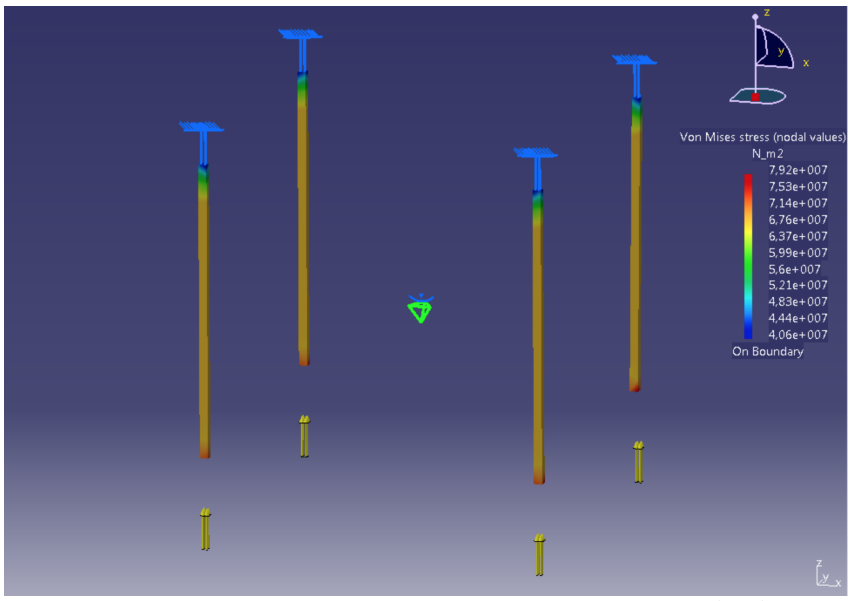

Figure 5.4: Structural analysis of the struts of the tug in CATIA.

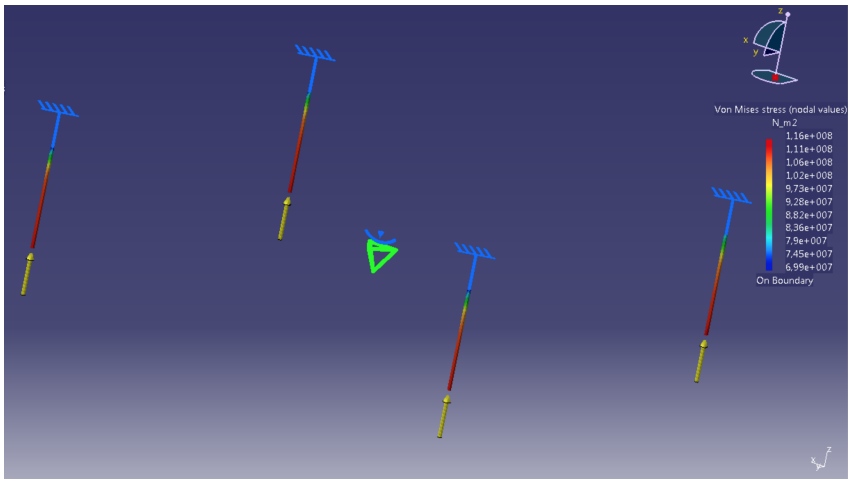

Figure 5.5: Structural analysis of the struts of the lander in CATIA.

stress of 79.2 MPa. Moreover, the maximum stress on the landing struts is 116 MPa. Referring back to the safety margins incorporated during the launch loads sizing, the model can be validated in the sense that the same safety margins were included and thus the structure does not fail during launch.

Product Verification

To verify the full structures subsystem, the compliance matrix, Table D.3 and Table D.4, was used. It can be noted that the temperature and radiation results are still to be determined: MTP-STR-TR02, MTP-STR-TR04, MTP-STR-LA05 and MTP-STR-LA06. All components used in the thermal and radiation control such as radiators and MLI are off-the-shelf and proven to work in space [24]. Though

the components are verified, due to time constraints, a detailed analysis was not performed. Thus it is still to be determined if the requirements are met.

Using the MSS, the tug, lander and habitat are able to couple and decouple: MTP-STR01, MTP-STR02, MTP-STR-LA02, MTP-STR-LA03. As the MSS is off-the-shelf material, there is confidence the component will work for this mission, as demonstrated during the Rosetta mission [28]. However, to prove the MSS will perform its functions on the PICARD, a coupling and decoupling test is necessary.

Furthermore, the lander can dock to Phobos using the harpoons and screws attached to the legs of the landing gear, which are off-the-shelf components as well. Again, an elaborate test has to be performed to gain confidence in the landing phase, with special attention for the anchoring mechanisms. A test that can be performed at the moment is for the landing mechanism, which was based on the Philae landing mechanism. Therefore, the same test facilities can be used [29].

Lastly, it was verified that the tug, lander and landing struts are able to withstand the loads. Based on the calculations performed, the requirements are met: MTP-STR-TR01, MTP-STR-LA01 and MTP-STR-LA04. To verify the structural subsystem, a loading test is required to be performed. Taking all of this into account, the structures subsystem will be verified to be ready to launch.

Product Validation

The best way to validate the structures subsystem is to test the structure with different types of tests. The load carrying structure can be tested by applying loads and vibrations on the tug and the lander, checking for signs of failure. Other tests that need to be performed on the structure is a test for the thermal and radiation control. This can be done by a mission scenario test on Earth by use of a vacuum room and applying radiation and thermal rays. Furthermore, the landing mechanism can be tested with the lander and habitat attached to it. In that way, the complete structural subsystem can be validated to work successfully.

5.2 Navigation

Navigation is one of the biggest elements in designing the PICARD mission. It encompasses two major elements: astrodynamics and orbit determination and control. In the Mid-Term Report [1], several decisions were made on how to tackle navigation. As the tug is equipped with electric propulsion, a low-thrust trajectory will be followed to Mars. From this Martian orbit, the lander will perform a Hohmann transfer to travel to Phobos using chemical propulsion. For the orbit determination and control, it was opted to use a semi-autonomous system, which relies on the DSN and on-board inertial measurement units.

This section is subdivided into two parts. The first one being the detailed design part, which starts with the tools used for calculating the trajectory. This is followed by a chronological breakdown of the travel itself. Eventually, the first part ends with the discussion on the on-board hardware for the orbit determination and control. It should be noted that spacecraft mass inputs used for the detail design are not the ones presented in chapter 2, but are the ones presented in Appendix B. This, due to the iterative nature of the development process as further elaborated on in Appendix B. The second part is dedicated to the verification and validation of all trajectory calculations made.

5.2.1 Detailed Design

Tools Used

In order to solve the problem of finding a suitable satellite trajectory, two auxiliary tools were used. The first tool was a Python program, used to establish estimations for the trajectory. The second tool was a full mission simulator: NASA's General Mission Analysis Tool (GMAT). Final results used by other subsystems are those obtained with the Python tool, due to a thorough understanding of its working, and easy optimisation of parameters. For a more detailed analysis with more accurate results, a deeper understanding of the GMAT tool is required.

Python [21] is an open source programming language used in this case for creating and executing simplified computational analyses. Unlike GMAT, it enables the user to define and consider each problem separately to obtain specific outputs in a sort of problem oriented programming. A benefit of using this

tool is that the user defines the method used for solving each problem and can thus easily keep track of the assumptions and simplifications used, with their consequences on the results. Another benefit is that none of the results are dependent on each other: when one problem solver for e.g. eclipse times returns an erroneous output, a solver for a different problem such as transfer time calculation can still give a correct result. This means that using the Python tool increases robustness of the problem solvers and their answers. A downside is that each problem solver requires additional assumptions and simplifications, as to make computational solving easier or even possible.

GMAT [30] is an open source design tool for space missions, created by NASA. Every few years a new version of this program is released, introducing new features such as electric thrusters or electric propellant tanks. The version employed is GMAT R2016a, one of the first versions which enables electric propulsion[6]. Although GMAT allows for very precise and detailed simulations of full mission trajectories, it is also capable of simulating very simplified trajectories. Simplifications can be made or removed by implementing different levels of irregular gravity fields, solar pressure radiation and third body perturbations. Despite this level of accuracy, GMAT is unable to perform actual calculations (e.g. ΔV calculation for a predetermined trajectory) and is therefore nominally used as a validation tool for previously made calculations. Note that GMAT calculates trajectories in 3D, while the Python program was simplified to 2D calculations.

Launch

Before spacecraft operations can begin, the spacecraft has to be launched first. This is done using the SLS Block II, currently being developed by NASA [11]. Note that the use of the SLS Block II is one of the key requirements, Table D.2. Other options which allowed for similar payload masses had a much lower Technology Readiness Level (TRL) and were thus less suitable for the mission. This choice ensured realism of the mission, while also setting clear constraints on the spacecraft shape. To find the optimal delivery orbit, some analyses were performed.

The first analysis was to investigate the capacity of the chosen launcher. The SLS Block II is capable of launching a 130 tonne spacecraft up to an altitude of 400 km, or to launch a 50 tonne spacecraft to a trans-lunar trajectory [11]. This is interpreted as the SLS Block II being able to launch a 130 tonne payload into a circular 400 km LEO orbit, while the trans-lunar orbit will remain a highly elliptical orbit. It is also assumed that to achieve this trans-lunar orbit, the SLS will bring the payload into a 400 km altitude circular orbit, followed by a raising of the apoapsis to a lunar orbit radius. The periapsis remains unchanged at 400 km. This is a fairly conservative assumption, since the actual apoapsis of a trans-lunar orbit will be more than the lunar orbit radius, thus the launcher will have a higher capacity than the one accounted for. Since little information is publicly available this interpretation is used to determine the available launch delivery orbit.

To find a preferred shape of the delivery orbit also a small analysis was performed. Considering that Mars has a larger orbit radius around the Sun than Earth, more energy has to be added to the spacecraft trajectory when leaving Earth SOI to achieve a successful transfer to Mars [31]. Due to the low, continuous thrust properties of the spacecraft propulsion system, this extra energy will require longer periods of burning to be achieved. This burning can happen either in interplanetary space, but can also already partially happen in Earth SOI. Spending more time in Earth SOI relative to interplanetary transfer is an advantage since it enables less demanding trajectory adjustments as shown in Figure 5.6. The change in trajectory is related to the ratio between start velocity and end velocity, but also to the change in inclination. When these are kept constant, while start velocity is increased (as for interplanetary when compared to manoeuvres in Earth SOI), the ΔV can be found to be much smaller within Earth SOI. Besides this, signal travel time will be less as well. To maximise the energy gain in Earth SOI, a higher energy orbit when leaving Earth SOI is preferred over a lower one.

To achieve this higher energy orbit within Earth SOI, it would mean to achieve an escape orbit with both apoapsis and periapsis being as large as possible and thus being a circular orbit on the edge of the SOI. Since a low-thrust trajectory with continuous thrust was chosen for the spacecraft towards interplanetary space, the delivery orbit by the SLS Block II will also have to be circular to enable achieving this.

[6] URL `https://gmat.gsfc.nasa.gov/` [cited: 12 Jun 2017]

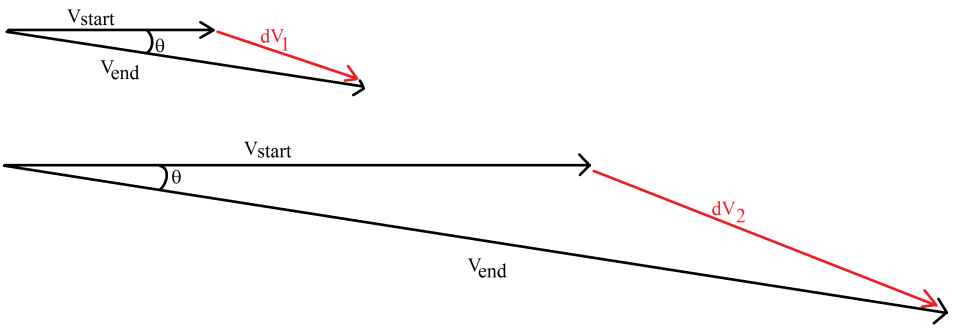

Figure 5.6: ΔV-difference for trajectory corrections based on a different start velocity explained.

The next analysis is performed to find the maximum achievable circular delivery orbit. With the SLS Block II being able to launch a 50 tonne payload from 400 km circular orbit to a trans-lunar elliptical orbit, the ΔV required for this performance can be calculated using equations 5.13 and 5.14. This is found to be 3,085.38 m/s.

$$V = \sqrt{G_c \, m_{centralbody} \, (\frac{2}{r} - \frac{2}{r_a + r_p})} \tag{5.13}$$

$$\Delta V = v_2 - v_1 \tag{5.14}$$

Keeping in mind the need for a circular starting orbit, a maximum circular delivery orbit radius can be calculated, as achievable with the available ΔV from the SLS. This orbit is found to have a radius of 21,102.6 km when transforming Equation 5.13.

The last analysis is made to investigate any benefits of using another delivery orbit within the available range. Originally, a launch delivery orbit similar to that of the ISS was assumed, as given by the project guide for this mission [32]. However, it was found that a higher altitude delivery orbit proves that it could benefit the mission by limiting the exposure of the spacecraft to the inner Van Allen belt. This exposure would be a one time, short duration passing instead of an exposure of multiple orbits while spiralling upwards through the belt. Furthermore it would effectively half the remaining travel time in Earth SOI when compared to the ISS orbit starting point. Travel time reduction occurs due to skipping atmospheric effects such as drag, but also by eliminating the most time intensive part of the low-thrust trajectory: the initial altitude raising phase. Note that travel time estimations are explained further on, while the simulations are explained. Using the same arguments as presented above, the habitat payload (50 tonnes) is most likely also launched by the SLS Block II, and thus it can also be brought up to the higher orbit starting point without further consequences for docking.

Finally the delivery orbit is optimised by taking into consideration the outer Van Allen belt. For this reason the delivery orbit is lowered from the maximum achievable radius of 21,102.6 km to a radius of 19,000 km. This will allow for the, potentially timely, docking procedures to be performed in a less radiation heavy environment, reducing risk of electrical equipment failure and degradation of other systems. This lowering of orbits allows for a small margin in the 50 tonne spacecraft mass restriction put into place by this new delivery orbit.

Note that although the lander (7,807 kg) has a weight margin for launch, the mass of the transportation tug (78,517 kg) is too high to use this higher initial orbit. However, this problem can be solved by launching the tug without fuel (fuel weight = 36,166 kg), and fuelling it in-orbit, which was proven feasible in the past, e.g. through refuelling the Mir space station[7]. Another way to solve this problem would be by launching the tug batteries and/or the solar panels (power subsystem weight = 34,773 kg) with the lander, and assembling them with the tug in-orbit. Beside these solutions, the current design is far from optimised and can thus be expected to lose a lot of its current weight, potentially enabling different ways of getting the tug launch mass under 50 tonnes. An example would be that currently the batteries are required to power the propulsion system even during eclipse times, requiring extreme battery masses. When trajectory becomes optimised these weights can be heavily reduced.

[7]URL `https://history.nasa.gov/SP-4225/mir/mir.htm` [cited: 19 June 2017]

Van Allen Radiation Belts

The Van Allen radiation belts are two semi-toroidal shaped layers of energetic charged particles surrounding Earth. The particles are kept into place by the attractive forces from Earth's magnetic field. Generally, there are two Van Allen belts, an inner and an outer one. These are represented in Figure 5.7. However in reality, the number of belts and their size depends on the amount of solar energy present[8].

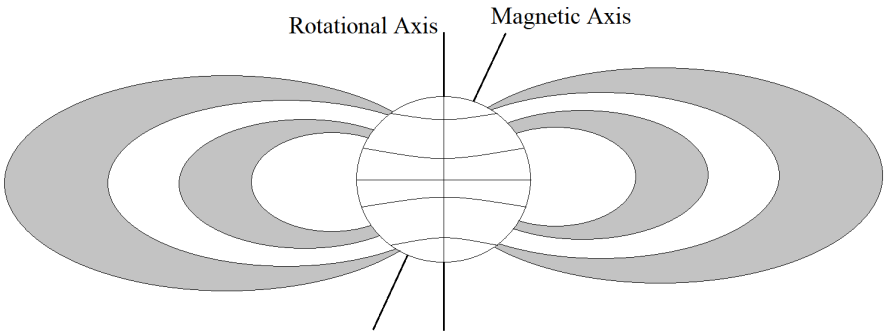

Figure 5.7: A depiction of the Van Allen radiation belts surrounding Earth.

The inner Van Allen belt stretches from 1,000 to 6,000 km above Earth's surface, while the outer radiation belt extends from 13,000 to 60,000 km. The inner and outer belt differ from each other on two levels: in particle composition and in intensity. The inner belt consists mainly of protons, while the outer belt consists of electrons. Furthermore, the outer belt is the most dynamic and therefore most dangerous radiation belt.

As explained before, it was opted to bring the transportation tug and habitat to a radius of 19,000 km, which equals a height of 13,000 km above the Earth's surface. This decision was taken to decrease the travel time and to diminish the time in the Van Allen belts. Leaving at a height of 13,000 km allows the spacecraft to quickly rush through the inner belt with the SLS Launcher, whereafter it only needs to thrust through the outer belt. According to the GMAT program, the spacecraft will travel for exactly 284 days within this outer Van Allen belt.

Fortunately, the radiation belts have no direct influence on the trajectory[9]. Therefore, measures for this radiation are deemed unnecessary from a navigational perspective. However, the travel time through the Van Allen belts was passed on to the structures subsystem for radiation protection.

Escaping Earth Sphere of Influence

Before the transfer from Earth to Mars can start, the spacecraft will first have to escape Earth's SOI. This means the spacecraft will have to achieve an orbit with radius larger than $924{\cdot}10^3$ km. This altitude was determined using equations 5.15 and 5.16. Here r_{SOI} is the radius of Earth's SOI while r_{SE} is the distance between the Sun and Earths SOI.

$$r_{SOI} = r_{SE} \sqrt{\frac{m_{Earth}}{m_{Sun}}} \tag{5.15}$$

$$r_{SOI} = 1\,AU - r_{SE} \tag{5.16}$$

Having determined the launcher delivery orbit and the escape orbit radius, a trajectory can be predicted with given mass and engine properties. Due to the low and continuous thrust available, the trajectory will be spiral shaped. It can be noted that, although the radius is steadily increased, the trajectory at any point in time remains close to circular. What is wanted as output from this segment to be used for other subsystem design is: the travel time, the ΔV required, the fuel burnt, the escape velocity, the number of orbits performed around Earth and solar eclipse times.

[8] URL `https://www.nasa.gov/content/goddard/van-allen-probes-spot-impenetrable-barrier-in-space` [cited: 12 Jun 2017]

[9] Based on personal conversation with Dr. A. Menicucci, Assistant Professor at TU Delft [cited: 19 June 2017]

Eclipse times were estimated as follows. Since Earth orbits the Sun, some of the sunlight will always be blocked by Earth. In a three dimensional environment this space in which sunlight is blocked will be conical: the shadow cone or umbra. Around this shadow cone there will also be an area that receives partial sunlight instead of having full illumination: the half-shadow zone or penumbra. The shadow cone and half-shadow zone are visualised as Figure 5.8.

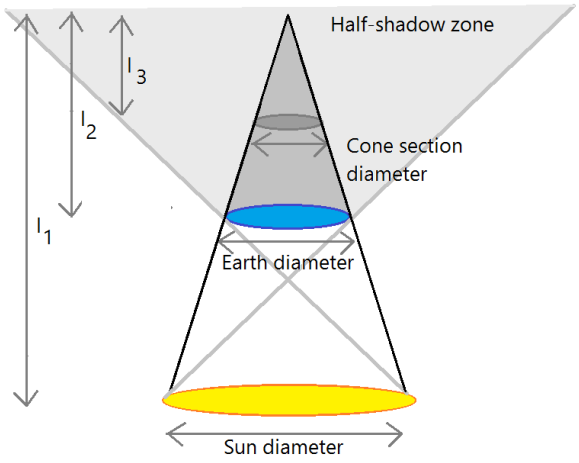

Figure 5.8: Representation of shadowcone.

To find the eclipse period per orbit, one can estimate this by calculating the cone section diameter for the related satellite orbit radius around Earth. Dividing this cone section diameter by the total orbit circumference gives a percentual estimate for distance travelled through the shadow cone. This same percentage applies to the time spent in the shadow cone relative to the total period: the eclipse period. Note that in reality the distance travelled through the shadow cone will not be a straight line, but a curved orbit section. However, if the radius of the orbit considered is large enough this effect can be neglected. The shadow cone diameter as a function of orbit radius can be calculated using equations 5.17 and 5.18.

$$l_2 = \frac{d_{Earth}}{d_{Sun} - d_{Earth}} l_1 \tag{5.17}$$

$$d_{cone}(r) = d_{Earth} \frac{l_2 - r}{l_2} \tag{5.18}$$

Due to the non-linear relation between decreasing cone diameter but decreasing satellite velocity with increasing orbit radius, a maximum eclipse time will occur somewhere during the Earth escape trajectory. Through iteration using the Python tool this maximum eclipse time is found to be 5.07 hours and to occur at an orbit radius of 460,881 km. Note that the time of illumination at this orbit would be 2,450.29 hours per orbit.

However, as shown on Figure 5.8 there is also a half-shadow zone, or penumbra. This penumbra is harder to define due to partial and non-linear illumination effects, and was estimated by simply doubling the eclipse time as a preliminary estimation[10]. The estimated maximum eclipse time including penumbra was thus 10.14 hours.

To perform a first estimate for the other trajectory parameters, a trajectory simulation in Python was deemed the most efficient solution. This was done by giving the spacecraft an initial mass, velocity and position with respect to Earth and combine thrust and gravitational accelerations to linearly integrate total acceleration and velocity over a certain time step as shown in equations 5.19, 5.20 and 5.21 using a Cartesian frame. The equations given show the integration for X-coordinates, but also apply to the Y-coordinates. It should be noted that the central body (e.g. the Sun for interplanetary transfer, or

[10]Based on personal conversation with K. Cowan, Professor at TU Delft

Earth for Earth escape), is assumed to be at the origin of the coordinate system.

$$a_x = \frac{-x}{\sqrt{x^2+y^2}} \frac{G\, m_{centralbody}}{\sqrt{x^2+y^2}} + \frac{F_T}{m_{spacecraft}} \frac{v_x}{\sqrt{v_x^2+v_y^2}} \tag{5.19}$$

$$v_{x_{new}} = v_{x_{old}} + a_x\, dt \tag{5.20}$$

$$x_{new} = x_{old} + v_x\, dt \tag{5.21}$$

This way a new spacecraft position in space can be obtained for every time step. However, since the spacecraft is following a non-linear curved trajectory and to ease the computational load, the time step is made to vary with the angular step. This angular step or $d\theta$ is kept constant on 0.01 rad, so that small angle approximations remain valid. Since increasing altitude will see the spacecraft have a decreasing angular velocity the time step dt of each velocity and orbit radius will not be constant and are found using Equation 5.22. Note that in this equation a small angle approximation was applied for simplicity.

$$dt = d\theta\, \frac{r}{V} \tag{5.22}$$

$$\dot{m} = \frac{F_T}{I_{sp}\, g_0} \tag{5.23}$$

It should be noted that the spacecraft mass is made to vary with fuel used. For this reason a mass flow $\dot{m}$ was obtained through Equation 5.23 and was multiplied per time step to obtain a fuel mass burnt per time step. Finally this step mass is subtracted from the remaining mass.

Some additional assumptions were made to run this simulation. Most importantly, no third-body perturbations were taken into account. Especially effects due to the moon could have consequences on the final trajectory of the spacecraft. However, to take these into account using the relatively primitive Python tool would require extra development time, more complex programming and longer computational times. For these reasons it was deemed out of the scope for these estimations. The second assumption made was that atmospheric effects can be neglected due to the spacecraft's higher starting altitude. In this way there is no need for complex atmospheric models, which would again require extra development time, more complex programming and longer computational times. Another assumption is that all motion is two dimensional. This way the simulation can run with only two vectors for position, velocity and acceleration instead of three, hence decreasing computational time and complexity. This is a valid assumption since inclinations of all celestial bodies considered are very low and thus effects will be negligible [33].

Finally with the method explained and assumptions identified, the simulation is run until the spacecraft orbit radius as shown in Equation 5.24 surpasses the Earth SOI.

$$r_{satellite} = \sqrt{x^2+y^2} \tag{5.24}$$

After running the simulation the wanted outputs can simply be obtained as follows:

- **Travel time**: The sum of all dt.
- $\boldsymbol{\Delta V}$: The sum of all dv, with dv as shown in Equation 5.25.
- **Fuel burnt**: The final mass subtracted from the initial mass, or the sum of all step fuel masses burnt.
- **Number of orbits**: Sum of all $d\theta$ divided by $2\,\pi$.

$$dv = \frac{F_T}{m(t)}\, dt \tag{5.25}$$

These outputs are further compared to a next simulation, described below, and summarised in Table 5.6

The second and therefore final simulation of the Earth escape phase was made in GMAT. This simulation is more accurate than the simulation made in Python, as the environment through which the spacecraft travels is much more realistically represented. For every stage of the mission, two GMAT output sets were calculated. The first set is always the most simplistic one, generated for validation of the Python model. The second set uses the same inputs as the first input, but gives a more realistic trajectory. This simulation incorporates disturbances such as third-body perturbations or atmospheric drag.

In order to enable recreation of the GMAT simulation, a full explanation is provided per phase, showing the set-up of all parameters.

To initialise a new GMAT mission, a few tools need to be programmed first. First of all, a coordinate system with the Earth as origin was established. This coordinate system was called 'EarthMJ2000Eq' and was used as a reference throughout the program. The generated spacecraft in GMAT - equipped with an electric tank, two electric thrusters and a solar power system - was given a Keplerian initial state in the EarthMJ2000Eq coordinate system:

- **Semi-major axis**: 19,371.0 km
- **Eccentricity**: 0.001
- **Inclination**: 0 deg
- **Right ascension of ascending node**: 0 deg
- **Apoapsis**: 0 deg
- **True anomaly**: 0 deg

With starting conditions defined, in order to make GMAT run the program it needs two further inputs: a propagator and a mission sequence. The propagator determines the iterative method used to simulate the trajectory and chooses its accuracy. The mission sequence imposes boundary conditions or an endpoint for the simulation. The boundary conditions are expressed as time, altitude or thrust constraints.

The propagator initialised for this phase is called the 'NearEarth' propagator. This propagator uses a Runge-Kutta integrator for its iterative trajectory determination. Furthermore, the propagator also defined the difference between the simplified and non-simplified GMAT code. The parameters that varied between both simulations are summarised in Table 5.5.

Table 5.5: The difference in propagator between the simplified and non-simplified GMAT simulation.

	Simplified	Non-simplified
Primary Body	Earth	Earth
Gravity Model	JGM-2	JGM-2
Irregularity of Gravity Field	Low	High
Drag	None	JacchiaRoberts Model
Third-Body Perturbations	None	Moon, Sun
Solar Radiation Pressure	No	Yes

The mission sequence defines where the simulation ends. In this phase of the mission, the specific boundary condition was set for the spacecraft to propagate no higher than an altitude of 924,000 km, which equals the end of the Earth's SOI, in a single, finite burn.

To conclude this phase, Table 5.6 displays the most important outcomes of both programs. Note that for the GMAT program, eclipse times were not calculated since the program has not yet been optimised for electric propulsion, causing incompatibilities. Overall, the Python and GMAT simulations resulted in similar output values. It is remarkable how the non-simplified GMAT simulation gives the most efficient trajectory: the lowest ΔV, lowest fuel burnt and lowest transfer time. This despite the influence of solar radiation and third-body perturbations. One reason for this could be a slight gravity assist or pull by the Moon, acting as a gravitational tractor.

Table 5.6: Trajectory parameters for Earth escape.

Data	Python Simulation	GMAT Simulation (simplified)	GMAT Simulation (non-simplified)	Unit
ΔV	3,913.0	3,946.1	3,895.4	m/s
Fuel burnt	10.453	10.387	10.258	tonnes
Transfer time	1.426	1.429	1.412	years
Number of orbits	711	$\pm$700	$\pm$650	orbits
Escape velocity with respect to Earth	724.86	706.67	703.87	m/s

Interplanetary Trajectory

Having achieved Earth escape, next the spacecraft will be travelling through interplanetary space before reaching Mars. This interplanetary phase will most likely be the most time and fuel intensive phase, since solar orbits at the relevant orbit radius have long periods. The wanted outputs from analysis of the trajectory of this phase are again the travel time, the ΔV required, the fuel burnt, the Mars orbit entry velocity and the number of orbits around the Sun before arrival.

Note that during Earth escape also the eclipse times had to be calculated. However, on the transfer orbit scale, any shadow cones created by other celestial objects such as planets or moons were minimal, almost non-existent. For this reason no eclipse times were deemed relevant for this phase and it is assumed the spacecraft always undergoes full illumination.

To estimate the other parameters, as with the Earth escape phase, also here it was deemed possible and necessary to use a simulation of the full trajectory to Mars. The first simulation was performed using the Python tool, a second one again using GMAT.

For the first simulation a number of assumptions were implemented as to shorten development time and computational time. These assumptions also reduce complexity of the program, which decreases risk of obtaining erroneous outputs. All assumptions mentioned for the Earth escape phase apply to this simulation. Besides this, effects due to solar pressure or gravity field irregularities from the Sun are also neglected in this simulation due to their effects being expected to have minimal effect on the overall trajectory of the spacecraft at given altitudes [4].

The starting point of this simulation is a solar orbit with a radius equal to that of Earth's orbit around the Sun. The velocity at that point is the velocity of an object in a circular orbit at that point, plus any excess or escape velocity present during Earth escape. The starting mass of this simulation was the total mass minus the estimated fuel mass burnt during Earth escape.

The end point of the simulation was achieved when the spacecraft achieves a distance from the Sun equal to that of Mars' orbit around the Sun. The velocity at this point, aka the excess velocity, will be translated into orbital velocity when the spacecraft enters Mars' SOI for the next phase of the trajectory. For simplicity it is assumed that the wanted excess velocity should be equal to the velocity of an object in circular orbit around Mars at SOI radius, or 272.67 m/s. This way very little burning should be performed to prevent failed capture, but also some other simplifications can be made during the capture phase simulation as explained further on. It should be noted that in reality the velocity vector of the spacecraft will not be completely aligned with the velocity vector of Mars at capture, thus the excess velocity at Mars capture might deviate. The misalignment angle between the velocity vectors was calculated from the simulation to be 5.52°, meaning a small ΔV correction of 26 m/s is required. For this reason, a small burn should suffice which has very little effect on the overall mission and was thus not further analysed.

To achieve this excess velocity when intersecting Mars' orbit, the trajectory can be deviated slightly from an ideal constant burn spiral. This was done by iterating burn time as opposed to total transfer time. First of all, burning beyond the intersection point of the spacecraft's trajectory will increase the excess velocity at Mars arrival. After engine shutdown the spacecraft will continue its trajectory towards an apoapsis, after which the spacecraft will start returning to a lower orbit altitude until it crosses Martian orbit altitude for the second time. The velocity at this second intersection is dependent on the engine shutdown altitude: the higher the altitude, the higher the velocity will be at intersection due to energy being added to the orbit. This principle is illustrated in Figure 5.9a. The shutdown

altitude is limited mostly by the requirement for the spacecraft shutdown orbit periapsis to be lower than Martian orbit altitude, so that an intersection remains possible. A second limitation is the use of no further engine activations, which might not be the optimal case. The other method for changing the excess velocity at Mars intersection is halting the burn before the spacecraft reaches Martian orbit. This will lower the excess velocity at the intersection point. The same principle as above entails that the spacecraft momentum will ensure a further climbing in orbit radius until intersection with Mars' trajectory. This principle is illustrated in Figure 5.9b. The minimum shutdown altitude is limited mostly by the requirement for the spacecraft shutdown orbit apoapsis to be higher than Martian orbit altitude, so that an intersection remains possible. A more optimal way of varying the excess velocity might be achievable by including multiple burns in the trajectory, however limiting the number of reactivations and shutdowns limits the computational and development time required for this simulation. Besides this it limits the complexity and as such increases its accuracy and robustness. This limitation can be further investigated in later iterations of the development process to find a true optimum.

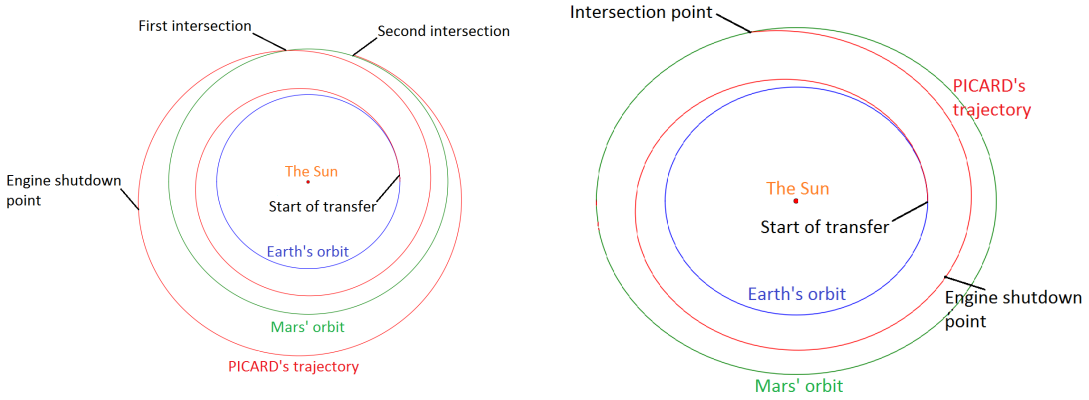

(a) Earth-Mars transfer with two intersections.

(b) Earth-Mars transfer with one intersection.

Figure 5.9: Comparison of two possible transfer trajectories.

Results of this first simulation using Python are found in Table 5.8, where it was found that a transfer with one intersection and pre-intersection engine shutdown is most optimal.

The second simulation for the interplanetary trajectory was made in GMAT. The simulation - as for the Earth escape phase consisting of a simplified and non-simplified trajectory - was based on the same orbital principles as described above. The spacecraft starts from an orbit with the same distance from the Sun as Earth orbit and travels towards an orbit with the same altitude as Mars. The same spacecraft configuration was used for this mission phase as in the escape of the Earth phase, however some variables had to be adjusted. First of all, the initial mass of the spacecraft is its original wet mass minus all consumed fuel up until the interplanetary phase. Secondly, the coordinate system 'SunEcliptic' was created. This is the coordinate system with the Sun as the origin and was used to visualise the interplanetary transfer. As the interplanetary phase follows directly from the escape out of Earth's SOI, the spacecraft position outputs of the first phase were used as inputs for this second phase. The inputs were described as Cartesian coordinates in the SunEcliptic coordinate system.

- **x-coordinate**: -106,028,450.74 km
- **y-coordinate**: -106,443,987.32 km
- **z-coordinate**: 364,174.27 km
- **x-velocity**: 20.04 km/s
- **y-velocity**: -20.80 km/s
- **z-velocity**: 0.11 km/s

Again a propagator was defined. This time the propagator used a Prince-Dormand integrator. A Prince-Dormant integrator is a six-function type of Runge-Kutta integrator and was the recommended

integrator for this phase of the mission[11]. Also for this phase the propagator was used to make a simplified and non-simplified simulation. The differences between these simulations are presented in Table 5.7. Note that the central body for this simulation is the Sun.

Table 5.7: The difference in propagator between the simplified and non-simplified GMAT simulation.

	Simplified	Non-simplified
Primary Body	None	None
Gravity Model	None	None
Irregularity of Gravity Field	None	None
Drag	None	None
Third-Body Perturbations	None	Sun, Luna, Earth, Jupiter, Mars, Neptune, Saturn, Uranus, Venus
Solar Radiation Pressure	None	Yes

The trajectory sequence for the transfer, as explained before, demanded a finite burn from start to a predefined percentage of the travel time. The remainder of the trajectory was covered without thruster burning. The simulation outputs of the Python model and both the GMAT models can be found in Table 5.8. However, in order to find these values, several iterations were performed with the GMAT program due to difficulties in achieving the correct trajectory.

First of all, iterations for the launch window were performed. For some launch windows, the spacecraft - after escaping Earth SOI - dropped to an orbit with smaller radius around the Sun before climbing again and could not reach Mars. For other launch windows, the spacecraft did reach Mars orbit, but only after a significantly longer travel time than the Python model predicted. To solve this problem the Python tool was used to find an optimal launch window for which the spacecraft reached Mars orbit in less than three revolutions around the Sun.

This launch window iteration was followed by an iteration on finding the optimal thrusting time as a percentage of the total travel time for optimising the excess velocity, as explained for the Python simulation. From the GMAT iteration it was concluded that the thrusting time should equal 72.16 % of the trajectory. Table 5.8 shows that the simplified and non-simplified GMAT simulations are very much alike. The non-simplified simulation accounts for third-body perturbations and solar radiation pressure, but due to the distance scale in which the transfer happens, these effects are almost negligible. The similarity can also be partially explained due to the limited amount of revolutions of the spacecraft around the Sun. This in contrast to the escape from Earth, where 700 revolutions did show a difference between the simplified and non-simplified simulation.

Although the Python and GMAT model simulate the same environment, the obtained output parameter values differ quite a bit. These differences can be explained by the difference in interpretation: first of all, the initial conditions of both simulations differ slightly. While the Python program assumes the initial location and velocity vector to be aligned with Earth's position and velocity, the GMAT program takes into account the outcome of the Earth escape phase and thus this alignment will not be perfect. This results in a slingshot of PICARD in an orbit with a lower radius than Earth itself. Iterations have been performed to minimise this deviation, but the effect remains visible: it takes the PICARD about 183 days before it reaches an orbit with a higher radius than Earth's orbit around the Sun. This deviation from the wanted trajectory can be seen in Figure 5.10. Note that the Z-axis is always pointing outwards, according to the right-hand-rule, the X-axis is pointing upwards, the Y-axis to the left. The Earth orbit is indicated in green, the Mars orbit in yellow, the trajectory in red.

Secondly, the Python tool assumes planar motion, while GMAT includes also a third dimension to the simulation. The deviations that occur in this z-direction result in a certain amount of ΔV correction, meaning a more demanding transfer for the GMAT simulation. This, since a higher ΔV results in a higher fuel burnt and longer burn times. As the GMAT program has a longer travel time - due to the initial slingshot - the time at engine shutdown is also later. The Python engine shuts down the engines

[11] URL `http://gmat.sourceforge.net/doc/nightly/help.html` [cited: 25 June 2017]

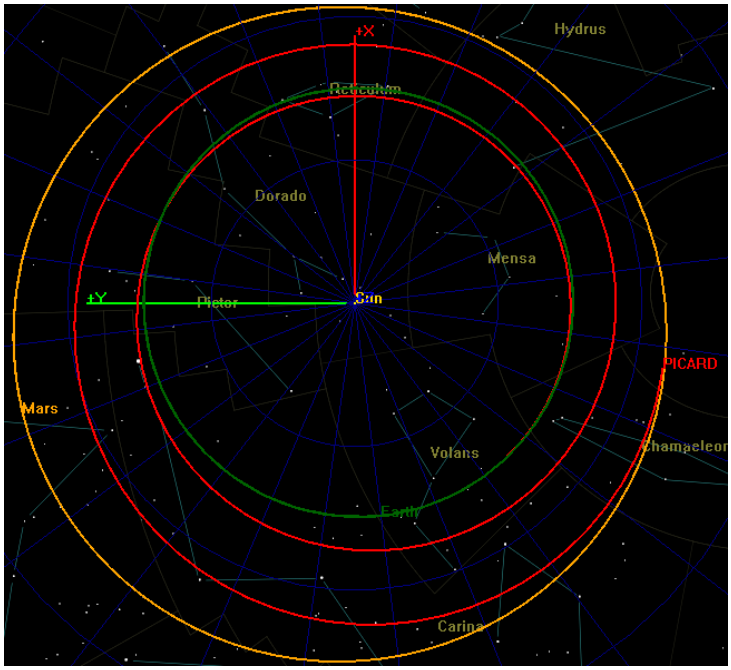

Figure 5.10: Representation of the GMAT trajectory.

at 88.11 % of the trajectory and GMAT at 72.16 %. These percentages differ quite a lot, but can be due to the extra rotations the GMAT simulations makes.

At last, the excess velocities. Both programs aimed at obtaining an excess velocity of about 270 m/s and both succeeded trough several iterations of the full transfer trajectory. Yet, although the GMAT simulation is performed in 3D, end results are translated and interpreted in 2D for simplification. This simplification is necessary for comparison with the Python simulation outputs. At the end of the GMAT interplanetary phase, the PICARD has an out-of-plane deviation of 881,903 km. Since this is less than 0.1 % of the other orbital dimensions, this deviation is neglected. The velocity vector deviation in this direction is also assumed zero, which can cause some differences in actual excess velocity when arriving at Mars.

Table 5.8: Trajectory parameters for Earth-to-Mars transfer.

Data	Python Simulation	GMAT Simulation (simplified)	GMAT Simulation (non-simplified)	Unit
ΔV	4,613.54	8,345.86	8,345.86	m/s
Fuel burnt	11.299	14.458	14.458	tonnes
Transfer time	1.780	2.734	2.734	years
Time at engine shutdown	1.542	1.973	1.973	years
Orbit radius at engine shutdown	1.406	1.524	1.524	AU
Number of orbits	1.290	± 2	± 2	orbits
Excess velocity at intersection	271.6	273.10	272.51	m/s

Mars Capture

The next step in the trajectory of the spacecraft towards Phobos is the capture of the PICARD into a so-called Mars capture orbit. This means going from interplanetary flight into a stable Mars orbit with chosen radius by thrusting retrograde. From this orbit further operations can continue. Wanted outputs from analysis of the trajectory towards the capture orbit are travel time, the ΔV required, the fuel burnt, the number of orbits before arrival and the solar eclipse times.

The chosen capture orbit radius is 10,000 km, being slightly larger than Phobos' orbit radius. Any smaller orbit would require the tug to propel the full spacecraft for a longer duration, needing more fuel before separating and continuing on its own. This, while any smaller capture orbit (while remaining larger than Phobos' orbit) would decrease the fuel required for the lander to perform the landing. Another thing that was kept in mind was the the recurring relative position period of the spacecraft with Phobos, which should be kept relatively small as explained further on. Some iterations between these variables were performed and an optimum was found to be a capture orbit of 10,000 km.

Eclipse times were calculated with the same method as described for the Earth escape phase. The maximum eclipse time, however, was calculated only for the relevant orbit radius range (SOI to 10,000 km orbit radius), and not for the whole sphere of influence. The maximum eclipse times were found to be 5.07 hours.

For the other parameters, the capture problem was split up into two sections: the initial orbit lowering from Mars SOI radius to a 19,000 km radius, and the further decrease to 10,000 km radius. This split up was made due to some practical difficulties in applying the linear integration model with constant thrust to the initial radius lowering stages where the spacecraft velocity is relatively low.

To solve this problem a simplified simulation is performed for the first phase where the ΔV for a low-thrust transfer is roughly estimated by subtracting the circular velocities of the ending orbit with the beginning orbit as shown in Equation 5.26 [34].

$$\Delta V = abs(v_{circular_{start}} - v_{circular_{end}}) \tag{5.26}$$

In this case the starting velocity and end velocity are equal to the velocities of an object in circular orbit at respectively the SOI of Mars and at 19,000 km, and can be calculated using Equation 5.27.

$$r = \frac{G\, m_{Mars}}{V^2} \tag{5.27}$$

With this estimation, a derivation can be made to obtain the transfer time, which for a continuous low-thrust trajectory is equal to the burn time. This derivation is shown in equations 5.28, 5.29, 5.30 and 5.31. The fuel burnt is estimated by multiplying transfer time with mass flow as calculated in Equation 5.23.

$$\Delta V_{total} = \int_{t_{start}}^{t_{burn}} a(t)_{thrust} dt = \int_{t_{start}}^{t_{burn}} \frac{F_T}{m(t)} dt \tag{5.28}$$

$$\Delta V_{total} = -\frac{F_T}{\dot{m}} \left[ln(m_{start} - \dot{m}\, t_{burn}) - ln(m_{start})\right] = -\frac{F_T}{\dot{m}}\, ln(1 - \frac{\dot{m}}{m_{start}}\, t_{burn}) \tag{5.29}$$

$$\frac{-\Delta V_{total}\, \dot{m}}{F_T} = ln(1 - \frac{\dot{m}}{m_{start}}\, t_{burn}) \tag{5.30}$$

$$t_{transfer} = t_{burn} = \frac{m_{start}}{\dot{m}} \left(1 - e^{-\frac{\delta V_{total}\, \dot{m}}{F_T}}\right) \tag{5.31}$$

Results for this estimation are presented in Table 5.9. Note that fuel burnt was obtained by simply multiplying the burn time by the constant fuel mass flow as determined before.

Table 5.9: Trajectory parameters for Mars capture (until 19,000 km).

Data	Estimation	Unit
ΔV	1227	m/s
Fuel burnt	2.768	tonnes
Travel time	0.364	years

For the second phase a simulation was deemed feasible and thus, the two tools, Python and GMAT, were again prepared to simulate this phase of the trajectory.

The first simulation using Python utilises again the already familiar linear integration model. This simulation is used for the same reasons as explained for previous phases, using the same integrational methods as explained in the Earth escape phase. Simplifications used for this simulation are similar to those used for Earth escape: no gravitational perturbances, no third-body perturbances and no

atmospheric effects are taken into account. It is also assumed all trajectories are 2D, meaning inclinations are neglected. This for the same reasons as explained before: reducing overall development time and increasing output reliability. Gravitational perturbances and atmospheric effects are small due to the relatively large distance between the spacecraft orbits and Martian surface. Third body perturbations due to Martian moons are small due to the minimal size of the moons of Mars. Third body perturbations due to other planets and the Sun are small due to the relatively small spacecraft orbit radii around Mars. Inclinations of Earth, Mars and Phobos with respect to each other are also very small and thus planar motion can be assumed [33].

The starting point of the simulation is a spacecraft with a mass equal to the total initial mass minus all burnt fuel as estimated by previous simulations. The initial velocity of the spacecraft is taken equal to the circular velocity of an orbit with radius 19,000 km, which is the end point of the estimation made above.

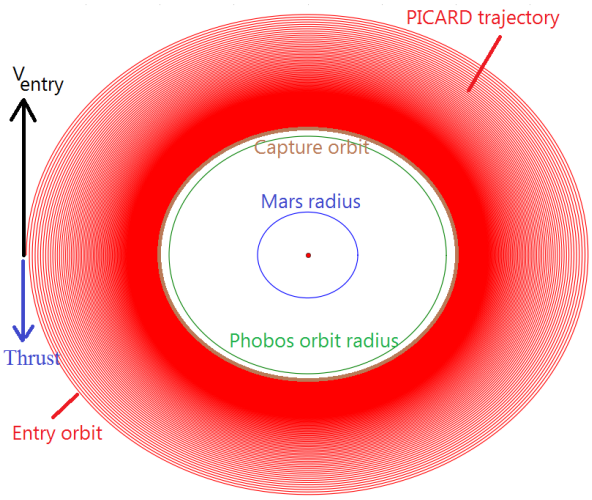

Figure 5.11: Mars capture trajectory explained.

The end point of the simulation is when the spacecraft achieves a circular orbit at the wanted altitude after lowering its orbital radius. This orbital lowering happens in a low-thrust spiral shaped trajectory, similar to the Earth escape trajectory, although this time reversed as illustrated in Figure 5.11. Results for this simulation are presented in Table 5.11.

The same procedure was followed for the GMAT simulation. Note that again only the second part of the entry phase - travelling from 19,000 to 10,000 km - was modelled in GMAT. As the spacecraft starts in an orbit at 19,000 km altitude, it was given an initial velocity of 1,489 m/s, the velocity corresponding to a spacecraft in circular trajectory. The initial mass was set equal to the total wet mass minus all used propellant. The initial conditions were implemented in a Cartesian state in the 'MarsInertial' coordinate system. This coordinate system is a body-inertial coordinate system, using Mars as its origin. In order to implement these start conditions spacecraft inputs were defined as follows.

- **x-coordinate**: 19,034.270 km
- **y-coordinate**: 0.000 km
- **z-coordinate**: 0.000 km
- **x-velocity**: 0.000 km/s
- **y-velocity**: 1.485 km/s
- **z-velocity**: 0.000 km/s

The propagator programmed for the Mars entry was called 'NearMars' and implemented a Prince-Dormand integrator. For both the simplified and non-simplified model the central body is Mars. The used gravity model to represent this central body is Mars-50C, a standardised gravity model for Mars from GMAT. The differences between the simplified and non-simplified simulation can be found summarised in Table 5.10.

Table 5.10: The difference in propagator between the simplified and non-simplified GMAT simulation.

	Simplified	Non-simplified
Primary Body	Mars	Mars
Gravity Model	Mars-50C	Mars-50C
Irregularity of Gravity Field	Low	High
Drag	None	None
Third-Body Perturbations	None	Sun, Phobos
Solar Radiation Pressure	No	Yes

The mission sequence was kept as simple as possible. The initiation of a finite burn was requested, followed by the propagation to an altitude of 10,000 km. The sequence ends with the shutdown of the finite burn. The most important adaptation made for a successful propagation into a Martian orbit was made in the characteristics of the electric thrusters. The origin of their local coordinate system was set to Mars instead of Earth or the Sun. Although their thrust was kept to a value of 11.4N, the sense of the first thrust direction (X-direction) was switched to negative to represent retrograde thrusting.

Table 5.11 displays the results from all simulations. Once again, both GMAT variations lean towards each other. This can be explained by the relative low gravity perturbations at relative altitudes (compared to Earth), Phobos' micro-gravity and the minor influences from the Sun. Outputs from the Python and simplified GMAT simulation are also quite alike. This is the result of the same input values used and two trustworthy programs.

Table 5.11: Trajectory parameters for Mars capture (from 19,000 km).

Data	Python Simulation	GMAT Simulation (simplified)	GMAT Simulation (non-simplified)	Unit
ΔV	567.05	524.46	524.46	m/s
Fuel burnt	1.285	1.136	1.136	tonnes
Transfer time	0.175	0.155	0.155	years
Number of orbits	120	$\pm$ 140	$\pm$ 140	orbits

Lander Transfer

The next phase in the total mission is the decoupling of the transportation tug from the lander and the transportation of the lander to Phobos surface. The decoupling manoeuvre itself is not of importance for overall trajectory design and navigation, but the transfer of the lander with habitat from Mars capture orbit to the surface of Phobos has to be analysed. Wanted outputs from an analysis of this phase are the transfer time and the ΔV required. Since fuel usage has no further effect on other phases of the trajectory this parameter is delegated and further determined by the propulsion subsystem.

As mentioned before the capture orbit with 10,000 km radius was deemed optimal for Mars capture because of its relative closeness to Phobos itself, and as such keeping the required lander propellant for transfer low, while also keeping the recurring relative position period of the spacecraft with Phobos low.

Due to the extremely low gravity of Phobos, a normal landing, using gravity to fall downwards, cannot be performed to reach the surface [33]. In fact, the landing procedure up until the final stages of hovering and touch down can be compared to docking with another satellite in orbit. Since the lander has chemical propellant and engines with relatively high thrust, a Hohmann transfer is a viable option. Because a Hohmann transfer is almost always the most efficient and by far the simplest transfer to analyse, this trajectory is chosen over another low-thrust trajectory [31]. A Hohmann transfer consists of two engine burns, in which the velocity is changed instantaneously (or over a very short period of time) as illustrated in Figure 5.12. The first burn lowers the periapsis of the departure orbit to the target orbit altitude, while the second one lowers the transfer orbit apoapsis from departure orbit altitude to target orbit altitude as to achieve a new circular orbit. Note that the same procedure can be performed in reverse, as to raise the orbit radius instead of lowering it. To find the ΔV, four velocities have to be estimated: the circular velocity at capture orbit (v_1), the velocity at periapsis of the transfer orbit (v_2), the velocity at apoapsis of the transfer orbit (v_3), and the circular velocity at Phobos orbit (v_4). This

can be done using Equation 5.13. The total ΔV of the Hohmann transfer will then be the sum of the two burns as indicated in Equation 5.32. Note that the smaller the difference between departure and target orbit radius, the less ΔV is required, and thus also the less fuel.

$$\Delta V = (v_2 - v_1) + (v_4 - v_3) \tag{5.32}$$

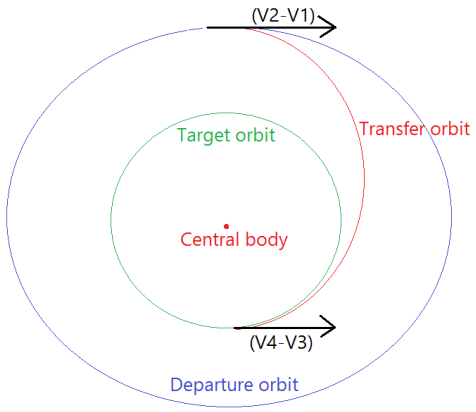

Figure 5.12: Hohmann transfer to Phobos explained.

The reason for not lowering the departure orbit further, although it would mean using less fuel for the landing, is to keep the recurring relative position period between the spacecraft in departure orbit and Phobos low enough. This period determines how long it takes before Phobos and the spacecraft return to one relative position with respect to each other in Martian orbit. This period is determined by the difference in angular velocity between objects considered. The lower this difference, the longer the period, meaning that objects with orbit radii close together will take a long time to return back to the same relative position from each other. This period is important to enable lander transfer to Phobos within reasonable time from arriving at the capture orbit without having to wait unnecessary amounts of times. A short period would also enable skipping a landing opportunity and waiting for the next chance to transfer, decreasing the sensitivity of the landing to the timing of the Mars capture. The recurring position period can be estimated using equations 5.33 and 5.34, here the angular velocity of an object in circular orbit is indicated as ω. In this case object 1 is the object with largest orbital radius or lowest angular velocity, and object 2 has the highest angular velocity. The final Phobos-lander recurring relative position period, with the spacecraft being in an orbit with radius 10,000 km is given in Table 5.12.

$$\omega_{object1}\, t_{recurring} = \omega_{object2}\, t_{recurring} - n\, 360. \tag{5.33}$$

$$n = integer\left(\frac{\omega_{object2}}{\omega_{object1}}\right) \tag{5.34}$$

Results of a simple analytical analysis using formulas described above and implemented in Python are presented in Table 5.12.

Table 5.12: Python trajectory parameters for Phobos landing.

Data	Value	Unit
Travel time	8.043	Hours
Required ΔV	67.51	m/s
Recurring position period	5.787	days

The Hohmann transfer was also programmed in GMAT. As chemical propulsion was used for the Hohmann transfer, GMAT had to be reconfigurated. The lander was created with a chemical tank and chemical thrusters on-board. The initial values were implemented in a Keplerian state in the previously mentioned 'MarsInertial' coordinate system.

- **Semi-major axis**: 10,000.0 km
- **Eccentricity**: 0.001
- **Inclination**: 0 deg
- **Right ascension of ascending node**: 0 deg
- **Apoapsis**: 0 deg
- **True anomaly**: 360 deg

To recreate a Hohmann transfer, two impulsive burns were also generated in GMAT, both operating in the 'MarsInertial' system. Since burning fuel decreases mass, a variable fuel tank mass was also implemented. No new propagators or coordinate systems were initialised.

As GMAT is more accustomed for chemical propulsion trajectories, the Hohmann transfer could be programmed very detailed as a mission sequence. First of all, the lander should propagate to the wanted position in its 10,000 km altitude orbit, after which it performs a Hohmann transfer, followed by a day propagating in the new orbit, the Phobos orbit.

The programming of a Hohmann transfer is much more complicated than programming a low-thrust trajectory. First of all a target must be defined, which in this case was performing a transfer using two impulsive burns. In order to reach this target, several iterations of different parameters were required. As these iterated parameters reach their optimal value, the attaining of the ultimate target becomes closer. The solver used for these iterations is a boundary value solver, which searches for a solution to the iterative problem, while respecting the imposed boundary conditions. It was decided to use the default GMAT settings for this one. The generated solver automatically applies a Newton Raphson algorithm with a forward-difference derivative method to the problem.

In order to reach the overall target of performing a Hohmann transfer, several intermediate steps and targets were defined. The first step is making sure that the magnitude of the first impulse is allowed to vary between a minimum and maximum value. It was decided that the impulse should vary between 0 and π. The allowed perturbation was set to a bare minimum, 0.0001. Next, this ΔV should be applied to perform the actual manoeuvre. As the Hohmann transfer needed to bring the lander to a lower orbit, an impulse in the opposite sense was expected. This was followed by propagating to the periapsis of the new orbit. More details of the periapsis are defined later in an intermediate target, which obeys the program to go to the periapsis of the Phobos orbit. At this periapsis, the second impulsive burn was initiated and was also varied between 0 and π, with a maximum allowed perturbation of 0.0001. This ΔV was then applied in the positive, forward sense. After this step, the second intermediate target should be met: achieving an eccentricity of 0.005, being nearly circular. Using the earlier defined boundary value solver, the transfer converged to a solution. After performing the Hohmann transfer to Phobos orbit, the landing or docking procedures are left up to propulsion, ADCS and C&DH to analyse.

Table 5.13: Python trajectory parameters for Phobos landing.

Data	Value	Unit
Travel time	10.742	hours
Required ΔV	61.50	m/s

Tug Disposal

When lander and transportation tug have separated, also the tug requires another operation: bringing it to a disposal orbit. Together with the C&DH subsystem it was determined the tug could be reused as relay station for communications, so that the lander can be made lighter and thus more efficient.

For disposing the tug into a graveyard orbit, it is preferable to keep it as close to the capture orbit as possible, as to keep the fuel required low. Keeping it far from Martian surface also has other benefits, since the decay rate due to gravitational irregularities and atmospheric drag. The decay rate will become negligible this way[12], keeping the disposal sustainable. An upper limit would be that the tug should remain below Phobos orbit, as to enable easy communication relaying for maximum periods.

[12] URL `https://www.space.com/20346-phobos-moon.html` [cited: 23 June 2017]

This is based on preferred lander positioning on the Martian side of the tidal-locked Phobos. To find a minimum distance between Phobos and the tug, some analyses were performed, showing that anything closer than 100 km to Phobos increases the communication eclipse times, as explained in section 5.5, to an unacceptable level due to the angular velocity of the relay and Phobos becoming too close to each other. For this reason a circular disposal orbit with 9,278 km radius was chosen.

Wanted outputs of the navigational analysis for this stage are ΔV, fuel required and transfer time. Another simulation using Python and the linear integration method explained for the Earth escape is performed.

Starting conditions are the tug mass with remaining fuel, with the tug being in a circular orbit around the capture orbit of 19,000 km.

Ending conditions are when the tug has spiralled down to a disposal orbit with radius 9,278 km.

The same assumptions as for the Mars capture simulation are used for this simulation too. Results from this analysis are presented in Table 5.14.

Table 5.14: Trajectory parameters for tug disposal.

Data	Python Simulation	Unit
ΔV	76	m/s
Fuel burnt	0.082	tonnes
Transfer time	0.011	years
Disposal orbit radius	9,278	km

Launch Date

With all transfer times known, a launch date could be calculated. This date is based on the transfer time to get from Earth departure orbit at 19,000 km radius to Mars SOI, t_{TTM}, Mars and Earth's current angular position relative to each other θ_{now}. Also taken into account is θ_{flown}: the angle flown by the spacecraft around the Sun during t_{TTM}. The relation between these terms is given as Equation 5.35, with the goal of finding t_{wait}. This t_{wait} represents how long a launch will have to wait from today before the trajectory enables the spacecraft to intercept Mars. It should be noted that, due to $t_{recurring}$, the relative position recurrence period between Earth and Mars, more than one possible t_{wait} are possible. However, due to the requirement to have a habitat ready on the surface of Phobos by 2033, t_{wait} is limited to a range corresponding to a maximum $t_{arrival}$ as shown in Equation 5.36. Equation 5.37 finds the possible departure dates based on the previous constraints. In these equations n and m represent integer numbers, used to keep all angles below 360°. Found data and results are presented in Table 5.15.

$$\theta_{flown} - 360\,n = \theta_{now} + \omega_{Mars}\,t_{TTM} - (\omega_{Earth} - \omega_{Mars})\,t_{wait} - 360\,m \tag{5.35}$$

$$t_{arrival} = t_{departure} + t_{transfer} \tag{5.36}$$

$$t_{departure} = t_{now} + t_{wait} \tag{5.37}$$

It should be noted that the data, such as transfer times, presented here is based on the Python simulation tool, since other outputs from this tool were also used as the basis for other subsystems. As to enable sufficient development time for the mission, the last launch date will be the launch date for the mission.

Table 5.15: Launch date results.

Data	Value	Unit
t_{TTM}	3.206	years
Total travel time	3.759	years
$t_{recurrence}$	783	days
Date at first $t_{departure}$	09/01/2018	dd/mm/yyyy
Date at last $t_{departure}$	31/09/2028	dd/mm/yyyy
Phobos arrival date at last $t_{departure}$	04/07/2032	dd/mm/yyyy

Full Trajectory Parameters

With all mission phases analysed and output parameters determined in the form of simulation outputs, a summary of the total mission is presented in Table 5.16. Note that the parameters presented are those obtained through the Python simulations, for the reasons mentioned before.

Table 5.16: Full trajectory simulation results.

	TransportationTug	**Lander Craft**	
Data	Estimation	Estimation	Unit
ΔV	10,396.59	67.51	m/s
Fuel burnt	25.833	-	tonnes
Active Travel time	3.759	0.0009	years
Burn time	3.519	-	years

Hardware

In the Mid-Term Report [1], it was determined that both tug and lander should be equipped with a semi-autonomous navigation system. A semi-autonomous system requires both an on-board and an external component. It was opted to use inertial measurement units and star trackers as the on-board component, and the DSN as the external component. Since these components are integrated in the spacecraft and were designed in consultation with the ADCS and communication subsystem respectively, an elaboration on the separate components can be found in the respective sections.

At last, the Guidance, Navigation & Control (GN&C) computer was designed. It was decided to base this design on NASA's Orion spacecraft. Just as Orion's GN&C computer, an IBM PowerPC 750FX processor chip will be used [35]. This 32-bit processor, running at 900 MHz, has a real memory of four gigabytes [36]. The goal of this GN&C computer is to process the received data from the on-board sensors and the DSN, and to give inputs to the associated effectors and other mechanisms. The GN&C computer is a central system in the spacecraft, which indicates its connection to most of the different subsystems. The GN&C system is connected to avionics, propulsion, structures, docking mechanisms and wiring.

The software of the Orion computer was developed by Honeywell and was further refined by NASA and Lockheed Martin. It is advised to follow the same procedure for software development for this mission [35].

5.2.2 Verification & Validation

To obtain the trajectory simulation and to individually determine some of the required output parameters, physical models were constructed. These models require verification and validation, as to prove the reliability of their outputs.

GMAT Model Verification & Validation

GMAT is a very complicated program. The complexity of the program originates from its rather theoretical approach of the problem compared to Python. GMAT allows its users to initiate iterative methods, however GMAT computes an optimal solution to these on its own. The parameters used as inputs are mostly predefined or already validated and thus require no further verification and validation. Therefore, only GMAT itself needs to be verified and validated. Note that GMAT does allow the implementation of MATLAB modules to enable easier optimisation of trajectories, which would require verification and validation. However, this option was not utilised due to the development time constraint.

In its development phase, GMAT has gone through several verification and validation procedures. These procedures were executed by ten full-time NASA engineers over a period of 18 months. Their verification and validation philosophy can be summarised in "Eat your own dogfood", meaning they used their own product to validate the product itself. A flow chart shows how the verification and validation took place at the highest level. See Figure 5.13 [37].

The engineers tested GMAT for any flaws by performing six types of tests [37]:

- **Numeric tests**: Test both mathematical and physical model by comparing their output to actual data.

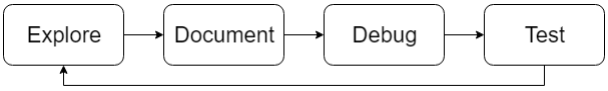

Figure 5.13: The verification and validation flow chart.

- **Functional tests**: Verifies all non-numeric functionality. E.g. plotting styles or file formats.
- **Input validation**: Tests if invalid user input is recognised and if error messages appear correctly.
- **End-to-end tests**: These tests compare the output of a full engineering problem to a real-world solution of the problem. E.g. a lunar transfer or orbital manoeuvre.
- **Stress tests**: Test the system by exploiting and exasperating the system's resources.
- **Edge corner tests**: Test how GMAT behaves near numerical singularities.

Using these tests, six component areas were investigated. First of all the 'Dynamics Models' were verified and validated. The dynamics models encompass the numerical models used for orbit propagation, coordinate system models, epoch representations, celestial body modelling,... Second, the 'Powered Flight' area was examined. This area consists of everything related to impulsive or finite manoeuvring, including tanks and thrusters. Third was the 'Solver Infrastructure', where all algorithms used for boundary value solvers and optimisation solutions were checked. Fourth was the 'Programming Structure'. In this area, the connection between all component areas was verified and validated. This includes user defined variables, the astrodynamic computations, the control flow and the interfaces. Fifth is the 'Output/Utils'. This area must be checked in order to make sure the graphical and data output is legitimate and precise. At last, the sixth component area is 'Application Control', which focuses on user interface [37].

In order to perform these tests, the team required a suitable verification and validation environment. This environment contains the right set of tools, necessary to bring the verification and validation procedures to a good end. The most often used tool was MATLAB. In MATLAB various test environments were created for the GMAT program.

To conclude, the NASA engineers completely verified and validated the models, components and functionality of GMAT. They also resolved critical system defects and updated some specifications. However since GMAT is regularly updated, the verification and validation becomes a continuous process [37].

Python Model Verification

In Python a model was created, consisting of different modules or units, as to obtain the required outputs from the navigation subsystem. These units are a fuel module, a recurring position module, a launch window module, an eclipse time module, and the most complex one: a positioning module. To verify the Python module, first of all unit testing was done as to ensure all units or modules give reliable outputs independently from each other.

The first module, to calculate the fuel used per mission phase, uses a simple fuel used per time step integration. The time step varies as explained in the Earth Escape detail design with Equation 5.22, but the mass flow remains constant, since thrust is kept invariable throughout the burn time as explained with Equation 5.23. The resulting fuel mass per phase was checked with estimates obtained separately by the propulsion subsystem and proved not to deviate above a 10 % difference. Besides this also the robustness of the program was tested by e.g. doubling the thrust, or halving the total burn time and seeing what happens. Results remained within expected and predictable ranges and thus the module was verified.

The second module, the recurring position module was also verified. The methods for calculating this recurring position are explained in the detail design section. When Earth and Mars are used as inputs for the recurring position, a period of 2.16 years was returned as output. This period matches the well known actual value[13], and thus it is assumed the module works correctly. To test its robustness some extreme cases were also tried. First the two orbits were made to coincide, after which the recurring

[13] URL `https://mars.nasa.gov/allaboutmars/nightsky/mars-close-approach/` [cited: 14 June 2017]

position period became almost infinitely large, as would happen in real life. Secondly when one orbit becomes very large and the other very small, the period converges towards zero, also being the expected result. For these reasons the recurring position module was verified.

The next module, the launch window module was next for verification. The value obtained for the found launch opportunities is hard to compare with other references, however the value is expected to be within a certain range. The first available launch opportunity requires a waiting time which cannot be less than zero, and it cannot be more than the recurrence period of Mars and Earth. The found waiting time of 184 days (from starting date 08/06/2017) falls well within this range and is thus a realistic value. To test the extreme cases with this program, the relative angle of Mars with respect to Earth was set to zero and the travel time was set to exactly one Mars orbit period, while setting the angle travelled also to one full orbit. The resulting departure date was found to be zero days, meaning an instant launch would apply. This value matches the expectations, thus proving the robustness of the module.

Another module that requires verification is the eclipse time module. A first check was to compare the eclipse times found for Mars to those found for Earth, which prove to be within the same order of magnitude. This check shows that no large anomalies or variations are present within the outputs. Another check for realism and anomalies is to plot the eclipse time for each orbital radius. The expected curve should be a continuous, smooth line without vertical asymptotes. This curve will not be a straight line due to the non-linear relation between shadow-cone diameter and orbital velocity per orbital radius. The found curve matches these expectations as presented in Figure 5.14. This way also the eclipse time module was verified.

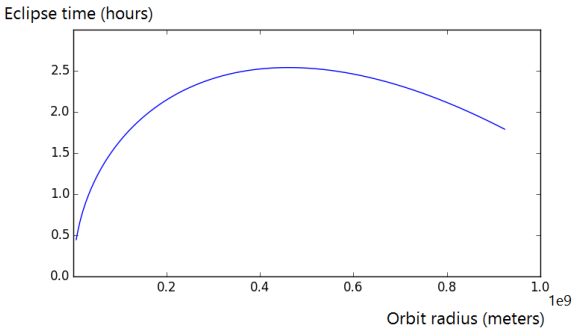

Figure 5.14: Eclipse times over radius for Mars orbit.

The last module requiring verification is the positioning module. This positioning module is the main simulator and finds the ΔV and transfer time per mission phase by simulating all accelerations acting on the spacecraft. The integration method used is explained in the detail design. One way to test the accuracy of the results is to adjust the time step of the integration and see if the results vary much. In this specific case the time step can be decreased by decreasing the angle step, as to test whether results start converging to the same output. The results of this process are shown in Figure 5.15, where each $d\theta$ is presented with its resulting $t_{transfer}$ and ΔV. Actually it can be seen that outputs have minimal deviation and are thus already converging before the first step. This convergence proves the model accuracy is being maximised. Results presented in the detail design are all obtained using an angular step below the convergence limit.

The second test performed on the outputs of the simulation is by comparison with outputs from other estimation methods. One way to estimate the ΔV for a low-thrust transfer is explained in the detail design: by subtracting the circular velocities of the starting with the beginning orbit.

Results from both estimations are presented in Table 5.17 together with results from the simulation. Besides the transfer, differences in ΔV do not exceed 24 m/s, differences in fuel burnt do not exceed 0.091 tonnes and differences in transfer time do not exceed 0.293 years. Considering the scale of the total mission, these differences are relatively small, even with the roughness of the estimation. The transfer from Earth to Mars deviates more than the other estimations, as expected, since not a circular orbit was obtained as final orbit, but the burn was stopped prematurely to obtain excess velocity at Mars orbit as explained in the detail design. When a separate simulation is performed with a spacecraft that stops burning at the first intersection with Mars orbit radius, the difference with the estimation drops below 1%.

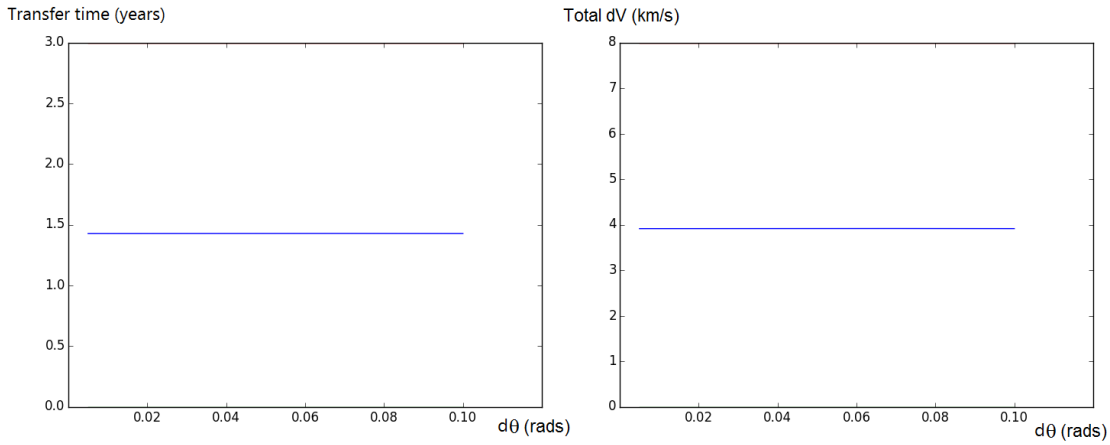

Figure 5.15: Proof of convergence for simulation outputs.

To test the program with extreme inputs, only an extremely small orbital trajectory is considered feasible for testing. A too large trajectory would simply take a huge amount of computational time to simulate. When the target orbit is put equal to the starting orbit, required ΔV and transfer time drop to zero. For the reasons presented above results of the positioning module are also verified.

Table 5.17: Comparison of Python simulation outputs with the estimation method.

	Data	Python Simulation	Estimation Method	Difference
Earth Escape	Fuel burnt (tonnes)	10.452	10.469	0.017
	ΔV required (m/s)	3,912	3,923	11
	Transfer time (years)	1.426	1.133	0.293
Earth-Mars Transfer	Fuel burnt (tonnes)	11.299	13.698	2.399
	ΔV required (m/s)	4,614	5,658	1,044
	Transfer time (years)	1.780	1.605	0.175
Mars Capture: first part	Fuel burnt (tonnes)	-	2.769	-
	ΔV required (m/s)	-	1,227	-
	Transfer time (years)	-	0.364	-
Mars Capture: second part	Fuel burnt (tonnes)	1.285	1.261	24
	ΔV required (m/s)	567	569	2
	Transfer time (years)	0.175	0.170	0.005
Tug Disposal	Fuel burnt (tonnes)	0.082	0.173	0.091
	ΔV required (m/s)	76	79	3
	Transfer time (years)	0.011	0.023	0.012

Python Model Validation

In order assure the validity of the Python model, the output will be compared to the GMAT model output. GMAT is known to be verified and validated extensively, which makes the program ideal to use in a comparison. Since the Python model uses a lot of simplifications - induced by the many assumptions - the simplified GMAT simulation will be used. This validation process took place for all phases in the astrodynamic trajectory. The comparison below always compares the graphical and data output.

The first phase to be compared is the escape out of Earth's SOI. As can be seen in Figure 5.16a and 5.16b, both trajectories are very similar. To see how similar they actually are, the error margin between both will be calculated for several parameters. The formula used to find this error margin can be expressed as Equation 5.38. Note that GMAT is considered to be the 'right' trajectory.

$$Margin[\%] = \frac{|GMAT - Python|}{GMAT} 100 \tag{5.38}$$

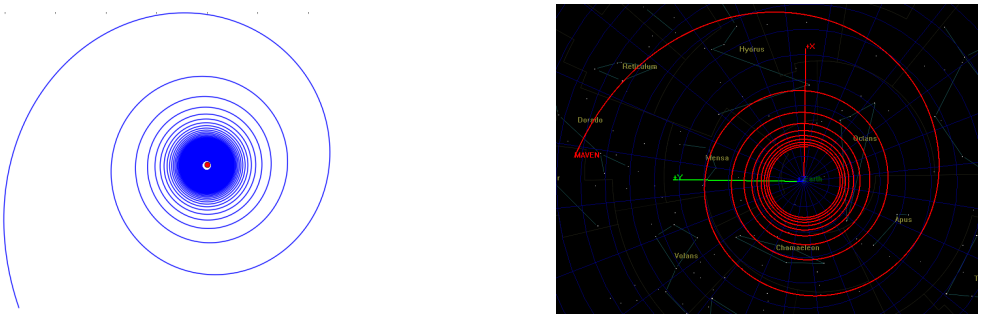

(a) Python simulation for Earth escape. (b) GMAT simulation for Earth escape.

Figure 5.16: Comparison of different simulated trajectories for Earth escape.

The results of the error margin calculations can be found in Table 5.18. It can be concluded that all margins are very small and are well below the maximum error margin of 10%. Thus, the Python simulation for escaping the Earth's SOI is hereby validated.

Table 5.18: Trajectory parameters for Earth escape.

Data	Python Simulation	GMAT Simulation	Unit	Margin [%]
ΔV	3,913.0	3,946.1	m/s	0.84
Fuel burnt	10.453	10.387	tonnes	0.64
Transfer time	1.426	1.429	years	0.2
Number of orbits	496	$\pm$700	orbits	1.57
Escape velocity with respect to Earth	707.74	706.67	m/s	2.57

The second phase of the mission is the interplanetary travel from Earth orbit to Mars orbit. A representation of the Python simulation can be found in Figure 5.9b, the representation for GMAT in Figure 5.10. Both trajectories seem to follow the same layout, however, the Python version looks much more efficient. The GMAT program needs more orbits to reach Mars orbit, and while doing so, first drops the orbits periapsis to a radius smaller than Earth orbit before raising its radius again. From Table 5.19, it can be concluded that the Python and GMAT simulation are far from the same. Most margins exceed the allowed 10%-margin and therefore the Python program cannot be verified with GMAT. As already mentioned in the detailed design of the interplanetary travel, this could be due to the initial values that differ in both simulations. Python assumes the spacecraft is free of any influence of the Earth, while the GMAT program does not. This could be solved by re-iterating the GMAT simulation. A new launch window needs to be found for which the influence of the Earth after escape is positive for the interplanetary trajectory instead of negative. Instead of forcing the PICARD in a lower orbit, Earth should force the PICARD in a higher orbit.

Table 5.19: Trajectory parameters for Earth-to-Mars transfer.

Data	Python Simulation	GMAT Simulation	Unit	Margin [%]
ΔV	4,613.54	8,345.86	m/s	44.72
Fuel burnt	11.299	14.458	tonnes	21.85
Transfer time	1.780	2.734	years	34.89
Time at engine shutdown	1.542	1.973	years	21.84
Orbit radius at engine shutdown	1.406	1.337	AU	5.16
Number of orbits	1.290	$\pm$2	orbits	35.50
Excess velocity at intersection	271.6	273.10	m/s	0.55

The third phase of the mission is the capture into a Martian orbit. As many assumptions were made

in this stage, both simulations are quite simplified. Both were given the same initial values, and it was thus expected to receive the same results. The Python simulation can be found in Figure 5.17a, the GMAT simulation in Figure 5.17b. Although both figures only show some indistinguishable lines, it becomes obvious that both estimations are roughly the same.

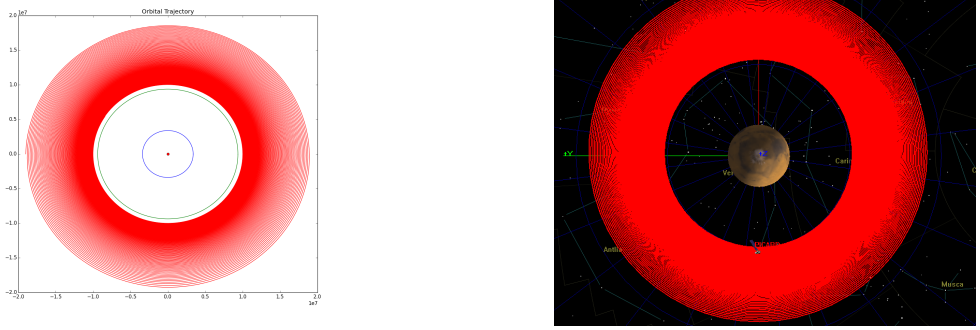

(a) Python simulation for Mars capture. (b) GMAT simulation for Mars capture.

Figure 5.17: Comparison of different simulated trajectories for Mars capture.

Table 5.20 on the other hand displays the more detailed parameters of each simulation. It can be seen that most variations remain around 11%, being slightly above the validation limit. This can be blamed on the roughness of the Python simulations, and is expected to drop with further refinement of the tools used. The only much larger deviation is the number of orbits performed before reaching the wanted orbit radius, but since this is not an output required for other subsystems, this difference will not influence the design significantly. Further investigation in this deviation is required for more detailed analysis.

Table 5.20: Trajectory parameters for Mars capture (from 19,000 km).

Data	Python Simulation	GMAT Simulation	Unit	Margin [%]
ΔV	567.05	524.46	m/s	11.6
Fuel burnt	1.285	1.136	tonnes	7.64
Transfer time	0.175	0.155	years	11.42
Entry orbit radius	19,034.268	19,034.268	km	0
Capture orbit radius	10,000.000	10,000.000	km	0
Number of orbits	114	$\pm$ 140	orbits	22.8

The last phase to be verified is the Hohmann transfer towards Phobos. This low-energy transfer is quite predictable and is therefore expected to deliver the same values for both models. Table 5.21 displays the individual parameters. Although the ΔVs are close to each other, there is a noticeable difference in the transfer time. This might be due to the GMAT program. In order to program this Hohmann transfer, the spacecraft should first propel to the apoapsis of its initial orbit. This propagation takes some time, but is included in the transfer time. The Python program on the other hand does not take this propagation into account, as it assumes the spacecraft is already present in the apoapsis.

Table 5.21: Trajectory parameters for Hohmann transfer.

Data	Python Simulation	GMAT Simulation	Unit	Margin [%]
Required ΔV	63.51	61.50	m/s	9.77
Transfer time	8.043	10.742	hours	25.13

Hardware Verification & Validation

As the GN&C computer of the PICARD is based on NASA's Orion navigation computer, the verification and validation of the latter was investigated. In the development of the Orion, NASA works in close cooperation with its major contractor, Lockheed-Martin. An engineering team, consisting of

both NASA and Lockheed-Martin engineers, was assigned to the complete verification and validation of Orion's GN&C computer. This team was called IGNC, which is short for Integrated GN&C, and was responsible for all verification and validation procedures on all subsystems and all segments of the program. Assuming the IGNC preformed well, the PICARD GN&C computer can also be assumed to be verified and validated.

Requirement Verification

In the end, a product verification check was performed on navigation. This check made sure all requirements imposed on navigation were fulfilled. The compliance matrix, which helps with this verification, can be found in Appendix D. Navigation only had to fulfil a handful of requirements and most of them were quite straightforward. As both tug and lander are equipped with a semi-autonomous navigation system, two requirements are already met. Semi-autonomous systems include an on-board system, which was asked for. The remaining requirements are also fulfilled as the tug is able to transport the complete spacecraft from an Earth orbit to a Mars orbit, and as the lander is able to perform a Hohmann transfer from a Martian orbit to Phobos.

5.3 Propulsion

The propulsion subsystem is divided in two parts, a separate propulsion system for the tug and one for the lander, which will be discussed separately. The first part in designing a propulsion system is the selection of engines, as performed in the Mid-Term Report [1]. After the selection of engines, the accompanying propellant mass, tank volume, tank mass and feed system mass was determined.

It was decided that for the tug VASIMR electric engines are used. The VASIMR engines were to use argon as its propellant. However, in light of new information, using xenon was shown to be the better choice. This is based on three arguments[14]. Firstly using argon as propellant would give a tank mass fraction of more than one, so a tank mass which is actually higher than the propellant mass itself, whereas xenon has a tank mass fraction of approximately 0.1 [38]. Secondly, the maximum yearly world production of xenon was underestimated. At first it was found that the amount of xenon propellant needed for this mission was actually higher than the maximum yearly production and therefore not a feasible option. However, it was later found that the production of xenon could easily be scaled up and is therefore again a feasible choice [39]. Also, xenon provides better overall efficiency for electric propulsion when compared to argon [40]. To provide the required thrust, two VASIMR VF-200 engines are used. They both provide a thrust of 5.7 N, have a specific impulse of 5,000 s and consume 200 kW of power.

For the lander it was initially decided that a liquid bi-propellant engine using Rocket Propellant 1 as fuel and liquid oxygen as oxidiser is the best choice. However, new information showed storing liquid oxygen for long amounts of time (as done in a transfer from Earth to Mars) would lead to heating up and therefore expanding of the oxygen. This would require either an extensive cooling system or very thick tank walls, to account for the higher pressures, both of which result in very high storage tank masses. It was therefore decided that using a Hydrazine + Dinitrogentetroxide (N_2O_4) engine is the better choice. This has the added advantage that the storage tanks for the propulsion system and ADCS can be combined, saving mass. It is however not the sustainable option, as Hydrazine is a toxic substance, but the advantages outweigh the disadvantages. To provide the means to perform the Hohmann transfer from Mars orbit to Phobos, as described in section 5.2, four Aestus engines, each with a thrust level of 29.6 kN and operating at a specific impulse of 324 s, are used. They run on Monomethylhydrazine, a variant of Hydrazine and N_2O_4.

With these important parameters and the required velocity increment, as described in section 5.2, the detailed design of the propulsion system can be performed.

5.3.1 Detailed Design

The detailed design of the propulsion systems encompasses the selection of the feed system and tank materials, and mass and dimension calculations. Firstly general equations applicable to both lander and tug are shown, after which the detailed design is split in two parts.

Equation 5.39 calculates the propellant mass m_p, in which m_d is the dry mass. The propellant volume V_p is generally calculated as shown in Equation 5.40. Equation 5.41 gives the tank radius r_t calculation.

[14] Based on personal conversation with Dr. Angelo Cervone, Assistant Professor at TU Delft

The tank thickness t_t calculation is shown in Equation 5.42. Equation 5.43 calculates the propellant tank mass m_t. In the calculation for the tank wall thickness a factor of safety (FoS) of 2 is taken into account, as found from SMAD [38][4]. Subscript p shows it is a propellant variable, subscript t shows it is a tank variable and σ_y is the yield stress of the material.

$$m_p = m_d(e^{\frac{\Delta V}{I_{sp}\ g_0}} - 1) \tag{5.39}$$

$$V_p = \frac{m_p}{\rho_p} \tag{5.40}$$

$$r_t = \sqrt[3]{\frac{V_p}{\frac{4}{3}\pi}} \tag{5.41}$$

$$t_t = FoS\ \frac{p_{max}\ r_t}{2\sigma_y} \tag{5.42}$$

$$m_t = \frac{4}{3}((r_t + t_t)^3 - r_t^3)\rho_t \tag{5.43}$$

Transportation Tug

With the specific impulse of the VASIMR engines of 5,000 s and a ΔV of 11.2 km/s, as found from the second to last iteration in section 5.2, the required propellant can be calculated. Note that due to the iterative nature of the design, the mass values found in this part are not fully accurate. In future iterations the new ΔV as present in section 5.2 should be used. However, using the second to last values should give some reasonably accurate results for this sizing. Using Equation 5.39, a propellant mass of 28.5 tonnes is found. This mass has to be scaled up taking into account average levels for loading uncertainty, off-nominal performance, off-nominal operations, mission margin or reserve and contingency for unforeseen propellant usage. This adds up to a scaling factor of 1.17, leading to a propellant mass of 33.4 tonnes [38]. This mass however does not take into account residual propellant. To allow for this, the minimum inlet pressure of the VASIMR engines has to be taken into account, which is found from reference electric engines to be 0.7 MPa [41] [42]. Taking this pressure as the pressure at which propellant cannot be retrieved from the tanks, the residual propellant is found to be 0.9 tonnes, giving a final propellant mass of 34.3 tonnes.

Then, from this final propellant mass and the optimal storage pressure of 14.8 MPa, the tank volume, radius, wall thickness and mass are calculated, as shown in Equation 5.40 to Equation 5.43 [43]. The material used for the tank is, as explained for sheet material in section 5.1, again Aluminium 7075-T73. This results in one central tank with $V_p = 25.4\ m^3$, $r_t = 1.82$ m, $t_t = 3.3$ cm and $m_t = 3.9$ tonnes.

The mass of the VASIMR engine can be calculated using Equation 5.44. This equation is based on models created for each individual component of the VASIMR engine, based on commercial and laboratory hardware, detailed designs and parametric modelling [44]. It gives a relationship between the electrical input power P_{VF} and the mass of the engine m_{VF}, as seen in Equation 5.44 [44].

$$m_{VF} = 1.2P_{VF} + 444 \tag{5.44}$$

Using the 200 kW input level, a VASIMR engine mass of 684 kg is found. This is however for the internal parts of the engine only. The VASIMR engines produce a lot of heat. This is mostly dealt with by the plasma being contained in the centre of the core of the engine by the magnetic field, but still a good heat rejection system has to be present. The actual cooling system of the engine is already included in the engine as described in [44], but this also still has to be transported outwards of the spacecraft. This can either be done by separate radiators for the VASIMR engines, or by the entire thermal control system. In future work, this should be investigated more deeply. The engines are placed on a gimbal, adding mass and requiring the feed system to be flexible. Reference data for electric engines show gimbals have an average weight of around 50 % of the thrusters itself [45]. This results in the gimbals having a mass of 342 kg. Besides the tank and engines, also a feed system to connect the two is required. Such feed systems generally have a low mass. Estimations based on reference data place it at 35 kg per engine. An example of a feed system is shown in the tug fuel block diagram in Figure 5.18 [41]. It shows the way in which the feed system could be designed. The actual detailed design is still to be performed in a later stage. Top down it shows the xenon tank, from which the propellant flows through a series of valves, measurement devices and pressure regulators to eventually flow into the two VASIMR engines, where a further separate feed system is present.

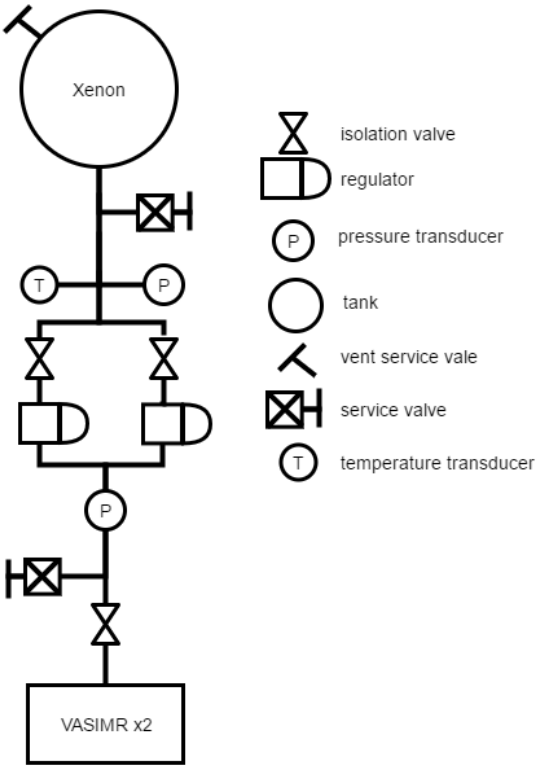

Figure 5.18: Fuel block diagram of the transportation tug.

Lander

Whereas the tug propulsion system just had one central tank, this is not the case for the lander. It instead consists of at least two tanks, as at least two are needed to store the oxidiser and fuel separately. Then, because more oxidiser than fuel is needed, two more tanks are present to provide for a symmetric spacecraft. Because the ADCS also makes use of a MMH + N_2O_4 engine, the storage tanks of both systems are combined. This allows for a simpler and lighter spacecraft.

Firstly, the required propellant for the propulsion system is calculated, using Equation 5.39, where I_{sp} is 324 and ΔV is 67.5 m/s. This results in a propellant mass of 1.1 tonnes. Then, to get the total required propellant, the propellant needed for the ADCS, as explained in section 5.4, is added. Resulting in a total propellant consumption of 2.7 tonnes. This mass has to be scaled up by a factor of 1.19, as opposed to the scaling factor of 1.17 for the xenon tank [38]. The difference with the tug scaling factor derives from the scaling factor now also including residual propellant. This adds up to a combined total propellant mass of 3.2 tonnes. Now, this propellant mass is split up in the fuel and oxidiser, which are again split up in two tanks.

Then, the engines require a feed pressure. The ADCS requires the highest minimum pressure of 2.4 MPa, so the propellant should always be at least at this pressure. It was decided to provide this pressure by means of a pressurant tank, as a relative low amount of propellant is used. This means the scaling benefit of turbopumps do not apply to this system. The actual shape of the full propulsion system is shown in the lander fuel block diagram in Figure 5.19. It again is a way in which the actual feed system may be designed. The actual detailed design is to be performed in a later stage. Top down it shows the helium pressurant tank, from which the required helium pressurant flows to the MMH and N_2O_4 tanks. Then, the actual MMH and N_2O_4 flows from their respective tanks to the four main engines and the 40 ADCS thrusters [46].

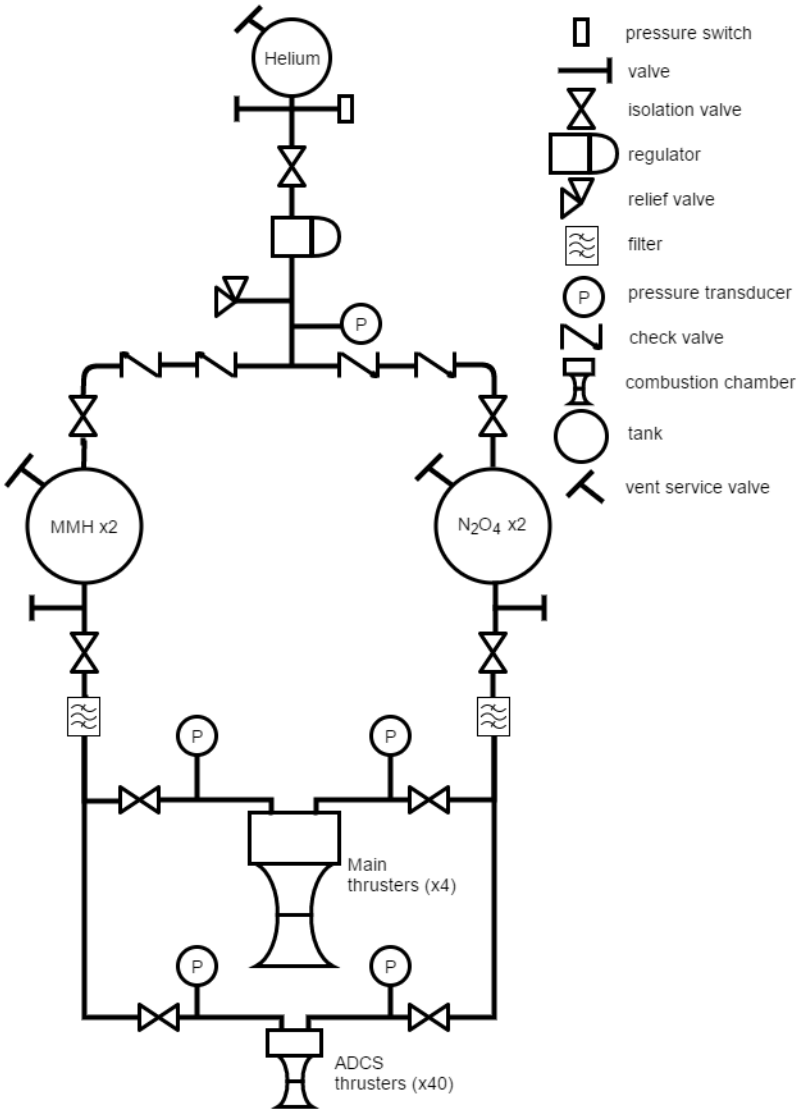

Figure 5.19: Fuel block diagram of the lander.

The pressurant mass is calculated, using Equation 5.45, to be 11.9 kg [4]. BOL is Beginning of Life, EOL is End of Life and subscript pr shows it is used for the pressurant.

$$m_{pr} = \frac{P_{EOL} V_t}{r_{pr} T_{EOL} - \frac{p_{EOL}}{\rho_{BOL}}} \tag{5.45}$$

Then, again using Equation 5.40 to Equation 5.43, the volume, radius, wall thickness and mass of the two oxidiser and fuel tanks and the pressurant tank were calculated and are presented in Table 5.22. For these tanks again Aluminium 7075-T73 is used.

Table 5.22: Values for the volume, radius, wall thickness and mass of the propellant tanks in the lander.

	Oxidiser (N_2O_4)	Fuel (MMH)	Pressurant (He)	Unit
Amount	2	2	1	-
Volume	0.71	0.65	0.31	m^3
Radius	0.55	0.54	0.42	m
Wall thickness	3.2	3.1	2.8	mm
Tank mass	353	322	176	kg

In contrast to the tug, no gimbals were deemed necessary. Since four engines are present, differential thrusting can be applied to provide attitude control and thrust corrections. These engines have an individual mass of 111 kg, resulting in a total engine mass of 444 kg[15]. These engines provide for their own cooling by making use of regenarative cooling. Some MMH flows through the hollow walls of the nozzles, extracting heat, and then flow into the combustion chamber to still react with the N_2O_4 [46].

5.3.2 Verification & Validation

The models to be verified and validated for the propulsion system are the model used to find the required propellant and the model used to find the propellant tank dimensions and mass. After model verification and validation, product verification and validation is discussed. Here, ways to verify individual parts are discussed, being the VASIMR engine, the Aestus engine, the feed systems and the tanks.

Model Verification

The model for calculating the propellant mass was verified by checking compliance with the values obtained from the navigation subsystem design. The propellant mass calculation from the astrodynamic model gives a total tug fuel consumption of 25.9 tonnes, while the propulsion model gives a mass of 28.5 tonnes. This means a deviation of 9.1 %. This is within the 10 % limit, but however is on the high side. First and foremost, the difference can be accounted for by the iterative nature of the design. The propellant mass as found from the navigation model is based on the latest iteration for the velocity increment, whereas the propellant mass from the propulsion model is based on the second to last iteration, which already accounts for a 6.9 % difference. Then, substracting this percentage from the total percentage, only a 2.2 % difference in models is left. This can be explained by two arguments. Firstly, in the navigation model the residual mass is not taken into account in the dry mass, leading to a lower propellant use. Secondly, the navigation model uses discretisation, therefore inherently is not fully accurate. Taking these arguments in account, it can be stated that the propellant calculation model is verified. Then, the model for the propellant tank mass is verified by checking its compliance with the model used for the ADCS tank mass and additional hand calculations. Both models showed the same end results when the same input values are used, therefore these models are verified. These two separate models were constructed because separate systems were required for the propulsion and ADCS, but in hindsight it might have been more efficient to create and verify just one model.

Model Validation

However, while the models are correct, the mass of the lander tanks is not in accordance to average levels. Reference data show an average tank mass as percentage of the propellant mass, or tankage fraction, of less than 10 % for chemical bi-propellants, while it is now at 40 % [38]. With this validation an error in the models used for the calculation of the chemical propellant tanks was identified. In these calculations the BOL pressure of the pressurant tank was used, while in reality a pressure transducer is placed between the propellant and pressurant tanks. This means the pressure on the propellant tanks is lower than used in the models, thus the actual mass of the lander fuel and oxidiser tanks will be lower too. Using this, a tankage fraction of around 4 % is found, which is more in line with reference data. In future iterations this should be taken into account. The tankage fraction for the xenon tank is 11 %, which is in line with reference electric propulsion tanks which have a tankage fraction of 12 % [47].

Product Verification

Then, the actual products are to be verified. The compliance to the requirements as stated under the propulsion tab in Table D.4 has to be shown. Firstly, MTP-PROP-TR01 states that the tug propulsion system is to deliver a velocity increment of 11.1 km/s. This velocity increment is delivered by the thrust of the VASIMR engines and has to be delivered within the time constraints as stated in section 5.2. This means a thrust level of 5.7 N has to be provided consistently by both engines for over 2 years. To verify this the engines need to be tested in a vacuum environment. This test is already planned to be performed on the ISS[16]. Another test for the engine placed on the gimbals is also needed to show whether

[15] URL `https://www.tudelft.nl/lr/organisatie/afdelingen/space-engineering/space-systems-engineering/expertise-areas/space-propulsion/system-design/analyze-candidates/motor-configurations/liquid-systems/year/2010/` [cited on: 14 june 2017

[16] URL `https://www.nasa.gov/audience/foreducators/k-4/features/F_Engine_That_Does_More.html` [cited: 14 June 2017]

the gimbals provide the required thrust vectoring for e.g. proper thrust alignment with the center of gravity of the spacecraft. Then, it has to be shown that the tank and feed system are capable of handling the required amounts of fuel. The capacity of the xenon tank can be verified by inspection. This can be done by filling it up with a liquid and measuring the total amount of liquid that fits in the tank. The tank is also required to withstand the maximum pressure. This can be tested by pressurising it with a, to be determined, gas to the maximum pressure for a set time. This is preferably done in a vacuum environment as this most accurately represents space conditions. The feed system test can be included in the actual VASIMR engine test at ISS. It has to be tested on the conversion of high tank pressure to VASIMR inlet pressure and the consistency of the gas flow. Lastly, MTP-PROP-TR02 states that the engine shall be able to restart. The VASIMR engine allows for restarting, as it is only a matter of providing power and fuel to the engine. The tug propulsion system is thus shown to comply to all posed requirements.

Then, MTP-PROP-TR02 states that the lander is required to provide a velocity increment of 67.5 m/s. This is delivered by the four Aestus engines all with a thrust level of 29.6 kN. The Aestus engines is flight proven and therefore does not require any further verification[17]. Then, the tanks of the lander can be verified in the same way as performed for the tug. The feed system has to be shown to provide the required propellant flow on a consistent level. Lastly, MTP-PROP-LA02 states that the engine shall be able to restart, which the Aestus engine is capable of [46]. This way, also the lander propulsion system is shown to comply to the requirements.

Product Validation

The last step is to validate the propulsion systems in its entirety. For the tug propulsion system this can be done by performing a ground test with the full engine configuration set up. The propulsion should both provide a consistent thrust level with the required efficiency levels. Also the performance of the gimbals, and thus also of the flexible feed system, should be shown while the engines are activated. The engines should also be deactivated and activated again to prove feasibility of engine reactivation. When all these things are shown to perform, the tug propulsion system can be said to be validated.

For the lander propulsion system the same approach can be followed. While all individual components are already verified, the way in which they work together needs to be shown. A full scale test with all tanks, the feed system and all four engines is required. When the full lander propulsion system is shown to work together while maintaining a constant thrust level, the thrust level can be throttled up and down and the system can be reactivated after shutdown, the lander propulsion system can be said to be validated.

5.4 ADCS

This section explains the sizing of the Attitude Determination & Control Subsystem. It is split into six parts, where first the mass distribution of the spacecraft and the disturbances are estimated. Based on these models the control systems for the tug and lander are designed. After these designs the attitude determination system is designed and lastly the verification and validation is performed for the calculations and design. All design calculations were based on the mass budget of the last iteration, which is shown in Table B.1.

5.4.1 Mass distribution

The basis of the entire ADCS model is the mass distribution. This model module calculated the spacecraft centre of mass and inertia tensor based on the shape and mass of the spacecraft. It was split into four main components, which were the habitat, the lander, the tug and the solar panels. For each component it was assumed it had a homogeneous mass distribution. The axis system was chosen in the way presented in subsection 2.1.1; the x-axis points in the direction of thrust, the y-axis points through the starboard solar panel and the z-axis completes the right handed reference frame. The origin for the centre of mass calculations was chosen at the centre of the bottom plate at the engine side of the tug.

The configuration was based on the layout presented in Figure 2.1. The habitat was given to be a cylinder. The axis of the cylinder was placed parallel to the z-axis and the habitat itself is located on top of the lander. The lander was assumed to be a cuboid. The lander had two options in the model,

[17] URL `http://projecte-hermes.upc.edu/Enginyeria%20Aeroespacial/2B/Sistemes%20Propulsius/Treball/Altres%20cursos/LL1%20AESTUS/Aestus.pdf` [cited: 14 June 2017]

which were wet and dry. Changing to other option only changed the mass of the lander. The tug was also assumed to be a cuboid. It was considered without the solar panels though. Similar to the lander it also had a wet and a dry option. The solar panels were split over a port and starboard panel. Each panel had two options, which were the extended and retracted mode. Selecting extended or retracted mode only influenced the moment of inertia of the solar panel.

Based on these components the centre of mass calculations were performed using Equation 5.46. This equation is for the x coordinate, but similar equations were used for the y and z coordinates. For the total moment of inertia Equation 5.47 was used. Similar equations were used for the other moments of inertia.

$$x_{cg} = \frac{\sum_{i=1}^{n} x_{cg_i} m_i}{\sum_{i=1}^{n} m_i} \tag{5.46}$$

$$I_{xx} = \sum_{i=1}^{n} I_{xx_i} + m_i \left(x_{cg_i} - x_{cg}\right)^2 \tag{5.47}$$

As a last step this module determined the maximum and minimum moments of inertia around each axis with the different possible configurations. The module calculated this for the situation where only the tug and lander are attached to each other, the situation where the tug, lander and habitat are connected, the tug alone and the lander and habitat connected. These situations were then passed on to the other modules.

5.4.2 Disturbance Estimation

During the entire mission the spacecraft is perturbed by disturbance torques, which have to be compensated by the ADCS. At each stage of the mission, different disturbance sources should be taken into account. The initially considered disturbance torques were aerodynamic (Equation 5.48), magnetic (Equation 5.49), gravity gradient (Equation 5.52), solar radiation pressure (Equation 5.50) and thrust vector misalignment (Equation 5.51) [4].

$$\tau_a = \frac{1}{2} \rho \, C_D \, A_r \, V^2 \left(cp_a - cm\right) \tag{5.48}$$

$$\tau_s = \frac{J}{c} A_s \left(1 + q\right) \left(cp_s - cm\right) \cos\beta \tag{5.50}$$

$$\tau_m = D_{res} \left(\frac{M}{R^3} \lambda_M\right) \tag{5.49}$$

$$\tau_t = T \cdot d_{cg-thrust} \tag{5.51}$$

$$\tau_{g,x} = \frac{3\mu}{2R} \left(I_{zz} - I_{yy}\right) \sin\left(2\phi\right) \tag{5.52}$$

The aerodynamic torques, calculated using Equation 5.48, were found to be negligible, due to the low atmospheric density at the starting orbit of 19,371 km. As the orbit altitude only increases after this and does not get below 9,134 km around Mars as found in section 5.2, it was neglected during the entire mission. The thrust vector misalignment was also neglected due to the gimbal that was placed on both of the VASIMR engines.

The disturbance model was then split into six different phases. These phases are waiting for departure at the launch orbit, the low-thrust departure trajectory between the launch orbit and geostationary orbit, the low-thrust departure trajectory above geostationary orbit, the heliocentric low-thrust trajectory, the low-thrust Mars orbit insertion trajectory and the relay orbit around Mars. The torques were split up into continuous and cyclic disturbances.

For each phase the total time in that phase was estimated or obtained from the navigation team. This was then used to calculate the change in angular momentum using Equation 5.53 [4]. The total angular momentum in a phase was then calculated by assuming that $\vec{\omega} \times \vec{H}$ is very small compared to $\vec{T}$, resulting in Equation 5.54. Then the change in angular momentum was integrated over time assuming that $\vec{T}$ is constant at the maximum value for that phase, which led to Equation 5.55. The cyclic disturbances were calculated the same way, but then over their cycle time.

$$\dot{\vec{H}} = \vec{\tau} - \vec{\omega} \times \vec{H} \tag{5.53}$$

$$\dot{\vec{H}} = \vec{\tau} \tag{5.54}$$

$$\vec{H}_{total} = \vec{\tau} \, t \tag{5.55}$$

Now the maximum disturbance torques, angular momentum accumulated over a phase and the largest angular momentum accumulated over a cycle were found. The maximum cyclic disturbance torques and maximum accumulated angular momentum were used to size the control moment gyroscopes. The

maximum continuous disturbance torques were used to size the thrusters and the angular momentum accumulated over all phases combined was used to determine the amount of propellant that is required.

5.4.3 Tug Attitude Control Detailed Design

In the Mid-Term Report it was decided that the tug would get Control Moment Gyroscopes (CMG), chemical and electric engines as attitude control actuators [1]. However, it was found during the early calculations of the final phase that the electric engines could be removed if the VASIMR engines would receive a gimbal. It saved almost two tonnes of the ADCS system in exchange for 0.7 tonnes added to the propulsion system. The current configuration contains only chemical thrusters and CMGs.

Thruster Sizing

In the Mid-Term Report, 216 N chemical bipropellant thrusters from the Automated Transfer Vehicle (ATV), which supplies the ISS, were used for preliminary sizing of the system [48]. In this report, it is proven that they meet the requirements.

The thruster sizing was based on the maximum required torque and the thruster arm. The maximum required torque from detumbling after launch (requirement MTP-ADCS-TR02), rotating the spacecraft (requirement MTP-ADCS-TR05) or counteracting disturbance torques (requirement MTP-ADCS-TR04) was used to size the thrusters.

To determine the required torque for detumbling the initial angular rate was assumed to be 1.0 deg/s based on the maximum initial angular velocity of the Ariane V, because this information could not be found for the SLS Block II [49]. Now the angular momentum was determined using Equation 5.56. Equation 5.53 was then used to determine the required torque to stop the tumbling.

$$\vec{H} = \bar{\bar{I}}\vec{\omega} \tag{5.56}$$

$$\dot{\vec{H}} = \bar{\bar{I}}\dot{\vec{\omega}} \tag{5.57}$$

The torque that is required to rotate the spacecraft at the required rate was determined by the rotation model shown in Figure 5.20. It was assumed that a linear angular acceleration occurs for burn time t_b. Then the spacecraft will rotate at a constant angular rate and it will then linearly decelerate to its initial angular rate. The angular acceleration was calculated by taking the derivative of Equation 5.56 and assuming that the moment of inertia remains constant, which resulted in Equation 5.57. The total rotated angle was then calculated by integrating the curve. Rearranging the terms led to Equation 5.58.

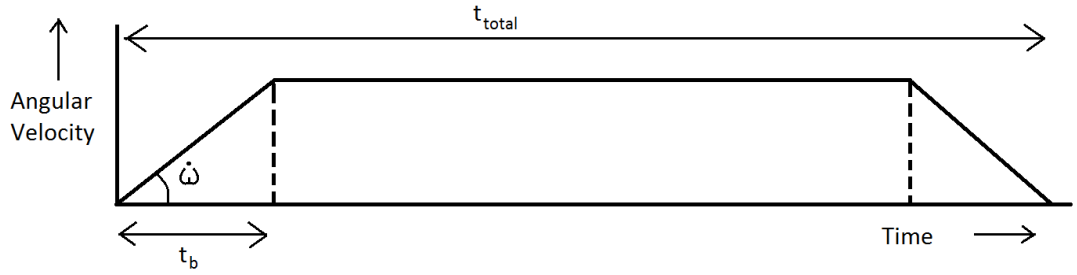

Figure 5.20: Rotation model for ADCS.

$$\tau_{thruster} = \frac{I \cdot \phi}{t_b\, t_{total} - t_b^2} \tag{5.58}$$

After comparing the results of the disturbance torques, the detumble torque and the rotation torque, the maximum required torque was found to be highest when the spacecraft has to be rotated, making MTP-ADCS-TR05 the driving requirement for the thrusters.

The calculated required thrust was found to be 130 N with an arm of 4.5 m. After this it was concluded that the thrusters selected in the Mid-Term Report were sufficiently powerful. Even though they are stronger than required, they were still selected, because they are off-the-shelf and because the required thrust dropped significantly in the last iteration.

The last design step to be performed was to determine the location of the thrusters. First of all the arm had to be at least 4.5 m. Second, the exhaust plumes should not hit any part of spacecraft, including the solar panels and the side of the spacecraft. The chosen locations are shown in Figure 5.21.

The thrusters could not be placed on top of the tug, because the lander is already there. The extending solar panels meant thrusters could not be placed on the sides of the solar panels. The habitat was also placed on top. Excluding these faces meant that thrusters were all placed on two sides, where some thrusters were angled away from the body to prevent burning it, but still providing full attitude control around all axes. In total sixteen thrusters are used on the tug. These provide attitude control around all three axes and allow for thruster failure around each axis.

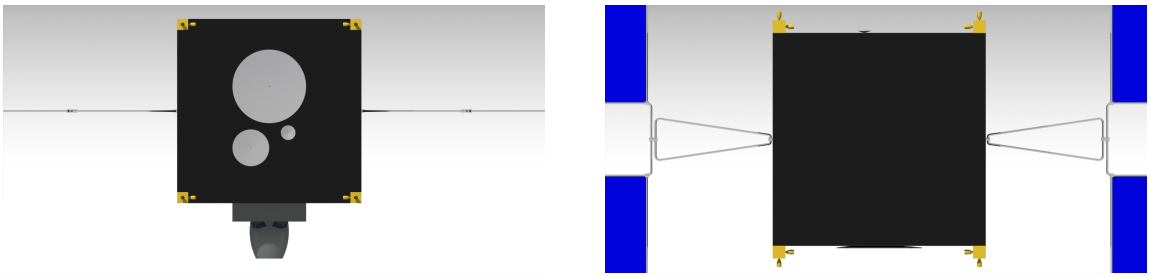

(a) Front view of the thruster locations for the tug. (b) Top view of the thruster locations for the tug.

Figure 5.21: ADCS thrusters locations on the tug with the solar panels on the sides. Circles are thrusters seen from the top, cones are thrusters seen from the sides.

Propellant Sizing

The required propellant was based on the maximum total angular momentum accumulated over the mission. Due to conservation of momentum, thrusters are used to dump this angular momentum. The selected ATV thrusters have an I_{sp} of 275 s and use MMH as fuel and N_2O_4 as an oxidiser [48]. The amount of fuel required to dump the angular momentum was calculated using Equation 5.61, which was derived using Equations 5.55, 5.59 and 5.60.

$$m = \dot{m}\, t \qquad (5.59) \qquad T = I_{sp} g_0\, \dot{m} \qquad (5.60) \qquad m = \frac{H_{total}}{I_{sp}\, g_0\, d} \qquad (5.61)$$

Combining the engine characteristics, the total angular momentum that must be dumped and the the fuel used during rotations resulted in a total ADCS fuel mass of 1,591 kg for the tug. This mass is split into 991 kg N_2O_4 and 600 kg of MMH, based on a nominal mixture ratio of 1.65 [48].

Tank Sizing

The tanks for the ADCS in the tug are sized using Equations 5.39 through 5.43 that were used for propulsion in section 5.3. It also uses helium as a pressurant to keep the pressure on the tanks, which removes the need for pumps. The xenon was already placed in the centre of the spacecraft and since there was not enough space left above or below this tank, it was decided that six ADCS fuel tanks would be used. Two of these tanks contain MMH, two contain N_2O_4 and two contains helium. This allowed for a symmetric mass distribution around the thrust axis.

For the tank design a FoS of two and a BOL pressure of 27.6 MPa were used based on SMAD [4]. The EOL pressure was taken from the required inlet pressure of the thrusters, which is 2.4 MPa [48]. This resulted in a helium mass of 6.0 kg These numbers led to the tank size in Table 5.23.

Table 5.23: Values for the volume, radius, wall thickness and mass of the ADCS tanks in the tug.

	Oxidiser (N_2O_4)	Fuel (MMH)	Pressurant (He)	Unit
Amount	2	2	2	-
Volume per tank	0.34	0.34	0.077	m^3
Radius	0.43	0.43	0.26	m
Wall thickness	2.7	2.7	1.7	mm
Mass per tank	173	173	42	kg

Fuel Block Diagram

To control the fuel flow from the tanks to the thrusters, a fuel block was made in Figure 5.22. This is still a preliminary design and should be improved in future iterations. It shows how the fuel tanks are connected to the thrusters, how the pressurant tanks are connected to the fuel tanks and what mechanisms are used to control the flow.

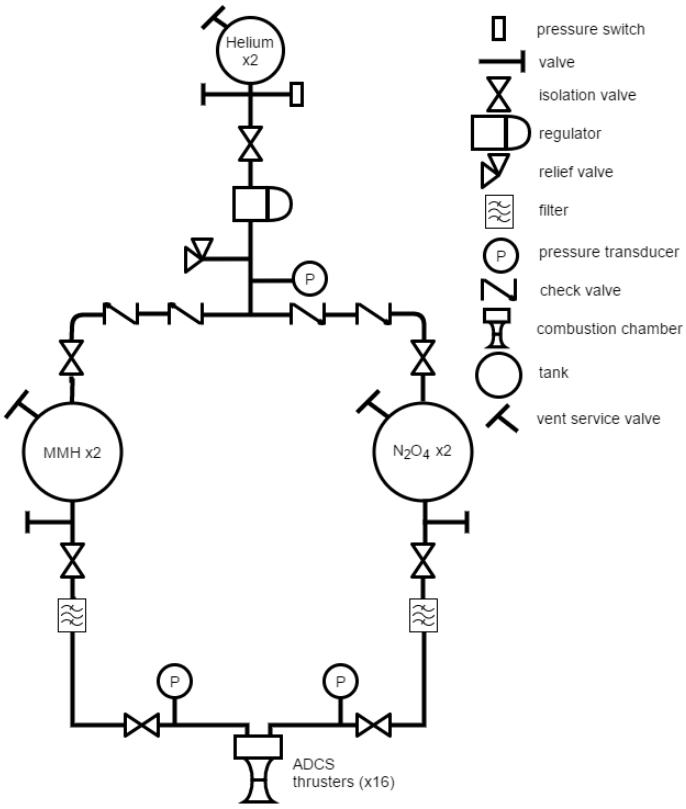

Figure 5.22: Fuel block diagram of the ADCS in the tug.

Control Moment Gyroscope Sizing

The sizing of the CMGs is mostly based on the CMGs on the ISS. The ISS uses four double axis controlled CMGs. In theory, two of these would be sufficient, but since two out of four have failed on the ISS, four CMGs will also be used on the tug [50].

The angular momentum that each CMG can store must be at least that of the largest amount of angular momentum peak during one cycle, because two CMGs are required to fully cover all directions. It may be the case though, that only one of them is able to provide torque around the axis the cyclic disturbance acts, because the other one may be parallel to that axis. Also, a FoS of 1.5 was applied to the maximum angular momentum per cycle.

To ensure effectiveness of a CMG, a maximum angle difference between the positions of minimum and maximum stored momentum during a cycle is set 90 degrees. Now the angular momentum of the CMG was determined using Equation 5.62, which is based on Figure 5.23 and the law of conservation of angular momentum. By further assuming the same angular velocity of the CMGs as the ISS, which is 6,600 rpm, the required wheel mass moment of inertia was determined using Equation 5.56 [51]. For the wheel material steel was chosen, because of its high density and low cost.

$$|\Delta\vec{H}| = 2|\vec{H}|\sin\left(\frac{\phi}{2}\right) \tag{5.62}$$

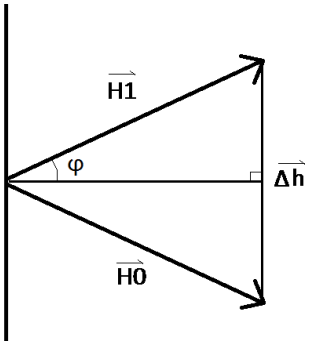

Figure 5.23: Momentum vector diagram from which Equation 5.62 was derived.

After the calculations the required size of each wheel were found to be a radius of 0.30 m and a thickness of 0.020 m. This resulted in a mass of 44 kg and had a maximum torque capability of 71 N, assuming a maximum rotational velocity equal to the CMGs of the ISS, which is 3.1 deg/s [51].

The CMGs also need a casing and a motor though. This mass was determined by multiplying the ratio between the total mass (272 kg) and the wheel mass (100 kg) of one ISS CMG with the 44 kg of a tug CMG. This resulted in a total mass for each CMG of 118 kg.

To determine the power each CMG uses, the power that is used by the M50 CMG produced by Honeywell was used as a reference and scaled up with the mass of the CMG [52]. This resulted in a peak power of 478 W and a standby power of 186 W for each CMG.

5.4.4 Lander Attitude Control Detailed Design

The lander has a simpler control system than the tug, because it only uses thrusters. This choice was made during the Mid-Term Report, mainly because the transfer time is short compared to the tug [1]. The tug ADCS also has the added task of performing the last stage of the landing, because the main engines from the propulsion subsystem are too strong to perform a precise landing. The sizing of the fuel tanks for the lander was done by the propulsion subsystem, because the ADCS and propulsion share fuel tanks in the lander.

Thruster Sizing

First the type of thruster and the required amount of thrusters were determined. The same thruster type was chosen as for the tug, which are the 216 N ATV thrusters, because it will further reduce development cost [48]. It was found that these thrusters would not have sufficient thrust to fulfil requirement MTP-ADCS-LA06. This was at a lower rotational time than the tug, because the lander must be able to land, which typically requires faster manoeuvres. To meet this requirement, the amount of thrusters around two axes was doubled to increase the torque around those axes.

The lander thruster locations were chosen to maximise the thruster arm and to prevent burning the habitat and the lander itself. The thruster placement is shown in Figure 5.24. This meant that the thrusters on the top had to be angled away from the habitat. To ensure that a rotation does not cause a small translation as well, the thrusters on the bottom were placed at the same angle. Due to the small margin between the solar panels and the lander at the sides, the thrusters were placed on the front and back. The total amount of thrusters on the lander is forty. This allows for control around all three axes and allows for thruster failure around each axis, while still meeting the performance requirements.

Propellant Sizing

The lander also uses the same propellant as the tug. To determine the required fuel for the lander ADCS, the landing was split up into different aspects. The first split that was performed was the split in attitude control functions (rotation) and landing functions (translation).

The fuel required for rotation was based on the fuel fraction reserved for attitude control by the Lunar Module, because it requires a simulation of all things that can go wrong during the landing. The ratio of attitude control fuel and the Lunar Module wet mass was found to be 1.7 % [53], which results in a attitude control fuel mass of 942 kg for the lander.

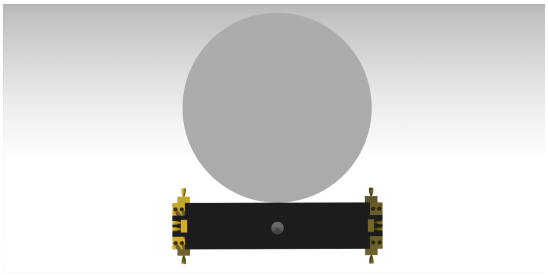

(a) Front view of the thruster locations for the lander.

(b) Side view of the thruster locations for the lander.

Figure 5.24: ADCS thrusters locations on the tug with the solar panels on the sides. Circles are thrusters seen from the top, cones are thrusters seen from the sides.

The landing functions were split into further segments, which were cancelling an initial velocity left by the Hohmann transfer, cancelling the free fall velocity, hovering for two minutes and manoeuvring to the right hovering spot. The maximum initial velocity was set at 2 m/s. To determine the free fall velocity, a starting altitude of maximum 5 km was set and then the end velocity was calculated assuming a constant gravitational acceleration. The hovering and manoeuvring values were obtained from the requirements. A FoS of 1.5 was put on the final ΔV value, because this model is simplified a lot. The final required ΔV the lander ADCS must be able to provide was found to be 30 m/s. Combining this with an I_{sp} of 275 s from the thrusters resulted in a fuel mass 634 kg for the lander translation functions [48].

5.4.5 Attitude Determination Detailed Design

In the Mid-Term Report it was determined that the attitude determination would consist of Sun sensors, star trackers and IMUs. These components are still included. For the final design each component has been selected from a manufacturer. The same components are used on both the tug and the lander.

For the Sun sensors, the Fine Digital Sun Sensor from NewSpace Systems was selected, because it has a very low mass (35 grams) and a large field of view (140 degrees) [54]. The location of the sensors on the tug can be seen in Figure 5.25. These locations have been chosen to ensure that almost the entire sky is covered. On each face double the amount required was placed to provide redundancy and to ensure the Sun can still be detected on that side. On the faces without a solar panel two Sun sensors are placed and on the sides with solar panels four Sun sensors were placed, because the solar panels may block the view of a single sensor. The lander uses eight sensors. The locations of these sensors are shown in Figure 5.26.

The Hydra Complementary Metal Oxide Semiconductor (CMOS) Star Tracker was selected with a three head configuration as a star tracker. Two heads are required to provide an accurate attitude around all three axes, so one head may fail and a single star tracker is still able to provide accurate information. The star trackers are placed in such a way that always at least three heads can point away from the Sun. Their location is shown in Figure 5.25. The same amount of star trackers was used on the lander, but their location is shown in Figure 5.26.

The selected Inertia Measurement Unit (IMU) was the Miniature IMU from Honeywell, because it is proven for deep space probe applications and provides the required accuracy [55]. Two of these are used to provide redundancy. They are located inside the spacecraft, because they require no external view.

5.4.6 Verification & Validation

To verify and validate the final ADCS design, first the verification of the individual calculations is given, after which the models are validated. Based on these models and calculations, the individual subsystem components are verified. The ADCS subsystem validation is done as a last step.

Model Verifcation

During the development of the ADCS, the complete model can be subdivided into a mass distribution model, a disturbance torque model, a rotation model and a tank model, which were separately verified and validated. Finally, the integration of these models was verified and validated.

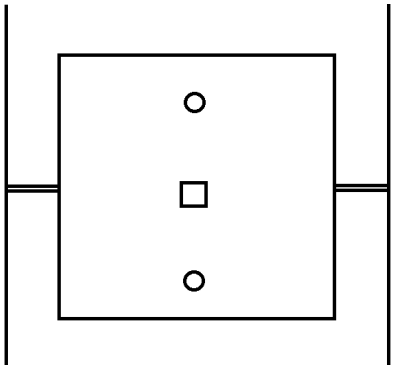

(a) Front view of the sensor locations for the tug.

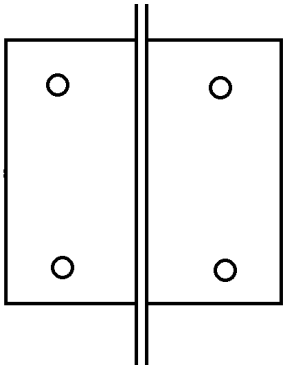

(b) Side view of the sensor locations for the tug.

Figure 5.25: ADCS sensor locations on the tug with the solar panels on the sides. Circles are Sun sensors and squares are star trackers.

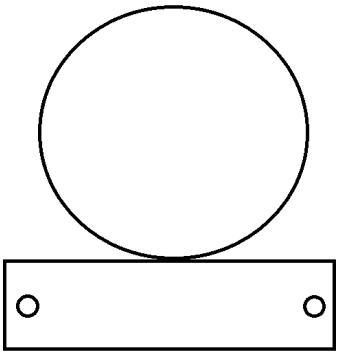

(a) Front view of the sensor locations for the lander.

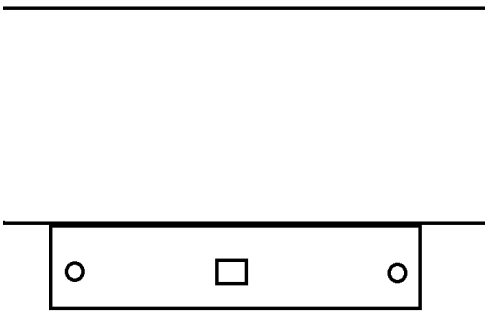

(b) Side view of the sensor locations for the lander.

Figure 5.26: ADCS sensor locations on the lander with the habitat on top. Circles are Sun sensors and squares are star trackers.

The model was constructed in Microsoft Excel. To minimise errors, hand calculations were done after an equation was inserted in a cell. If the cell was copied, it was checked whether the right cells were used as an input. Within each model blocks were defined, which made subcalculations. For each block a hand calculation was done as well to verify the output.

Model Validation

The mass distribution model calculated the centre of mass and the moment of inertia tensor, which has been described in subsection 5.4.1. The main assumption that simplified the model significantly is that each of the selected components in subsection 5.4.1 has a homogeneous mass distribution. To validate these results, it could be compared to a CAD model of the spacecraft. Due to time constraints this was not done though, but instead a sensitivity analysis was done to show that the spacecraft was divided into sufficiently small enough parts and that deviations in the centre of mass of a component would not impact the required performance significantly. This was done for a change in the tug centre of mass in x-direction only, because the tug is the largest component and can therefore influence the values the most. The results of this analysis are shown in Table 5.24. The analysis shows that even if a relatively large centre of gravity shift occurs, the performance only decreases if the centre of gravity shifts downwards. The largest performance differences occur in the fuel mass required and in the time to rotate around the y-axis, which is not a critical axis for the rotation criteria, because it has the smallest moment of inertia. Also the increased time to rotate around the z-axis stays well below the limit of requirement MTP-ADCS-TR05, which poses a limit of thirty minutes on a 180 degree rotation. The

pointing accuracy has no detectable change. Based on this sensitivity analysis it was concluded that the mass distribution model was sufficiently detailed for designing purposes and was therefore validated.

Table 5.24: Validation with a sensitivity analysis of the ADCS mass distribution model. The analysis was performed on the fully fuelled tug and lander with habitat attached and solar panels deployed.

Output	$x_{cg_{tug}}$ - 1 m	$x_{cg_{tug}}$	$x_{cg_{tug}}$ + 1 m	Unit	Δ% - 1 m	Δ% + 1 m
$x_{cg_{tug}}$	1.5	2.5	3.5	m	-40.0%	+40.0%
$x_{cg_{tot}}$	4.28	4.82	5.36	m	-11.2%	+11.2%
Fuel mass	1,691	1,591	1,482	kg	+6.3%	-6.9%
Time to rotate 180deg (x-axis)	18.2	18.2	18.2	minutes	0.0%	0.0%
Time to rotate 180deg (y-axis)	7.1	6.4	5.8	minutes	+10.9%	-9.4%
Time to rotate 180deg (z-axis)	18.1	17.4	16.9	minutes	+4.0%	-2.9%
Pointing accuracy	0.011	0.011	0.011	deg	0.0%	0.0%

The disturbance torque model determined the total angular momentum accumulated over the mission, as described in subsection 5.4.2. Each of the used equations shown in subsection 5.4.2 was also checked with the values from an example calculation in SMAD. With the available resources, it can only be validated up to the individual components of this model, which are the individual disturbances and the the spacecraft mass distribution. It was also tried to compare it to historical data, but no data could be found on how much fuel was reserved for attitude control, because it is typically shared with a propulsion system.

The rotation model described in subsection 5.4.3 calculated the required torque generated by the actuators to fulfil the rotational time requirements. This model was verified using hand calculations. The validation of this model was done using [12], which uses this model to determine rotations as well.

The tank model determined the tank size and mass based on the required propellant volume, which is described in subsection 5.4.3. To validate the tank sizing model, it was compared to the typical value of less than 10 % of the fuel mass [38]. For the tanks used by the ADCS this value is 43 %, which is significantly higher. This was found to mainly be caused by the high pressure in the tank, due to the maximum pressure in the pressurisation tank. It was overlooked though, that most systems have a pressure transducer between these tanks. This would significantly reduce the pressure on the fuel tanks and therefore the mass. This should be taken into consideration in the next iteration.

Product Verification

To show that the ADCS subsystem meets its requirements, each requirement is shown to be met, Table D.4 and Table D.5 . Firstly the pointing accuracy is demonstrated. This was not explicitly taken into account in the design phase, but taken from values that SMAD indicated should be able to be achieved [4].

The pointing accuracy comes from two sources, which are the knowledge accuracy and the control accuracy. The knowledge accuracy comes from the star trackers, which have an accuracy of at least 0.005°[56].

The control accuracy is determined by the CMGs and the thrusters. The CMGs can control their gimbal position with a 1° accuracy [52]. Assuming they are all orientated wrongly in the same direction, means a 0.017 deg/s rotational velocity of the entire spacecraft, using the lowest moment of inertia modelled for the tug. Using a control frequency of 10 Hz [52], the maximum deviation from the desired attitude by the CMGs is 0.0017. Adding the knowledge accuracy together, it results into a pointing accuracy of 0.0067 deg for the tug with the CMGs, which is well below the required 0.1°.

The thruster control accuracy is calculated by taking the smallest impulse they can give. It is assumed that this is done by two thrusters. The thrusters have a minimum impulse of 8 Ns, resulting in a minimum angular impulse of 36 Nms [48]. This corresponds to a rotational rate of 0.010 deg/s at the lowest modelled moment of inertia for the lander. The thruster pulse frequency is at worst 1 Hz [48], which results in a maximum deviation from the desired attitude by the thrusters of 0.010 deg. Adding the knowledge accuracy to the control accuracy results in a pointing accuracy of 0.015 degree, but slightly still well below the required 0.1 deg. This verifies requirement MTP-ADCS-LA01 is met.

The detumbling was calculated using the total angular momentum the tug and lander contain after launch at an angular velocity of 1 deg/s around the axis with the largest moment of inertia [49]. Assuming the redundant thrusters already failed during launch, which means only two thrusters can be used to detumble, a detumble time of at most one minute, which means requirement MTP-ADCS-TR02 is verified.

Requirements MTP-ADCS-TR04 and MTP-ADCS-TR06 are verified by checking the torque that the tug can generate is larger than 0.1 Nm and 0.25 Nm, which is 71 Nm using one CMG or 972 Nm using two thrusters. Requirement MTP-ADCS-LA02 was verified by checking that the torque the lander thrusters can output is larger than 0.1 Nm, which is the case at 972 Nm using two thrusters.

To determine whether the rotation performances are met, the rotating model in subsection 5.4.3 was used. Assuming two thrusters fire on the tug, the 180 deg rotation can be performed within twenty minutes, which is below the required time, verifying requirement MTP-ADCS-TR05. Assuming four thrusters fire on the lander for a rotation manoeuvre, a 180 deg rotation time of 2.2 minutes can be achieved, verifying requirement MTP-ADCS-LA06.

To verify requirements MTP-ADCS-LA03, MTP-ADCS-LA04 and MTP-ADCS-LA05 the total ΔV budget for translation is checked, which is 30.4 m/s. The hover time requires less than one m/s due to the low gravity on Phobos. This shows that the total ΔV budget from the ADCS is sufficient for these three requirements, which means MTP-ADCS-LA03, MTP-ADCS-LA04 and MTP-ADCS-LA05 are verified.

Product Validation

The ADCS consists of many components, so the validation must be done in steps, which start at components and end at the full subsystem test.

The tank must be able to hold the required propellant volume and it must be able to withstand the pressure. To validate the volume, it could simply be filled with a liquid and then emptied again, while the volume of the liquid that comes out is measured. It must also be able to withstand the pressure during the entire mission. This can be done by doing a pressure test.

The thrusters are off-the-shelf, so they will not have to be validated individually. Any valves and tubing was not considered in this report. Any of these components that are off-the-shelf also will not have to be individually tested, but the components that are newly designed for this mission should be tested and validated individually.

After the thruster, tank and fuel supply components are tested, a test must be done where all these components are integrated. This will check if all components together function as required. The control software for all components must also be used in this test. This test should consist of all components put together and then all possible operations and commands should be tested to see if they are carried correctly.

The individual CMG performance must be validated by testing. A CMG should be built, spun up and then a torque should be applied to it. The resulting rotation can be used to determine the actual performance of the CMG. Also lifetime tests must be performed to increase the reliability of the CMGs.

The four CMG assembly must also be tested with the control software for the CMG assembly. This will confirm that the four CMGs can work together properly using the control software. Rotational disturbances should be applied to the entire assembly and the reaction of the CMGs should be measured.

The final step to validate the control aspect of the ADCS is testing if the thruster and CMG assemblies together provide proper attitude control. These tests consist of momentum dumping tests, large rotation manoeuvres and fine attitude control.

All attitude sensors are off-the-shelf, so these do not need to tested individually. The integration of all sensors should be tested though by simulating sensor inputs to the navigation computer. These tests should also test the response if a sensor gives an incorrect output.

As a complete ADCS test, a test spacecraft could be launched to test the cooperation of the sensors and the controls. Before doing this, the added cost should be compared to the added certainty that

the thrust and controls work together properly and whether or not (almost) the same certainty can be obtained through simulation. It could also be tested in a simulated environment or it could be tested through a hardware-in-the-loop test.

The final step is testing the integration of the ADCS with other subsystems, which is described in chapter 12.

5.5 Communication

The telecommunication subsystem serves as an interface between Earth and the spacecraft. In the Mid-Term Report [1] a worst-case scenario was assumed, which resulted in a preliminary sizing of the communication subsystem. In this phase of the design, these preliminary values for data rates, antenna size and power consumption of both the tug and lander were optimised and finalised. Furthermore, communication eclipses and ground station availability were taken into account to determine the downlink and uplink duration. The Deep Space Network was chosen as a suitable ground station as it is connected to multiple Mars orbiters like the MRO and MAVEN.

As determined in the Mid-Term Report [1], the tug will be used as a relay after tug-lander separation and it will use four antennas: two for main communication with Earth (X- and Ka-band), one for communication with Earth during safety mode (X-band), and one for communication with the lander (X-band). The reason why two antennas are used at the same time for communication between tug and the DSN is because sending a signal twice at different frequencies allows for relative cancelling of space disturbances to enable precise distance determination of the PICARD[18]. A separate antenna on the tug is used for tug-lander communication and tug-DSN at the same time. The lander will have one antenna for communication with the tug. A visual representation of these specifications is given in Figure 5.28.

5.5.1 Detailed Design

To optimise and finalise the data rates, antennas' size and power consumption, a link budget was obtained using Equation 5.63 to Equation 5.70 for different phases of the mission. The margin between the required and received signal-to-noise ratio, calculated with Equation 5.63 should be higher than 3 dB to ensure proper communication [4]. The antennas gain was calculated with Equation 5.65 and Equation 5.66. The space loss was determined with Equation 5.67 and Equation 5.68. Lastly, the antenna pointing loss was obtained with Equation 5.69 and Equation 5.70. In the equations below, subscript r indicates the receiver and t the transmitter.

$$\frac{E_b}{N_0} = \frac{P\ L_l\ G_t\ L_a\ G_r\ L_s\ L_{pr}\ L_r}{R\ k\ T_s} \tag{5.63}$$

$$X[dB] = 10\ log(\frac{X}{X_{ref}}) \tag{5.64}$$

$$G_r = \frac{\pi^2\ D_r^2}{\lambda^2}\ \eta \tag{5.65}$$

$$G_t = \frac{\pi^2\ D_t^2}{\lambda^2}\ \eta \tag{5.66}$$

$$L_s = (\frac{\lambda}{4\ \pi\ l})^2 \tag{5.67}$$

$$l = \sqrt{d_{E-S}^2 + d_{S-P}^2 - 2\ d_{E-S}\ d_{S-P}\ cos(\theta)} \tag{5.68}$$

$$L_{pr}[dB] = Lp_{pr_t}[dB] + Lp_{pr_r}[dB] = -12\ [(\frac{e_{t_t}}{\alpha_{1/2_t}})^2 + \frac{e_{t_r}}{\alpha_{1/2_r}})^2] \tag{5.69}$$

$$\alpha_{1/2}[deg] = \frac{21}{f[GHz]\ D[m]} \tag{5.70}$$

A distinction was made between two phases of the mission: prior to and after separation of the tug and lander. After both phases were analysed, it was determined which phase was driving for the sizing of the subsystem. The assumptions made during the preliminary sizing phase that hold for both mission phases are:

[18] Based on personal conversation with Dr. Dominic Dirkx, assistant professor at TU Delft

- The tug was assumed to be at a maximum distance from Earth (378 million km). This is to ensure that maximum space loss is taken into account which is the most dominant factor in the link budget. However, at maximum distance the tug and DSN cannot communicate due to blockage of the Sun. Still, this maximum distance was taken to incorporate redundancy in the subsystem.
- The loss factors of the transmitter and receiver were assumed to have a minimal influence on the link budget. This loss factor was therefore chosen to lie between 0.8 and 0.9 which results in -1.0 and -0.5 dB for each link based on a Bispectral and Infrared Remote Detection (BIRD)-type satellite [57].
- The downlink frequencies for X- and Ka-band were set to a value that was most optimal for the link budget, assuming that every value in the frequency range is possible for downlink communication. This resulted in a value of 10 MHz for X-band and 27.5 MHz for Ka-band.
- Uplink frequencies of the DSN were based on frequency band limitations established by the International Telecommunication Union (ITU) [4]. This resulted in an uplink frequency of 8.4 MHz for X-band and 31 MHz for Ka-band.
- Uplink data rates of the DSN ranges from 1 to 2000 bits/s [4]. The uplink data rate was therefore set to 2000 bits/s assuming a worst-case scenario.
- The DSN consists of 34 m and 70 m diameter antennas. Because the number of 34 m antennas is larger, it was assumed the PICARD will mostly be connected to these antennas.
- For parabolic reflectors, the parabolic constant lies between 0.5 and 0.7 [58]. The constant was increased for the final link budget because it is achievable based on the fact that radio products for deep space are highly developed. Increasing this constant has an advantage on the link budget, increasing the antenna gain.
- The pointing offset of the ground station was assumed to be 10 % of the half-power angle which is calculated with Equation 5.70 [57].
- The transmission path loss was assumed to be negligible [4].
- The required signal-to-noise ratio of 4.5 dB was estimated using Figure 5.27. This value was minimised by using Binary Phase-shift Keying (BPSK) modulation and a Bit Error Probability (BER) of 10^{-5}. Although this modulation has a higher complexity, it has an excellent BER performance [4].
- The system noise temperature was based on typical system noise temperatures in satellite communication links [4].
- A margin of at least 3 dB between the received and required signal-to-noise ratio was assumed to be necessary.
- When a critical situation occurs both the X- and Ka-band antenna for main communication with the DSN are shut down and the safety antenna is activated to take over the communication between the tug and DSN using only 30 W and sending data with a low rate of 500 bits/s. A critical situation could be that less power is available due to malfunctioning of the power subsystem.

Prior to separation

To minimise attitude control during the mission phases up to the deployment of tug and lander, the largest X-band antenna (X-band) for communication with Earth will be turned off. This is due to the fact that the ADCS is mainly used for engine pointing and it is not convenient to use an antenna pointing mechanism or gimbal for large objects as this may cause attitude disturbances. Only the (smaller) Ka-band antenna will be used for downlink communication during this phase by using an antenna pointing mechanism. Based on the power sizing, it was determined that 500 W would be required for the communication system of the tug prior to separation.

The link budget in Table 5.25 resulted in a downlink data rate of at least 200 kbits/s at all times. At minimum distance between tug and Earth data rates up to 5 Mbits/s can be achieved. The data rate is higher than the preliminary value (100 kbits/s) due to optimisation of the link budget, the modulation method and the power input. The subsystem is only slightly overdesigned as a decrease in data rate will

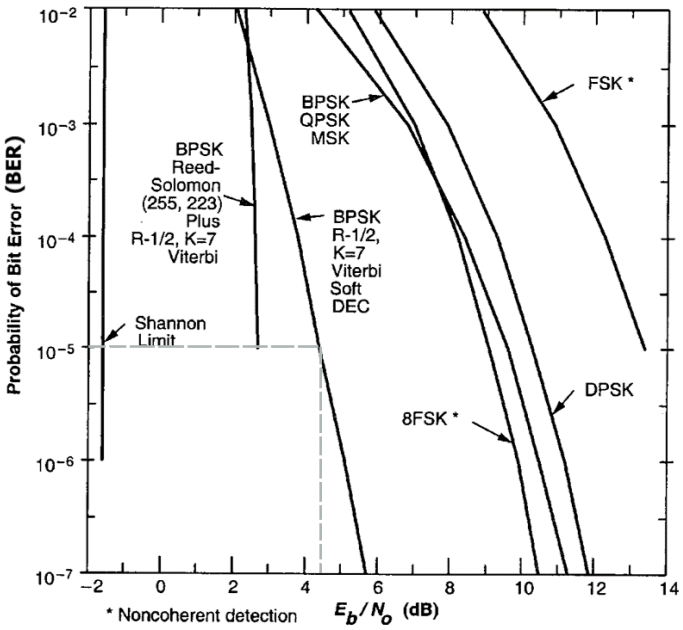

Figure 5.27: Bit error probability as a function of required signal-to-noise ratio [4].

not significantly change the overall size, mass and power consumption of the subsystem compared to the total spacecraft.

Table 5.25: Link budget for communication between the DSN and the tug prior to separation.

Quantity		Ka-band [dB]		Unit
		Downlink	Uplink	
P	Transmitter power	+ 27.0	+ 29.0	W
L_l	Loss factor transmitter	- 0.5	- 0.5	-
G_t	Transmitting antenna gain	+ 47.6	+ 79.3	-
L_a	Transmission path loss	0.0	0.0	-
G_r	Receiving antenna gain	+ 79.3	+ 47.6	-
L_s	Space loss	- 292.8	- 293.8	-
L_{pr}	Antenna pointing loss	- 0.3	- 0.3	-
L_r	Loss factor receiver	- 0.5	- 0.5	-
$1/R$	Required data rate	- 53.0	- 33.0	$(\text{bits/s})^{-1}$
$1/k$	Boltzmann constant	+ 228.6	+ 228.6	$(\text{J/K})^{-1}$
$1/T_s$	System noise temperature	- 26.3	- 28.8	K^{-1}
Quantity		Downlink	Uplink	Unit
$(E_b/N_0)_{rec}$	Received SNR	+ 9.2	+ 27.7	-
$(E_b/N_0)_{req}$	Required SNR	+ 4.5	+ 4.5	-
Margin		+ 4.7	+ 23.2	-

After Separation

After separation of the tug and lander, the tug moves to its relay orbit and two X-band antennas on the tug are switched on. One is a 2 m diameter antenna pointing to Earth and one is a 0.2 m antenna pointing to the lander (see Figure 5.28) . The lander communication system is switched on as well. A link budget for both the communication between the tug and Earth and between the lander and tug was obtained and summarised in Table 5.26 and Table 5.27.

The obtained link budget during the phase after separation was determined to be driving for the sizing of the subsystem. The largest antenna on the tug was decreased in size compared to the preliminary

value. Furthermore, a data rate ranging from 200 kbits/s to 5 Mbits/s equal to the previous phase can be achieved during this phase as well which is twice as much as the preliminary value. As mentioned above, the data rate was not decreased to the minimum value of 100 kbits/s stated in requirement MTP-COM-TR01 because it would not significantly change the mass, size and power consumption of the entire spacecraft. The results were obtained with the following assumptions:

- It was assumed that once in relay orbit, twice the amount of transmitter power (1000 W) will be available for the tug for communication with Earth because the propulsion system requires no power in the relay orbit.
- A maximum distance between tug and lander was assumed to take into account a maximum space loss which is the most dominant factor in the link budget. This maximum distance is equal to the distance from Phobos to Mars plus the distance from the tug in relay to Mars ($1.87 \cdot 10^4$ km). As mentioned above, even though communication is not possible at maximum distance, it was used to incorporate a small redundancy in the design.

Table 5.26: Link budget for communication between the Deep Space Network and the tug after separation.

Quantity		X-band [dB]		Ka-band [dB]		Unit
		Downlink	Uplink	Downlink	Uplink	
P	Transmitter power	+ 28.1	+ 43.0	+ 25.3	+ 29.0	W
L_l	Loss factor transmitter	- 1.0	- 1.0	- 0.5	- 0.5	-
G_t	Transmitting antenna gain	+ 44.9	+ 68.0	+ 47.6	+ 79.3	-
L_a	Transmission path loss	0.0	0.0	0.0	0.0	-
G_r	Receiving antenna gain	+ 68.0	+ 44.9	+ 79.3	+ 47.6	-
L_s	Space loss	- 284.0	- 282.5	- 292.8	- 293.8	-
L_{pr}	Antenna pointing loss	- 0.2	- 0.2	- 0.3	- 0.3	-
L_r	Loss factor receiver	- 1.0	- 1.0	- 0.5	- 0.5	-
$1/R$	Required data rate	- 53.0	- 33.0	- 53.0	- 33.0	$(\text{bits/s})^{-1}$
$1/k$	Boltzmann constant	+ 228.6	+ 228.6	+ 228.6	+ 228.6	$(\text{J/K})^{-1}$
$1/T_s$	System noise temperature	- 21.3	- 27.9	- 26.3	- 28.8	K^{-1}
Quantity		Downlink	Uplink	Downlink	Uplink	Unit
$(E_b/N_0)_{rec}$	Received SNR	+ 9.1	+ 38.9	+ 9.6	+ 27.0	-
$(E_b/N_0)_{req}$	Required SNR	+ 4.5	+ 4.5	+ 4.5	+ 4.5	-
Margin		+ 4.6	+ 34.4	+ 3.1	+ 23.2	-

Table 5.27: Link budget for communication between the tug and lander after separation.

Quantity		X-band [dB]		Unit
		Downlink	Uplink	
P	Transmitter power	+ 7.0	+ 10.0	W
L_l	Loss factor transmitter	- 1.0	- 1.0	-
G_t	Transmitting antenna gain	+ 24.9	+ 24.9	-
L_a	Transmission path loss	0.0	0.0	-
G_r	Receiving antenna gain	+ 24.9	+ 24.9	-
L_s	Space loss	- 197.9	- 197.9	-
L_{pr}	Antenna pointing loss	- 0.1	- 0.1	-
L_r	Loss factor receiver	- 1.0	- 1.0	-
$1/R$	Required data rate	- 53.0	- 33.0	$(\text{bits/s})^{-1}$
$1/k$	Boltzmann constant	+ 228.6	+ 228.6	$(\text{J/K})^{-1}$
$1/T_s$	System noise temperature	- 21.3	- 21.3	K^{-1}
Quantity		Downlink	Uplink	Unit
$(E_b/N_0)_{rec}$	Received SNR	+ 11.1	+ 34.1	-
$(E_b/N_0)_{req}$	Required SNR	+ 4.5	+ 4.5	-
Margin		+ 6.6	+ 29.6	-

The final values of the communication system are summarised in Table 5.28. Data rate and power are indicated as ranges. A visual representation of the subsystem including antennas, data rates and frequencies as well as the communication path is shown in Figure 5.28. Communication flow between the lander and existing Mars orbiters using Electra is shown as well. The Electra package is explained in more detail below. The mass of the subsystem was determined using the specific antenna mass of the Mars Reconnaissance Orbiter (MRO) which is 3.2 kg/m^2. Multiplying this result by the antenna surface of the PICARD results in a mass for the antennas. However, the antenna mass of the MRO was only 21 % of the total telecommunication mass [59]. The antenna mass of the PICARD was therefore divided by this percentage to take into account other components of the subsystem. This resulted in a total telecommunication mass of 62.2 kg and 0.5 kg for the tug and lander respectively. This mass is lower than the preliminary mass due to decrease in total antenna surface.

Table 5.28: Overview of antennas.

Transmitter	Receiver	Mode	Amplifier	Diameter [m]	Data Rate [kbps]	Power [W]
Tug	DSN	Nominal	X	2.0	200 - 5000	0.0 - 640
Tug	DSN	Nominal	Ka	1.0	200 - 5000	340 - 500
Tug	DSN	Safety	X	0.4	0.0 - 0.5	0.0 - 30
Tug	Lander	Nominal	X	0.2	0.0 - 2.0	0.0 - 10
Lander	Tug	Nominal	X	0.2	200 - 5000	0.0 - 5

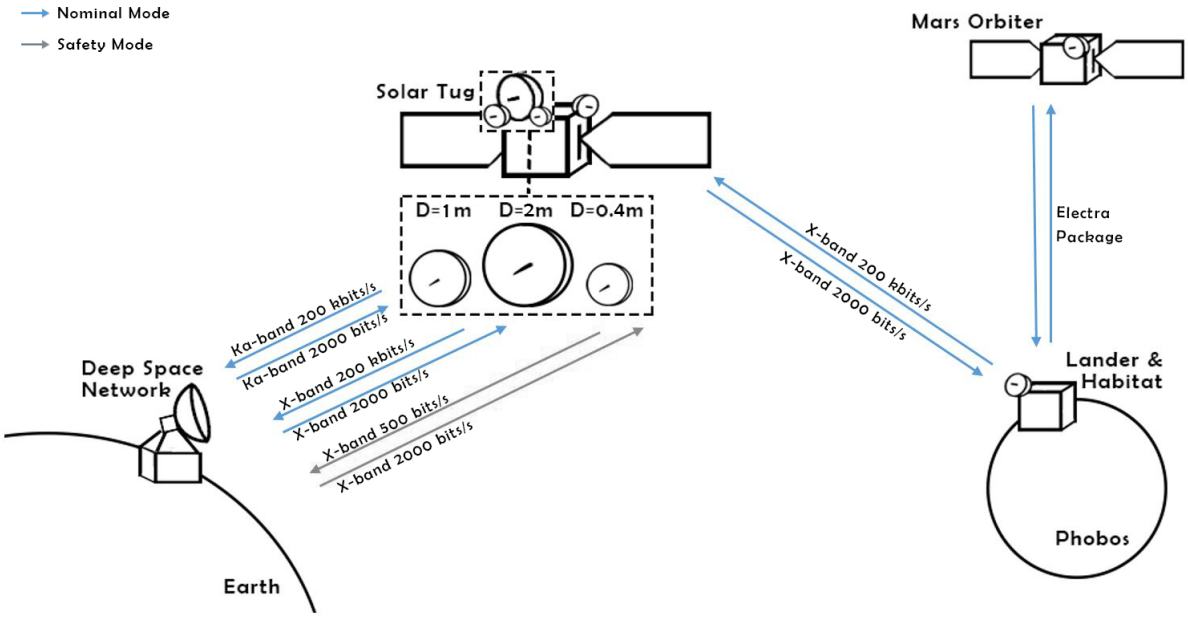

Figure 5.28: Communication flow diagram.

Electra Telecommunication Package

For communication with existing Mars orbiters, the lander will carry the Electra communication package on-board. The package is specifically designed for new incoming landers and can be used as a relay when necessary or as a tool for relative positioning between solar tug, lander and other Mars orbiters. The MRO is an example satellite that uses the Electra package[19]. Other space vehicles arriving after the PICARD like Orion could choose to incorporate this package as well. Including this piece of technology is essential to expand the communication network between spacecraft around Mars. Furthermore, the Electra package could be used when the antenna of the lander pointed to the tug fails to prevent a single point of failure.

[19] URL `https://mars.nasa.gov/mro/mission/instruments/electra/` [cited: 19 June 2017]

Communication Eclipses

The last aspect considered is communication eclipses which mainly influences the available downlink time and consequently the memory size of the C&DH system. During the mission three types of communication eclipses occur:

- The Sun blocks the link between the DSN and the tug.
- Mars blocks the link between the DSN and the tug.
- Mars blocks the link between the tug and lander.

Assuming that the tug is already in Mars orbit when the Sun blocks the link between the DSN and tug, the communication eclipse lasts approximately a total of 17 days every 26 months[20].

The blockage time due to Mars being between the DSN and the tug was mathematically determined with Equation 5.71 and was approximated to have a value of 0.88 hour per tug-orbit which corresponds to 7.5 hours per Earth day. The minimum distance between Mars and Earth was used to obtain the maximum value of this communication eclipse type. Equation 5.71 was obtained using Figure 5.29, in which t_{com} stands for communication eclipse time. Subscript M and $E-M$ stand for Earth and Earth-Mars respectively.

$$t_{com} = \frac{2\ tan^{-1}(\frac{R_M}{d_{E-M_{min}}})}{\omega_{tug}} \tag{5.71}$$

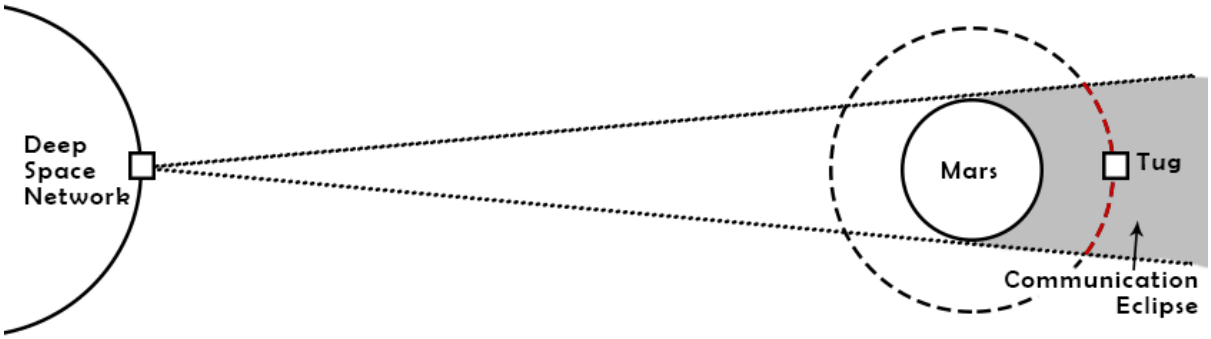

Figure 5.29: Blockage of link between the DSN and tug due to Mars.

To determine the communication eclipse time between tug and lander due to blockage of Mars, the relative velocity between tug and lander, obtained by the sizing of the navigation subsystem, was used. Equation 5.72 was obtained from Figure 5.30. In section 4.1 four suitable landing sites were investigated. What these landing spots have in common is that they face Mars constantly because Phobos is tidally locked. Therefore, a relay orbit at a lower altitude than Phobos was chosen to minimise communication eclipses. As mentioned in section 5.2, a minimum distance between Phobos' orbit and the relay orbit of 100 km was chosen to prevent that the relay and Phobos have an almost equal orbital speed. The reason why this is a problem is that the denominator in Equation 5.72 becomes very small, consequently increasing the eclipse time. The orbital velocity of Phobos, and thus lander, is $2.28{\cdot}10^{-4}$ rad/s and the orbital velocity of the tug in relay orbit is $2.32{\cdot}10^{-4}$ rad/s. Using relative velocity ω, Mars radius R_M and Phobos-Mars distance d_{P-M}, a communication eclipse approximation of 52.2 hours per 5.78 days was obtained. A visual representation of this communication eclipse is given in Figure 5.30.

$$t_{com} = \frac{2\ tan^{-1}(\frac{R_M}{d_{P-M}})}{\omega_{tug} - \omega_{Phobos}} \tag{5.72}$$

[20] URL `https://www.space.com/20501-mars-rover-curiosity-solar-conjunction.html` [cited: 12 June 2017]

Although multiple satellites are connected to the DSN at the same time, downlink time is limited due to dish capacity. Although no exact downlink duration was found, the limit was set to eight hours per day based on the daily downlink time of the Mars Reconnaissance Orbiter. When Mars blocks the link between the DSN and the tug, eight hours of downlink time per day can still be obtained. In case of the other two types of communication eclipses, this downlink time cannot be achieved. Therefore, a certain memory size is needed to temporary store the data when communication is not possible. The memory size was determined in the detailed design of the C&DH (section 5.6).

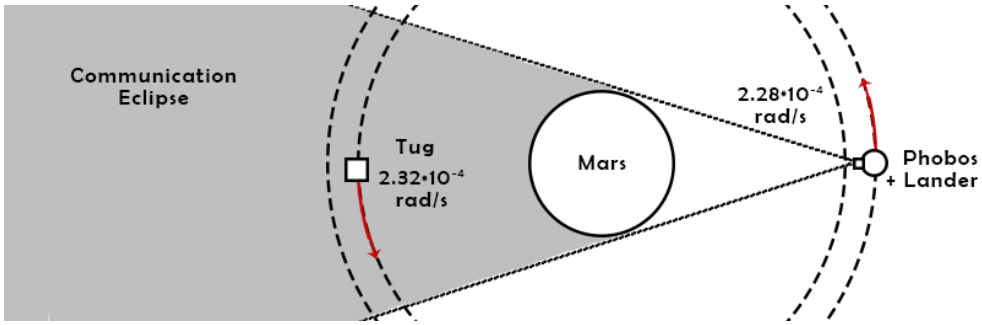

Figure 5.30: Blockage of link between the tug and lander due to Mars.

5.5.2 Verification & Validation

This section describes the verification and validation process of the communication system. First the model used for sizing was tackled, followed by the verification and validation of the subsystem product.

Model Verification

A tool was developed to perform the sizing of the communication system. This tool uses certain inputs to obtain a link budget and determine if the link closes, in other words if the margin is larger than 3 dB. To verify the model, the most influencing factors in the link budget are calculated by hand to see whether the produced values match. Furthermore a sanity check is performed to see whether a change in certain parameters affect the output as expected.

The most dominant factors were determined to be power P, antenna gain G_t and G_r, space loss L_s, data rate R, the Boltzmann constant k and the system noise temperature T_s. The antenna gain and space loss were calculated by hand with the same inputs as the model. The other factors are set values and were therefore not verified. The results are presented in Table 5.29. As shown in the table, the dominant output values of the simulation model accurately represent the physical model.

Table 5.29: Comparison model with hand calculations.

Quantity	Model [dB]	Hand calculations [dB]	Difference [dB]
G_t	44.872	44.872	0.000
G_r	67.967	67.967	0.000
L_s	-283.981	-283.981	0.000

For the sanity check, certain quantities were changed and a comparison was made between the expected outcome and the actual outcome. As shown in Table 5.30, the expectations precisely match the actual outcome.

Model Validation

Firstly, the model was based on an example model and on references [4] [57]. Furthermore, the model was validated by comparing the output values with reference values. According to the DSN Telecommunication Link Design Handbook, the gain of their 34 m diameter antennas using X-band is 68.41 dB [60]. The model output of the DSN antenna was estimated to be 67.97 dB which corresponds to 10.7 % change compared to the model value. This change is caused by the assumptions made regarding the uplink frequency and parabolic constant. Although the difference seems large, it does not influence the outcome significantly. If the antenna gain is higher in reality it will not negatively affect the link.

Table 5.30: Sanity check link budget model.

Quantity	Change	Expectations	Model
D_t	Increase with factor 2	G_t increases with 10 $\log(2^2)$ [dB]	True
		G_r remains the same	True
$f_{downlink}$	Increases with factor 1.2	G_t increases with 10 $\log(1.2^2)$ [dB]	True
		L_s decreases with 10 $\log(\frac{1}{1.2^2})$ [dB]	True
D_r	Decrease with factor 3	G_t remains the same	True
		G_r decreases with 10 $\log(\frac{1}{3^2})$ [dB]	True
S	Decreases with factor 2	L_s increases with 10 $\log(2^2)$ [dB]	True

Furthermore, according to the link budget of the Mars Observer the space loss at 0.37 AU is -267.8 dB for X-band and -277.9 dB for Ka-band [61]. Setting the value for distance in the simulation model to 0.37 AU results in a space loss of -267.3 dB for X-band and -276.1 dB for Ka-band. This results in a 10.9 % and a 33.9 % difference for X-band and Ka-band respectively caused by the assumed downlink frequency for both X- and Ka-band. The change for Ka-band is still within reasonable limits as the downlink frequency can be adjusted within its bandwidth from -275.8 dB to -279.3 dB. The same can be said for X-band.

Product Verification

The communication product is verified by referring back to the requirements to ensure they are met in the detailed design of the subsystem. Requirement MTP-COM-TR01 states that the tug shall transmit data to the ground station with a minimum bitrate of 100 kbits/s during all segments of the mission. This requirement is met by the two and one meter diameter antennas that will transmit data with a minimum rate of 200 kbits/s during all segments. What should be noted is that the safety antenna will have a lower bitrate than 100 kbits/s so it can be operational during critical situations while consuming low power. Furthermore, a similar requirement (MTP-COM-01) was established which states that the lander and tug transmit data to each other with a minimum data rate of 100 kbits/s during all mission phases. Again a 200 kbit/s data rate was achieved.

Another requirement that applies to the communication system is that the difference between the required and received signal-to-noise ratio shall have a minimum margin of 3 dB. This requirement was imposed on both the communication between tug and the DSN (MTP-COM-TR02) and between the tug and lander (MTP-COM-02). Between tug and the ground station a minimum of 3.1 dB margin was achieved by the Ka-band antenna. The two meter antenna and safety antenna have a higher margin. For the communication between the tug and lander a minimum SNR of 6.6 dB was achieved by the antenna on the lander.

Product Validation

The product can be validated by two tests: mission scenario test and an operation readiness test. Because the operational environment changes significantly during the mission, in terms of link distance, communication path and the amount of data required to send, a mission scenario test should be performed. This can be done, for example, in a radio-frequency anechoic chamber where the radiation pattern of the antenna can be studied [62]. Special attention should be paid to critical conditions in which the safety antenna should take over and function properly.

For the operation readiness test, the Deep Space Network is involved to test whether the interface between the ground station and the relay communication path is well integrated and the mission plan can be executed. This can be achieved by simulating the operational environment and perform mission procedures.

5.6 C&DH

To design the C&DH system, the main focus was on the microprocessor and memory. The processor was chosen based on historical data, whereas the memory required an extensive analysis of internal flows to come to the required storing capacity. Since the communication eclipse due to blockage of the Sun could take up to 17 days as described in section 5.5, choices on what subsystems should and should not generate

data during these periods were made. Before commencing a quantitative analysis, block diagrams for tug and lander were set up to describe the most important qualitative parameters exchanged with the C&DH system. This was done to show the interfaces between C&DH and other systems, as well as attaining an idea of data flows before quantifying them.

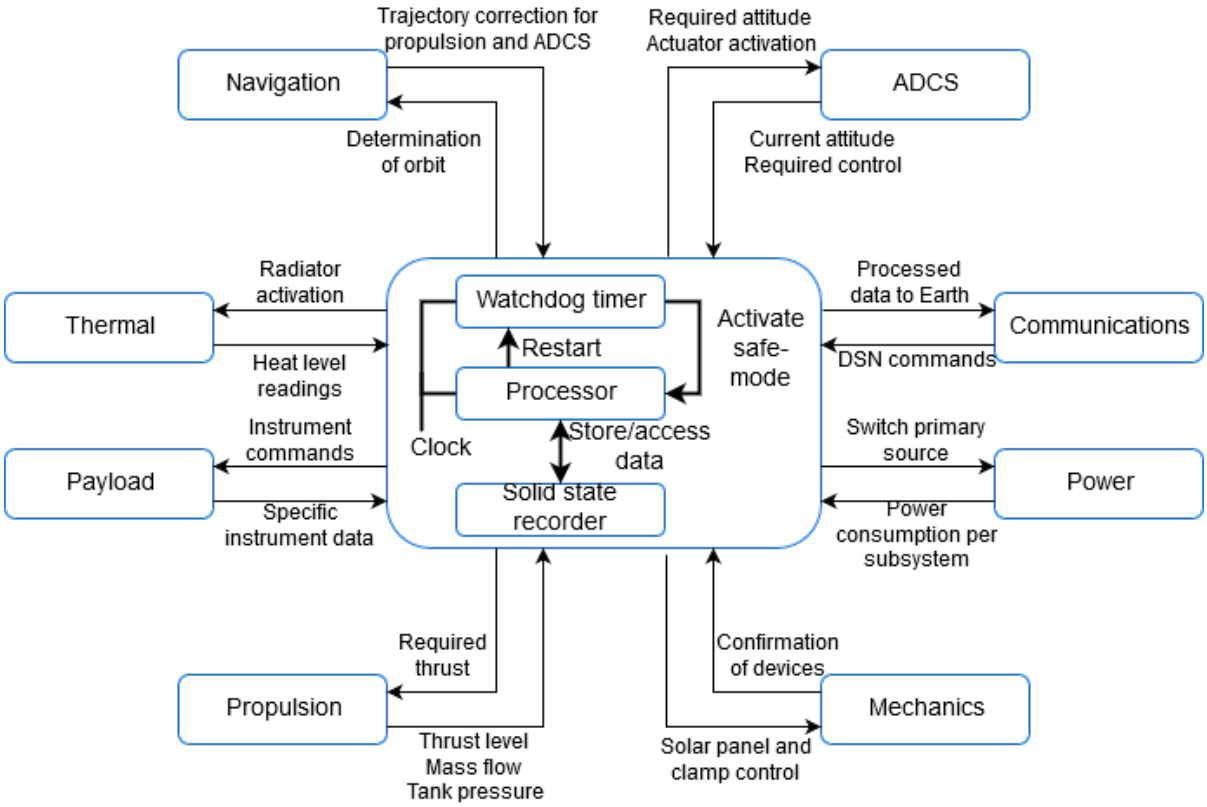

Figure 5.31: Qualitative data flows within the C&DH system of the tug.

Figure 5.31 describes these qualitative flows, showing the internal structure of the computer and flows going in and out. Since separation of tug and lander occurs, both should have their own C&DH system containing processor(s), memory and watchdog. Both watchdog and processor are connected to the same clock in order to prevent time differences. Whenever the computer would fail, it would be a catastrophic risk rendering the entire spacecraft to be unusable. Therefore, the processor is responsible for resetting the timer in the watchdog every period, whenever not, the watchdog makes sure the system is reset after a failure to respond to Earth's commands again. The lack of a watchdog would cause a shutdown due to the lack of a system reset and thus a non-responsive computer. This entire configuration is also present in the lander C&DH system, which is shown in Figure 5.32.

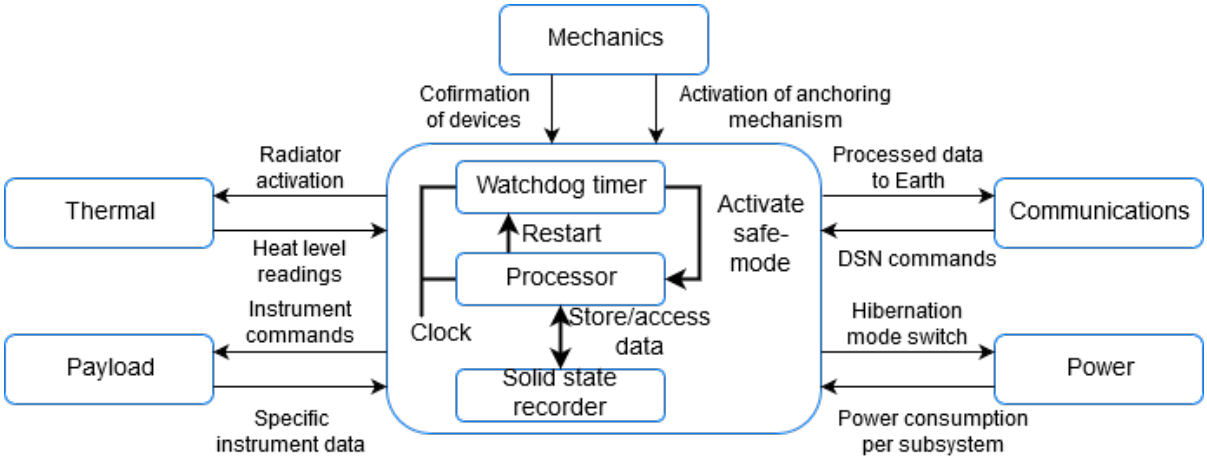

Figure 5.32: Qualitative data flows within the C&DH system of the lander, during the PSP.

5.6.1 Detailed Design

Choosing the microprocessor based on instructions per second is the sole justifiable option. Since no estimates can be done on the instructions, it was decided to base it on recent missions. Based on knowledge obtained in the Mid-Term Report, the Curiosity mission has demonstrated the use of the recent BAE Systems processor, proving it's feasibility for current and near future missions [1]. This RAD750 processor is thus also implemented in both tug and lander. The number of processors for both will be three. The third will primarily be turned off and not used. Processors one and two handle provided data. Whenever values deviate, the third processor comes into play. The third will run on different software, doing the same handling. The processor (first or second) that complies with the third processor will have the largest possibility of being correct, and thus that value will be processed, where the other is discarded [63].

Tug Memory

The memory was determined by estimating the data flows from each subsystem taking into account eclipse times. The data stored would be either that of payload or housekeeping. To minimise any overdesigning, the choice was made to turn off payload during communication eclipses. There is no necessity to keep payload on during eclipses. Housekeeping data would be the governing parameter for data to be stored. The different communication eclipse periods were evaluated, eventually designing for the longest: a 17 days eclipse due to blockage of the Sun. During this eclipse, all subsystems are considered to be turned on as worst-case scenario and thus providing maximum housekeeping data. The estimates are based on what data would be provided (and the amount of subcomponents providing that), the amount of significant numbers and the frequency with which it is requested. The significance per value was determined from what its predicted value of interest would be. It was assumed that one digit corresponds to eight bits or one byte. The tug is discussed first, followed by the lander. Tables 5.31-5.37 show all the estimates for the tug, with the update frequency written in the captions. The data rate per second is then determined by dividing the total bytes by the assigned update frequency.

Table 5.31: Propulsion data rate per 5 seconds.

Amount	Subcomponent Data	# of Digits
1	Mass flow	4
1	Tank pressure	4
2	Thrust level	6
1	Power consumption	6
1	Time stamp	6
	Total bytes	**32**
	Data rate	**6.4**

Table 5.32: Thermal data rate per 30 seconds.

Amount	Subcomponent Data	# of Digits
8	Subsystem temperature	5
2	Radiator cooling	4
1	Power consumption	6
1	Time stamp	6
	Total bytes	**60**
	Data rate	**2**

Table 5.33: Power data per 10 seconds.

Amount	Subcomponent Data	# of Digits
28	Solar array generation	6
80	Watthour per battery	5
1	Time stamp	6
	Total bytes	**574**
	Data rate	**57.4**

Table 5.34: ADCS data rate per second.

Amount	Subcomponent Data	# of Digits
3	Angles of S/C	5
3	Velocities of S/C	5
3	Accelerations of S/C	5
48	Thruster levels	4
4	Spin rates of wheels	4
6	Tank pressure	4
1	Power consumption	6
1	Time stamp	6
	Total bytes	**289**
	Data rate	**289**

Table 5.35: Communications data rate per 5 seconds.

Amount	Subcomponent Data	# of Digits
4	Downlink frequency	4
4	Downlink data rate	4
4	Uplink frequency	4
4	Uplink data rate	4
1	Power consumption	6
1	Round-trip light time	5
1	Time stamp	6
	Total bytes	**81**
	Data rate	**16.2**

Table 5.36: Navigations data rate per second.

Amount	Subcomponent Data	# of Digits
3	Position	6
3	Velocity	6
3	Acceleration	6
1	Power consumption	6
1	Time stamp	6
	Total bytes	**66**
	Data rate	**66**

Table 5.37: Mechanics data rate per second.

Amount	Subcomponent Data	# of Digits
1	Solar panels	1
1	Docking	1
1	Antenna	1
1	Time stamp	6
	Total bytes	**9**
	Data rate	**9**

Summing all these rates, a total of 446 bytes are generated every second of housekeeping data. Multiplying this value by the seconds of communications eclipse, 1,468,800 seconds (17 days), it was determined that a total of 655.1 megabyte storage space is required. The data can then be transmitted with a minimum downlink data rate of 200 kbps, as determined in section 5.5, over a period of approximately eight hours after the eclipse period. Adhering to the binary formats for memory, a radiation-hardened hard drive of 1,024 megabytes is required.

Lander Memory

The determination of the memory for the lander was obtained in the same fashion, except for the fact that more data-intensive payload is in use during the period the lander is active. From the Mid-Term Report [1], the descent imager was found to be the scaling factor for the lander memory. Its images had to be saved during descent, and since they could not directly be sent due to constraints of the communications system, a memory of 2,048 megabytes was allocated [1]. This value was compared to the housekeeping data on the lander and its corresponding eclipse. A 52.2 hour eclipse per 5.78 days, as determined in section 5.5, was found to be constraining for the lander. However, since many of the housekeeping data is similar to that of the tug, not all tables will be provided to prevent repetition. Instead, Table 5.38 shows the changes from tug to lander.

Table 5.38: Changes in amounts of subcomponents providing data.

Subsystem	Subcomponent Data	Tug Amount	Lander Amount
Propulsion	Pressure in tanks	1	5
	Thrust level	2	4
Thermal	Active cooling	2	0
Power	Watt per solar array	28	0
	Watthour per battery	80	50
ADCS	Thruster levels	48	40
	Spin rates of wheels	4	0
	Tank pressure	6	0
Communications	Downlink frequency	4	1
	Uplink frequency	4	1
	Downlink data rate	4	1
	Uplink data rate	4	1

Note that the 'pressure in tanks' differs between tug and lander, but this is because some tanks are shared, whereas others are not. In the case of the tug, no tanks are shared, whereas in the lander, all tanks are shared. All five were grouped under propulsion.

Coming back to the memory for the lander, based on the changes from Table 5.38 a data rate of 357.5 bytes per second was obtained. This comes down to approximately 67.2 megabytes of storage space if designed for the eclipse of 52.2 hours. As mentioned earlier, 2,048 megabytes was allocated to the lander, but at this point a change in design was made. Aforementioned memory was solely for the most consuming instrument, the descent imager, but did not take into account any housekeeping. So, since housekeeping data can be directly sent to Earth, designing such large main memory for the entire lander would not seem sensible. Any failure of memory would indicate a complete dependency on the direct communications, making it infeasible to transfer large data files due to data overflows.

Concluding, the spectrometer, infrared camera, on-board camera and descent imager will each have a memory of 2,048 megabytes of their own. Whenever there is a necessity to turn an instrument on, there is allocated memory to store. Whenever certain memory fails of an instrument, the lander's main computer will be used with 2,048 megabytes memory to prevent the loss of instrument data. This suffices for the housekeeping data, but also in case of failure of the memory for one of the individual payloads.

5.6.2 Verification & Validation

This section incorporates the verification and validation of the memory model, as well as the watchdog unit and multiple processors for redundancy.

Model Verification

The model used was a calculator for the different data volumes from the different subsystems. This volume was then divided by the frequency in order to obtain a rate per second. The values that have been checked in the model concern the megabytes per seconds, eclipse times in seconds and the total amount of megabytes. These values are shown in Table 5.39 where the significant number rule is adhered for the hand values.

Table 5.39: Model verification depicting deviation of values.

		Tool Values	Hand Values	Unit	Difference
Tug	Bytes per second	446	446	B/s	0.00%
	Eclipse time	1,468,800	1,468,800	s	0.00%
	Total bytes	655,084,800	655,000,000	bytes	0.01%
Lander	Bytes per second	357.53	357.5	B/s	0.00%
	Eclipse time	187,920	188,000	s	0.04%
	Total bytes	67,187,664	67,181,400	bytes	0.03%

Model Validation

Validating the model would require a proper source to prove that these memory values actually make sense. This implies the general memory for both tug and lander, but also the separate dedicated memory

modules for the payload. The resources used would be historical data from Mars missions comparing that similar module sizes are used with similar payload. Again, the analogy with the Curiosity mission is striking. Comparing to the values of the rover, it was found that its main memory is the size of 2,048 megabytes[21]. With this comparison, the size in megabytes was proven to be exactly the same. Note though that the size of memory can be anywhere in this range, a somewhat smaller or larger module would also be feasible. The aspect that primarily had to be validated was the order of magnitude of these sizes.

Product Verification

The third objective would be to verify that the memory modules actually store the data that was calculated. They were not chosen from a specific company, since this information is hardly available. This verification can be done with inspection by simply plugging the memory modules in the on-board computer whilst still in the testing facility. The cameras should then shoot the maximum amount of images and see whether these amounts comply with the intended value they should have according to the design. This would then prove that MTP-C&DH-TR02 and MTP-C&DH-LA02 are met.

Verifying the watchdog might be one of the most vital parts for the C&DH, since computer failure is a realistic risk and could give the mission a catastrophic turn. Therefore it should be certain that it resets the computer whenever the timer has not been reset. This method requires a somewhat more surprising approach, that is to load erroneous software on the computer. The processor fails to reset the timer and it can be verified whether the watchdog does indeed reset the system to be able to process commands again.

Thirdly, the RAD750 has to be verified. This choice of processor did not explicitly meet requirements MTP-C&DH-TR01 and MTP-C&DH-LA01, since solely the clock rate of the processor is known, not the data rate it can handle. Since it has been used in recent missions, it is most certain to work properly, but a test has to prove this. In this test, both maximum data rates have to be sent through the processor to see whether it can cope with the data.

Product Validation

Lastly, the validation of the three processors and memory modules was conducted. The idea of the three processors is to rule out any disagreements among the two processors. Validation was done in a similar manner as the watchdog unit. A proposal to check the set-up is by running data through the system in a hardware-in-the-loop configuration. With proposed 'fake' data to both processors, the third should turn on and supply a verification for one of the two values. Another argument for this method of ruling out the disagreements, is the implementation in the Space Shuttle [63]. Although that configuration used a total of five processors, with the fifth being the checker, it is still based on the same idea.

The multiple amount of memory modules is to provide enough redundancy to prevent a memory error. Validating this could be done by unplugging a memory module when shooting images with the payload, whereafter it should automatically switch to the main memory module. If not, and images are not saved hereafter, the memory is not properly designed and should be reconfigured to a working, redundant configuration.

5.7 Power

The Electrical Power System (EPS) was designed by using a program especially created for this mission. This chapter describes the design process of this subsystem and highlights the reasons for the different design choices. Furthermore, the interaction of the tug and the lander EPS with the other subsystems is presented by means of Electrical Block Diagrams (EBDs). The design of the main components like solar arrays and batteries is also explained in detail. Finally, the model used to size the components of the power system and the actual product were verified and validated.

5.7.1 Detailed Design

The sizing of the EPS was mainly performed separately for the tug and the lander, as they consist of different components. However, during the sizing of the tug's EPS, the power requirements of the lander had to be taken into account, since its secondary batteries have to be charged before detachment, as

[21] URL `https://mars.jpl.nasa.gov/msl/mission/rover/brains/` [cited: 13 June 2017]

explained in chapter 3. In the Mid-Term Report, photovoltaics and batteries were chosen after a detailed trade-off which took into account the most important criteria for the mission considered [1].

Tug

Initially, the EPS of the tug configuration was chosen. It is depicted in Figure 5.33. This figure shows the EBD, a graphical representation of the electrical interfacing between subsystems, which also shows the equipment used by the EPS to generate, control and distribute the power of the spacecraft. To regulate the power output of the solar arrays, a shunt voltage limiter is added. It avoids short circuits and it prevents the current to run from the batteries back to the panels during eclipse times. The inclusion of a charge control unit regulates the rate at which electric current is added or drawn from the batteries. It also prevents over- and deep charging of the batteries, which increases their life time and reduces risks. The discharge bypass unit equalises and balances the batteries during charging. If a battery has a higher charge level, the bypass regulator lets some of the current flow so it receives fewer amp-hours, while the other batteries still get 100%. Once the input power is regulated, the Power Control Unit (PCU) distributes the electric current over the different subsystems. Overall, the tug consists of a larger amount of subsystems compared to the lander due to the greater number of functions it has to perform.

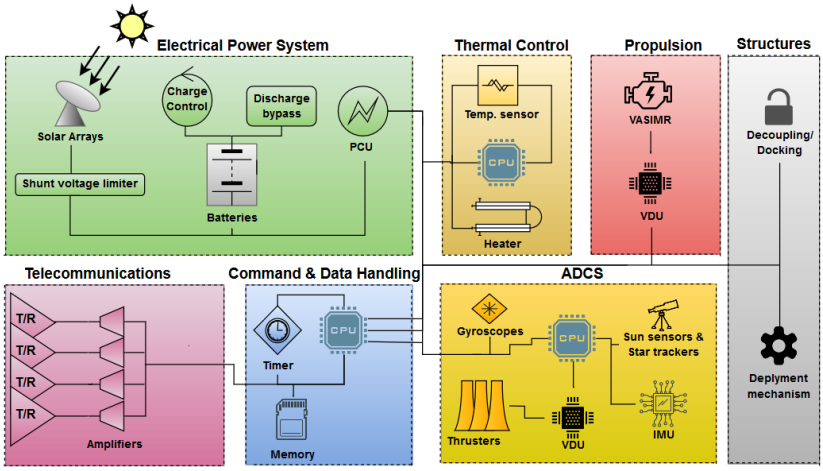

Figure 5.33: EBD of transportation tug.

Solar arrays and batteries were sized simultaneously because batteries must be able to deliver power during eclipse time t_e. In order to do that, they have to be charged during the sunlight time t_{sun} by the solar arrays. This means that the power delivery by the solar array is strictly related to the energy requirements of the batteries. The sizing procedure followed this logic. It was decided to size for three different travel situations, each being one of three main mission segments: Earth escape, Earth-to-Mars transfer and Mars capture. This was done because of the varying power availability and subsystem power requirements throughout the mission. The segment's characteristics are shown in Table 5.40. To give the reader an understanding of how these characteristics affected the power subsystem sizing, numerical values that were influenced in the sizing equations were included in the table.

Table 5.40: Characteristics of the three main mission segments, crucial for the sizing of the EPS.

	Earth Escape	Earth-to-Mars Transfer	Mars Capture	Values Influenced
Presence of eclipse times	Yes	No	Yes	t_{sun}, t_e
43% energy density	No	Yes	Yes	P_{sp}, P_δ
Charging of lander's batteries	No	No	Yes	P_{avg}, P_{SA}

For the first and third mission segments, it was decided to size the power subsystem for the orbit with the largest t_e. This decision was made after an iterative testing process. This consisted in obtaining orbital data, t_e and t_{sun} from the navigation department for a set of orbits. It was noticed that varying t_{sun} resulted in minor changes in the sizing of the power subsystem, while a different t_e had the largest impact. Regarding the second mission segment, sunlight is always present, therefore battery sizing was

not applicable and t_{sun} was considered equal to the full transfer time. The orbits chosen for sizing the EPS are shown in Table 5.41.

Table 5.41: EPS sizing orbits for the different mission segments.

	Earth Escape	Earth-to-Mars Transfer	Mars Capture	Unit
t_{sun}	2,450.29	17,520	2,978.20	hours
t_e	10.14	N.A.	4.00	hours

Once the segments' characteristics and defining orbits were identified, the last step before sizing the solar arrays and batteries was to gather power requirements of all tug subsystems. Operational and stand-by power consumption of each subsystem were collected for each mission segment as shown in Table 2.2. Before the actual sizing of the solar arrays, experimental GaAs/GaInP MJ cells were chosen as type due to their high performance characteristics [64]. The exact amount of junctions used was not fixed as this depends on the actual photovoltaics level of development in 2033. Solar arrays could then be sized with Equation 5.75 and Equation 5.76 for the single critical orbit per mission segment shown in Table 5.41. In both equations, a specific power P_{sp} of 250 W/kg and power density P_δ of 400W/m^2 were chosen based on reference data on experimental GaAs/GaInP MJ arrays and performance trends[22] [64]. These references provide solar array and single cell data separately. The solar array specifications were selected and they were assumed to include the inherent degradation I_d, which takes into account the inefficiencies of an assembled solar array. Furthermore, based on a 0.5 % MJ array degradation per year and a relatively short mission lifetime, the lifetime degradation L_d value resulted in being higher than 99.9%, indicating a nearly non-existent solar array performance decrease throughout the mission [4]. At this design stage, feasibility to point solar panels in order to gather rays at 90° was assumed by introducing the use of proven alignment mechanisms known as SADM[23]. Afterwards, the solar array power P_{SA} was calculated. It includes the power that must be delivered by the solar arrays in order to maintain the other subsystems functional during sunlight time and to charge the batteries in view of the eclipse time.

$$P_{SA} = \frac{P_{avg}\left(\frac{t_{sun}}{\eta_{sun}} + \frac{t_e}{\eta_e}\right)}{t_{sun}} \tag{5.73}$$

$$P_{avg} = \frac{\sum_{i=1}^{n}\left(P_{req,on_i}\, t_{on} + P_{req,stand-by_i}\, t_{stand-by}\right)}{t_{sun} + t_e} \tag{5.74}$$

P_{SA} was determined using Equation 5.73, where η_{sun} and η_e were given values of 0.85 and 0.65, respectively, based on reference data [57]. Considering the Sun SOI segment, as it does not involve any eclipse ($t_e = 0$), Equation 5.73 becomes independent of t_{sun} (since it is both multiplied and divided by this value) in this segment, meaning t_{sun} does not influence the sizing of solar arrays. Also, batteries could not be sized for this segment because of the absent eclipse times. It was assumed that the batteries are used for peak power requirements only, which is not a critical sizing condition. Looking back at Equation 5.73, P_{avg} is the average power to be delivered by the EPS to all tug subsystems during the critical orbit and it was determined using Equation 5.74. In this equation, the energy required to run each subsystem during the critical orbit was determined based on the subsystem's required power while operating, $P_{req,on}$, and their required power during stand-by, $P_{req,stand-by}$. Furthermore, it includes the time per orbit during which each specific subsystem is operating or in stand-by mode, t_{on} and $t_{stand-by}$, respectively. The required power values and operating or stand-by times are given in Table 2.2. Eventually, three sets of results were obtained, each including a m_{SA} and A_{SA} value, one for each mission segment. The values of choice were presented in chapter 2. These correspond to the worst-case scenario, thus they are the maximum values found.

[22] URL `https://fagerstrom.engineering/?p=120` [cited: 13 June 2017]

[23] URL `http://www.esa.int/Our_Activities/Space_Engineering_Technology/Mechanisms/Solar_Array_Drive_Mechanisms_SADM` [cited: 19 June 2017]

$$m_{SA} = \frac{P_{SA}}{P_{sp}} \tag{5.75}$$

$$A_{SA} = \frac{P_{SA}}{P_{\delta}} \tag{5.76}$$

The next step concerned the sizing of batteries. First, the Li-Ion type was chosen given its relatively high performance characteristics in terms of specific energy and energy density and current development focus from the industry. Other battery types, such as Li-poly and AgO-Zn, have similar or higher performance, but Li-Ion was preferred because of its large scale proven application on the ISS, which can somewhat be compared to the Phobos mission from a size perspective[24]. After this choice, sizing could be performed. The two sizing quantities of interest, in this case, are the battery mass m_{bat} and the battery volume V_{bat}. These values were determined using Equation 5.77 and Equation 5.78, respectively. Research was conducted on the specific energy E_{sp} and energy density E_{δ} of batteries and values of 300 Wh/kg and 400 Wh/l were chosen, respectively, based on current Li-Ion battery data and future trends of their performance[25] [65]. The eclipse energy E_e is found using Equation 5.79 and it is the energy that batteries must be able to store in order to distribute the average power among the tug subsystems during the eclipse time. The Depth of Discharge (DOD) was chosen as high as 80 % because the tug batteries have to go through a relatively limited amount of cycles throughout the mission, 571 to be exact. Compared to the Phobos mission, the ISS batteries go through 60,000 cycles[24]. The battery discharge efficiency η_{BAT} includes battery efficiency and discharge efficiency, and was chosen to be 90 % from reference data [57]. Once again, three sets of results were obtained following the solar array sizing approach. The maximum values corresponding to the worst-case scenario were chosen and presented in chapter 2. The actual amount of batteries to be used on the tug was estimated in collaboration with the C&DH department and was chosen to be 80.

$$m_{bat} = \frac{E_e}{E_{sp}} \tag{5.77}$$

$$V_{bat} = \frac{E_e}{E_{\delta}} \tag{5.78}$$

$$E_e = \frac{P_{avg}\, t_e}{DOD\, \eta_{BAT}} \tag{5.79}$$

The final step involved is the sizing of the tug's Power Management & Distribution (PMD) and EPS. The PMD includes controllers required to regulate the power level and wiring for power distribution throughout the tug's subsystems. In this case, sizing only concerns mass values, as volumes and placement of the PMD is too detailed to be determined in this design phase due to time constraints. The EPS could be sized using Equation 5.80, where m_{EPS} is the electrical power system mass. Based on reference data, the PMD mass m_{PMD} was evaluated using Equation 5.81 [57]. Therefore, by substituting m_{PMD} with $0.33 m_{EPS}$ into Equation 5.80, the EPS could be obtained using the previously determined critical solar array and battery sizing values. Once m_{EPS} was obtained, m_{PMD} could be calculated using Equation 5.81.

$$m_{EPS} = m_{SA} + m_{bat} + m_{PMD} \tag{5.80}$$

$$m_{PMD} = 0.33\, m_{EPS} \tag{5.81}$$

Regarding the tug, feasibility is questionable because the final battery mass value was found to be very high, see chapter 2, and no mission for comparison exists. An alternative power source to aid batteries during eclipse time, or even used to substitute solar arrays and batteries was tested in the power tool. The remaining feasible power source that could be tested was the Radioisotope Thermoelectric Generator (RTG) technology. Having a set of combinations of solar arrays/batteries/RTGs resulted in expensive systems, due to the high cost of nuclear technology, but showed EPS mass improvements of a couple of thousands kg. On the other hand, it was decided to maintain the current developed system (solar arrays and batteries) due to the two following reasons. First, RTGs were ruled out after a thorough trade-off carried out in the Mid-Term Report [1]. Second, in order to meet the tug power requirements, more than

[24] URL `https://www.nasaspaceflight.com/2017/01/spacewalkers-upgrading-iss-batteries/` [cited: 13 June 2017]
[25] URL `http://ir.baystreet.ca/article.aspx?id=151` [cited: 13 June 2017]

100 RTGs would have to be used in all the tested power configurations. This is not feasible because of launch restrictions (RTGs cannot be folded like solar arrays).

The most important results concerning the tug power system are presented in Table 5.42.

Roll-Out Solar Array Deploy Mechanism

NASA puts priority on sustainability when developing new technologies. Taking a step away from chemical propulsion techniques, future deep space missions will be driven by electrical propulsion systems using renewable energy sources like the Sun. However, bringing large cargo like habitats or humans and their life support systems beyond Earth requires huge amounts of power. Therefore, up to this day flexible and deployable solar arrays are not commonly used for interplanetary travel. Reasons for that are the complicated deployment mechanisms which usually exceed the mass budgets and therefore lower the overall specific power W/kg of the photovoltaic system[26]. The solution that NASA's Space Technology Mission Directorate (STMD) worked out are high power, flexible solar arrays that are stronger, lighter and more storage efficient than current rigid solar arrays[27]. This new technology is called Roll-Out Solar Arrays, or short ROSA. As the name already suggests, ROSA is a new type of solar panel that rolls up around a shaft to form a compact cylinder for launch. Once in orbit, during the first stage of the deployment, the solar wings are deployed via strain energy similar to a spring, where the shafts form the outer structure. In the second stage, the panels roll off the shafts to form the final wing. The solar cells get structural support by a lightweight mesh material[26]. Figure 5.34 to Figure 5.36 further represent the deployment and roll-out procedure. This new technology is not only more storage efficient and therefore cost saving, but due to its simple mechanism it also is more reliable [66]. For excessive power levels as they are required for this mission, multiple ROSAs are required [66]. To achieve a constant power generation of 476,054 W, 28 ROSAs were chosen, each with an area of around 100 m^2 that form two solar wings with a total area of 2,753 m^2.

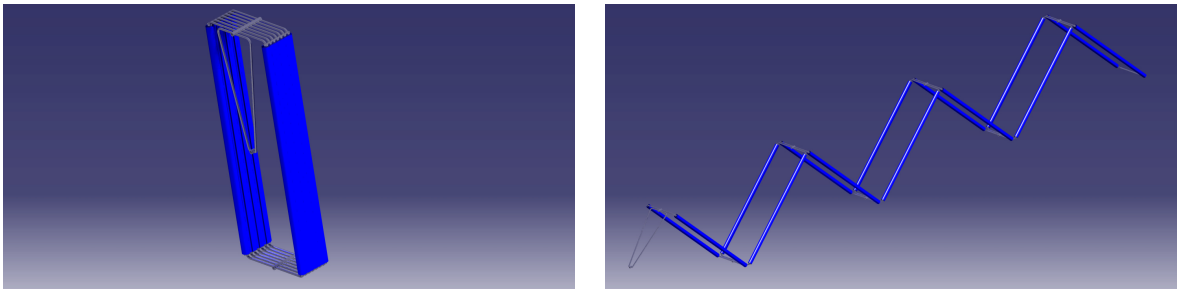

(a) Undeployed solar wing with folded arrays. (b) Partly deployed solar wing with folded arrays.

Figure 5.34: Deployment steps of folded solar arrays.

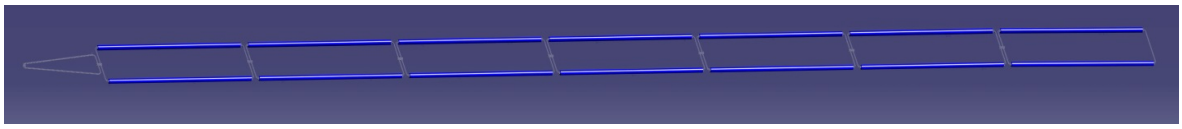

Figure 5.35: Deployed but folded solar arrays.

Lander

The EBD of the lander is depicted in Figure 5.37. When inspecting the figure and comparing it to the tug's EBD, it can be seen that the EPS for the lander purely relies on secondary batteries for power generation. The batteries are charged by the solar arrays just before the separation of the tug and lander.

[26] URL `https://www.nasa.gov/mission_pages/station/research/experiments/2139.html` [cited: 22 June 2017]

[27] URL `https://www.nasa.gov/feature/roll-out-solar-array-technology-benefits-for-nasa-commercial-sector` [cited: 8 June 2016]

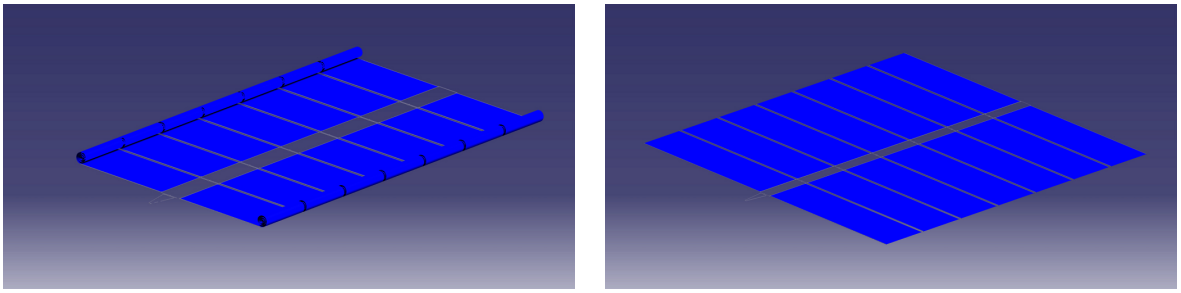

(a) Deployed solar wing with partly folded arrays. (b) Deployed solar wing with unfolded arrays.

Figure 5.36: Unfolding of solar arrays.

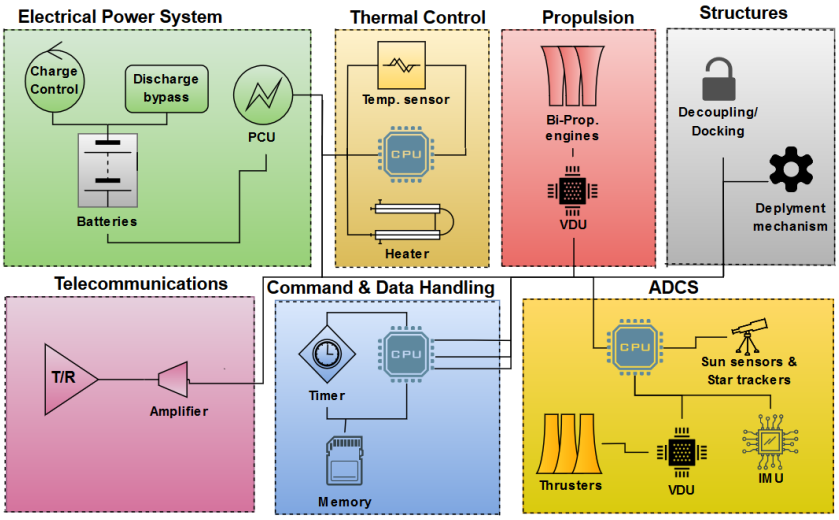

Figure 5.37: EBD of lander module.

Sizing the lander meant obtaining values for batteries, PMD and EPS. These components were sized for two segments during which the lander is detached from the tug, instead of focusing on the previously used mission segments. This is because, before detachment, the lander subsystems are not required to function actively. Both of these segments are part of Mars SOI: one is the pre-landing phase, which is the time between the detachment from the tug and the Phobos landing, and the second one is the Phobos staying phase, which includes the time spent by the lander on Phobos. The equations used in the sizing of batteries, PMD and EPS are the same as for the tug, except for Equation 5.79 where the DOD is not taken into account because the battery is not being recharged. Thus, E_e is calculated using Equation 5.84, where however, the power requirements for the subsystems are different, as the lander has diverse subsystems and performs different functions relative to the tug. This directly influences the P_{avg} value. These power requirements are shown in Table 2.3. Also, since the batteries cannot be recharged due to the absence of charging systems on the lander, the final mass and volume of the batteries is taken as the sum of the values found for the two segments, instead of the maximum one as in the tug sizing, as shown in Equation 5.82 and Equation 5.83. For the PMD and EPS, the total battery mass was taken into account as shown in Equation 5.85. The final sizing values were reported in chapter 2. Once again, the actual amount of batteries to be used on the lander was estimated in collaboration with the C&DH department and was chosen to be 50.

$$m_{bat} = M_{bat_{PLP}} + M_{bat_{PSP}} \tag{5.82}$$

$$V_{bat} = V_{bat_{PLP}} + V_{bat_{PSP}} \tag{5.83}$$

$$E_e = \frac{P_{avg}\, t_e}{\eta_{BAT}} \tag{5.84}$$

$$m_{EPS} = m_{bat} + m_{PMD} \tag{5.85}$$

All equations used for the sizing of the power subsystem were taken from [57]. However, a part of these equations underwent changes due to the specific sizing approach used for this mission.

The most important results concerning the lander power system are presented in Table 5.42.

5.7.2 Verification & Validation

This section incorporates the verification and validation of the solar array and battery sizing model as well as the product verification and validation of the type of solar cell, battery and deployment mechanism used for this mission.

Model Verification

The tool used to size solar arrays, batteries, PMD and EPS was verified by performing the following measures. Hand calculations ensured no flaws within the tool. The results from the tool were compared to the outcome of the hand calculations. A representation of this comparison is found in Table 5.42, where it can be seen that the difference between both results is $\leq 1\%$. This is due to rounding of numbers for hand calculations. Due to this very small deviation in numbers it can be concluded that this tool was verified.

Table 5.42: Comparison between tool values and hand calculated values, including their difference.

Quantity		Tool Values	Hand Values	Unit	Difference
Tug	m_{SA}	4,403.91	4,408.61	kg	0.11%
	A_{SA}	2,752.44	2,755.38	m^2	0.11%
	m_{bat}	18,893.66	18,892.26	kg	0.00%
	V_{bat}	14.17	14.17	m^3	0.00%
	m_{PMD}	11,474.92	11,476.55	kg	0.01%
Lander	m_{bat}	1,001.99	1,002.23	kg	0.02%
	V_{bat}	0.60	0.60	m^3	0.00%
	m_{PMD}	493.51	493.64	kg	0.03%

Model Validation

For the tool to be validated, first it had to be checked that its outcomes were useful for the design. This means outcomes had to include solar arrays, battery, PMD and EPS mass/area/volume values. These values were successfully delivered as presented in Table 5.42, thus validating part of the tool. Moreover, the equations used, even if customised for the current mission, are all based on actual sizing equations from reference methods [4], [57]. This last step proves that the tool is reliable as it is based on proven mathematical procedures. Based on the previous facts, it can be stated that the power sizing model was validated.

Product Verification

The requirements given to the EPS (Table D.6) were imposed by the other on-board subsystems. MTP-POW-TR01 states that at each moment of the mission, all electrical components of the mission have to be provided with sufficient power levels to ensure proper functioning of the entire system. This requires a continuous power generation of 404,269 W, which the system will be able to provide by using 2,752 m^2 of solar arrays. MTP-POW-TR03 states that the tug batteries need to have a capacity of 5,668,099 Wh, which was achieved by bringing on board 18,893.66 kg of batteries. MTP-POW-TR04 and MTP-POW-TR05 cannot be verified at this early design stage, since the power required by the docking and solar array deployment mechanisms was not determined yet. As stated under MTP-POW-LA01, the lander batteries need to have a capacity of 240,477 Wh, which was achieved by a battery mass of 1,001.99 kg. The model that sized the EPS took technical parameters from existing technologies. All except the DOD, which is determined to be extremely high due to the low amount of cycles the batteries must undergo. As mentioned in chapter 2, a similar type of Li-Ion batteries as recently installed on the ISS were used[24]. In terms of power generation, GaAs/GaInP MJ solar cells were chosen, which have been previously tested by Spectrolab. These tests have demonstrated the technical properties of the solar cells [64]. Using the acquired experience and sizing the photovoltaic system for the worst-case scenario as explained previously in this chapter, the conclusion is drawn that sufficient power levels will be reached

to support the entire system with enough power at every moment of the mission. Therefore, the product is verified.

Product Validation

The type of solar cells that are used for this mission have not yet been used for existing missions. However, Spectrolab has performed tests with the outcome that ultra-thin GaAs/GaInP MJ solar cells can successfully be implemented into future designs [64]. Furthermore, the size and mass of the solar arrays are comparable to the solar arrays attached to the ISS[24]. So the conclusion is drawn that these type of solar cells are a valid product to use for the application in this mission. In terms of batteries, the same Li-Ion batteries recently installed on the ISS were used[24]. However, to ensure a safe operating performance of the battery pack configuration, the batteries should undergo a set of validation test. Those could be performance testing, abuse testing and compliance testing [67]. Performance testing validates that the batteries will perform accordingly in the intended environment. It includes discharging, recharging, cycling and thermal testing. Abuse testing checks the systems performance when being used else than for its intended purpose. To mention just a few, it includes short circuits, overcharge and vibration testing. Lastly, compliance testing verifies whether the batteries meet certain standards like safety, transportation and electromagnetic radiation. These test are recommended for future engineers to be performed before the finalisation of this design. Once these tests are conducted and the batteries perform sufficiently, it can be said that this product is validated.

Chapter 6 Post-design Operations

This chapter outlines all activities to be performed by the team from the end of the Design Synthesis Exercise (DSE) to the start of the actual mission. Different aspects of these activities were analysed in order to have a clear view on the actual mission feasibility. Section 6.1 discusses all activities starting afher the end of the DSE up to the start of the production plan, section 6.2 deals with activities ranging from the start of the production plan to the mission beginning, section 6.3 aims at planning all the previous activities by placing them in a schedule and section 6.4 identifies how the different costs are associated to the different activities.

6.1 Project Design & Development Logic

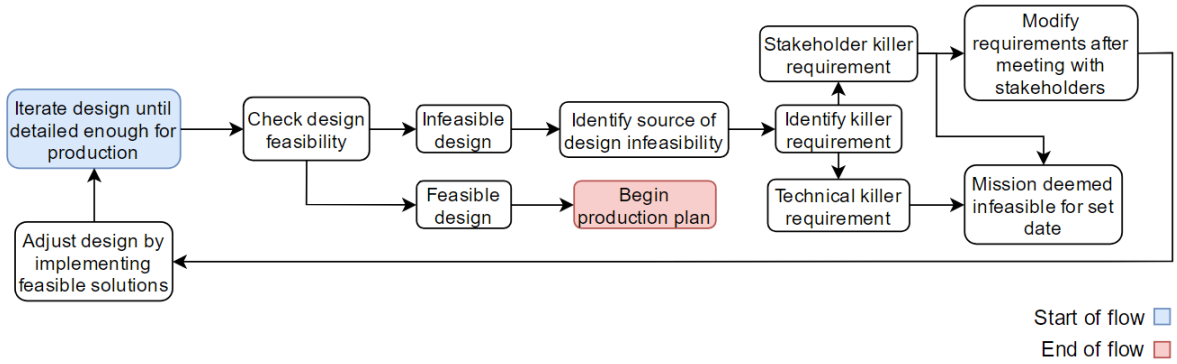

Figure 6.1: Project Design & Development Logic flow diagram of the PICARD.

The Project Design & Development (PD&D) Logic consists of a flow diagram, Figure 6.1, displaying activities to be performed by the design team between the end of the DSE and beginning of the PICARD production plan. Once this DSE is concluded, the design is still in a preliminary phase, meaning more iterations have to be performed to finalise it in view of production. After final verification and validation procedures, if the design is considered feasible, its production plan can be started. On the other hand, if the design is infeasible, the design team has to identify the source of the infeasibility, which is most likely related to a killer requirement. If the killer requirement is of technical nature, the design is deemed infeasible for the set date, which can be seen as an alternate ending to the flow. This occurs because the team would be forced to use a technology which makes the mission infeasible. For example, technology might still be in development, meaning risks would result in being too high, or technology might be too expensive. In case the killer requirement is a stakeholder requirement, a discussion with the stakeholders can be carried out hoping to come to an agreement which would change the killer requirement itself. Assuming it was agreed to change the requirement, the next and final step involves changing the design based on the new requirement and re-iterate through the whole procedure until the production plan is ready to be carried out.

6.2 Operations & Logistics

This section deals with all activities performed by the design team from the beginning of the PICARD production plan up to the launch phase.

6.2.1 Production Plan

The production plan, as illustrated in Figure 6.2, is a general plan indicating a time ordered outline of activities required to construct the product from its constituent parts [68]. The start of the production plan is indicated in the PD&D logic diagram, Figure 6.1, as the completion of a preliminary design. From this design a preliminary investigation for required subsystem components can be performed, simultaneously with the development of a more detailed version of the design. When the preliminary component investigation is performed, a first search for suppliers should be performed to enable outsourcing of manufacturing to external experts or partners. In the meanwhile, the detailed design will lead to a more thorough and definite investigation of parts required for assembly. This investigation involves preparing

the engineering data required for part production, e.g. material and part specifications. The found suppliers are then updated with this information [4].

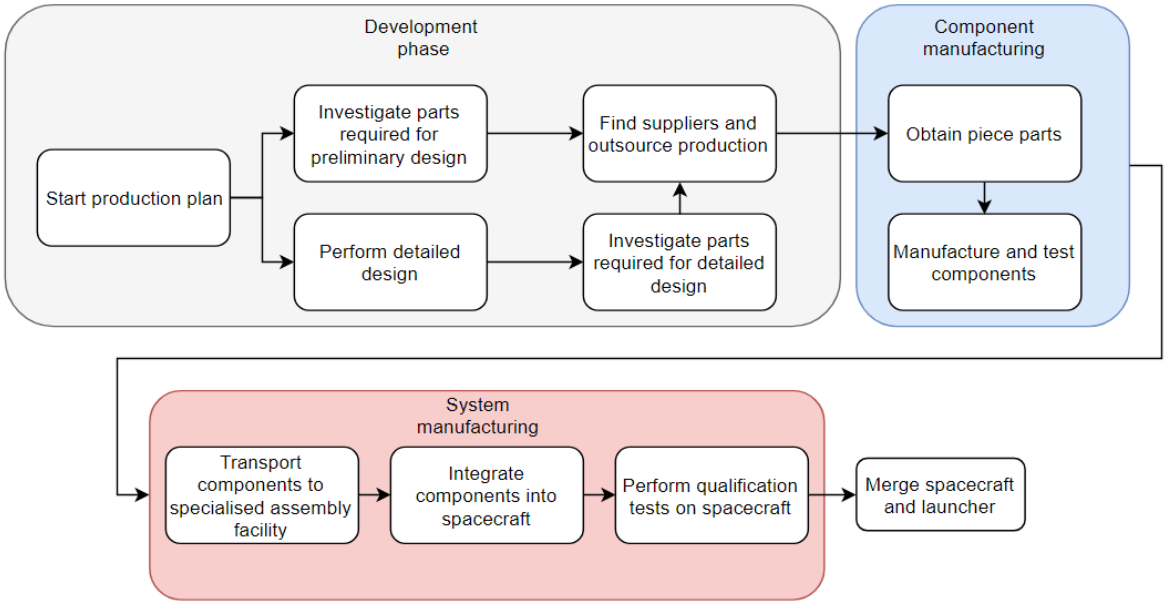

Figure 6.2: Production plan of the PICARD.

Next, the manufacturers will start production of the required components, which includes manufacture planning, parts procurement and testing, component assembly, and component acceptance testing. Hereafter delivery to the spacecraft assembly facility will take place [4].

Delivery of these components to the spacecraft assembly facility can prove difficult due to the size or frailness of some components such as fuel tanks or solar panels. For this reason different transportation possibilities should be considered to enable transport for all main components of the spacecraft. To tackle this problem, NASA acquired specialised methods of transportation for heavy and unusual payloads, e.g. the Super Guppy cargo aeroplane. This aircraft is capable of carrying anything with dimensions up to 7.62 m diameter and 33.83 m in length. The maximum payload weight capacity is 20.4 tonnes[1]. These specifications enable every single component to be transported when it comes to size and volume, since the mass and volume budget and mass estimations during the detailed design show that no single component exceeds these specifications. When weather or other circumstances do not permit air transportation, or when it is simply not necessary to have such a high capacity, other transportation methods should be used. For this reason cargo trucks or modified cargo trucks are available. These cargo trucks can carry large weights, and can even include cranes to load-unload the cargo themselves [69]. These cargo trucks are limited in diameter-wise dimensions though, meaning the largest components such as propellant tanks will have difficulties being transported. However, since NASA is a US governmental agency, there is some flexibility towards transporting large objects on public roads[2].

After assembly and integration of the spacecraft, the spacecraft has to be qualified as a whole. This is done by steps explained in Table 6.1, as found in [4]. Loading of e.g. propellant and batteries for launch are usually done when the spacecraft is already mounted on the launcher. This is the last step in production of the spacecraft.

[1] URL `https://jsc-aircraft-ops.jsc.nasa.gov/guppy/aircraftspecifics.html` [cited: 16 June 2017]

[2] URL `http://www.dailymail.co.uk/travel/travel_news/article-4540604/The-biggest-things-moved-road-revealed.html` [cited: 16 June 2017]

Table 6.1: Steps in the design of a spacecraft qualification program, as taken from SMAD [4].

1. Identify Spacecraft and Payload Functions	Test each spacecraft and payload function for proper operation. Identify the top functional requirements of the spacecraft. In the top system specification, obtain subsystem functions from the subsystem specifications.
2. Identify Environments	Environments for transportation and storage, launch, and orbit include vibration, shock, temperature, vacuum and radiation.
3. Correlate Functions and Environments	During transportation the spacecraft is shut down, although sensitive components may be powered. During launch, some equipment will be in standby and some will be operating. Test the operating equipment during spacecraft vibration and check all modes of on-orbit operation.
4. Identify Main Configurations	Include boost configuration and one or more orbital configurations.
5. Devise Functional Tests for each Major Configuration	Test each function appropriate to a particular configuration, including all equipment and software.
6. Lay Out the Sequence of Functional Tests and Environmental Exposures	
7. Identify Span Times and Special Facility Requirements	

6.2.2 Pre-launch Operations

Pre-launch operations include all activities coming after testing the spacecraft up to and including transportation and placement of the launcher and spacecraft on the launch pad. These are crucial activities for the mission feasibility and are verified to the highest possible extent in this text. The flow of activities in chronological order is depicted in Figure 6.3.

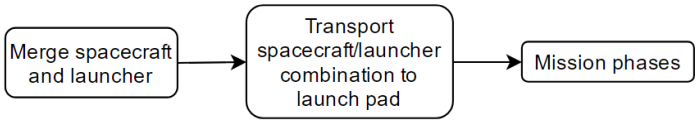

Figure 6.3: Pre-launch operations flow diagram of the PICARD.

Once the spacecraft passes all relevant tests, it must either be placed in the launcher or transported to the launch pad. For relatively large space vehicles such as the PICARD, the first choice is the most common one[3]. Initially, fairing encapsulation procedures are applied to the spacecraft. This involves lifting the spacecraft with cranes and enclosing it within the fairing before connecting it to the full launcher [70]. It is considered feasible to lift the PICARD with no fuel on-board, as its total dry mass is 52,613 kg and some cranes can reach 70,000 kg capacity, since they have to be able to move rocket parts for assembly too[4]. Moreover, since it was chosen to have two separate launches, the total PICARD mass is not handled at once, but it is split into two parts, making it even easier for the cranes. In the meantime, the launcher is assembled and then the spacecraft is merged. This can be done using a horizontal or vertical assembly approach. As this is a NASA mission, a vertical assembly approach is used since this is the organisations common procedure [71].

Next the launcher-spacecraft combination has to be transported to the launch site. This may be an issue as the wet mass of the spacecraft is 91,989 kg (which is planned to be split in two launches) and the SLS Block 2 mass is 2,948,350 kg [11] for a total of less than 3,040,340 kg liftoff mass. Prior to transportation, spacecraft and launcher have to be placed vertically on a Mobile Launcher Platform

[3]URL `http://www.savethelut.org/MLDocs/ML_History.html` [cited: 16 June 2017]
[4]URL `http://www.assemblymag.com/articles/92586-crane-lifts-spacecraft-to-new-heights` [cited: 16 June 2017]

(MLB). The MLB should be able to withstand these loads as it was originally designed to carry the ready-for-liftoff Saturn V which has a mass of 2,800,000 kg[5] (all these considerations are made not taking into account the service structure). In case the MLB is not able to withstand the loads, minor reinforcements are needed, since it can already carry 92 % of the total weight and the actual spacecraft mass will be lowered due to the separate launches. The final consideration concerns the feasibility of transporting all previous equipment to the launch pad. This can be done with the heavy duty crawler transporter, a vehicle capable of carrying more than 5,715,264 kg [72]. As its carrying capacity is much larger than the launch mass of the Phobos mission, this set of operations is considered feasible.

The assembly and launch site of choice is John F. Kennedy Space Center due to its appropriate and specialised infrastructure to launch the SLS[6]. Another benefit of using this launch site is the possibility to use the more beneficial west-east orbit (due to its coastal location), giving the launcher an extra boost[7].

6.3 Project Gantt Chart

The post-DSE activities and processes mentioned in section 6.2 are crucial to the completion and realism of the mission: they contain design iteration steps, design approval, production and launch steps. The manufacturing and launch schedule were estimated according to general estimations used for space mission manufacturing [4]. Design iteration and engineering data preparation scheduling was estimated using similarly large scale space missions[8] [9]. It should be noted that the last step, the launch, happens on September 31 2028, matching the last launch opportunity available for completing the mission and arriving on Phobos before 2033. This last launch opportunity was selected based on the time required for further development and manufacturing, as not to constrain the schedule to an impossible extent.

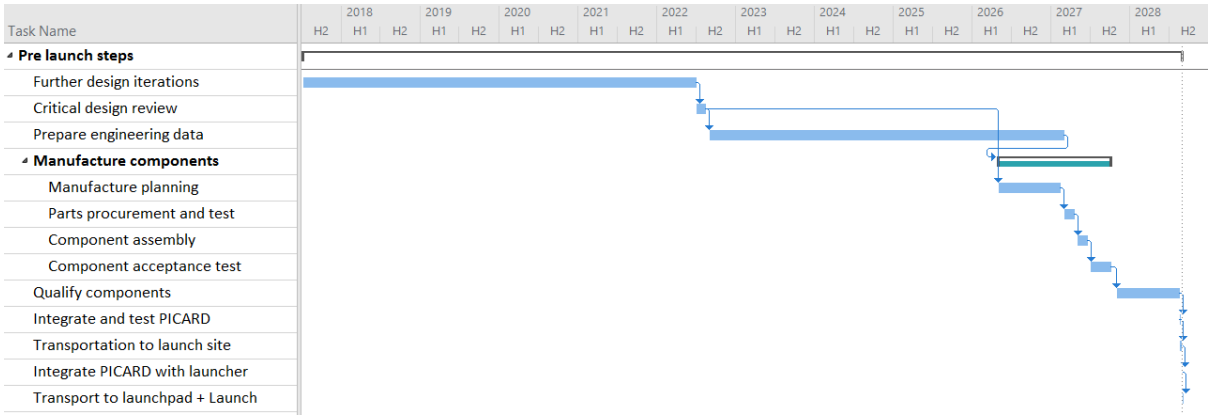

Figure 6.4: Project Gantt chart.

6.4 Cost Breakdown

This section elaborates on the cost breakdown of the mission and supports this elaboration by a Cost Breakdown Structure (CBS), represented in Figure 6.5. A CBS shows all elements that will form a part of the available budget and must therefore be complete to provide a right estimation. The CBS shown below splits the mission into three big segments: manufacturing, logistics and operations, but does not differentiate between tug and lander. These three segments provide a complete picture of how the budget should be divided. Note that Figure 6.5 mentions wages or personnel. These costs should be interpreted as number of personnel multiplied by the wage multiplied by the amount of worked hours. The actual costs should be compared to the available budget, as presented in section 7.1.

[5] URL https://www.nasa.gov/audience/forstudents/5-8/features/nasa-knows/what-was-the-saturn-v-58.html [cited: 16 June 2017]
[6] URL https://www.nasa.gov/exploration/systems/ground/pad_b_flame_trench.html [cited: 20 June 2017]
[7] URL https://www.nasa.gov/centers/kennedy/launchingrockets/sites.html [cited: 16 June 2017]
[8] URL https://www.universetoday.com/123036/nasas-space-launch-system-passes-critical-design-review-drops-saturn-v-color- [cited: 16 June 2017]
[9] URL https://www.space.com/12085-nasa-space-shuttle-history-born.html [cited: 25 June 2017]

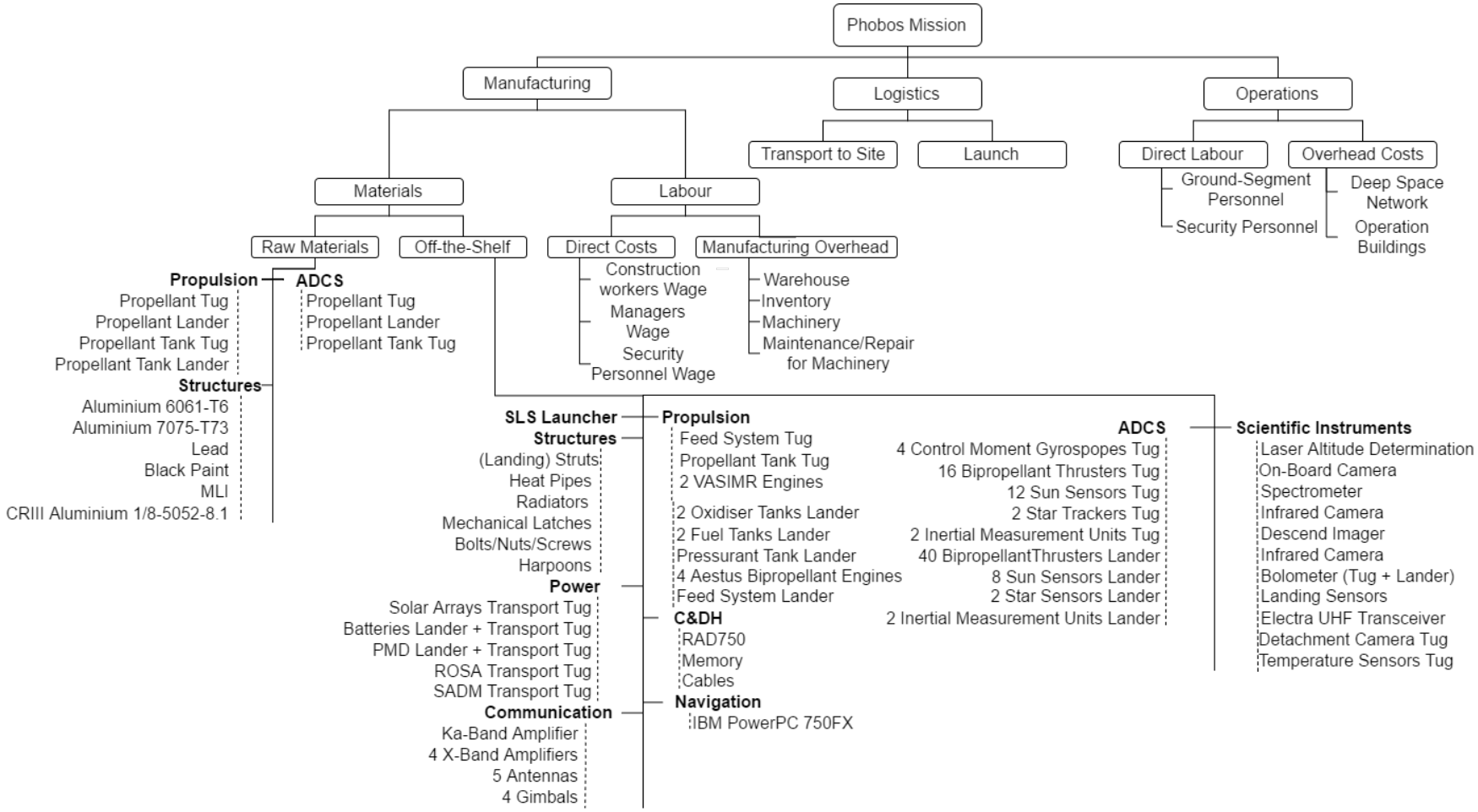

Figure 6.5: The CBS of the entire mission.

With the cost breakdown performed, a quantitative analysis was performed to determine the expected costs per subsystem. For this purpose, the subsystem development and the subsystem manufacturing were considered and any extra costs were included.

In determining the development cost two estimations were performed. This was done because these kind of estimations are generally not representative of the cost on their own, but when multiple estimations are performed the estimation gets closer and closer to the actual cost. Initially the development cost was estimated using a statistical approach, regressing between reference missions to find the cost per kilogram of each subsystem [4]. With this regression a subsystem development cost was determined based on the mass budget. A total development cost of $6.4 bn (billion) is found at this point.

Another development cost estimation was also based on reference data[10]. Again, a regression analysis was performed, this time not based on subsystems, but on complete reference spacecraft. In this case, the development cost of the PICARD was calculated based on the mass of the tug and lander. It was estimated to be $12.8 bn, as opposed to $6.4 bn found from the approach focusing on subsystems. The actual value of the development cost is expected to be within the $6.4-12.8 bn range. For this reason the average was used to scale the individual subsystem development costs using the same percentage-wise distribution.

Furthermore, the TRL of the individual subsystems was taken into account as well in the development cost estimation. A percentage was added based on Table 6.2 [5]. This percentage was included because the TRL level can significantly influence the development costs due to a more extensive verification and validation process including tests. For example, the propulsion system uses engines with a TRL of five and therefore a percentage of 15 % was added to the subsystem development cost. Based on this, a total added cost due to TRL level was estimated $0.6 bn which resulted in a total development cost of $6.3 bn.

Table 6.2: Added development costs based on technology readiness [5].

Technology Readiness Level	Definition of Space Readiness States	Added Cost [%]
1	Basic principle observed	≥25
2	Conceptual design formulated	≥25
3	Conceptual design tested	20-25
4	Critical function demonstrated	15-20
5	Breadboard model tested in environment	10-15
6	Engineering model tested in environment	≤10
7	Engineering model tested in space	≤10
8	Fully operational	≤5

Operation and tracking costs are expected to be on the same level as those found in the Cassini mission[10]. The launch cost is taken to be $3.6 bn, since the number of launches required has doubled since the analysis performed in the Baseline Report to a total of two launches [6]. Note that the costs for launching the habitat are not included, as throughout this design process it was assumed that the habitat is already in the orbit at which docking with the tug and lander occurs. In this analysis transportation costs are included in the manufacturing costs, since this split up is usually only performed for international logistics[11].

At last, software costs were taken into account. In order to create an accurate cost estimation the COCOMO II software cost estimation tool was used[12]. This tool estimates software costs based on the Source Lines of Code (SLOC), which is the number of lines in a program. The SLOC was estimated to equal 1,093,868, which is the same number of lines as NASA's Orion spacecraft [73]. As Orion is a spacecraft intended to transport humans, its code will be more complex than the PICARD's software code. However the Orion is capable of performing unmanned flights as well, which makes it a suitable reference. This number was entered in the COCOMO II calculator, together with an estimation of

[10] URL `https://www.hq.nasa.gov/office/codeb/budget/LIFCY982.htm#ISS` [cited: 2 june 2017]
[11] URL `http://www.clresearch.com/research/detail.cfm?guid=BA3372D9-3048-79ED-9971-5B3CAA36FF37` [cited 20 June 2017]
[12] URL `http://csse.usc.edu/tools/cocomoii.php` [cited 20 June 2017]

labour rates at $120. For this input, the calculator determined both the software development cost and the acquisition cost. However as for the PICARD, the acquisition cost is almost negligible and the development cost is based on creating a completely new operating system - while in reality parts of older software can be reused or modified - it was decided to only take into account the software development cost. This overestimated development cost compensates the neglected acquisition costs. In total, this came to $ 136,455,474.

Manufacturing costs are based on previously determined costs, combined with the estimated total monetary budget. These estimated manufacturing costs are then divided among subsystems using again a statistical regression between reference missions [4]. This step, together with the above mentioned estimates, is presented in Table 6.3.

The total budget is divided among subsystems and the additional costs. The subsystem costs are determined to be a total of $ 10.6 bn, as shown in Table 6.4. Here, the individual total cost including development and manufacturing cost per subsystem is also presented. One final note to make is that all these cost estimates are an upper estimation, as to prove the project fits within the allocated budget of $ 15 bn. A lower estimation would be the presented results minus 10%, due to the current TRL of the mission and spacecraft.

Table 6.3: Subsystem cost estimation [4], [6].

Development Cost			**Manufacturing Cost**			**Additional Cost**	
Subsystem	%	Cost [bn$]	Subsystem	%	Cost [bn$]	Additions	Cost [bn$]
Structures	3.3	0.206	Structures	12.3	0.507	Operating	0.736
Thermal	0.3	0.021	Thermal	15.0	0.621	Tracking	0.054
ADCS	19.1	1.209	ADCS	19.8	0.820	Launch	3.600
Power	24.1	1.524	Power	17.1	0.706	Software	0.136
Propulsion	53.0	3.358	Propulsion	11.0	0.456	**Total**	**4.526**
C&DH	0.1	0.004	C&DH	9.9	0.410		
Communication	0.1	0.008	Communication	15.0	0.621		
Total	**100**	**6.331**	**Total**	**100**	**4.142**		

Table 6.4: Total subsystem Cost Breakdown.

Subsystems	Structures	Thermal	ADCS	Power	Propulsion	C&DH	Comm.	Extra	**Total**
Cost [bn$]	0.714	0.643	2.030	2.230	3.813	0.415	0.629	4.142	**15.000**
% of Total	4.8	4.3	13.5	14.9	25.4	2.8	4.2	30.18	**100**

[THIS PAGE WAS INTENTIONALLY LEFT BLANK]

Chapter 7 Market Analysis

A proper market analysis shows what position the design will have in the market and subsequently what influence the design will have on the market as to obtain an estimate of the allowable budget for further technical design. Firstly, an estimation of the budget available for a Mars exploration project is given in section 7.1. Secondly, influences the design has on further research or other market activities are determined in section 7.2. Lastly, potential fund raising sources are stated in section 7.3.

7.1 Financial Plan

When the available amount of money for a Mars exploration mission is to be estimated, a few things should be considered. First of all, all parties which could provide in the funding of such a mission have to be determined. Overall, for this kind of space missions only public funding can be considered. This is only for the budget estimation though, because private investors can be used to raise additional funds or discounts. The additional options can be found in section 7.3.

In terms of public funding, governmental instances from all over the world can be considered willing to provide money for a space project. For example, multiple space agencies provided different parts and funding for the ISS. However, the amount provided by non-US countries only contributes to 17 % of the total ISS budget [74]. For future projects a similar contribution is assumed to be representative when an international collaboration is formed. However, an international cooperation adds a complexity factor to the organisation. The gained budget following from an international collaboration does not add up to the increased complexity. Hence, when estimating the available budget for a Mars exploration mission it is assumed sufficient to only take the contribution formed by the US, through NASA, into account [75].

As of now the yearly NASA spending budget is \$19.1 bn, of which a total amount of \$8.5 bn is reserved for human space exploration [74]. The remaining amount can be further split up in parts funding the ISS, researching the Orion spacecraft, designing the SLS, Human Exploration and Operations Mission Directorate (HEOMD) Support & Research, Exploration Technology Development and finally new projects [74]. New projects consist of the Mars missions required to put humans on Mars and possible other projects. At this moment, NASA's budget is completely consumed without leaving room for new projects. However, the ISS project is planned to be decommissioned in 2024, with a possible extension to 2028. This would give a rise in budget for new projects of about \$4 bn [74]. Additionally, the budget for human space exploration can be assumed to grow annually. Most optimistic estimations state an annual rise of 2.5 % to the budget [74]. This would mean that by the year of 2033 human space exploration can expect a budget of around \$12.5 bn.

This implies that by 2033 human Mars project will have received a budget of \$74 bn. However, the Phobos mission is only one of multiple Mars missions. Hence, a rough estimate of the actual budget the *Boots on Phobos* mission will have received by 2033 is \$15.1 bn, 20 % of the total budget, as estimated in Pathways to Exploration Rationales and Approaches for a U.S. Program of Human Space Exploration [74].

7.2 Market Shift

The main assumption made when evaluating markets is that the lander safely lands on Phobos and the overall mission is thus successful. Due to this success, a shift in the current markets will be set into motion. The change in current markets will be evaluated per topic. Each element addresses a different market, the expected changes and the expected largest shareholders.

- **Interplanetary travel**: The market that will undergo the greatest change will probably be that of interplanetary travel systems. Up until now, space agencies have mostly been focusing on researching systems related to LEO spaceflight. However, once interplanetary human travel is proven feasible, general development for these kind of missions will likely experience an increase. This means that research into e.g. low-thrust-high-impulse propulsion will experience a raise. This will especially be the case for the VASIMR-engine, since the engine hasn't been proven yet for such a large scale mission. Also, the research in high efficiency batteries will be a main focus for the power department. The further development in these technologies will be very interesting for future interplanetary travel. If the Phobos mission is eventually executed, more research will be

put into these subjects during the design phase, with NASA being the main investor. Thus, the overall share in this market will be significant for NASA.

- **Launchers**: Since the launchers have to carry a significantly high-weight payload, further research will likely go into heavier, more capable launchers. This enables for example more and heavier equipment to be landed besides the habitat or to land equipment at other planets. This is mainly beneficial for large space agencies able to purchase or produce these large launchers[1].
- **Docking**: The more mass is transported with large configurations, the more docking will be required to assemble these configurations. This involves a significant amount of risk and time, making it attractive to increase the research in this topic. This could either be in the way of automation or docking strategies, having increasing time-effectiveness and safety, thus decreasing the risks and time related costs for all partnered space agencies.
- **Shielding of humans**: The current knowledge on humans in space with respect to radiation goes as far as the ISS and Moon travel. The first unmanned missions to Phobos are expected to acquire data on radiation levels, which shall be used to understand the influences on humans. Especially the knowledge on Van Allen belts will be particularly interesting, since the degradation of instruments and damage to humans has to be investigated for the travel time in these belts. A plan can subsequently be devised to shield the humans in future journeys to distant planets. This research can be used by other space agencies and companies, providing a potential boost in competition from the private sector towards manned interplanetary travel.

As mentioned, this mission will not only alter current markets, but also introduce new markets. Currently these markets are at this moment not or marginally existent with most research still being in the theoretical phase.

Next to the aforementioned technical market changes, also some changes in markets related to other aspects are expected. Note that this is aimed at the very distant future, where human landings on Phobos are reality.

- **Medical effects on humans**: Once the landing of humans becomes more realistic, more in-depth research will have to be performed. Humans staying on Phobos for longer periods will have a lot of medical and psychological needs. Since little is known about living on these planets, the market for this will be in a rise.
- **Achieving regular life**: This part is a continuation of the previous item, since it partly offers a solution. To make sure the astronauts adapt as quickly as possible, life should be able to continue as regularly as possible. Research into achieving this during long term missions is necessary to ensure humans are able to properly stay healthy both physically as mentally.

7.3 Potential Customers & Funding

So far, only NASA was considered as an investor as they are also the primary customer. However, companies or other space agencies may want to use the tug once it has proven its value during this mission to Phobos. There may also be additional funding from other programs to take a (micro)satellite as a secondary payload to Mars. The last source of potential funds is selling relay time.

7.3.1 Future Tug Users

The designed tug can place a 50 tonne payload in an orbit around Mars, near Phobos. This provides new capabilities to future large payloads to Mars, as the SLS block II can only launch 45 tonnes into Mars transfer orbit. From the 45 tonnes a portion would still have to be used for orbit insertion around Mars. Using the SLS Block II to launch something directly into Mars transfer orbit requires only one launcher though, compared to the two launches it requires to use the tug, because one launch is needed for the tug and one for the payload.

The first and most obvious potential user is NASA itself. They may reuse the design of the tug in future missions to Mars, saving development costs, risks and time on those missions. The tug design could also be sold to other governments and companies that want to transport large objects to Mars orbit or even want to land on Mars.

[1] URL `https://www.nasa.gov/exploration/systems/sls/index.html` [cited: 04-05-2017]

7.3.2 Secondary Payloads

Besides using the entire tug for other missions, some extra funds can also be raised by bringing a secondary payload. This is divided into two types, which are bringing the scientific equipment on the tug itself and bringing a separate satellite to Mars.

Due to the large mass and power generation of the tug, having additional scientific instruments will have a relatively small impact. This could be used to gain additional funds from companies, other governments or other programmes.

CubeSats are gaining popularity, but interplanetary CubeSats still face two main problems, which are propulsion for course corrections and long range communications capabilities[2]. In combination with selling relay time discussed in subsection 7.3.3, CubeSats could be brought to Martian orbit. These spots can be sold to customers, allowing for cheaper scientific missions.

7.3.3 Relay Time

The last possible option to generate additional funds for the mission is selling relay time to other Mars missions. This can be combined very well with bringing secondary payloads, discussed in subsection 7.3.2. Also other missions could use the relay, reducing the mass for their communications subsystem. This can also be part of an extended lifetime mission after the habitat has been left, but there is still fuel to maintain the attitude and sufficient power generation capabilities by the solar panels.

[2]URL `http://www.planetary.org/blogs/guest-blogs/van-kane/0708-marco-planetary-cubesats.html` [cited 19 June 2017]

[THIS PAGE WAS INTENTIONALLY LEFT BLANK]

Chapter 8 RAMS

Space missions carry a sure level of uncertainty with them. In order to reduce the uncertainty and elevate the satisfaction of stakeholders, a Reliability, Availability, Maintainability and Safety (RAMS) analysis should be performed. As Mattew Lemke, Orion's manager of avionics, declares (2015) "The whole goal is reliability". RAMS includes four vital elements which are explained individually [76]:

- **Reliability**: "The probability that a system will perform in a satisfactory manner for a given period of time when used under specified operating conditions." (Verhagen, 2017, slide 38)
- **Availability**: "The degree, percent, or probability that a system will be ready or available when required for use." (Verhagen, 2017, slide 38)
- **Maintainability**: "The ease, accuracy, safety, and economy in the performance of maintenance actions." (Verhagen, 2017, slide 38)
- **Safety**: "The freedom from hazards to human and equipment." (Verhagen, 2017, slide 38)

These four items are interrelated according to a certain pattern. One element is able to influence the other, but this is not necessarily reversible. The relations between elements can be found in Figure 8.1. From the figure it is concluded that both reliability and maintainability are two key elements that influence the other two items. Hence, availability is the output of maintainability and reliability. Safety has a large influence on reliability and drives it to a certain extent. Maintainability directly impacts safety [76].

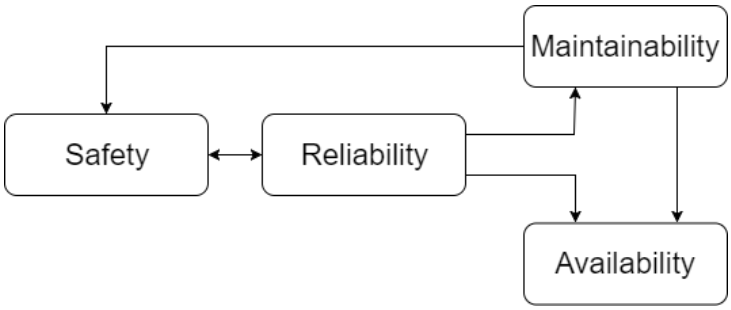

Figure 8.1: A representation of the interaction between all RAMS-elements.

8.1 Reliability

As for space missions reliability is inherently the most important aspect, it will be further investigated in this section. Failures are considered accordingly, as reliability is closely related to failure. The best way to make a spacecraft reliable is to avoid failures. This can be done by including design margins, by selecting proven parts (off-the-shelf) and by inspecting the spacecraft under production. The types of failure are listed below [76]:

- **Fatigue failures**: These failures are related to the amount of cycles the spacecraft has gone through.
- **Design failures**: These failures occur when the designers/engineers made a mistake in e.g. the internal stresses.
- **Manufacturing failures**: Failures like these occur when the properties of the actual product deviate from the design.

Fatigue failures are quite predictable. They occur after a certain amount of cycles and can thus be taken into consideration during the design process. Design and manufacturing failures can lead to catastrophic results or even failure of the mission. In further design iterations, these failures must be taken into account and design margins must be established. Table 8.1 shows the frequency of failures for several spacecraft components, from a study of 1,584 spacecraft launched between 1990 and 2009 from [4].

Table 8.1: Frequency of spacecraft failures, [4].

Spacecraft Component	Frequency of Failure
Telemetry Tracking and Command	18 %
Thrusters and Fuel	16 %
Solar Array (deployment and operating)	12 %
Attitude Control	11 %
Structures, Mechanisms and Thermal	11 %
Batteries	10 %
Electrical Distribution	10 %
Unknown	5 %
Control Processor	4 %
Payload Instrument	3 %

As reliability is such a big aspect of space missions, it must be taken into account in the design phases. The design stage is subsequently followed by 'Development and Fabrication', 'Integration and Test' and 'Operations'. In all these phases reliability must be incorporated. For the development and fabrication phase, compliance must be ensured with the hardware and software characteristics determined in the design phase. Furthermore, unanticipated failure behaviour must be reported. During integration and testing, the results are checked for conformance or deviation from the expected failure behaviour, with an analysis of the data for conformance with the failure rates. During mission operation data is reviewed for anomalies to incorporate those failures into future requirements [4].

One example of where reliability in spacecraft is of major importance is in software. Software largely influences the spacecraft operations. It can be found in the spacecraft, but also in the ground segment. In the past, there have been major launch and on-orbit failures due to a defect in the software. In general, there are two categories of software failures: deterministic and random failures. The former failures occur consistently for a given input data set. A disciplined software development process can be used to find and remove deterministic failures. In this process, requirements are formulated and validated, the design is analysed, the code is checked, peer reviews are conducted and testing is performed at multiple levels of integration. The latter failures are related to conditions external to the software. These occur because of a timing problem or another transient condition that make them difficult to reproduce. These failures can be addressed stochastically as software reliability cannot be predicted without empirical data, but can be measured [4].

In order to make the design as reliable as possible - and thus minimise the amount of failures - a design margin must be incorporated in all stages. Furthermore, the spacecraft must be able to continue operating after a failure occurred, which is also called fault tolerant [26]. This is related to system functions where design margins are inadequate. To apply fault tolerance in this spacecraft, redundant components are required. Besides, a way to detect failures and a transfer mechanism to switch to the redundant component are also required.

For this PICARD design, the general approach was to design for the worst scenario. As an example, the power subsystems was designed for the longest eclipse time possible. Therefore, most subsystems are oversized. Thus, the amount of failures are minimised. Besides, off-the-shelf technologies were used. This means the design choice is more reliable, as these technologies were used before. The on-board computer for orbit determination and control is an example of a reliable off-the-shelf component. Another off-the-shelf component is the decoupling mechanism to split the tug and lander. This decoupling mechanism is proven to function during the Rosetta mission and includes an emergency release if the primary decoupling mechanism does not function. The most redundant subsystem is ADCS, where all components (e.g. Sun sensors and thrusters) are doubled for redundancy. Another example of the redundancy philosophy can be found in the landing phase, where multiple anchoring systems are used to increase the reliability. To communicate with Earth, it is crucial to incorporate redundancy, as this subsystem fails frequently, see Table 8.1. The two main antennas work on a different frequency level and the spacecraft is equipped with a safety antenna to increase reliability. Furthermore, the payload memory is split from the other memory. At last, there are three identical processors, but one of them runs on a different software in case of deviation between the first two processors.

Table 8.2 shows the different subsystems and their respective failure rate. The 'ground systems development and operations' is related to the SLS launch system, found in [77]. Using Equation 8.1, the according reliability percentage was calculated as well, considering the above discussed redundancy philosophy. This reliability calculation considers the failure rates found in the appendix of [58], which is based on a series model and does not take into account redundancy. This reliability analysis takes into account the partial redundancy incorporated in the PICARD. Note that the VASIMR engine is not incorporated in this reliability calculation as the reliability of these engines is not known at this moment. In Equation 8.1, R equals the reliability, γ is the failure rate and t is the operational time (five years). Using all individual reliability percentages, the reliability of the complete system was determined to be 86.4%. Note that since γ equals the failure rate, $\frac{1}{\gamma}$ is the mean time between failures.

$$R = e^{-\gamma t} \tag{8.1}$$

Table 8.2: Spacecraft subsystem failure rate and reliability.

Subsystem	Failure Rate, Failures/Spacecraft/Year	Reliability [%]
Reaction Control System	0.0068	96.6
ADCS	0.0032	98.4
Ground Systems Development and Operations	0.0024	98.8
Electrical power system	0.0040	98.0
Mechanism	0.0029	98.6
Telemetry, Tracking and Control	0.0035	98.3
Thermal	0.0064	96.8
Result		**86.4**

8.2 Availability

The PICARD must be available throughout the entire mission duration. This mission duration differs for both tug and lander. The tug is required to bring the habitat and lander to Phobos and serve as a relay satellite, while the lander - after safely landing the habitat on Phobos - ends it mission after maintaining the habitat. Just like reliability, availability is closely linked to failures. To maximise the availability of the spacecraft, recoverable failures must be solved in a minimal amount of time. This can be done by autonomous recovery or recovery by interaction of the ground control station [4]. The most important availability requirement is that the habitat needs to be available on Phobos by 2033.

Availability thus takes into account the life span of the spacecraft, but also the downtime, which is the time the spacecraft is unavailable due to an internal failure or any other cause. In order to estimate the availability of the spacecraft, Equation 8.2 is used, in which A is availability and Total Time is the sum of uptime, the time the spacecraft is available, and downtime.

$$A = \frac{Uptime}{Total\,Time} \tag{8.2}$$

At last, a check on the launch availability was performed. The launch availability percentage of the SLS combines the overall reliability of the system, the likelihood of failure and time to restore from an irregularity. Eventually, the launch availability of the SLS was set to 96.7 % [78].

8.3 Maintainability

This aspect of the RAMS is less relevant for a spacecraft, as it is not possible to maintain the spacecraft once operational. Therefore, there are only a small amount of topics to be discussed for maintainability.

In general, a possible approach to maintain a system is to fix when something breaks [26]. It is the simplest approach, but infeasible for a spacecraft. Other maintenance approaches are maintenance on a predetermined schedule or maintenance to prevent failures. In the latter, failure mechanisms and design solutions are analysed to prevent failures. The preferred maintainability approach is the reliability-centred maintenance, which is a combination of the above discussed approaches. It applies the smallest amount of maintenance at minimum cost. As it is based on indicators of crucial system failures, it increases the reliability. To use this approach, a thorough analysis of the failure modes and its effects are necessary. Furthermore, the spacecraft can be equipped with built-in fault detection systems to give a warning whenever the spacecraft fails. Besides, detailed tests - such as a non-destructive test - must be performed.

As the spacecraft has to be maintenance-free after launched, physical maintenance is only possible for the ground system. This means the launch site has to be controlled and maintained to successfully launch the spacecraft. The software on-board of the spacecraft must also be maintained. The spacecraft should be able to interact with the ground system to update the software when corrections need to be made.

8.4 Safety

The last element of RAMS is safety. In space missions, safety implies the safety of humans and the system [79]. As the PICARD will not transport humans, the human factor of safety decreases a great extend. The launch is the only mission phase where humans are involved. As the launch is a very energy intensive phase, measures must be taken to safeguard the complete staff and possible spectators. These measures are called safety requirements. They include the assurance for safety of all people involved and surrounding the launch and prevention of damage by launcher stages descending back to Earth.

In order to assure the successful execution of the mission, the safety of the system must be assured as well. The safety requirements imposed on the system include the avoidance of collisions in space and of fuel leakage.

At last, to prevent major damage in case something goes wrong, there should be the possibility of destroying the spacecraft during launch. An example of a safety-critical function - a component where safety is critical to the succeeding of the mission - are the batteries. Batteries tend to impact the design significantly. They are meant to store a large amount of energy in a small volume [4]. Due to overcharging or rapidly discharging, the batteries might cause fire or explosions. They should therefore be designed to prevent these events in order to assure the safety of the mission.

As mentioned before, the PICARD is designed for worst case scenario. Therefore, safety margins are included during the detailed design phase. A good example is the safety antenna, in case the other two malfunction. Another example is the emergency release included in the decoupling system to separate the tug and lander. Furthermore, safety margins were considered, e.g. for the stresses in the structure and for the propellant tanks. These examples show the PICARD includes sufficient safety to successfully fulfil the mission.

Chapter 9 Risk Management

Risk can be seen as the measure of uncertainty of attaining a goal, objective, or requirement in terms of technical performance, cost and schedule [79]. A proper risk management strategy is of special importance for an unmanned space mission like *Boots on Phobos*. This is due to the lack of possibility for in situ modifications to the spacecraft.

The risk strategy chosen for the development of this mission is the following. At first, the risks were identified for the different mission segments. This process is described in section 9.1. This was followed by an assessment of the risks in terms of probability of occurrence and severity of consequence. This is further elaborated on in section 9.2. The risks are presented according to their ranking in Figure 9.1. In case they were ranked to an unacceptable extent, risk mitigation strategies were proposed which are further described in section 9.3. This section also includes a 'posterior' risk map which shows the effect of that mitigation.

9.1 Risk Identification

Risk identification was performed throughout every step of the project. To ensure an up-to-date status of technical risks and to identify new ones, the risks of all subsystems were re-evaluated on an almost daily basis. The list of technical risks and their assessment can be found in Appendix E. This list also includes risks with respect to costs as they are closely related to the technical aspects of the mission. Additionally, a list of organisational risks is included in Appendix E. The list includes the risks that were expected and/or occurred during this DSE regarding the team members and their cooperation and with respect to scheduling.

9.2 Risk Assessment

The characterisation of magnitude and likelihood of risks was performed by looking at the probability of occurrence and the severity of consequence in case of occurrence. Within these two criteria, the risks of each individual subsystem were ranked according to the following scale:

Table 9.1: Probability of occurrence.

Probability	Description
High	Feasible in theory
High-Moderate	Working laboratory model
Moderate	Existing (of topic) engineering
Moderate-Low	Extrapolated from existing design
Low	Proven design

Table 9.2: Severity of consequence.

Severity	Description
Negligible	Inconvenience or non-operational impact
Marginal	Minor reduction in technical performance
Critical	Major reduction in technical performance
Catastrophic	Mission failure

Figure 9.1 shows the risk map with unacceptable risks. The colouring of the map was chosen as: **Green**=Negligible Risks, **Yellow**=Acceptable risks or acceptable after mitigation and **Red**=Unacceptable risks, so mitigation is necessary [80].

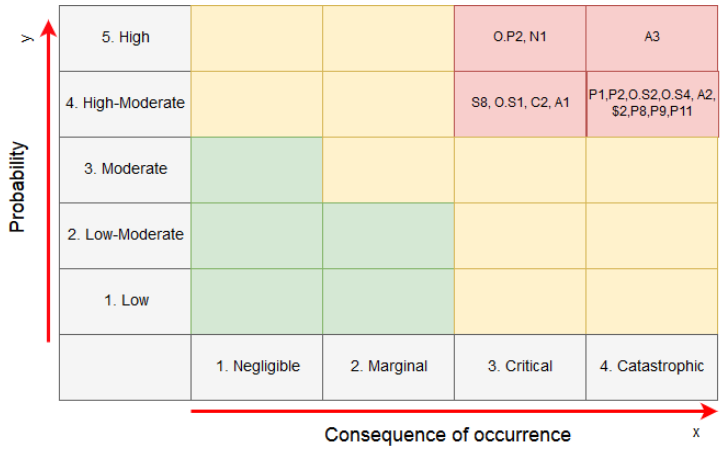

Figure 9.1: Risk Map with unacceptable risks.

9.3 Risk Mitigation

Risk mitigation can be understood as the disposal of unacceptable risks. To approach the minimisation of risks, two measures can be taken:

- (Pre-)development/Prototyping
- Change in design:
  - Choose a different technology, which decreases the probability of occurrence.
  - Change the way of operating, which decreases probability and criticality of occurrence.
  - Apply margins or redundancy, which decreases the probability of occurrence.

Figure 9.2 shows the 'posterior' risk map that takes mitigation into account. The mitigation strategy that was assigned to the different risks can be found below the figure.

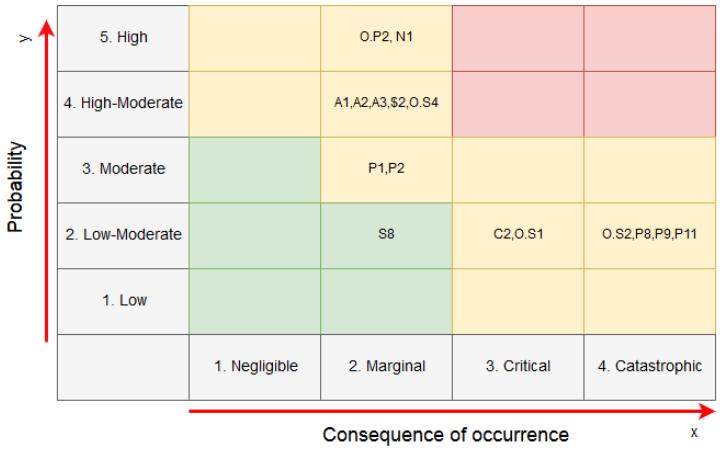

Figure 9.2: Risk Map after mitigation.

Power & Propulsion

- P1 - Solar panel failure:
  Mitigation 1: Include margins and redundancy to ensure sufficient power generation even if parts of the panels malfunction or get hit by space debris.
- P2 - Battery failure:
  Mitigation 1: Include margins and redundancy to ensure sufficient power storage capability even if some batteries malfunction.
- P8 - VASIMR misalignment resulting in wrong trajectory:
  Mitigation 1: Place VASIMR-engines on gimbals.
- P9 - Power support failure:
  Mitigation 1: Add emergency cabling and bring back-up PCU.
- P11 - Running out of fuel:
  Mitigation 1: For the tug and lander include margins in the fuel amount.

Structure

- S8 - Capsizing of the habitat at Phobos' surface:
  Mitigation 1: Stiffen the joint.
  Mitigation 2: Enable habitat to function even if misplaced.

Navigation

- N1 - Navigating through van Allen belts:
  Mitigation 1: Limit time in van Allen belts.
  Mitigation 2: Include radiation protection in design.

Communication & C&DH

- C2 - Pointing offset:
  Mitigation 1: Use of gimbals.

ADCS

- A1 - Sensor failure:
  Mitigation 1: Redundancy on all sensors.
- A2 - Thruster failure:
  Mitigation 1: Each thruster pair has a redundant pair.
- A3 - CMG failure:
  Mitigation 1: Double the required amount of CMGs are used.

Organisation

- O.P2 - Disagreements:
  Mitigation 1: Respect members opinion and discuss problem in civilised manner.

Costs

- $2 - Budget cuts:
  Mitigation 1: Use of commercially available resources like external audits and reviews.

Schedule

- O.S1 - Missing deadlines:
  Mitigation 1: Use of Gantt Chart and daily wrap-up meetings stating progress status.
- O.S2 - Performance cutbacks to do misapplication of resources:
  Mitigation 1: Allocate resources (students, time) according to importance of mission aspect.
- O.S4 - Political delay of mission:
  Mitigation 1: If 2028 launch window is lost, back up for arrival at 2035 can be designed.

[THIS PAGE WAS INTENTIONALLY LEFT BLANK]

Chapter 10 Sustainability

This chapter explains in what ways the final design is sustainable. For a space mission, sustainability considers the impact on Earth and all other environments that are passed through. This is discussed in section 10.1. Also, given that this mission is a stepping stone to the exploration of Mars, the impact on society is also considered in section 10.2.

10.1 Environment

The environment aspect of sustainability considers the impact of the mission on the different environments it passes through. The considered environments are the Earth surface, Mars surface and the environments of the orbits through which the spacecraft travels. To analyse the sustainability, five aspects are discussed, which are the COSPAR Planetary Protection Policy (PPP), the debris left in orbit, the propellants used, the power source and the use of off-the-shelf technology.

10.1.1 COSPAR Planetary Protection Policy

The COSPAR PPP aims to protect Earth from possible extraterrestrial contamination and to protect other celestial bodies that may contain life or biological components. This sustainability aspect is reflected in requirement MTM-SYS-KEY08. Contamination of Earth by extraterrestrial matter is called backwards contamination and must be prevented, because it is potentially dangerous. A retrieved rock might contain anything from a disease that is lethal to humans to things that disrupt the ecosystem, which may cause food shortages and the extinction of animal species [16]. Other environments, such as the Martian surface, can be contanimated by the spacecraft, reducing the reliability of future research into life on Mars. This contamination of other planets is called forwards contamination.

To ensure the protection of both Earth and other planets, COSPAR has set up guidelines which minimise the chance of a contamination event. To determine the measures that must be taken, the PPP contains categories for missions, where each category is determined by the body that is visited and the type of mission (fly-by, landing or sample return). Each category requires certain measures to be taken to reduce contamination risks. This mission is a category III mission, because it was considered a Mars fly-by mission and no restrictions are currently placed on landing on Phobos.

The PPP places a requirement on the orbital lifetime of spacecraft around Mars. The tug must have a probability lower than 1 % to crash into Mars within 20 years after launch and a probability lower than 5 % to crash into Mars within 50 years. As aerobreaking increases the chance of crashing into Mars, the choice was made not to use aerobreaking.

10.1.2 Mission Debris

Leaving debris in orbit may be dangerous to new missions. The amount of debris that this mission will leave was analysed to determine the impact of the mission on the orbital environment.

Firstly, the debris left in orbit after launch was considered stage by stage. The boosters and payload fairing will not get into orbit and also the main core will fall into the ocean [81]. The upper stage will remain near the target altitude at 13,000 km. During the joining of the lander and the habitat no debris is created, assuming no problems occur.

When the spacecraft arrives at Mars, the tug and lander separate. Due to the selected separation mechanism no debris will be generated during separation. After separation the tug is left in an orbit around Mars, where it functions as relay for up to two years. When it is shut down, it is left in that orbit. This leaves one piece of debris in orbit. To prevent any risk of explosion, the spacecraft will also be passivated to remove any risk of explosions, which means the removal of any remaining energy sources [82]. This procedure consists of first depleting the xenon tank by opening the valve to the engine without activating the engine to relieve the pressure. The second step consists of burning the remaining ADCS fuel and despinning the CMGs. The last step consists of shutting down the power generation and depleting the batteries by sending a signal at maximum power into space.

The lander will be left on the surface of Phobos, because it poses no threat to Mars at that location within the fifty year limit imposed by the COSPAR PPP discussed in subsection 10.1.1. Only when Phobos starts breaking up and crashes into Mars, the lander will crash as well.

These results show that the nominal mission leaves three pieces of debris in orbit. One piece between low- and medium Earth orbit, one in an orbit around Mars and one on the surface of Phobos.

10.1.3 Propellant

Requirements MTM-LA-PROP-KEY02 and MTM-TR-PROP-KEY02 state that the used fuel shall have minimal effect on the environment. The xenon selected for the tug propulsion fulfils this requirement. The ADCS fuel for both the tug and the lander and the propulsion system for the lander use MMH and N_2O_4 though, which are both toxic. However, the performance would drop to unacceptable levels if other fuels would be used. Cold gas thrusters for the ADCS would have a too low I_{sp} for example. For propulsion, using liquid oxygen was not an option, because of its bad storability over long amounts of time.

An alternative thruster could be one that uses hydrogenperoxide and ethanol, which are a lot less toxic than MMH and N_2O_4 [83]. This thruster is a relatively new concept and is currently at a TRL of three, which is too low according to requirement MTM-SYS-KEY02, which requires a TRL of at least five. It is recommended though that an analysis is performed at a later stage to determine whether it is feasible to invest in a fast development of this thruster. Changing the thruster and propellant will probably not change the design a lot, because the performance of the green thruster is similar to that of the MMH and N_2O_4 thrusters. The tanks would also require only minor adjustments, because the densities of ethanol and MMH differ only slightly and the densities of H_2O_2 and N_2O_4 are similar as well.

10.1.4 Power Generation

Two main power options exist for interplanetary missions, which are nuclear and solar power. The trade-off between these two power sources was done in the Midterm Report [1]. The chosen power source was solar energy, partially because it is a more sustainable option. Nuclear power generation was considered unsustainable, because of the radiation it generates and because it uses rare elements. Particularly in the event of a launch failure the radiation poses an environmental threat.

10.1.5 Off-the-Shelf Technology

Both the tug and lander use as much off-the-shelf technology as possible. This not only reduces the cost and risk off the mission, but also reduces the environmental impact. The reduced environmental impact is caused by the reduction in resources spent in development and testing.

It was already stated in subsection 10.1.3 that the chosen MMH and N_2O_4 for propellants are toxic. The total use of these chemicals is reduced by using off-the-shelf thrusters, because it requires fewer tests to be performed. This reduces the total amount of MMH and N_2O_4 used.

10.2 Society

A mission should have a sustainable impact on human society as well. The considered societal aspects are the survival of the human race and the potential scientific advances.

10.2.1 Human Survival

When looking at the bigger picture, this mission contributes to the exploration of Mars. This could lead to the colonisation of Mars, which reduces the risk of human extinction due to possible meteorite impacts, volcanic eruptions or other natural causes. Also human caused disasters including climate change and a nuclear war may render the Earth inhabitable.

10.2.2 Scientific Advances

Scientific data about Phobos is limited. Three missions have been send to Phobos, which all failed to land on the surface [84, 85]. The scientific advances of travelling to Phobos mainly exist in two areas: understanding the solar system and investigating if Phobos can be used to mine resources.

The understanding of the solar system mainly applies to the origin of Phobos. It is still not understood whether Phobos accreted in Mars orbit from a debris disk or whether it is a captured asteroid. If Phobos is accreted from a disk, its composition may also hold clues to the origin and composition of Mars.

For this mission, Phobos is only used as a final step before landing on Mars. Depending on the composition of its surface, it may also be used as a refuelling outpost [85].

Chapter 11 Sensitivity Analysis

When changing major design parameters, an entire design could either change significantly, or require marginal adjustments. That is exactly the scope of the sensitivity analysis; to evaluate influential assumptions which have a high likelihood of changing. This is dealt with by describing per subsystem what could change of the major parameters and in what manner. These manners which have a change are then evaluated in the subsections, to see what would happen to other subsystems or the system.

11.1 Causes

One of these parameters is the use of xenon in the VASIMR engine, which could change to krypton or argon in the case of xenon not working properly. If so, the tank mass could increase with a factor of 10 in the case of argon or 3.5 in the case of krypton. This then also means that there is a increase in height of the spacecraft, since the main driver behind its height are the propellant tanks.

Furthermore, both power density and specific power for the solar arrays are based on small scale tests for solar panels, but have actually never been demonstrated on the large scale the PICARD intends to have. Also, the energy density and specific energy are based on current battery data, and then extrapolated based on predicted trends in near future. Whenever these parameters change in the future, they could cause larger arrays or more batteries.

Lastly, the thrust for the VASIMR was assumed to be constant and at required thrust level whenever necessary. This does not take into account any degradation of the engine or any other factors (negatively) influencing the propulsion, causing the requirement for more propellant.

11.2 Effects

Effects from section 11.1 are evaluated in terms of mass and schedule. The evaluation of dimensions follows as a direct consequence of the mass increase.

11.2.1 Change in mass

As seen from the introductory part, one of the changes that could occur is a change in mass. Testing the sensitivity for mass, an increase is simulated to see how other parameters change to this increase. To prevent going too much into detail and actually executing an entire iteration, this analysis will be kept top level. This means that only values directly related to mass in the models are evaluated. An ADCS changes due to a mass increase as well, but introduces far more complication. It would require a new design if so. It was decided to increase the mass by 5%. Note that this number is arbitrary and is to illustrate. The results of this increase are shown in Table 11.1.

Table 11.1: Change in major parameters after mass increase.

		Before mass increase	After mass increase	Procentual increase
Earth escape	Travel time	1.4262 years	1.4720 years	3.21%
	Fuel burnt	10.45 tonnes	10.79 tonnes	3.25%
Transfer	Travel time	1.7639 years	1.7903 years	2.03%
	Fuel burnt	11.85 tonnes	12.09 tonnes	1.50%
Mars insertion	Travel time	0.1747 years	0.1816 years	3.95%
	Fuel burnt	1.28 tonnes	1.33 tonnes	3.91%
Propulsion	Tank mass	3.85 tonnes	4.05 tonnes	5.19%

Note that more propulsion parameters could be included, but since they scale with the tank mass according to the model, it is not necessary to repeat that increase of percentage multiple times.

From the table it can be seen that (except for tank mass) travel time and burn of fuel are not as effected as the mass itself, which changes by 5%. They might not be as sensitive, but the travel time is especially important in this case. Since a launch window can be successfully met, but whenever the transfer takes too long, the time in low-thrust trajectory increases as well. The ultimate goal of reaching Mars can then still fail, since Mars its position changes in the mean time as well. This would subsequently be a single point of failure. Therefore, the travel time is not as sensitive as the mass, up to the point where transfer windows are missed.

From a sustainable point of view, the fuel used is percentually lower than the mass increase, which means that they are not linearly related. From this perspective, it actually does relatively influence the sustainability positively when increasing the payload mass, because the fuel mass increase is relatively less.

11.2.2 Change in Dimensions

This change in mass may lead to different dimensions. Currently, the design is roughly 8.5 meters tall, mainly due to the fuel tanks. Whenever these fuel tanks would increase in mass, its size increases proportionally. This means that the tanks could increase up to 25 meters in height, since that would still fit within the SLS launcher. Whenever the tanks would also take space in other directions, there would be space left for 0.9 meters in diameter. Overall, the design would not be sensitive regarding the size.

11.2.3 Change in schedule

Lastly, the idea of change in time (or delays) is addressed. Whenever the launch window is missed, it will take another 2.16 years before the most efficient window is available again. However, this launch window is based on efficiency and availability, and more launch opportunities are available. Of course, one could wait for the next launch window and the design could remain the same. Postponement will however lead to a dramatic increase in costs, to which each design is extremely sensitive. The other option is to redesign for a less efficient trajectory. These options do complicate the design a lot, since the required ΔV and travel time will both increase drastically. This will mainly ask for a complete change in the propulsion system, but other subsystems could be affected by this trajectory as well. Regarding the fact that the SEP was already very difficult to realise with this most efficient trajectory, the propulsion will not be able to cope with a more ΔV intensive trajectory. It will either lead to the conclusion of infeasiblity, or the conclusion of the SEP being a killer requirement, leading to the use of chemical propulsion. The latter can then be regarded as very sensitive.

Chapter 12 System Verification & Validation

Subsystem models and products are verified and validated individually in chapter 5, which can be considered as unit tests. In this chapter, the verification and validation process on a system level is described in section 12.1 and section 12.2, respectively. A system test is discussed as well, to assure proper integration of each unit into the full system.

12.1 Verification

To perform the product verification, the requirements in the compliance matrix in Table D.2 were used. In this section the compliance to all key requirements is shown, as these are the relevant requirements for the stakeholders. Argumentation on how these key requirements are met is given below. Requirements that were not met are identified as killer requirements.

- **MTP-KEY-SYS01**: An investigation on landing sites was conducted in section 4.1 to find a stable area to land. The trajectory was designed to land on Phobos on 15 October 2032.
- **MTP-KEY-SYS02**: Scientific instruments described in section 2.4 were incorporated in the design for monitoring the habitat and supportive equipment.
- **MTP-KEY-SYS03**: See explanation MTP-KEY-SYS02.
- **MTP-KEY-SYS04**: Each risk, both on system and subsystem level, was assessed and a mitigation strategy was provided in chapter 9. More detailed attention was paid to the mitigation strategies of catastrophic risks to prevent any single point of failure (SPF).
- **MTP-KEY-SYS05**: The initial elimination of design choices in the Mid-Term Report was based on feasibility. In other words, design options with a TRL lower than five were discarded [1].
- **MTP-KEY-SYS06**: Predictions were made to predict the TRL of hardware before launch. All hardware components are expected to achieve a TRL of eight. However, definite compliance to this requirement cannot be assured at this stage of the design process.
- **MTP-KEY-SYS07**: The PICARD and its individual components were designed to fit into the SLS Block II launcher. The tug and lander combined have a base of 5 m by 5 m with a height of 8.5 m without taking into account the solar panels. Before launch the solar panels are retracted and folded to enable fitting in the launcher. The SLS launcher has a diameter of 8.3 m and a height of 25 m and thus compliance was achieved.
- **MTP-KEY-SYS08**: The maximum number of SLS Block II launches is four for pre-Mars missions [9]. Assuming that one SLS Block II is needed to launch the habitat and one for the Orion capsule that transfers the crew to Phobos, that leaves two launchers for the lander and tug. There are multiple options on how to bring the PICARD up in space. Although no definite choice was made on how to launch the PICARD, it was determined that two is the maximum number of SLS launches for the considered options.
- **MTP-KEY-SYS09**: The EOL strategy of both tug and lander are described in section 3.8.
- **MTP-KEY-SYS10**: The mission adheres to COSPAR regulations because the PICARD was designed in such a way that there is no probability of crashing into Mars within 50 years [16]. This was achieved by designing an EOL solution in which the relay tug is put into a higher orbit in which the orbital decay is negligible.
- **MTP-KEY-SYS11**: Each phase of the mission was analysed individually in chapter 10 to ensure debris is minimised. After separation of tug and lander in Mars orbit, the tug will be used as relay satellite. In other words, a new purpose was found for the tug which minimises debris left in orbit. After its relay function is fulfilled, the tug will have an EOL strategy as described in section 3.8.
- **MTP-KEY-SYS12**: A CBS in section 6.4 was established to ensure compliance with NASA's current budget for human spaceflight. The whole mission including development, manufacturing and additional costs are expected to be $ 15 bn, equal to NASA's available budget.

- **MTP-KEY-SYS13**: As mentioned above, scientific payload is incorporated in the design. A communication system was designed to send data retrieved from the scientific instruments to the DSN at high data rates for approximately eight hours per day (section 5.5). Communication eclipses were taken into account and temporary storage in terms of memory was included in the C&DH of both tug and lander (section 5.6). The lander lands in 2032 and the crew is expected to leave in 2033. It is therefore feasible to collect data six months beforehand.
- **MTP-KEY-SYS14**: The maximum payload mass of the SLS Block II is 143.2 tonnes. The estimated mass of the tug and lander combined is 92.2 tonnes.
- **MTP-KEY-LA-ADCS01**: As described in section 5.1, the lander will have a maximum approach speed of 0.25 m/s to ensure a soft landing. This is achieved with downwards thrust by the ADCS. Furthermore, a four-legged landing gear ensures damping during touch-down, (section 5.1).
- **MTP-KEY-LA-ADCS02**: As mentioned above the ADCS will provide downward thrust to slow down during the descent. The thrusters provide 864 N to ensure a hover period of at least two minutes.
- **MTP-KEY-PROP01**: As described in chapter 10, both the propulsion system and ADCS use toxic propellants for the lander. The propulsion system uses a combination of Hydrazine and Dinitrogentetroxide because the storage of a more sustainable propellant would increase the fuel volume to unacceptable extends. The propellant used for the ADCS was chosen to ensure proper performance of the system, although being toxic. However, in the scope of the full mission its effect is still assumed to be low, therefore this requirement is decided to be partially met, while still giving the recommendation to look into this in further design. A more detailed explanation can be found in chapter 10.
- **MTP-KEY-PROP02**: Xenon used by the VASIMR engines adheres to this requirement. However, as mentioned above, propellant used for the ADCS is toxic to ensure proper performance of the system. However, in the scope of the full mission its effect is still assumed to be low, therefore this requirement is decided to be partially met, while still giving the recommendation to look into this in further design. A more detailed explanation can be found in chapter 10.
- **MTP-KEY-TR-PROP01**: A suitable trajectory to transfer the lander, habitat and supportive equipment to Mars orbit was established and a propulsion system to provide this transfer was designed. A more detailed explanation on how this was achieved is described in section 5.2 and section 5.3.
- **MTP-KEY-TR-PROP02**: Two VASIMR electric engines using xenon as propellant will be used as propulsion system for the tug as described in section 5.3.
- **MTP-KEY-TR-PROP03**: It was determined that designing the tug with an electric capacity of 100 kWe would be a killer requirement that would drive the design to an unacceptable extend. Therefore, in consultation with stakeholders, it was agreed upon to increase the electric capacity to 400 kWe.
- **MTP-KEY-LA-PROP01**: A suitable trajectory to transfer the habitat and supportive equipment to Phobos was established and a propulsion system to provide this transfer was designed. A more detailed explanation on how this was achieves is described in section 5.2 and section 5.3.

As mentioned earlier, the requirements that were not met are identified as killer requirements. Killer key requirements are MTP-KEY-PROP01, MTP-KEY-PROP02 and MTP-KEY-TR-PROP03. Killer requirements drive the design to unacceptable extends and therefore it was decided to deviate from these requirements in consultation with the stakeholder to achieve the objective of the mission.

12.2 Validation

Multiple tests can be performed to validate the final product. Some of these methods were mentioned on subsystem level product validation but can be applied to the full system validation in chapter 5 as well. These methods include:

- **End-to-end information test**: These will be used to analyse the compatibility of the system. This test is mainly focused on the software interface of the system and shows how the system reacts

on simulated space-like data input. In other words, how is certain information processed and what procedures are taken by the system to respond to this input properly.

- **Mission scenario test**: It will be used to demonstrate the performance of the system in a space-like environment. Both hardware and software are tested whether they are integrated properly in a simulated environment according to the mission design. The launch environment could for example be simulated by applying maximum vibrations or loads to test the bearing strength of all integrated hardware. A possible location for this test could be the vibration and acoustics test facility of NASA[1].
- **Operation readiness test**: It will be used to simulate the mission timeline. This test is meant to demonstrate whether the ground segment including people, facilities, hardware and software work properly to fulfil the mission from beginning to end. For the PICARD this test could be performed in cooperation with the DSN. The DSN uses multiple facilities for radio frequency testing, for example the DSN testing facility at the Kennedy Space Center in Florida[2]. This is a suitable location for testing because the SLS Block II including tug and lander is launched at Cape Canaveral.
- **Stress testing and simulation**: It is a method that will be used to simulate faults in the system and variations in system performance. How the full system processes these changes and reacts are analysed in this test. Furthermore, SPF can be detected.

In section 6.3 and section 6.4, time and costs were assigned to perform these type of system tests. Based on the TRL of the individual subsystems an overall budget for verification and validation (incorporated in the total development costs) of 6.3 $bn was reserved. The reserved time period for verification and validation is shown in Figure 6.4. Task names "Qualify components" and "Integrate and test PICARD" refer to this process, not only on system level but also on subsystem level.

By executing each of these methods, the full system can be validated properly. The overall focus in these tests should lie on the interface of subsystems, how they perform under different conditions and whether the system indeed fulfils the mission.

[1] URL `https://www.nasa.gov/centers/johnson/engineering/human_space_vehicle_systems/vibration_acoustics_test_facility/` [cited: 23 June 2017]

[2] URL `https://www.nasa.gov/content/communications-tests-go-the-distance-for-maven/` [cited: 23 June 2017]

[THIS PAGE WAS INTENTIONALLY LEFT BLANK]

Chapter 13 Conclusion

A mission to Phobos with the Sun as primary energy source has been proven to be a very challenging task. To return to the design question posed at the introduction - 'Is solar electric propulsion a possible option for a mission to Mars and if so, how would its detailed design look like when considering all the design challenges?' - it can be concluded that the current design is optimal for this mission. This is achieved with the PICARD design that has been shown in chapter 2. The Mission Objective is also adhered to, since the launch is executed on the 31th of September 2028 from Cape Canaveral, expecting arrival at Phobos to be on the 4th of July 2032.

The total spacecraft with a TRL$\geq$5 consists of three main parts, which all have a rectangular shape. This is one tug, one lander and a fairing in between. This configuration is powered by two VASIMR engines, available whenever that is required according to the navigation computer. This independent computer calculates all the points where a finite burn is required to create a low-thrust trajectory leaving Earth, around the Sun as well as for insertion into Mars obit. During the transfer, the spacecraft is powered by a large array of solar panels, which are alternated by batteries when in eclipse periods. Whenever communications is required, the ADCS is capable of pointing the spacecraft with an accuracy of 0.1 degree. Communications will then happen on Ka- and X-band to achieve a link with Earth's DSN. This ADCS accuracy is possible for the lander as well, which has a independent and own ADCS system. This lander is powered by chemical propulsion which will help with the execution of a Hohmann transfer to Phobos, where it will be able to land softly. After arriving, its power will be supplied purely by batteries which will be loaded by the tug's solar arrays before separation.

Throughout this entire design sustainability has been a key driver when making decisions. Especially when coming up with an EOL solution, which concluded with the tug in a relay orbit and the lander remaining on Phobos. For the landing of the tug, a total of four possible landing sites were selected. Also, whenever catastrophic risks or SPFs were detected during the design phase of these two designs, mitigation strategies were implemented. All of the severe risks with a too high chance of occurrence have been mitigated, which is in line with a proper risk strategy for space missions.

The post-design operations have been evaluated by looking at the production, cost and schedule after the design. It was concluded that the production is feasible within the time limit. However, not all elements of the production process and - where necessary - transportation have been verified. This was also confirmed by the Gantt chart, which was able to fit in all the elements of all post-design operations. Overall, the cost analysis showed that every element of the mission fits within the \$15.1 bn budget, proving its feasibility in terms of costs.

With the help of a RAMS analysis, the reliability of the PICARD has been determined to be 86.4% up until this point. Not only the spacecraft is important, also the availability of other factors like the SLS have been found to be in place. With the help of redundancy in subsystems and a maintenance-free spacecraft, its safety and maintainability have also been approved.

Transporting a 50 tonne habitat to Mars, an enormous mass on its own, is possible. The current design makes it possible. The PICARD has made the use of SEP feasible as main energy source, together with a working propulsion system, which has been extremely challenging. This also was one of the key requirements, of which the most important ones are met with the help of the extensive verification and validation process. The reliability confirms that this is not 'hot air', but a trustworthy system.

[THIS PAGE WAS INTENTIONALLY LEFT BLANK]

Chapter 14 Discussion

In this chapter criticism on the detailed design and design process is discussed and recommendations regarding further improvement are given. This is done by looking at different aspects of the development of this design and the design itself. Recommendations were give on both subsystem and system level. Post design operations and the organisational approach were discussed as well.

Subsystem

Each subsystem has its own criticism and recommendations. These recommendations and possible improvement strategies are given below.

The first subsystem is the **structures** subsystem. As of now the structure of the spacecraft is overdesigned. With a better CATIA model, the load and vibrational analysis of the entire structure can be performed. This will optimise the structure by making it lighter. With an optimised design, the actual structure should be tested with these loads. The separate structural systems such as the coupling system and the landing mechanism should also be tested under realistic loads. Further calculations and tests for shocks and acoustic vibrations should be performed to complete the full stress tests. A last recommendation for the structures subsystem is to further investigate the materials used in the spacecraft. At this point, only metals are used, while different materials such as composites can be used for many different applications. Further investigation into these materials can further optimise the structure.

The **thermal** and **radiation** control is now designed with little analysis. Elaborate models should be built to have a detailed design. For the radiation control the SPENVIS[1] program could be used. Using this the effect on all components and its consequences could be analysed. For example, the star sensors have a maximum radiation value. If this is too low, a different sensor should be chosen.

The first major decision made in **navigation** was to simulate all trajectories using a simplified Python tool, and a more complex GMAT tool. Final results presented and used are those obtained with the Python tool, due to a thorough understanding of its working, and easy optimisation of parameters. For a more detailed analysis with more accurate results, a deeper understanding of the GMAT tool is required. With this understanding a more reliable output could be generated, increasing the realism of the mission.

Furthermore, a major assumption within the determination of the trajectory is that all computations are performed in 2D. This was done to reduce complexity of the programs while keeping computational times to a minimum. For more detailed analysis and more accurate results the inclusion of the third dimension would be required.

Moreover, the trajectory determination required many different, sometimes seemingly unrelated, parameters as output(such as eclipse times and fuel burnt). The shear number of these outputs required many assumptions and simplifications to be made, as to obtain reasonable results within a minimum of development time. For this reason not a lot of detailed optimisation was performed, which, if done, could make the mission much more effective and less cost heavy. An example of this is the assumption of using only one continuous burn per phase in the simulations. This caused the power subsystem to include large batteries in the tug design, as to also power the engines during eclipse periods. After some initial "back-of-the-envelope" calculations it was found that shutting down the engines during eclipse times did not effect the total transfer time or fuel required by much, avoiding the mass increase from a large battery array. Another point that could have decreased the travel time and fuel burnt would be the use of gravity assists, which was deemed out of the scope for the current design iterations. Eventually arriving at Mars, a more detailed analysis of Mars capture should be performed. The current estimation has been proven to give reasonable results, but does not say anything about the procedures required by the PICARD for successful capture (thrust levels, burn times, etc.).

The last recommendation for further analysis would be a thorough investigation in launch windows. For now only launch dates are given, which are an estimate for times when a launch is recommended for enabling successful trajectory completion. However, these launch dates do not include a time-range during which the launch applies. Initial estimates show this would be in the range of hours, not days, and are thus fairly sensitive to the mission. Related to this is the possibility to perform in-flight trajectory corrections, which also require further investigation. These corrections would enable successful trajectory completion, even when the launch window is not followed. These corrections could serve as a mitigation plan for missing the launch opportunity, while also allowing for a more certain flight path.

[1] URL `https://www.spenvis.oma.be/` [cited: 22 June 2017]

The **propulsion** system is equipped with two VASIMR engines. These VASIMR engines have a TRL of five and are thus assumed to be ready before launch. However there is a possibility that the engines will not be flight ready on time, leading to the system requiring a different propulsion system or waiting for a later launch window. This will significantly change or delay the design. A recommendation is to further investigate the possibilities of other SEP thrusters to replace the VASIMR if necessary. Furthermore, only two engines are used, which is less preferable for navigation since it has low thrust, but preferred by the power subsystem. The trade-off for more engines should further be investigated. Lastly, the propulsion system includes a feed system. This feed system could be designed into further detail for a full detailed design.

In this phase of the design, the landing procedure by the **ADCS** was simplified. In further stages of the design a more detailed model is required which could be achieved by investing existing or newly developed software that simulates the landing. Furthermore, a more detailed analysis regarding CMG's is required because these are not off-the-shelf models. This level of detail could be achieved by optimisation of the rotational model.

For the **communication** system a preliminary estimation was made on the communication eclipses. However, the estimation was simplified and therefore the level of detail is limited. Further investigation is required in blockage of the communication signal by other components of the spacecraft, blockage due to priority of other subsystems to be pointed in a certain direction (e.g. engines) or blockage by planets. These aspects could be tested with small scale models. Another point of criticism are the gimbals used for the pointing of a few antennas. Up until now, it was assumed that these gimbals are capable of pointing in any direction when the ADCS is not available for antenna pointing. Research into existing gimbals and their rotational capability is required. Furthermore, in a further stage of the mission design the DSN should be involved and their permission should be requested. This is essential to ensure availability of ground-based antennas and to finalise downlink and uplink durations. Lastly, the concept of the Electra telecommunication package was introduced. However, an end-to-end information test is required to ensure its compatibility with the other components of the communication system.

Although the determination of processor and memory of the **C&DH** has been justified, the choice of processor is still based on a preliminary analysis. Generally, processors are expressed in clock rates, describing the amount of instructions per second they are capable of handling. The bitrate they are capable of handling is actually not a parameter, but was required in this case. Ideally, proposing the required bitrate to the manufacturer should show whether it is possible or not. A hardware-in-the-loop test could subsequently show whether the processor does indeed perform sufficiently, and prevents data loss due to overflows. This introduces the second point, since the required data rate is built up from estimates. All system throughput parameters that could be thought of were noted down, with the amount of significant digits required. All of these estimates were based on qualitative ideas, where the amount of throughput parameters could change together with its significance. Again, a hardware-in-the-loop should give a proper estimate of the data flowing through the system, to prove whether the memory is sufficient.

The last subsystem is the **power** subsystem. The most remarkable point about this subsystem is the enormous amount of batteries required, which is inefficient. One way to decrease this mass would be by decreasing the thrust level during eclipse, thus decreasing the power required by the VASIMRs and in turn leading to a changing trajectory. Another recommendation would be to investigate the development of a power source with a higher specific energy to replace these batteries. Further design calculations should be performed to determine the exact amount of batteries to be used since right now the value is based on C&DH estimations. This would help in the exact mass distribution of batteries within the spacecraft. Moreover, research on batteries series or parallel configuration should be performed, as this influences the overall subsystem performance. The C-rate should be determined as this quantity gives an estimate of how much current (and power) can be delivered per unit time by the batteries from a practical point of view. A more in-depth design of smaller components, such as voltage regulators, is also part of future detailed design.

System

Following from the subsystems a holistic analysis was performed from which recommendations on system level were determined.

To minimise all the **risk**, a clear mitigation strategy is needed. For future work a risk catalogue should be made explaining different types of scenarios and a specific mitigation strategy. In this catalogue a combination of failure of different aspects could be written and designed for.

In the detailed design of the ADCS and propulsion system, it was found that the most **sustainable** solutions were not capable of delivering the required performance. Sustainable alternatives for the ADCS exist in the form of a new concept that uses hydrogenperoxide and ethanol, and therefore extensive research is required in this type of thruster to determine its feasibility. If feasibility is proven, investment in fast development is needed. The propellant of the propulsion system is another point of criticism. Similar research to the ADCS regarding sustainable propellants is required.

In the **verification** of the full system, key requirements were analysed to see whether they were met. Compliance to requirement MTP-KEY-SYS06 which states that all mission hardware should have a TRL of at least eight before launch is up to this point uncertain. Extensive research and investment in fast development combined with tests is required to fulfil this requirement. Another point of improvement is the level of detail in **validation** methods proposed. These validation processes require cost, manpower, time and facilities of which some aspects are covered in the post-design operations in chapter 6 but only up to a certain level.

Post Design Operations

Other aspects considered were post-design operations. From these operations the following recommendations were established.

In the design phase a **production plan** with a preliminary schedule was established. This schedule shows the main activities but to a limited detail. Activities like "Further design iterations" and "Prepare engineering data" are dominant in the schedule but could be subdivided into multiple tasks. This is helpful to analyse progress during post-DSE activities.

After the **RAMS** analysis a Failure Mode and Effect Analysis can be performed. This helps to identify potential failure modes based on experience with similar products and processes, or based on common physics of failure logic. Effects analysis refers to studying the consequences of those failures on different system levels. These analyses will help structure the risk and mitigation strategies.

Organisational

The last aspect to be analysed was the organisation of the group. At the very beginning of the project, there was no clear project manager. Whenever organisational problems arose, it was the chairman's responsibility to fix it. This was eventually solved by appointing a project manager, but lacked during the first week and a half. A better understanding of the responsibilities for each role could have helped in understanding the need for such a role.

Moreover, a division of technical roles was set up in the very beginning, taking into account personal preference. This has not been changed any more, for the sake of 'not having to read in into another system, taking too much time'. Looking at the relevant importance of each subsystem, some parts were overestimated, and some underestimated. This importance could have been evaluated to a somewhat further extent, to come to a better technical division.

[THIS PAGE WAS INTENTIONALLY LEFT BLANK]

Bibliography

[1] Akkerhuis, I., Bianchi, A., Ghys, E., Govaert, T., Sasse, F., Schornagel, F., Schoutetens, F., Touw, M., Van der Grift, R., and Van Tent, N., *DSE - Steps to Mars - Boots on Phobos - Mid-Term Report*, May 2017, (unpublished).

[2] Stooke, P. and Thomas, P., "Phobos - Shaded Relief," Image, `https://www.astro-urseanu.ro/imagini/invata/planete/marte/sateliti/phobos-harta.jpg`.

[3] Ulamec, S. and Biele, J., "Surface elements and landing strategies for small bodies missions – Philae and beyond," *Advances in Space Research*, Vol. 44, 2009, pp. 847–858.

[4] Wertz, J., Everett, D., and Puschell, J., *Space Mission Engineering: The New SMAD*, Microcosm Press, Hawthorne, CA, 2011.

[5] Miller, D., Keesee, J., and Jilla, C., "Space Systems Cost Modeling," Tech. rep., MIT Aeronautics and Astronautics Course, 2003.

[6] Akkerhuis, I., Bianchi, A., Ghys, E., Govaert, T., Sasse, F., Schornagel, F., Schoutetens, F., Touw, M., Van der Grift, R., and Van Tent, N., *DSE - Steps to Mars - Boots on Phobos - Baseline Report*, May 2017, (unpublished).

[7] Zamaro, M., *Natural and artificial orbits around the Martian moon Phobos*, Ph.D. thesis, University of Strathclyde, Glasgow, October 2015.

[8] TU Delft - Faculty Aerospace Engineering, Kluyverweg 1, 2629 HS Delft, *Simulation, Verification and Validation*, Lecture Notes, (unpublished).

[9] Hubbard, S., Logsdon, J., Dreier, C., and Callahan, J., "Humans Orbiting Mars," Tech. rep., Planetary Society, September 2015.

[10] Szopa, C., "Mass spectrometry in the history of the solar system exploration," Tech. rep., Laboratoire Atmosphères Milieux Observations Spatiales, Sep 2012.

[11] E. Kyle, *Space Launch Report - Space Launch System Data Sheet.*, June 2017, Fact sheet.

[12] Fortescue, P., Swinerd, G., and Stark, J., *Spacecraft Systems Engineering*, John Wiley and Sons, Chichester, 4th ed., 2011.

[13] Hopkins, J. and Pratt, W., "Comparison of Phobos and Deimos as destinations for human exploration and identification of preferred landing sites," *AIAA Space 2011 Conference & Exposition*, American Institute of Aeronautics and Astronautics, September 2011, pp. 1–13.

[14] Pavone, M., Castillo-Rogez, J., Nesnas, I., Hoffman, J., and Strange, N., "Spacecraft\Rover hybrids for the exploration of small Solar system bodies," Tech. rep., NASA, September 2012.

[15] Basilevsky, A., Lorenz, C., Shingareva, T., Head, J., Ramsley, K., and Zubarev, A., "The surface geology and geomorphology of Phobos," *Planetary and Space Science*, Vol. 102, 2014, pp. 95–118.

[16] Kminek, G. and Rummel, J., "COSPAR's planetary protection policy," *Space Research Today*, Vol. 193, August 2015, pp. 1–14.

[17] CATIA, Software Package, Ver. 5R21, Dassault Systems, Vélizy-Villacoublay, France, 2016.

[18] Rogers, W., "Apollo experience report - lunar module landing gear subsystem," Tech. rep., NASA, June 1972.

[19] Hexcel, Stamford, Connecticut, *HexWeb Honeycomb Energy Absorption Systems - Design Data*, 2005.

[20] Gernhardt, M., Bekdash, O., Li, Z., Abercromby, A., Chappell, S., Beaton, K., Bielski, P., and Crues, E., "Human Exploration Missions to Phobos Prior to Crewed Mars Surface Missions," *Aerospace Conference, 2016 IEEE*, IEEE, Big Sky, MT, USA, March 2016, pp. 1–20.

[21] Python, Software Package, Ver. 2.7.10, Python Software Foundation, Beaverton, OR, 2015.

[22] NASA, *Radioisotope Heater Units (RHUs)*, December 1999, Fact sheet, Document No: 400-1634.

[23] Gilmore, D. G., *Spacecraft Thermal Control Handbook*, The Aerospace Press, El Segundo, California, 2002.

[24] Boeing, *Main ISS ATCS Overview*, December 1999.

[25] Adams, J., Hathaway, D., Grugel, R., Watts, J., Parnell, T., Gregory, J., and Winglee, R., "Revolutionary Concepts of Radiation Shielding for Human Exploration of Space," Tech. rep., Marshall Space Flight Center, March 2005, Document No: NASA/TM-2005-213688.

[26] W.J.Larson and Wertz, J., *Space Mission Analysis and Design*, Microcosm Press, Torrance, CA, 1998.

[27] "Materials Data Book," Cambridge, 2003.

[28] Thiel, M., Stöcker, J., Rohe, C., K. N., Kargl, G., Hillenmaier, O., and Lell, P., "The Rosetta lander anchoring system," *Proceedings of the 10th European Space Mechanisms and Tribology Symposium*, edited by R. Harris, ESA Publications Division, Noordwijk, Netherlands, 2003, pp. 239–246.

[29] Witte, L., Schroeder, S., Kempe, H., Van Zoest, T., Roll, R., Ulamec, S., Biele, J., and Block, J., "Experimental Investigations of the Comet Lander Philae Touchdown Dynamics," *Spacecraft and Rockets*, Vol. 51, No. 6, 2014, pp. 1885–1894.

[30] GMAT, Software Package, Ver. R2016a, NASA, Goddard Space Flight Center, Maryland, 2016.

[31] B.A.C. Ambrosius, R. N., "Introduction to Aerospace Engineering II (Space)," Lecture slides.

[32] Cowan, K., *Project Description - Steps to Mars Boots on Phobos*, Delft University of Technology, Delft, The Netherlands, 2017.

[33] Williams, D. R., *Mars Fact Sheet*, NASA Goddard Space Flight Center, December 2016, Fact sheet.

[34] Stansbury, S., "ASEN 5050 - Low Thrust Transfer to GEO: Comparison of Electric and Chemical Propulsion," Tech. rep., University of Colorado Boulder, December 2009.

[35] Von Ehrenfried, D., *Exploring the Martian Moons: A Human Mission to Deimos and Phobos*, Springer, Texas, USA, 2017.

[36] International Business Machines (IBM), *IBM PowerPC 750GX RISC Microprocessor Revision Level DD1.X - Datasheet*, Oct 2005, Version SA14-2765-02.

[37] Hughes, S., Qureshi, R., Cooley, S., Parker, J., and Grubb, T., "Verification and Validation of the General Mission Analysis Tool (GMAT)," Tech. rep., NASA Goddard Space Flight Center, August 2014.

[38] Sutton, G. and Biblarz, O., *Rocket Propultion Elements*, John Wiley & Sons, Inc, Hoboken, New Jersey, 9th ed., 2001.

[39] Spores, R., Monheiser, J., Dempsey, B., Wade, D., Creel, K., Jacobson, D., and Drummond, G., "A Solar Electric Propulsion Cargo Vehicle to Support NASA Lunar Exploration Program," *International Electric Propulsion Conference*, Vol. 29, Aerojet Corporation, Lockheed Martin, NASA Glenn Research Center and Colorado Power Electronics, Princeton, NJ, October 2005, pp. 1–22.

[40] Lorand, A., Duchemin, O., Zurbach, S., Le Mehaute, D., and Cornu, N., "Alternate propellants for PPS® Hall-Effect Plasma Thruster," *International Electric Propulsion Conference*, Vol. 33, Snecma, SAFRAN group, Space Propulsion Division, Washington, DC, October 2013, pp. 1–3.

[41] Snyder, J., Randolph, T., Hofer, R., and Goebel, D., "Simplified Ion Thruster Xenon Feed System For NASA Science Missions," *International Electric Propulsion Conference*, Vol. 31, Jet Propulsion Laboratory, Ann Arbor, MI, September 2009, pp. 1–16.

[42] Bushway III, E., Engelbrecht, C., and Ganapathi, G., "NSTAR Ion Engine Xenon Feed System: Introduction to System Design and Development," *International Electric Propulsion Conference*, Vol. 25, Jet Propulsion Laboratory and Moog, Inc, Cleveland, OH, October 1997, pp. 289–294.

[43] Welle, R., "Propellant Storage Considerations for Electric Propulsion," *International Electric Propulsion Conference*, Vol. 22, The Aerospace Corporation, Viareggio, Italy, October 1991, pp. 1–10.

[44] Squire, J., Carter, M., Chang Diaz, F., Giambusso, M., Glover, T., Ilin, A., Oguilve-Araya, J., Olsen, C., Bering III, E., and Longmier, B., "VASIMR® Spaceflight Engine System Mass Study and Scaling with Power," *International Electric Propulsion Conference*, Vol. 33, Ad Astra Rocket Company and University of Houston and University of Michigan, Washington, D.C., October 2013, pp. 1–10.

[45] Hofer, R. and Randolph, T., "Mass and Cost Model for Selecting Thruster Size in Electric Propulsion Systems," *Journal of Propulsion and Power*, Vol. 29, No. 1, 2013, pp. 166–177.

[46] Turner, M., *Rocket and Spacecraft Propulsion*, Springer, Leicester, UK, 3rd ed., 2009.

[47] Martinez-Sanchez, M. and Pollard, J., "Spacecraft Electric Propulsion - An Overview," *Journal of Propulsion and Power*, Vol. 14, No. 5, October 1998, pp. 688–699.

[48] Cortés Borgmeyer, S., "Chemical Bi-propellant thruster family," Tech. rep., Airbus Safran Launchers, Orbital Propulsion, Robert Koch-Straße 1, 82024 Taufkirchen, Germany, 2016.

[49] Lagier, R., *Ariane 5 User's Manual, Issue 5 Revision 2*, Arianespace, October 2016.

[50] Gurrisi, C., Seidel, R., Dickerson, S., Didziulis, S., Frantz, P., and Ferguson, K., "Space station control moment gyroscopes lessons learned," *Aerospace Mechanisms Symposium*, Vol. 40, NASA Kennedy Space Center, May 2010, pp. 161–176.

[51] L3 Space & Navigation, 450 Clark Drive, Budd Lake, NJ 07828, *Control Moment Gyro*, Fact sheet.

[52] Honeywell Defense & Space, P.O. Box 52199, Phoenix, AZ 85072-2199, *M50 Control Moment Gyroscope*, January 2006.

[53] Grumman, *Lunar Module - Quick Reference Data*, Fact sheet.

[54] NewSpace Systems, 12 Cyclonite Street, The Interchange, Somerset West 7130, South Africa, *Fine (Digital) Sun-Sensor*, Fact sheet.

[55] Honeywell, *Miniature Inertial Measurement Unit*, September 2003, Fact sheet.

[56] Dikmen, S., *Development of Star Tracker Attitude and Position Determination System for Spacecraft Maneuvering and Docking Facility*, Master's thesis, LuleåUniversity of Technoloy, Department of Computer Science, Electrical and Space Engineering, 2016.

[57] Cervone, A., "Aerospace Design and Systems Engineering Element II," Lecture slides.

[58] Zandbergen, B., *Course AE1222*-II - *Aerospace Design & System Engineering Elements* I - *Part: Spacecraft (bus) Design & Sizing*, Delft University of Technology, November 2015.

[59] Taylor, J., Lee, D., and Shambayati, S., "Mars Reconnaissance Orbiter Telecommunications," Tech. rep., NASA, September 2006.

[60] Chang, C., *DSN Telecommunications Link Design Handbook*, Jet Propulsion Laboratory, California Institute of Technology, May 2017, DSN No. 810-005.

[61] Rebold, T., Kwok, A., Wood, G., and Butman, S., "The Mars Observer Ka-Band Link Experiment," *The Telecommunications and Data Acquisition Progress Report*, Vol. 42-118, May 1994.

[62] Sellers, J., Astore, W., Giffen, R., and Larson, W., *Understanding Space - An Introduction to Astronautics*, McGraw Hill, 3rd ed., September 2005.

[63] Berlin, P., *Satellite Platform Design*, Department of Space Science of the Universities of Luleåand Umeå, 5th ed., 2007.

[64] Law, D. C., Edmondson, K., Siddiqi, N., Paredes, A., King, R., Glenn, G., Labios, E., Haddad, M., Isshiki, T., and Karam, N., "Lightweight, flexible, high-efficiency III-V multijunction cells," *World Conference on Photovoltaic Energy Conversion*, Vol. 4, May 2006, pp. 1879–1882.

[65] Pathel, M. R., *Spacecraft Power Systems*, CRC Press, 2005.

[66] Hoang, B., White, S., Spence, B., and Kiefer, S., "Commercialization of Deployable Space Systems' roll-out solar array (ROSA) technology for Space Systems Loral (SSL) solar arrays," *2016 IEEE Aerospace Conference*, March 2016, pp. 1–12.

[67] A123 Energy Solutions, *Battery Pack Design, Validation,and Assembly Guide using A123 Systems AMP20 M1 HD-A Nanophosphate®Cells*, February 2014, Document No: 493005-002.

[68] Cowan, K., *Project Guide Design Synthesis Exercise*, Delft, The Netherlands, 2017, (unpublished).

[69] MAN Truck & Bus AG, Postfach 50 06 20, D-80976 München, *Moving large objects. Efficient MAN crane vehicles.*, Fact sheet.

[70] *Falcon 9 Launch Vehicle payload user's guide, Revision 2*, October 2015.

[71] NASA, Kennedy Space Center, FL 32899, *America's Spaceport*, Fact sheet, Document No: NP-2010-04-072-KSC.

[72] *Crawler-Transporter*, Kennedy Space Center, FL 32899, Fact sheet, Document No: FS-2012-04-085-KSC.

[73] Prokop, L., "A requirements-based, bottom-up SLOC estimate and analysis of NASA's Orion crew exploration vehicle spacecraft flight software," *Innovations System Software Engineering*, Vol. 101, No. 2, October 2012, pp. 93–101.

[74] National Research Council, *Pathways to Exploration: Rationales and Approaches for a U.S. Program of Human Space Exploration*, The National Academies Press, Washington, DC, 2014.

[75] Hogan, T., *Mars Wars - The Rise and Fall of the Space Exploration Initiative*, NASA, Washington, DC, 2007, NASA SP-2007-4410.

[76] Verhagen, W., "AE3221-I Systems Engineering and Aerospace Design Lecture 8 - Risk Management & Reliability Engineering," Lecture slides.

[77] Gillespie, A. and Monaghan, M., "Allocating Reliability & Maintainability Goals to NASA Ground Systems," *Proceedings - Annual Reliability and Maintainability Symposium (RAMS)*, January 2013, pp. 1–6.

[78] Staton, E., Cates, G., Finn, R., Altino, K., Burns, K., and Watson, M., "Use of DES Modeling for Determining Launch Availability for SLS," *SpaceOps Conference 2014*, NASA, Pasedena, CA, May 2014, pp. 1–14.

[79] Gill, E., "System Engineering and Aerospace Design Notes," Lecture slides.

[80] Belingheri, M., Eckardstein, D. V., and Tosellini, R., "Programmatic Risk Management in Space Projects," *ESA Bulletin*, Vol. 103, August 2000, pp. 86–91.

[81] NASA, *Space Launch System (SLS) Program Mission Planner's Guide (MPG) Executive Overview*, August 2014, Document No: SLS-MNL-201.

[82] NASA, *NASA Procedural Requirements for Limiting Orbital Debris*, May 2009, Document No: NPR 8715.6A.

[83] Woschnak, A., Krejci, D., Schiebl, M., and Scharlemann, C., "Development of a green bipropellant hydrogen peroxide thruster for attitude control on satellites," *Progress in Propulsion Physics*, Vol. 4, 2013, pp. 689–706.

[84] Sagdeev, R. and Zacharov, A., "Brief history of the Phobos mission," *Nature*, Vol. 341, October 1989, pp. 581–585.

[85] Murchie, S., Britt, D., and Pieters, C., "The value of Phobos sample return," *Planetary and Space Science*, Vol. 102, November 2014, pp. 176–182.

[THIS PAGE WAS INTENTIONALLY LEFT BLANK]

Appendix A Human Resources

To give an introduction of the design team and project management, this section provides insight in the planning. Realistically speaking, the only real resource the team had access to throughout this project was the brainpower of 10 enthusiastic and ambitious members. For 40 hours a week over a window of 11 weeks, the total time available added up to about 4,400 hours. This valuable resource had to be split up over the great number of tasks to attain the final objective of safely landing a habitat on Phobos. This required detailed planning from day one. The workforce was divided based on the importance of certain aspects of the mission. The two most important bits of the design were astrodynamics and system integration, with 20% and 25% of the overall project importance, respectively. Therefore, two members were assigned the technical role of navigators and two members were assigned the organisational role of system engineers. The next fundamental aspect of the mission was remote sensing and planetary science with 15% of the total. This resulted into two members taking up the technical role with respect to communication and C&DH. Propulsion and power each scored 10% of the total importance. However, the design choice of the propulsion system was limited by the requirement of using a SEP system. As that implied a major challenge for the electrical power supply, only one member was assigned to propulsion while two members were assigned to power. Of least importance was stability and control, operations, sustainability and structures all scoring 5% of the total. In order to efficiently allocate the time for these tasks, the system engineers did a great job in estimating the time necessary to complete the task to a certain level of detail. Over the span of the project these time indications helped immensely to organise the group which resulted into meeting the deadlines every single time while still producing a product of high quality in the form of a detailed design. An overview of the design team and the project management can be found in Figure A.1.

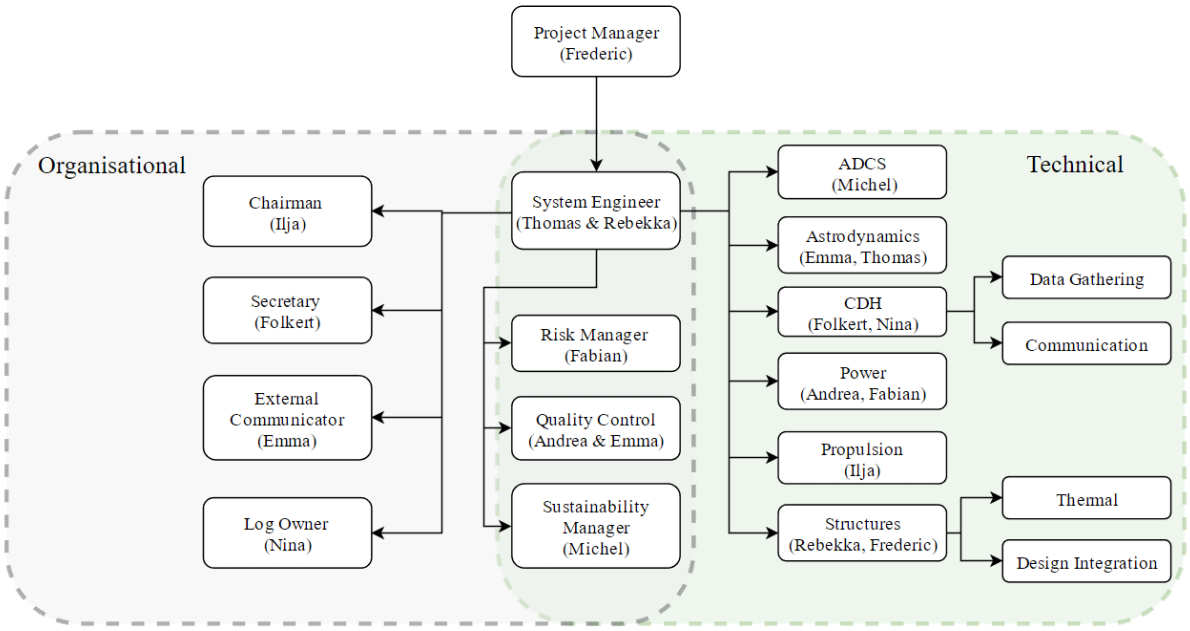

Figure A.1: The updated organogram showing organisational and technical roles.

[THIS PAGE WAS INTENTIONALLY LEFT BLANK]

Appendix B Old Mass Budget

Since the design of a complex system such as a spacecraft is a highly iterative process, parameters such as mass budgets are constantly updated. As to keep these iterations organised and correct, these iterations must happen simultaneously between all subsystems, while communicating changes. The results presented in this report, including the mass budget, are those obtained through the final of these iterations performed. However, as to enable recreating the method used for obtaining the results, also inputs should be mentioned. For this reason the mass budget of a previous iteration is shown, which was used as input for obtaining the results presented in this report as Table B.1. Thus, this mass budget was used to size all the subsystems before ending with the final values presented in chapter 2.

Table B.1: Old mass budget of the PICARD design.

Mass budget [kg]	Tug	Lander
Structures	4,484	713
Thermal	200	100
Navigation	1	1
Propellant main prop	29,086	3188
Propellant ADCS	1,840	0
Propulsion	6,460	1,961
Power	34,766	1,641
ADCS	1,388	98
CDH	20	10
Communication	135	15
Payload	1	80
Total Wet Mass	**78,381**	**7,807**
Total Dry Mass	**47,455**	**4,619**

[THIS PAGE WAS INTENTIONALLY LEFT BLANK]

Appendix C Functional Diagrams

This appendix shows the functional diagrams for the final design. The functional flow diagram is shown in section C.1 and the functional breakdown structure is given in section C.2.

C.1 Functional Flow Diagram

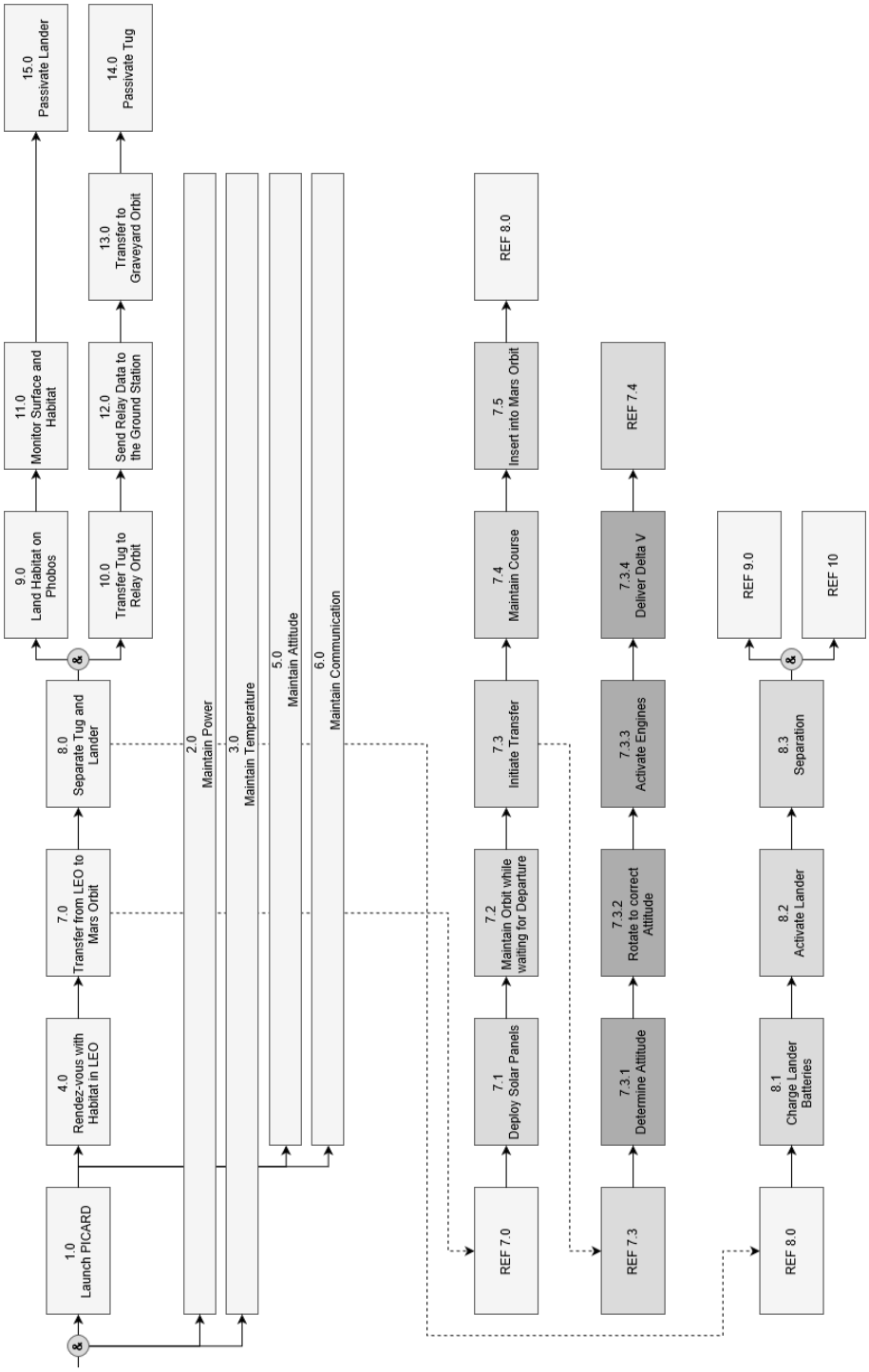

Figure C.1: Part one of the Functional Flow Diagram.

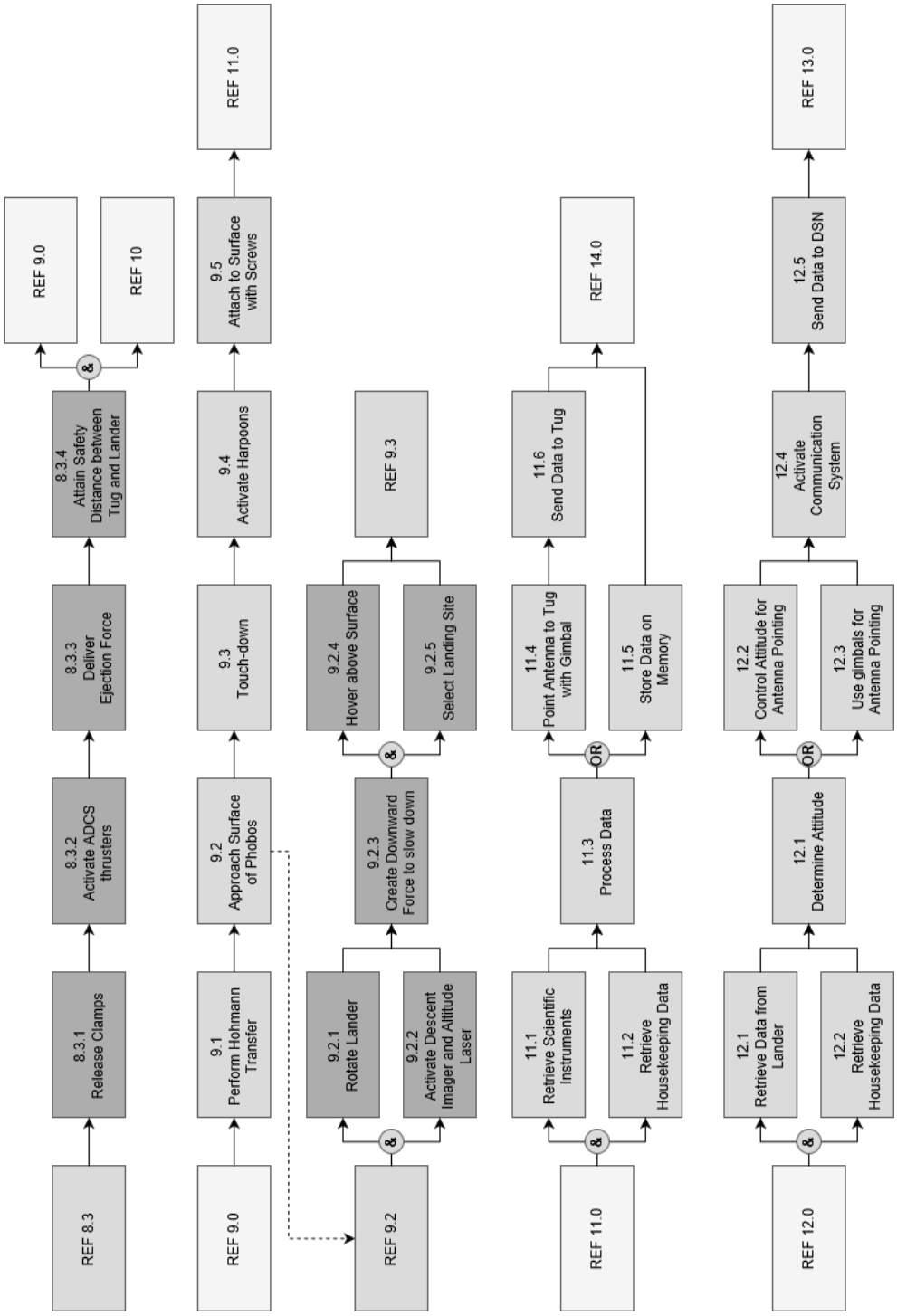

Figure C.2: Part two of the Functional Flow Diagram.

C.2 Functional Breakdown Structure

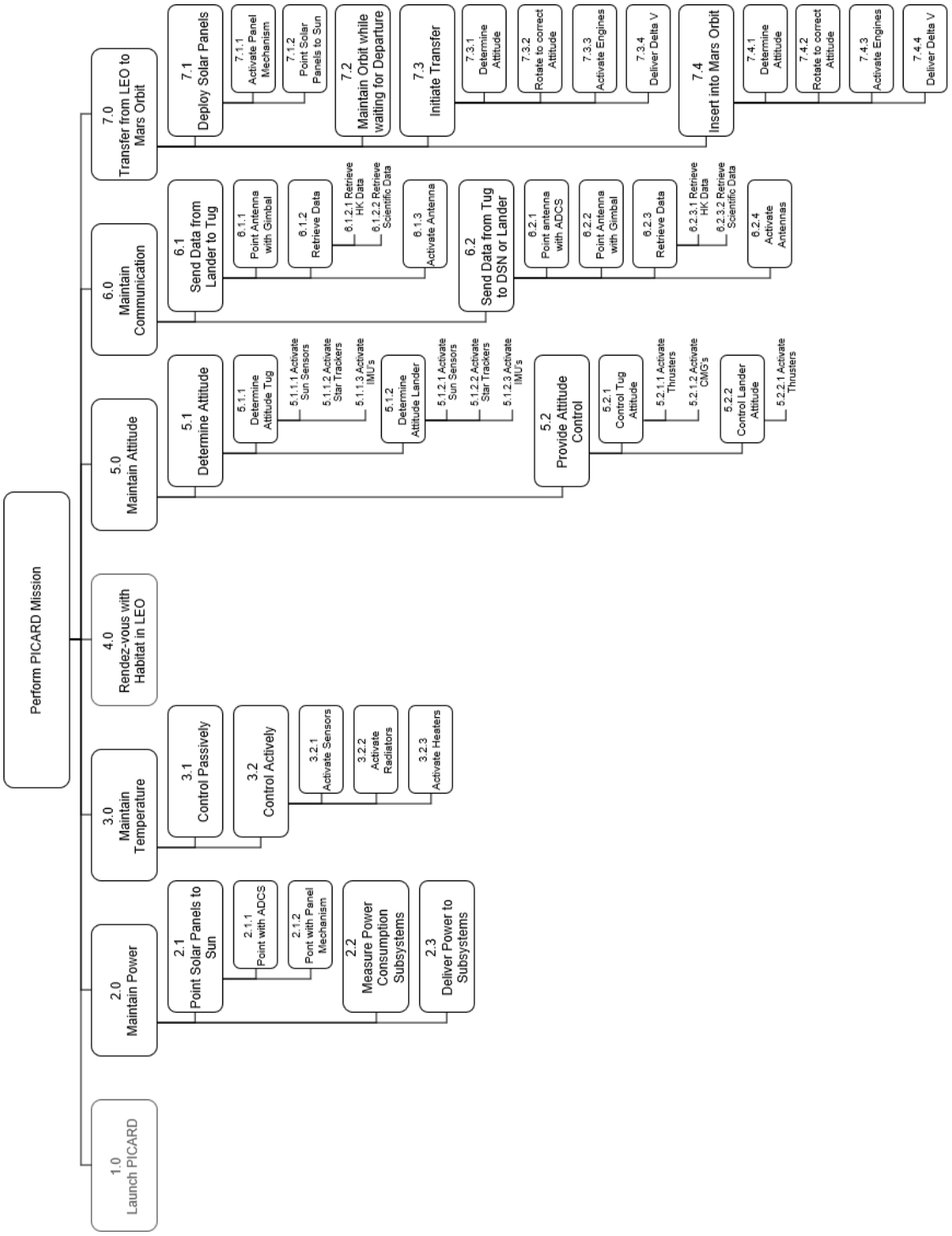

Figure C.3: Part one of the Functional Breakdown Structure.

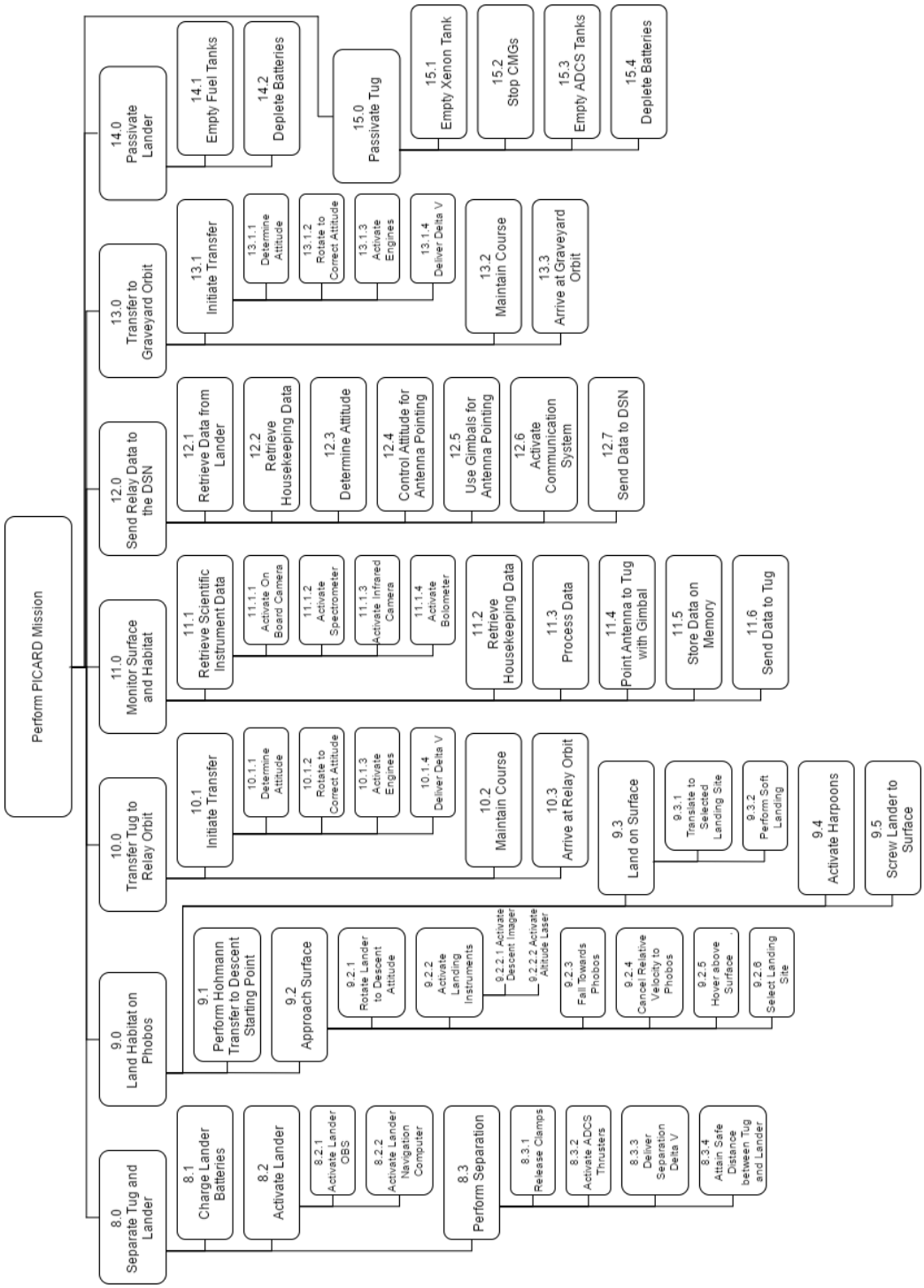

Figure C.4: Part two of the Functional Breakdown Structure.

Appendix D Compliance Matrix

This appendix gives the full list of requirements in the form of compliance matrices in Table D.2, Table D.3, Table D.4 and Table D.5. The requirements are as identified in the Baseline Report [6], but reformulated and restructured to clearly show what requirements apply to what. Also, some are added for completeness. In the first row the requirement and its identifier are given. The second row states whether the requirement is met, a 'Y' shows the requirement is met, a 'N' shows it is not met, a 'U' shows it is unknown at this point and more investigation has to be performed, a P shows it is partially fulfilled and more investigation is required and a C indicates a killer requirement was found which was changed accordingly. The third row shows the actual value that needs to be met and the fourth row the value which is achieved. The compliance to the subsystem requirements is discussed in the respective parts in chapter 5. The key and other requirements are discussed in chapter 12. The identifiers used for the requirements are explained in Table D.1 [6].

Table D.1: Explanation of identifiers used for the requirements.

Identifier	Explanation	Identifier	Explanation
MTP	Mission to Phobos	TR	Transportation Tug
LA	Lander	COM	Communication
NAV	Navigation	STR	Structural
PROP	Propulsion	SENS	Sensor
ADCS	ADCS	SYS	System
POW	Power	KEY	Key
OTH	Other		

Table D.2: First part of key requirements.

Requirement	Met	Requirement	Achieved
Key requirements			
MTP-KEY-SYS01 *The Habitat shall be in a stable position on Phobos' surface by the end of 2032.*	Y	End of 2032	15 October 2032
MTP-KEY-SYS02 *The Habitat shall be monitored on Phobos' surface.*	Y	Monitored	Monitored
MTP-KEY-SYS03 *Scientific instruments shall monitor Phobos' surface conditions when at Phobos.*	Y	Scientific instruments	On-board camera, etc.
MTP-KEY-SYS04 *The vehicle design shall have no Single Point of Failure (SPF).*	Y	No SPF	No SPF
MTP-KEY-SYS05 *Mission hardware used shall have a minimum Technology Readiness Level (TRL) of at least five.*	Y	TRL 5	TRL 5
MTP-KEY-SYS06 *Mission hardware shall achieve a minimum TRL of eight before launch.*	U	TRL 8	-
MTP-KEY-SYS07 *The Space Launch System (SLS) up to Block II shall be capable of launching all hardware.*	Y	d 8.3 x h 25 m	5 x 5 x 8.4 m
MTP-KEY-SYS08 *The maximum number of SLS Block II launches shall agree with the Humans Orbiting Mars (HOM) report [9].*	Y	2 launches	2 launches
MTP-KEY-SYS09 *A clear end-of-life strategy shall be included.*	Y	EOL	EOL
MTP-KEY-SYS10 *The COSPAR regulation for planetary protection shall be adhered to [16].*	Y	COSPAR	COSPAR
MTP-KEY-SYS11 *The amount of debris at all mission stages shall be minimised.*	Y	Minimal	Minimal
MTP-KEY-SYS12 *The total cost of the mission shall fit within NASAs current budget for human spaceflight as presented in [9].*	Y	15.1 bn $	15.1 $bn
MTP-KEY-SYS13 *The data collected by the scientific instruments shall be available on Earth six months before humans leave Earth for Mars*	Y	6 months	6 months
MTP-KEY-SYS14 *The total spacecraft mass shall be compatible with the SLS*	Y	143.2 mt	92.0 mt

Table D.3: Second part of key requirements and structures requirements.

Requirement	Met	Requirement	Achieved
Key requirements			
MTP-KEY-LA-ADCS01 *The Phobos lander shall provide a soft landing.*	Y	2 m/s	0.25 m/s
MTP-KEY-LA-ADCS02 *The Phobos lander shall provide a hovering capability for at least two minutes.*	Y	120 s	120 s
MTP-KEY-PROP-01 *The propellant used shall have minimal effect on the environment.*	P	Minimal	Partially toxic
MTP-KEY-PROP-02 *The propellant used shall have minimal effect on biological organisms.*	P	Minimal	Partially toxic
MTP-KEY-TR-PROP01 *The transportation tug propulsion system shall transfer the spacecraft to an orbit around Mars.*	Y	Mars	Mars
MTP-KEY-TR-PROP02 *The transportation tug shall use a solar electric propulsion system (SEP).*	Y	SEP	SEP
MTP-KEY-TR-PROP03 *The transportation tug electric propulsion system shall have an electric capacity of 100 kWe.*	C	100 kWe	400 kWe
MTP-KEY-LA-PROP01 *The lander propulsion system shall transfer the habitat and supportive equipment to Phobos.*	Y	Phobos	Phobos
Structures requirements			
MTP-STR01 *The tug shall have docking capabilities with the lander.*	Y	docking	MSS
MTP-STR02 *The tug shall have undocking capabilities with the lander.*	Y	undocking	MSS
MTP-STR-TR01 *The structure of the transportation tug shall be able to withstand a load of $3.08{\cdot}10^6$ N.*	Y	$3.08{\cdot}10^6$ N	$3.14{\cdot}10^6$ N
MTP-STR-TR02 *The tug shall remain functioning up to a radiation level of $<$ tbd $>$ mrad.*	U	$<$ *tbd* $>$ mrad	To be determined
MTP-STR-TR04 *The temperature in the tug shall be in between component limits.*	U	15 and 30 °C	Exact model still to be made
MTP-STR-LA01 *The structure of the lander shall be able to withstand a load of $3.06{\cdot}10^5$ N.*	Y	$3.06{\cdot}10^5$ N	$3.15{\cdot}10^5$ N
MTP-STR-LA02 *The lander shall be able to dock with Phobos.*	Y	dock	Harpoons and leg screws
MTP-STR-LA03 *The lander shall be able to dock with the habitat.*	Y	dock	MSS
MTP-STR-LA04 *The landing struts shall be able to withstand a load of 12,324 N.*	Y	12,324 N	12,330 N

Table D.4: Structures continued, navigation, propulsion and ADCS requirements.

Requirement	Met	Requirement	Achieved
MTP-STR-LA05 *The temperature in the lander shall be in between component limits.*	U	15 and 30 °C	Exact model still to be made
MTP-STR-LA06 *The lander shall remain functioning up to a radiation level of < tbd > mrad.*	U	< *tbd* > mrad	To be determined
Navigation requirements			
MTP-NAV-TR01 *The tug shall have on-board orbital navigation capabilities.*	Y	on-board	on-board
MTP-NAV-TR02 *The tug shall deliver the full spacecraft from Earth SOI to Mars SOI.*	Y	Mars SOI	Mars SOI
MTP-NAV-LA01 *The lander shall have on-board orbital navigation capabilities.*	Y	on-board	on-board
MTP-NAV-LA02 *The lander shall deliver the lander and habitat from an orbit around Mars to Phobos.*	Y	Phobos	Phobos
Propulsion requirements			
MTP-PROP-TR01 *The tug propulsion system shall be able to deliver a ΔV of 11.1 km/s.*	Y	11.1 km/s	11.1 km/s
MTP-PROP-TR02 *The tug propulsion system shall be able to restart.*	Y	restartable	restartable
MTP-PROP-LA01 *The lander propulsion system shall be able to deliver a ΔV of 67.5 m/s.*	Y	67.5 m/s	67.5 m/s
MTP-PROP-LA02 *The lander propulsion system shall be able to restart.*	Y	restartable	restartable
ADCS requirements			
MTP-ADCS-TR01 *The tug ADCS shall have a pointing accuracy of 0.1 degree.*	Y	0.1°	0.011°
MTP-ADCS-TR02 *The tug ADCS shall be able to detumble after launch within one hour.*	Y	1 hour	1 minute
MTP-ADCS-TR04 *The tug ADCS shall handle 0.1 Nm torque in the transfer from Earth orbit to Mars orbit.*	Y	0.1 Nm	71 Nm
MTP-ADCS-TR05 *The tug ADCS shall be able to rotate 180 degrees within 30 minutes.*	Y	30 minutes	20 minutes
MTP-ADCS-TR06 *The tug ADCS shall handle 0.25 Nm torque in the relay orbit.*	Y	0.25 Nm	71 Nm
MTP-ADCS-LA01 *The lander ADCS shall have a pointing accuracy of 0.1 degree.*	Y	0.1°	0.015°

Table D.5: ADCS continued, communication and C&DH.

Requirement	Met	Requirement	Achieved
MTP-ADCS-LA02 *The lander ADCS shall handle 0.1 Nm torque during the transfer from Mars orbit to Phobos.*	Y	0.1 Nm	71 Nm
MTP-ADCS-LA03 *The lander ADCS shall provide 120 s hover capability.*	Y	120 s	120 s
MTP-ADCS-LA04 *The lander ADCS shall provide 10 m/s manoeuvre capability at Phobos.*	Y	10 m/s	10 m/s
MTP-ADCS-LA05 *The lander ADCS shall be able to provide 7.6 m/s vertical deltaV at Phobos.*	Y	7.6 m/s	7.6 m/s
MTP-ADCS-LA06 *The tug ADCS shall be able to rotate 180 degrees within 3 minutes.*	Y	3 minutes	2.2 minutes
Communication requirements			
MTP-COM-TR01 *The tug shall have a minimum bitrate of 100 kbits/s with Ground Control during all segments of the mission.*	Y	100 kbits/s	200 kbits/s
MTP-COM-TR02 *The tug shall communicate with Ground Control with a maximum SNR of 3 dB.*	Y	3 dB	3.1 dB
MTP-COM-01 *The lander and tug shall have a minimum bitrate of 100 kbits/s with each other after separation of the tug and lander.*	Y	100 kbits/s	200 kbits/s
MTP-COM-02 *The tug and lander shall communicate with each other with a maximum SNR of 3 dB.*	Y	3 dB	6.6 dB
C&DH requirements			
MTP-C&DH-TR01 *The tug C&DH system shall be able to process 484.6 bytes/s*	U	484.6 bytes/s	Requires testing
MTP-C&DH-TR02 *The tug shall have memory to store all housekeeping data generated during eclipse periods*	Y	3.52MB	2048MB
MTP-C&DH-LA01 *The tug C&DH system shall be able to process 359.93 bytes*	U	359.93 bytes/s	Requires testing
MTP-C&DH-LA02 *The lander shall have memory to store all housekeeping data generated during eclipse periods*	Y	712MB	1024MB

Table D.6: Power and other requirements.

Requirement	Met	Requirement	Achieved
Power requirements			
MTP-POW-TR01 *The tug solar arrays shall be able to provide a maximum of 404,269 W to the subsystems during the mission.*	Y	404,269 W	404,269 W
MTP-POW-TR02 *The solar arrays shall be able to charge the tug batteries to a capacity of 5,668,099 Wh during sun time.*	Y	5,668,099 Wh	5,668,099 Wh
MTP-POW-TR03 *The tug batteries shall be able to provide 5,668,099 Wh to the subsystems during eclipse.*	Y	5,668,099 Wh	5,668,099 Wh
MTP-POW-TR04 *The tug batteries shall provide tbd Wh to ensure docking after SLS launch.*	U	tbd Wh	tbd Wh
MTP-POW-TR05 *The tug batteries shall provide tbd Wh to deploy solar arrays after docking.*	U	tbd Wh	tbd Wh
MTP-POW-LA01 *The lander batteries shall be charged to 240,477 Wh before detachment of tug and lander.*	Y	240,477 Wh	240,477 Wh
MTP-POW-LA02 *The lander batteries shall provide a total of 240,477 Wh to the subsystems after detachment from the tug up to arrival of astronauts.*	Y	240,477 Wh	240,477 Wh
Other requirements			
MTP-OTH-01 *The lander shall be able to detect the landing position.*	Y	landing position	landing position

Appendix E List of Risks

Table E.1: Technical risks part one.

P = Power & Propulsion		
Identifier	Location	Description
P1	[4,4]	Solar panel failure
P2	[4,4]	Battery failure
P3	[4,2]	Cable failure
P4	[3,3]	Software failure (Control & Distribution)
P5	[3,2]	Unexpected eclipse times
P6	[2,5]	External impacts (Collision, Radiation, Temperature)
P7	[4,2]	VASIMR failure during transfer
P8	[4,4]	VASIMR misalignment resulting in wrong trajectory
P9	[4,4]	Power support failure
P10	[2,3]	Control failure resulting into reduction of performance
P11	[4,4]	Running out of fuel
C = Communication & C&DH		
Identifier	Location	Description
C1	[4,3]	Antenna failure
C2	[3,4]	Pointing offset
C3	[4,3]	Power support failure
C4	[3,2]	Insufficient SNR
C5	[2,3]	Insufficient data rate
C6	[2,3]	Unavailability of Deep Space Network
C7	[2,3]	Malfunctioning of instruments
C8	[3,2]	Disagreement between 1st and 2nd processor
C9	[2,1]	Overflow of memory
S = Structure		
Identifier	Location	Description
S1	[4,3]	Structure cannot withstand launch loads
S2	[2,2]	Structure cannot withstand landing loads
S3	[3,2]	Failure of thermal control
S4	[3,3]	Failure of clamping mechanism
S5	[4,2]	Solar panel deploy mechanism failure
S6	[3,3]	Wrong planning of system allocation within structure
S7	[4,2]	Structure does not fit the launcher
S8	[3,4]	Capsizing of the habitat at Phobos' surface

Table E.2: Technical risks part two.

N = Navigation		
Identifier	Location	Description
N1	[3,5]	Navigating through van Allen belts
N2	[4,2]	Deviation from trajectory
N3	[4,3]	Failures during design stage (miscalculation)
N4	[3,2]	Increased radiation due to Solar activity
A = ADCS		
Identifier	Location	Description
A1	[3,4]	Sensor failure
A2	[4,4]	Thruster failure
A3	[4,5]	CMG failure
A4	[2,3]	Underestimation of disturbances
A5	[2,3]	Selected off the shelf products no longer produced at construction date
A6	[4,1]	Tank failure
Costs		
Identifier	Location	Description
$1	[3,3]	Overshooting cost budget
$2	[4,4]	Budget cuts

Table E.3: Organisational risks.

Project Group		
Identifier	Location	Description
O.P1	[2,5]	Shortfall of group member
O.P2	[3,5]	Disagreements
O.P3	[2,3]	Dissatisfaction
O.P4	[3,2]	Failure of performance
Schedule		
Identifier	Location	Description
O.S1	[3,4]	Missing deadlines
O.S2	[4,4]	Performance cutbacks due to misapplication of resource
O.S3	[3,3]	Poor planning of coach meetings
O.S4	[4,4]	Poitical delay of main mission

Appendix F Work Division

Table F.1: Work division part one.

Section	Writer	Contributor	Quality Control
Preface	Folkert		Andrea, Frederic, Ilja, Rebekka, Emma, Fabian
Summary	Folkert		Andrea, Frederic, Ilja, Michel, Emma, Rebekka, Fabian
1 Introduction	Folkert	Emma	Andrea, Frederic, Rebekka, Emma
2 PICARD Specifications			
2.1 Configuration	Fabian		Andrea, Frederic, Emma , Fabian
2.2 Performance	All		Andrea, Frederic, Folkert , Fabian
2.3 Resource Allocation	Andrea, Ilja and Rebekka		Andrea, Frederic, Michel, Folkert, Fabian
2.4 Instruments	Folkert		Andrea, Frederic, Michel
2.5 Hardware Diagram	Frederic		Andrea, Emma
3 Mission Phases			
3.1 Launch	Rebekka	Thomas	Andrea, Frederic, Ilja, Thomas, Folkert
3.2 Rendez-vous with Habitat	Rebekka	Thomas	Andrea, Frederic, Ilja, Thomas, Folkert
3.3 Escaping Earth's Sphere of Influence	Rebekka	Thomas	Andrea, Frederic, Ilja, Thomas, Folkert
3.4 Transfer to Mars	Rebekka	Thomas	Andrea, Frederic, Ilja, Thomas, Folkert
3.5 Separation of Tug & Lander	Rebekka, Thomas		Andrea, Frederic, Ilja, Thomas, Folkert
3.6 Land on Phobos	Thomas		Andrea, Frederic, Ilja, Thomas, Folkert
3.7 Mission on Phobos	Rebekka		Andrea, Frederic, Ilja, Thomas, Folkert
3.8 End of Life	Thomas		Andrea, Frederic, Ilja, Folkert
4 Mission Design			
4.1 Landing Design	Michel and Nina		Andrea, Frederic, Emma
4.2 End of Life Design	Michel and Nina	Thomas	Andrea, Frederic, Emma

Table F.2: Work division part two.

Section	Writer	Contributor	Quality Control
5 PICARD Detailed Design			
5.1 Structures	Rebekka (Loading, Thermal, Radiation and Integration) and Frederic (Landing, Clamping, Material and Integration)		Andrea, Ilja, Nina, Thomas
5.2 Navigation	Emma (GMAT) and Thomas (Python)		Andrea, Emma, Ilja, Rebekka, Thomas
5.3 Propulsion	Ilja		Andrea, Rebekka, Thomas, Folkert
5.4 ADCS	Michel		Andrea, Ilja, Rebekka, Folkert
5.5 Communication	Nina	Folkert	Andrea, Ilja and Folkert
5.6 C&DH	Folkert	Nina	Emma, Frederic, Ilja, Nina
5.7 Power	Andrea (Detail design procedure and Model V&V) and Fabian (EBD, ROSA and Product V&V)		Andrea, Emma, Frederic, Folkert
6 Post Design Operations			
6.1 Project Design & Development Logic	Andrea		Emma, Frederic, Ilja, Folkert
6.2 Operations & Logistics	Andrea and Thomas		Emma, Frederic, Folkert, Ilja
6.3 Project Gantt Chart	Thomas		Emma, Frederic, Folkert, Ilja
6.4 Cost Breakdown	Emma, Thomas and Ilja	Nina	Frederic, Nina, Folkert
7 Market Analysis			
7.1 Financial Plan	Ilja		Emma, Frederic, Folkert
7.2 Market Shift	Folkert		Emma, Frederic, Ilja, Nina
7.3 Potential Customers & Funding	Michel		Emma, Frederic, Nina, Folkert
8 RAMS			
8.1 Reliability	Emma and Frederic		Frederic, Rebekka, Folkert
8.2 Availability	Emma	Frederic	Frederic, Rebekka, Folkert
8.3 Maintainability	Frederic	Emma	Frederic, Rebekka, Folkert
8.4 Safety	Emma and Frederic		Frederic, Rebekka, Folkert
9 Risk Management			
9.1 Risk Identification	Fabian		Emma, Frederic, Folkert
9.2 Risk Assessment	Fabian		Emma, Frederic, Folkert
9.3 Risk Mitigation	Fabian		Andrea, Emma, Frederic, Folkert

Table F.3: Work division part three.

Section	Writer	Contributor	Quality Control
10 Sustainability			
10.1 Environment	Michel		Emma, Frederic, Ilja, Nina
10.2 Society	Michel		Emma, Frederic, Ilja, Nina
11 Sensitivity Analysis			
11.1 Causes	Folkert		Emma, Frederic, Ilja
11.2 Effects	Folkert		Emma, Frederic, Ilja
12 System Verification & Validation			
12.1 Verification	Nina	Ilja	Emma, Frederic, Rebekka
12.2 Validation	Nina	Ilja	Emma, Frederic, Rebekka
13 Conclusion	Folkert		Emma, Frederic, Rebekka
14 Discussion	Rebekka, Folkert, Nina and Thomas	Andrea	Emma, Frederic, Michel
Bibliography	Michel	Folkert	
A Human resources	Fabian		Frederic, Ilja, Michel, Folkert
B Old Mass Budget	Rebekka and Thomas		Frederic, Michel, Folkert
C Functional Diagrams			
C1 Functional Flow Diagram	Nina	Michel	Frederic, Folkert
C2 Functional Breakdown Structure	Michel and Nina		Frederic, Folkert
D Compliance Matrix	Ilja	All	Frederic, Michel, Folkert
E List of Risks	Fabian	All	Frederic, Michel, Folkert
F Work Division	Nina	All	Frederic, Michel, Folkert